

MICROGRID MODELLING AND ONLINE MANAGEMENT

Faisal A. Mohamed



TEKNILLINEN KORKEAKOULU
TEKNISKA HÖGSKOLAN
HELSINKI UNIVERSITY OF TECHNOLOGY
TECHNISCHE UNIVERSITÄT HELSINKI
UNIVERSITE DE TECHNOLOGIE D'HELSINKI

MICROGRID MODELLING AND ONLINE MANAGEMENT

Faisal A. Mohamed

Dissertation for the degree of Doctor of Science in Technology to be presented with due permission of the Faculty of Electronics, Communications and Automation, for public examination and debate in Auditorium AS1 at Helsinki University of Technology (Espoo, Finland) on the 7th of March, 2008, at 12 noon.

Helsinki University of Technology
Faculty of Electronics, Communications and Automation
Department of Automation and Systems Technology

Distribution:

Helsinki University of Technology
Department of Automation and Systems Technology
P.O. Box 5500
FI-02015 HUT, Finland
Tel. +358-9-451 5201
Fax. +358-9-451 5208
E-mail: control.engineering@tkk.fi
<http://www.control.tkk.fi/>

ISBN 978-951-22-9234-9 (printed)

ISBN 978-951-22-9235-6 (pdf)

ISSN 0356-0872

Yliopistopaino

Helsinki 2008

Available on net at <http://lib.tkk.fi/Diss/2008/isbn9789512292356>



ABSTRACT OF DOCTORAL DISSERTATION		HELSINKI UNIVERSITY OF TECHNOLOGY P.O. BOX 1000, FI-02015 TKK http://www.tkk.fi	
Author Faisal A. Mohamed			
Name of the dissertation MicroGrid Modelling and Online Management.			
Manuscript submitted September 17, 2007		Manuscript revised January 17, 2008	
Date of the defence March 7, 2008			
<input checked="" type="checkbox"/> Monograph		<input type="checkbox"/> Article dissertation (summary + original articles)	
Faculty	Electronics, Communications and Automation		
Department	Automation and Systems Technology		
Field of research	Control Engineering		
Opponent (s)	Dr. Matti Vilkkö and Associate Professor Mohamed Abido		
Supervisor	Professor Heikki Koivo		
<p>Abstract</p> <p>Modern power network owners have to respond to a number of challenges such as significant load changes and growth in the geographical distribution of the customers. On the other hand, the environmental policy and economic requirements from the market are constantly growing. The presence of these problems has led to an increased interest in the local renewable energy generation at the distribution level. The Microgrid (MG) concept assumes a cluster of loads and microsources operating as a single controllable system that provides both power and heat to its local area. Not much is known about Microgrid behavior as a whole system. Some models exist which describe the components of the Microgrid. This thesis aims to model Microgrids at steady state and study their transient responses to changing inputs. Currently models of a Diesel Engine, a Fuel Cell, a Microturbine, a Windturbine, a Photovoltaic cell, and Battery storage have been developed. In this thesis, a generalized formulation is introduced to determine the optimal operating strategy, the goal to minimize the operating costs as well as the reduction of the emission costs and level for a MicroGrid. To solve such a management problem it is first formulated as a nonlinear constrained cost optimization problem. Since the management problem poses a number of simultaneous objectives and constraints a Multiobjective optimization problem is formulated by considering the emission level reduction. A daily income from sold power and cost to be paid to the utility of the purchased power is added to the problem. The model takes also into consideration the reduction of emissions caused by NO_x, SO₂ and CO₂. The optimization is aimed to minimize the operating costs of the system, while constraints are adjusted to meet the customer demand and the safety of the system. Different optimization techniques are applied to solve the problem, such as Mesh Adaptive Direct Search, Sequential Quadratic Programming, Genetic Algorithms, and Game Theory. Test cases provide comparison and evidence of the efficiency of the proposed methods.</p>			
Keywords Microgrid, Diesel Engine, Fuel Cell, Microturbine, Windturbine, Photovoltaic, Battery storage, Optimization, Emission level			
ISBN (printed) 978-951-22-9234-9		ISSN (printed) 0356-0872	
ISBN (pdf) 978-951-22-9235-6		ISSN (pdf)	
Language English		Number of pages 143	
Publisher Helsinki University of Technology, Department of Automation and Systems Technology			
Print distribution Helsinki University of Technology, Department of Automation and Systems Technology			
<input checked="" type="checkbox"/> The dissertation can be read at http://lib.tkk.fi/Diss/			

Preface

I joined Helsinki University of Technology, Control Engineering Laboratory as postgraduate student in July 2003.

First of all I would like to thank Allah for blessing me with the ability to complete this work. This work couldn't be complete without help and support of several people.

First my deep gratitude goes to my advisor, Professor Heikki Koivo who has provided me invaluable support, guidance, patience, and encouragement over the past years. I would like to thank all my Libyan friends here in Helsinki, and in Libya for their care and encouragement. I wish also to thank all the my friends and colleagues in the Control Engineering Laboratory, for creating a friendly and stimulating atmosphere.

I would like to express my appreciation to the pre-examiners Professor Salman K Salman and Associate Professor Mohamed Abido for their honest and faithful comments.

My deep appreciation are for all my family and relatives at home, for their support and encouragement. Also I thank my wife and my children for their patience, ultimate support, great generosity, and lovingness.

This thesis has been supported by grant from Omar Al-Mukhtar University- El-Beida -Libya. The author has received grants that are gratefully acknowledged, from FORTUM FOUNDATION.

Thanks to everyone who has contributed to this work directly or indirectly.

FAISAL A. MOHAMED

Contents

Preface	v
Contents	vii
List of Notations	xi
List of Figures	xix
List of Tables	xxiii
1 Introduction	1
1.1 Introduction	1
1.1.1 Definition of Microgrids	1
1.1.2 Reasons for Microgrids	3
1.2 Motivation	4
1.3 Management of Microgrid	5
1.4 Optimization	5
1.4.1 Genetic Algorithms	5
1.4.2 Mesh Adaptive Direct Search	6
1.4.3 Game Theory	6
1.5 Objectives and Contributions of the Thesis	7
1.5.1 Modelling of Microgrid	7
1.5.2 Problem Model Formulation	7
1.5.3 Management of Microgrid	8
1.6 Outline of the Thesis	9
2 System Modelling	11
2.1 Introduction	11
2.2 Diesel Generator	11
2.2.1 Modelling of Diesel Engine	12
2.2.2 System Description	13
2.2.3 Diesel Generator Costs	14
2.3 Fuel Cell	14
2.3.1 Characteristics	16
2.3.2 Fuel Cell Workings	17
2.3.3 Modelling of SOFC	17

2.3.4	Characterization of the exhaust of the channels	18
2.3.5	Calculation of the partial pressures	19
2.3.6	Simulation Results	22
2.3.7	Fuel Cost of Fuel Cell	24
2.4	Microturbines	25
2.4.1	Construction of Microturbines	25
2.4.2	Microturbine Modelling	26
2.4.3	Simulation Results	28
2.4.4	Microturbine Fuel Cost	31
2.5	Wind Turbine	31
2.5.1	Wind Turbine Generating System	32
2.5.2	Doubly Fed (Wound Rotor) Induction Generator and Direct Drive Synchronous Generator	32
2.5.3	Wind Turbine Modelling	33
2.5.4	Rotor Equation	34
2.5.5	Generator Equation	35
2.5.6	Simulation Results	38
2.5.7	Wind turbine optimization model	42
2.6	Photovoltaic	43
2.6.1	Modelling	44
2.6.2	Simulation Results	45
2.6.3	PV optimization model	47
2.7	Battery Storage optimization model	49
2.8	Conclusions	50
3	Online Optimal Management of MicroGrid using Mesh Adaptive Direct Search (MADS)	51
3.1	Introduction	51
3.2	Optimization Overview	52
3.3	Direct Search	52
3.3.1	The MADS algorithm	52
3.3.2	Description of MADS algorithm	53
3.4	Optimization Model	54
3.5	Proposed Objective Functions	54
3.5.1	Scenario 1	55
3.5.2	Scenario 2	56
3.5.3	Scenario 3	57
3.6	Golden Search	58
3.7	Implementation of the Optimization Algorithm	60
3.8	Results and Discussions	60
3.8.1	Scenario 1	62
3.8.2	Scenario 2	64
3.8.3	Scenario 3	66
3.9	Conclusions.	72

4	MicroGrid Online Management Using Multiobjective Optimization	73
4.1	Introduction	73
4.2	Optimization Problem	75
4.2.1	Proposed Objective Function	75
4.2.2	Operating Cost	75
4.2.3	Emission Level	76
4.3	Implementation of the Algorithm	77
4.4	Multiobjective optimization problem	77
4.4.1	Weighted Sum	79
4.5	Results and Discussion	81
4.5.1	Scenario 1	81
4.5.2	Scenario 2	85
4.5.3	Scenario 3	89
4.6	Conclusions.	96
5	MicroGrid Online Management Using Multiobjective Genetic algorithms	97
5.1	Introduction	97
5.2	Genetic algorithms	97
5.3	Multiobjective genetic algorithms (MOGA)	100
5.4	Results and Discussion	100
5.4.1	Scenario 1	100
5.4.2	Scenario 2	101
5.4.3	Scenario 3	103
5.5	Conclusions.	107
6	MicroGrid Online Management Using Game Theory	109
6.1	Introduction	109
6.2	Game Theory	109
6.3	Results and Discussion	112
6.3.1	Scenario 1	112
6.3.2	Scenario 2	114
6.3.3	Scenario 3	115
6.4	Conclusions	119
7	Conclusions and Future Work	121
7.1	Conclusions	121
7.2	Modelling of the MG components	122
7.2.1	Modelling of the Diesel Engine	122
7.2.2	Modelling of the Fuel Cell	122
7.2.3	Modelling of the MicroTurbine	122
7.2.4	Modelling of the Wind Turbine	123
7.2.5	Modelling of the Photovoltaic Cell	123
7.3	The Online Management of the MG	124
7.3.1	Online Management using MADS	124
7.3.2	Multiobjective using MOMADS	124

7.3.3	Multiobjective using MOGA	124
7.3.4	Multiobjective using MOGT	124
7.4	Microgrid Modelling and the Future	125
7.5	Final Remarks and Future Work	125
References		127
A Appendix		135
A.1	The General Pattern Search Algorithm	135
A.1.1	Generalized pattern search	135
A.1.2	The Basic GPS Algorithm	136
A.2	Mesh Adaptive Direct Search (MADS) Methods	137
A.2.1	Features of the MADS algorithm	137
A.2.2	The MADS algorithm Description	138
A.2.3	Initialization	138
A.2.4	Search Step	138
A.2.5	Poll Step	138
A.2.6	Parameters update	139
A.2.7	Termination	139
A.2.8	Convergence Analysis	140
B Appendix		143
B.1	The numerical values used to simulate Fuel Cell model	143
Table of ContentsContents		

List of Notations

Symbols

A	Swept Area of Rotor Disc
A_{cf}	Curve Fitting Constant
C_p	Power Coefficient
C_{FC}	Fuel cost of the fuel cell
$C_{DG,i}$	Diesel generator fuel cost
C_{nl}	Natural gas price to supply the fuel cell
C_i	Fuel costs of generating unit i
CO_3^{2-}	Carbonate Ion
CO_2	Carbon Dioxide
C_p	Tariffs of the purchased power
C_s	Tariffs of the sold power
$DCPE_i$	Daily purchased electricity if the load demand exceeds the generated power in $\$/h$
e^-	Electron
E_0	Voltage associated with the Reaction Free Energy
E_g	No Load DC Voltage
E_{GO}	Band Gap for Silicon
EF_{ik}	Emission factor of generating unit i and emission type k
F	Faraday's Constant
F_i	Fuel consumption rate of generator unit i
$f(\mathbf{P})$	objective function
G	Solar Irradiation
G_{ING}	Incident Irradiance
G_{STC}	Irradiance at STC $1000 \text{ W}/\text{m}^2$
H_m	Equivalent Inertia Constant of the Generator Rotor
H_2O	Water
H_2	Hydrogen
H^+	Hydrogen ion
$I(s)$	Input Current
I^r	Stack Current
I_D	Diode Current
I_{SCR}	Short Circuit Current

I_{or}	Cell Saturation Current
I_{os}	Cell Reverse Saturation Current
I_{sh}	Shunt-Leakage Current
$IPSE_i$	Daily income for sold electricity if the generated power exceeds the load demand in $\$/h$
I_L	Load Current
I_{mpp}	Current at Maximum Power Point
I_{ph}	Light-Generated Current
J_r	Inertia of the Shaft
K	Valve Constant
k	Temperature coefficient of power
K_1	Engine Torque Constant
K_2	Fuel Actuator Gain
K_3	Actuator and the Current Driver Constant
K_I	Short Circuit Current Temperature Coefficient
K_0	Process Gain
K_r	Constant Defined for Modelling Purposes
K_v	Voltage Constant
K_B	Boltzmann Constant
K_{H_2O}	Valve Molar Constant for Water
K_{H_2}	Valve Molar Constant for Hydrogen
K_{an}	Anode Valve Constant
K_{OM}	Proportionality constant
L_m	Mutual Inductance
L_r	Rotor Leakage Inductances
L_s	Stator Leakage Inductances
LHV_f	Fuel lower heating rate (kJ/kgf)
M	Emission types (NO _x , or CO ₂ , or SO ₂)
N	Number of generating units i
N_0	Number of Cells Associated in Series in the Stack
N_i^0	Flow Rates Reactant at the Cell Output
N_i^{in}	Flow Rates Reactant at the Cell Input
O_2	Oxygen
$OH - H^+$	Hydroxy Ion
OM_i	Operation and maintenance cost of generating unit i
O^{2-}	Oxygen Ion
P	Active Power
P_m	Input Power
P_{H_2O}	Partial Pressure of Water
P_{H_2}	Partial Pressure of Hydrogen
P_{minpp}	Minimum Power Point
P_{mpp}	Maximum Power Point
P_J	Net electrical power produced at interval J

$P_{DG,i}$	Output power of the diesel generator
P_{el}	Net electrical output power
P_{ru}	Pressure Upstream
$P_{th,rec}$	The thermal power recovered (kW)
P_+	Charge power
P_-	Discharge power
P_L	Power demanded by the load [kW]
P_i	Decision variables, representing the power output from generating unit i
P_i^{max}	Maximum operating power of unit i
P_i^{min}	Minimum operating power of unit i
P_{PV}	Output power of the photovoltaic [kW]
P_{STC}	Module maximum power at STC
$P_{WT,r}$	Wind turbine rated power
P_{WT}	Output power of the wind turbine [kW]
P_{an}	Pressure Inside the anode Channel
P_{batt}	Output power of the battery [kW]
P_r	Cell Pressure
Q	Reactive Power
q	Electron Charge
q_{H_2O}	Molar flows of Water
q_{H_2}	Molar flows of Hydrogen
$q_{H_2}^r$	Hydrogen Molar Flow Take Part in the Reaction
$q_{H_2}^{in}$	Input Hydrogen Molar Flow
$q_{H_2}^{out}$	Output Hydrogen Molar Flow
R	Resistance
R_{gass}	Gas Constant
R_{sh}	Shunt Resistance
R_s	Series Resistance
r	Reference Signal
r_{loss}	Ohmic losses of the stack
r_s	rotor slip
SOC_{max}	Maximum state of charge
SOC_{min}	Minimum state of charge
STC_i	Start-up cost in \$/h
T	Cell Temperature
$-T_{off,i}$	The time a unit has been off
$T(s)$	Mechanical torque of Diesel Engine
T_r	Reference Temperature
T_t	Load Torque
T_c	The cell temperature
t	Time
$\Phi(s)$	Fuel Flow

ω_m	Mechanical Frequency of the Generator
ω_s	Stator Electrical Frequency
ω	Electrical Angular Frequency
ω_w	Angular Speed of a Flywheel
ψ	flux Linkage
ρ	Viscous Friction Coefficient
τ_1	Time Delay
τ_2	Actuator Time Constant
τ_{H_2}	Time Constant of the System Associated with the Hydrogen Flow
ϑ	Density of Air
i	Current
n_{H_2}	Number of Hydrogen Moles in the Anode Channel
η_l	Total efficiency of the microturbine
η_J	Cell efficiency at interval J
m	Mechanical Shaft Torque for the no Loss System
m_f	Mass flow rate of the fuel(kg/s)
U	Terminal Voltage of the PV cell
U_f	Fuel Utilization
U_{max}	Maximum Fuel Utilization
U_{min}	Minimum Fuel Utilization
U_{oc}	Open Circuit Voltage
U_{opt}	Optimal Fuel Utilization
v	Voltage
V^*	Output Voltage from the Control Unit
V_w	Wind Velocity
V_{LL}	Voltage Induced on the Generator Terminal
V_{dc}	DC Voltage
V_{mpp}	Voltage at Maximum Power Point
V_O	Cell Volume
W	Mass Flow
W_{an}	Mass Flow Through the Anode Valve
σ_i	The hot start-up cost
$\sum P_i$	Total power generation [kW]
$\varepsilon_{start-stop}$	Number of the starts and stops
U_{batt}	The battery capacity
V_r	Rated wind speed
V_{ac}	Actual wind speed

V_{an}	Volume of the Anode
V_{ci}	Cut-in wind speed
V_{co}	Cut-out wind speed
V_{sys}	System voltage at the DC bus
X	Feasible region
α_k	Externality costs of emission type k
δ_i	Cold start-up cost
τ_i	Unit cooling time constant of unit i

Abbreviations

AFC	Alkaline Fuel Cell
AH	Ampere hour
AVR	Automatic Voltage Regulator
CHP	Combined Heat and Power
CI	Compression Ignition
CO ₂	Carbon Oxides
DG	Diesel Generator
DYSC	Dye-Sensitised Solar Cells
FC	Fuel Cell
GA	Genetic Algorithms
GP	General Problem
GPS	Generalized Pattern Search
IGBT	Insulated Gate Bipolar Transistor
MADS	Mesh Adaptive Direct Search
MCFC	Molten Carbonate Fuel Cell
MG	MicroGrid
MO	Multiobjective
MOMADS	Multiobjective Adaptive Direct Search
MOSQP	Multiobjective Sequential Quadratic Programming
MPPT	Maximum Power Point Tracking
MT	Micro Turbine
MUT/MDT	minimum up/down time limits
NOCT	Normal Operating Cell Temperature
NO _x	nitrogen Oxides
O G	Total Optimal Generated Power .
OM	The operating and maintenance costs
P.P	Total Purchased Power.
PAFC	Phosphoric Acid Fuel Cell
PCC	Point of Common Coupling
PEMFC	Proton Exchange Membrane Fuel Cell
PMSG	Permanent Magnet Synchronous Generator
PV	Photovoltaic
PWM	Pulse Width Modulation
S.P	Total Sold Power.
SD	Separation Device
SI	Spark Ignition
SOC	State of Charge
SOFC	Solid Oxide Fuel Cell
SO ₂	Sulfur Oxides

SQP Sequential Quadratic Programming
STC Start-UP Cost
T C Total Operating Cost
T E Total Emissions
UPS Uninterruptible Power Supply
WT Windturbine

List of Figures

1.1	MicroGrid Architecture.	2
1.2	Example of MG on Kytnos Island (PV MORE and MODE projects.)	3
2.1	The transfer function of the actuator model where K_3 is the current drive constant, current $I(s)$ the input and fuel-flow $\Phi(s)$ the output	12
2.2	The Engine Model.	12
2.3	The Block diagram of the Diesel Engine System.	13
2.4	Fuel consumption of DNAC 50 Hz diesel engine.	15
2.5	Operation principle, cathode reactions, and the mobile ion associated with most common fuel cell types.	15
2.6	Fuel cell. principles of operation.	17
2.7	SOFC system dynamic model.	22
2.8	Responses output voltage, output current, real power output due to the power demand input.	23
2.9	Response of pressure difference between hydrogen and oxygen.	23
2.10	Response of Fuel Utilization.	23
2.11	Assumed efficiency curve for 50 kW PEMFC stack based on IFC PC-29. . .	24
2.12	Principle components of micro turbine unit(www.turbec.com).	25
2.13	Outline of a micro turbine generator.	26
2.14	The equivalent circuit.	26
2.15	The micro turbine generator model.	28
2.16	Power command to the microturbine system.	28
2.17	The output power of the microturbine P.	29
2.18	Shaft speed of the microturbine model ω . The red curve gives a detailed curve between 50-100 s.	29
2.19	DC link Voltage of the microturbine model V_{DC}	30
2.20	Rotor Speed of the microturbine model.	30
2.21	General working principle of wind power generation.	32
2.22	Generating systems used in wind turbines: direct synchronous generator (above) and doubly fed (wound rotor) induction generator (below). . . .	33
2.23	Performance coefficient C_p as a function of the tip speed ratio λ with pitch angle β as a parameter.	35
2.24	Power curve of wind turbine.	37
2.25	Wind Speed.	38
2.26	Generated active power P	38

2.27	Generated reactive power Q .	38
2.28	Pitch Angle.	39
2.29	Rotor Speed.	39
2.30	Generated active power due to different values of wind speed.	39
2.31	Pitch Angle due to different values of wind speed.	40
2.32	Rotor Speed due to different values of wind speed.	40
2.33	Measured sequence of wind speed.	40
2.34	Response of the generated active power due to the measured sequence wind speed input.	41
2.35	Response of the pitch angle due to measured sequence wind speed input.	41
2.36	Response of the rotor speed due to measured sequence wind speed input.	41
2.37	The actual and modeled power curve of AIR403.	42
2.38	Schematic diagram of small PV inverter for grid connected operation.	43
2.39	Equivalent circuit of a PV module.	44
2.40	I-U characteristic for a PV cell at a constant temperature of $25^{\circ}C$	46
2.41	P-U characteristic for a PV cell at a constant temperature of $25^{\circ}C$	47
2.42	I-U characteristic for a PV cell at constant $G= 1000W/m^2$	47
2.43	P-U characteristic for a PV cell at constant $G= 1000W/m^2$	48
2.44	I-U characteristic of PV for some set of G and T	48
3.1	The Optimization Model.	55
3.2	Minimization of the MT, FC, and DG costs.	59
3.3	The input wind speed to the model.	60
3.4	The input temperature data to the model.	61
3.5	The input irradiation data to the model.	61
3.6	Hourly load.	61
3.7	The hourly power curves using SQP scenario 1.	62
3.8	The hourly power curves using MADS scenario 1.	62
3.9	Hourly total cost of the microgrid using 2 different technique scenario 1.	63
3.10	Hourly fuel costs of the microgrid scenario 1.	63
3.11	Hourly emission costs of the microgrid scenario 1.	63
3.12	Hourly OM cost of the microgrid scenario 1.	64
3.13	The hourly power curves using SQP Scenario 2.	65
3.14	The hourly power curves using MADS Scenario 2.	65
3.15	Hourly total cost of the microgrid using 2 different technique Scenario 2.	65
3.16	Effect of sold power tariff on the MG optimal operation Scenario 3.	66
3.17	Effect of sold power tariff on the MG optimal operation Scenario 3.	66
3.18	Effect of sold power tariff on the MG optimal operation Scenario 3.	67
3.19	Effect of sold power tariff on the MG optimal operation Scenario 3.	67
3.20	Sold and purchased power using SQP method and Scenario 3.	67
3.21	Sold and purchased power using MADS method and Scenario 3.	68
3.22	Cost per day using SQP method and Scenario 3.	68
3.23	Cost per day MADS method and Scenario 3.	68
3.24	Effect of purchased power tariff on the MG optimal operation Scenario 3.	69

3.25	Effect of purchased power tariff on the MG optimal operation Scenario 3 .	69
3.26	Effect of purchased power tariffs on the MG optimal operation Scenario 3	70
3.27	Effect of purchased power tariff on the MG optimal operation Scenario 3 .	70
3.28	Sold and purchased power using SQP and MADS methods and Scenario 3.	70
3.29	Total cost per day using SQP, MADS methods and scenario 3.	71
4.1	Optimization algorithm Model.	75
4.2	Implementation of the algorithm flow chart.	78
4.3	Hourly load.	81
4.4	Convergence of the operating cost and emission objective functions using MOSQP and MOMADS Scenario 1.	82
4.5	Trade- off in operating cost and emission using MOSQP Scenario 1.	83
4.6	Trade- off in operating cost and emission using MOMADS Scenario 1.	83
4.7	The hourly power curves generated by different energy resource using MOSQP Scenario 1.	84
4.8	The hourly power curves generated by different energy resource using MOMADS Scenario 1.	84
4.9	Hourly operating cost using the MOSQP and MOMADS Scenario 1.	85
4.10	Hourly emission using the MOSQP and MOMADS Scenario 1.	85
4.11	Convergence of operating cost and emission objective functions using MOSQP and MOMADS Scenario 2.	86
4.12	Power Generation distribution case 1 using MOMADS Scenario 2.	87
4.13	Power Generation distribution case 2 using MOMADS Scenario 2.	87
4.14	Hourly operating cost using the MOSQP and MOMADS Scenario 2.	87
4.15	Hourly emission using the MOSQP and MOMADS Scenario 2.	88
4.16	Trade- off in operating cost and emission using MOSQP Scenario 2.	88
4.17	Trade- off in operating cost and emission using MOMADS Scenario 2.	89
4.18	The hourly power curves generated by different energy resource using MOMADS Scenario 2.	89
4.19	The hourly power curves generated by different energy resource using MOSQP Scenario 2.	90
4.20	Convergence of operating cost and emission objective functions using MOSQP and MOMADS Scenario 3.	91
4.21	Hourly operating cost using the MOSQP and MOMADS Scenario 3.	91
4.22	Hourly emission using the MOSQP and MOMADS Scenario 3.	92
4.23	Trade- off in operating cost and emission using MOSQP at Scenario 3 and for $P = 0.12$ and $S = 0$	92
4.24	Trade- off in operating cost and emission using MOMADS at Scenario 3 and for $P = 0.12$ and $S = 0$	93
4.25	Trade- off in operating cost and emission using MOSQP at Scenario 3 and for $P = 0.16$ and $S = 0.1$	93
4.26	Trade- off in operating cost and emission using MOMADS at Scenario 3 and for $P = 0.16$ and $S = 0.1$	94

4.27	Effect of purchased power tariffs on the MG optimal operation using MOMADS Scenario 3.	95
4.28	Effect of purchased power tariffs on the MG optimal operation using MOSQP Scenario 3.	95
4.29	Power Generation distribution using MOSQP Scenario 3.	96
4.30	Power Generation distribution using MOMADS Scenario 3.	96
5.1	Flow chart of a general form of the genetic algorithm	98
5.2	Crossover procedure	99
5.3	Mutation	99
5.4	Trade- off in operating cost and emission using GA Scenario 1.	101
5.5	The hourly power curves using GA Scenario 1.	102
5.6	Hourly operating cost and emission using MOGA Scenario 1.	102
5.7	Trade- off in operating cost and emission using GA Scenario 2.	103
5.8	The hourly power curves using GA Scenario 2.	103
5.9	Hourly operating cost and emission using MOGA Scenario 2.	104
5.10	Hourly operating cost and emission using MOGA Scenario 3.	104
5.11	Trade- off in operating cost and emission using MOGA Scenario 3 and for $P = 0.12$ and $S = 0$	105
5.12	Trade- off in operating cost and emission using MOGA at Scenario 3 and for $P = 0.16$ and $S = 0.1$	105
5.13	Effect of sold power tariff on the MG optimal operation using MOGA Scenario 3.	106
5.14	Effect of purchased power tariff on the MG optimal operation using MOGA Scenario 3.	106
6.1	Trade- off in operating cost and emission using MOGT Scenario 1.	112
6.2	The hourly power curves using MOGT Scenario 1.	113
6.3	Hourly operating cost and emission using MOGT Scenario 1.	113
6.4	The hourly power curves using MOGT Scenario 2.	114
6.5	Hourly operating cost and emission using MOGT Scenario 2.	114
6.6	Trade- off in operating cost and emission using MOGT Scenario 2.	115
6.7	Hourly operating cost and emission using MOGA Scenario 3.	116
6.8	The hourly power curves using MOGT Scenario 3.	116
6.9	Trade- off in operating cost and emission using MOGT Scenario 3 and for $P = 0.12$ and $S = 0$	117
6.10	Trade- off in operating cost and emission using MOGT at Scenario 3 and for $P = 0.16$ and $S = 0.1$	117
6.11	Effect of purchased power tariffs on the MG optimal operation using MOGT Scenario 3.	118

List of Tables

2.1	Summary of chemical reactions in different types of fuel cell.	16
2.2	Major fuel cell technologies.	16
2.3	Parameters for 80W PHOTOWATT panel PWZ750 at STC.	46
3.1	Externality costs and emission factors for NO _x ,SO ₂ , and CO ₂	58
3.2	Total Optimal Generation and Total Cost of the MG Scenario 1	62
3.3	Total Optimal Generation and Total Cost of the MG Scenario 2	64
3.4	Total Optimal Generation and Total Cost of the MG Scenario 3	71
4.1	The objective functions when optimized individually: Scenario 1	82
4.2	The best selection per day of the power generators of the MG using MO: Scenario 1	84
4.3	The objective functions when optimized individually: Scenario 2	86
4.4	The best selection per day of the power generators of the MG using MO: Scenario 2	88
4.5	The objective functions when optimized individually: Scenario 3	90
4.6	The effect of the Purchased and Sold tariffs on the optimal Generation: Scenario 3	94
4.7	Cost savings and emissions reductions of the MG using multiobjective op- timization: Scenario 3	95
5.1	The objective functions when optimized individually Scenario 1	100
5.2	The best selection per day of the power generators of the MG using MOGA Scenario 1	101
5.3	The The objective functions when optimized individually Scenario 2	102
5.4	The best selection of the power generators of the MG using MOGA Sce- nario 2	103
5.5	The objective functions when optimized individually using MOGA Sce- nario 3	104
5.6	The effect of the Purchased and Sold tariffs on the optimal Generation us- ing MOGA and Scenario 3	106
5.7	Cost savings and emissions reductions of the MG using multiobjective op- timization Scenario 3	107
6.1	The best selection of the power generators of the MG using MOGT: Sce- nario 1	113

6.2	The best selection of the power generators of the MG using MOGT: Scenario 2	114
6.3	The objective functions when optimized individually using MOGT: Scenario 3	115
6.4	The effect of the Purchased and Sold tariffs on the optimal Generation using MOGT: Scenario 3	117
6.5	Cost savings and emissions reductions of the MG using multiobjective optimization: Scenario 3	118

Chapter 1

Introduction

1.1 Introduction

Recent developments in the electric utility industry are encouraging the entry of power generation and energy storage at the distribution level. Together, they are identified as distributed generation units. Several new technologies are being developed and marketed for distributed generation, with capacity ranges from a few kW to 100 MW. The distributed generation includes microturbines, fuel cells, photovoltaic systems, wind energy systems, diesel engines, and gas turbines [1],[2].

1.1.1 Definition of Microgrids

The Microgrid (MG) concept assumes a cluster of loads and microsources operating as a single controllable system that provides both power and heat to its local area. This concept provides a new paradigm for defining the operation of distributed generation [3],[4]. The MG study architecture is shown in Figure 1.1. It consists of a group of radial feeders, which could be part of a distribution system. There is a single point of connection to the utility called point of common coupling (PCC). Feeders 1 and 2 have sensitive loads which should be supplied during the events. The feeders also have the microsources consisting of a photovoltaic (PV), a wind turbine (WT), a fuel cell (FC), a microturbine (MT), a diesel generator (DG), and battery storage. The third feeder has only traditional loads. The static switch (SD) is used to island feeders 1 and 2 from the utility when events happen. The fuel input is needed only for the DG, FC, and MT as the fuel for the WT and PV comes from nature. To serve the load demand, electrical power can be produced either directly by PV, WT, DG, MT, or FC. The diesel oil is a fuel input to a DG, whereas natural gas is a fuel input to fuel processor to produce hydrogen for the FC. The gas is also the input to the MT. The use of DG, or FC or MT with other fuel types can be modeled by changing the system parameters to reflect the change in the fuel consumption characteristics (e.g. fuel heating values, and efficiency of the engines).

Each component of the MG system is separately modeled based on its characteristics and constraints. The characteristics of some equipment like wind turbines and diesel generators are available from the appropriate manufacturers. Each of the local genera-

tion unit has a local controller (LC). This is responsible for local control that corresponds to a conventional controller (ex. automatic voltage regulator (AVR) or Governor) having a network communication function to exchange information between other LCs and the upper central controller to achieve an advanced control. The central controller also plays an important role as a load dispatch control center in bulk power systems, which is in charge of distributed generator operations installed in MG [5].

Furthermore, the central controller is the main interface between the uppergrid and

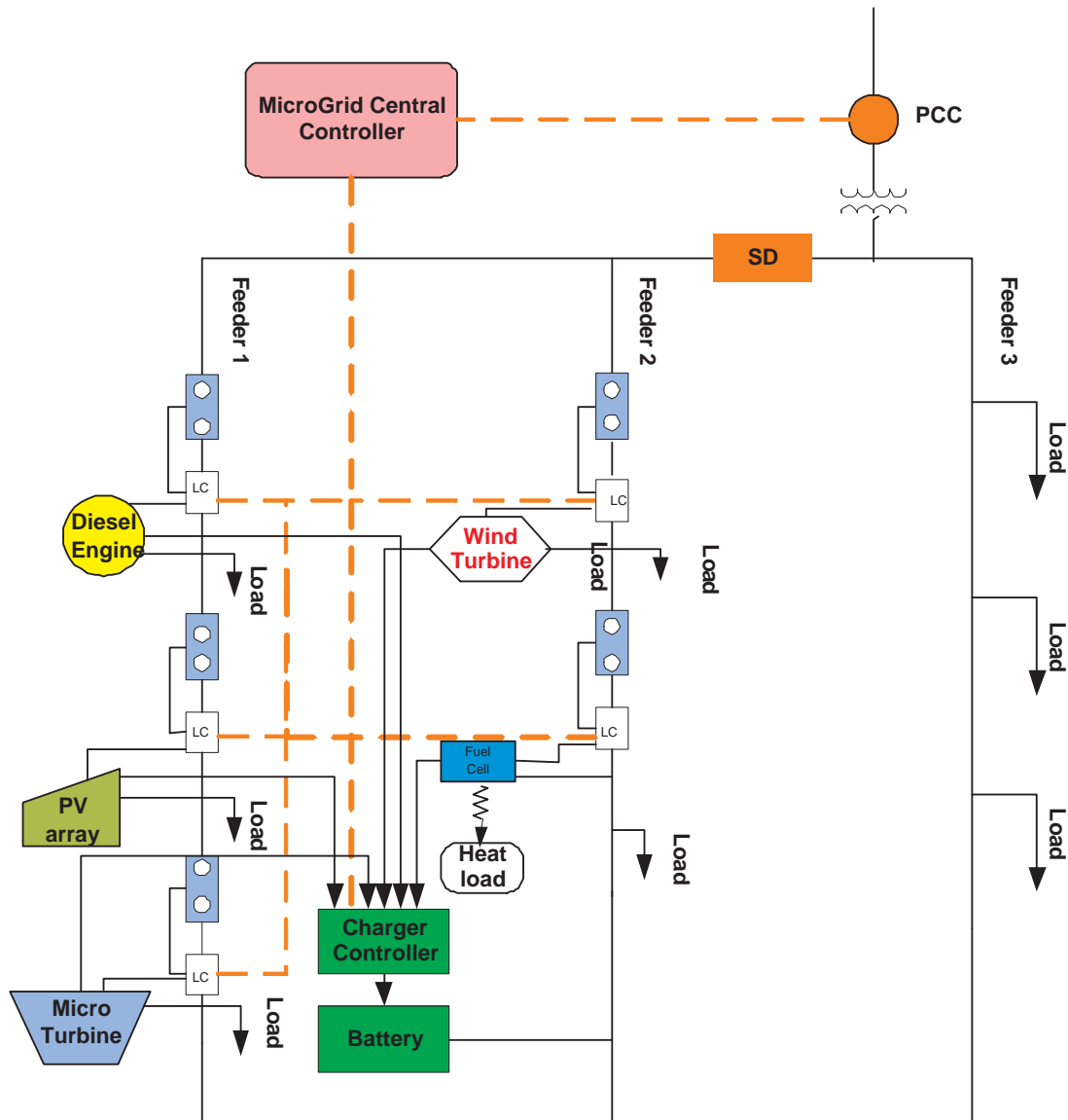


Figure 1.1: MicroGrid Architecture.

the Microgrid. The central controller has the main responsibility for the optimization of the Microgrid operation, or alternatively, it coordinates the actions of the local controllers to produce the optimal outcome.

MG technologies are playing an increasingly important role in the world's energy portfolio. They can be used to meet baseload power, peaking power, backup power, remote

power, power quality, and cooling and heating needs. Customers usually own small-scale, on-site power generators, but they may be owned and operated by a third party. If the distributed generator does not provide 100% of the customer's energy needs at all times, it can be used in conjunction with a distributed energy storage device or a connection with the local grid for backup power. The MG resources support and strengthen the central-station model of electricity generation, transmission, and distribution. The diagram depicted in Figure 1.1 shows how the grid looks after the addition of distributed resources. Although the central generating plant continues to provide most of the power to the grid, the distributed resources meet the peak demands of local distribution feeder lines or major customers. Computerized control systems, typically operating over telephone lines, make it possible to operate the distributed generators as dispatchable resources that generate electricity as needed. Figure 1.2 shows a demonstration system, which has been running successfully on the Greek island of Kythnos since April 2001 [6].

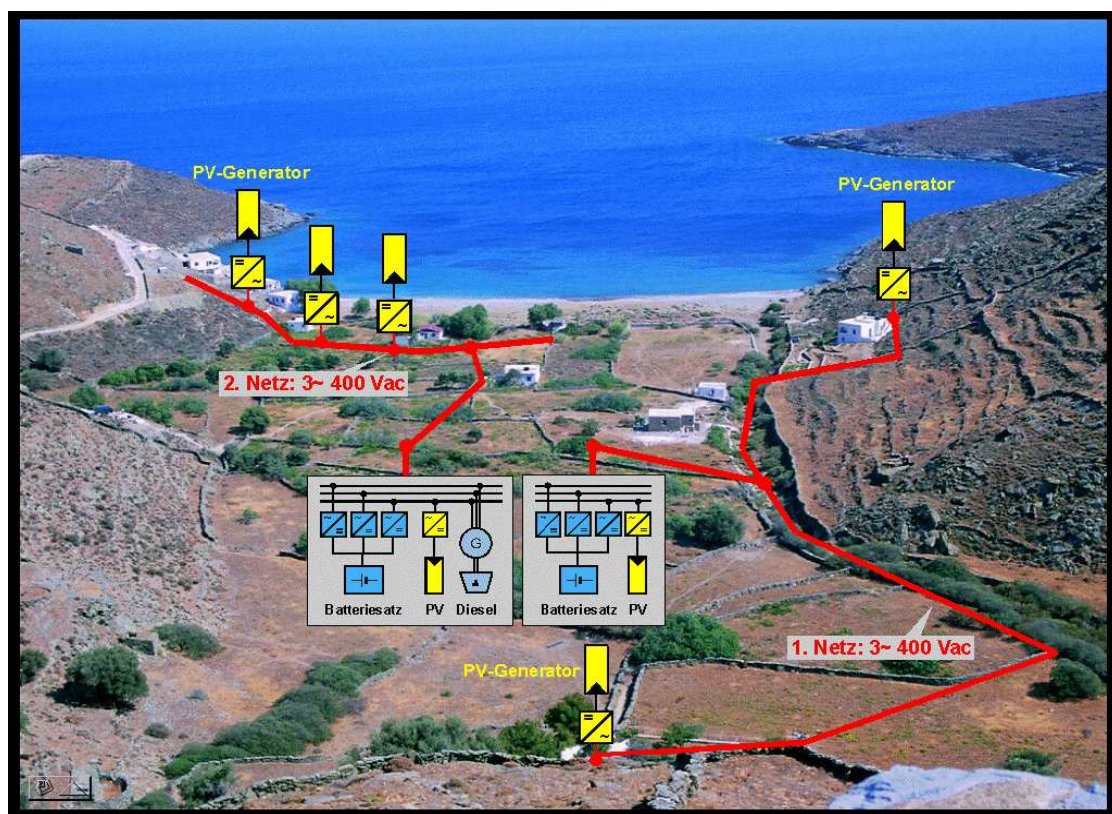


Figure 1.2: Example of MG on Kythnos Island (PV MORE and MODE projects.)

1.1.2 Reasons for Microgrids

The conventional arrangement of a modern large power system offers a number of advantages. Large generating units can be made efficient and operated with only a relatively small number of personnel. The interconnected high voltage transmission network allows the generator reserve requirement to be minimized, the most efficient generating plant to be dispatched at any time, and bulk power to be transported large distances with limited electrical losses. The distribution network can be designed for unidirectional

tional flows of power and sized to accommodate customer loads only. However, over the last few years a number of influences have combined to lead to the increased interest in MG schemes [1] and [7]. The policy drivers encouraging MGs are:

1. Reduction in gaseous emissions (mainly CO₂).
2. Energy efficiency or rational use of energy.
3. Deregulation or competition policy.
4. Diversification of energy sources.
5. National and global power requirements.

Reference [1] listed other reasons but with additional emphasis on commercial considerations such as:

- Availability of modular generating plants.
- Ease of finding sites for smaller generators.
- Short construction times and lower capital costs of smaller plants.
- Generating may be sited closer to load, which may reduce transmission costs.

1.2 Motivation

Currently a lot of research is being undertaken into MGs. Some model architectures have been proposed in the literature such as [3, 4, 5, 8, 9, 10]. Although components of the MGs are fairly well understood, the system as a whole is not. When several sources are connected to form a MG, the system behaviour is unpredictable. This being the case, modelling the system and simulating it, in order to develop an appropriate management system, is the heart of micro-grid research. Nowadays, several research groups around the world are investigating the feasibility and benefits that the MGs may provide. Some problems are encountered including dealing with the unbalanced loads and harmonics associated with the system. This work does not intend to address such problems, rather it is concerned with the modelling of the MG for management.

Modelling is an important component for power system energy management system. A precise model helps the electric utility to make unit commitment decisions and to reduce operating costs and emission level properly. Besides playing a key role in meeting the load demand, it is also essential to the reliability of the MG. The central controller uses the modelling result as a basis of off-line network analysis to determine if the system might be costly and have high emissions. If so, corrective actions should be prepared, such as power sales, power purchases and bringing units on line.

This thesis focuses on the modeling of MGs and discusses new management approaches for reducing the operating costs and emission level. Although the modeling and management techniques developed in this thesis are intended for MGs, with little modifications,

they can be extended to many other larger distributed generation system as well, for example, to capacity ranges up to 100 MW.

1.3 Management of Microgrid

Significant research is currently carried out regarding the operation and control of Microgrids [11], [12]. In this thesis, a novel management system is proposed, considering the following objectives:

- 1) Optimal use of local distributed resources;
- 2) Feeding of local loads;
- 3) Reducing the operating cost;
- 4) Minimizing the emission level.

Important research has been conducted in the area of MGs , which may take many different sizes and forms. Some model architectures have been proposed in the literature such as in [4]. Communication infrastructure operating between the power sources, to solve the optimization problem for the fuel consumption, have been proposed in [13] and a rational method of building MGs optimized for cost and subject to reliability constraints have been presented in [14].

Solving the environmental economic problem in the power generation has received considerable attention. An excellent overview on commonly used environmental economic algorithms can be found in [15]. The environmental economic problems have been effectively solved by the goal programming method [16], the classical technique [17], fuzzy satisfaction- maximizing approach [18], and genetic multiobjective optimization algorithm [19]. However, the computing speed of these solutions is unsatisfactory for online applications [20]. Additionally the optimization problem is treated as a single objective optimization without considering the emissions reduction [13], [21]. In [22], the problem is handled as multiobjective optimization problem without considering the balancing with upper grid, operation and maintenance and start-up costs.

1.4 Optimization

In constrained optimization, the general procedure is to transform the problem into an easier subproblem that can then be solved and used as the basis of an iterative process. The three optimization techniques used in this study are:

1.4.1 Genetic Algorithms

Genetic algorithms are global optimization techniques, which means that they converge to the global solution rather than to a local solution. However, this distinction becomes unclear when working with multi-objective optimization, which usually entails a set of solution points. Mathematically, a single global solution to a multiobjective problem does

not exist unless the utopia point happens to be attainable [23].

Genetic algorithms loosely parallel biological evolution and are based on Darwin's theory of natural selection. The specific mechanics of the algorithms involve the language of microbiology and, in developing new potential solutions, mimic genetic operations. A population represents a group of potential solution points. A generation represents an algorithmic iteration. A chromosome is comparable to a design point, and a gene is comparable to a component of the design vector [23].

1.4.2 Mesh Adaptive Direct Search

MADS is a generalization of the pattern search algorithm. These methods are intended for black box optimization problems. They are derivative-free methods in the sense that they do not compute nor even attempt to evaluate derivatives [24]. Mesh Adaptive Direct Search methods are designed to only use function values and require only a numerical value of the objective; no knowledge about the internal structure of the problem is needed. Mesh Adaptive Direct Search methods can easily and quickly adapt to nonlinear, non-convex non-differentiable, discontinuous, or undermined at some points [24].

1.4.3 Game Theory

A multiobjective design problem may be envisioned as a game in which each objective is a player competing to optimize his standing in a system subject to limit resources. Operation researchers and economists, in studying competitive systems, have developed theories for games which are readily applicable to engineering problems. Theories have been used to describe the interaction of players; the noncooperative theory, based on the concept of Nash equilibrium, and cooperative game theory, based on the concept of Pareto minimum solution [25].

The noncooperative theory of games assumes that each player is looking out for his own interests. Each player selects his own objective and does not care how his choice will affect the objectives of the other player. The players then bargain with each other, exchanging resources, until an equilibrium is reached. The resultant solution, referred to as Nash equilibrium, is a solution where no player may improve his objective by attaining some different amount of resources as long as the other players maintain their resources choices [25].

Cooperative game theory assumes that each player is a member of the team willing to compromise his own objective to improve the solution as a whole. In the cooperative solution, the team would want to allocate the resources with intent that all players should be as optimal as possible- in other words, a Pareto optimal solution. The team then must decide how to distribute the resources such that a gain for one player does not result in unacceptable loss for another player. One method is to distribute the resources such that all players are as far from their worst case as possible [26].

1.5 Objectives and Contributions of the Thesis

The main objective of this thesis is to develop a model and a management methodology that makes for the MG energy production low cost, environmentally friendly and highly efficient power generation. The approach is to first form models for MG components at steady state and study their transient responses when the inputs are changing. Based on these a new optimization power model is constructed. It is intended that the work completed in this thesis will lay the groundwork for further model development. The long term goal is to have a highly sophisticated and complete model of a MG, so as to allow a full understanding of how MGs behave.

This thesis focuses on modelling and management of Microgrids and its contributions can be classified into three main categories as follows:

1.5.1 Modelling of Microgrid

- **Modelling the MG components at steady state and study their transient responses to changing inputs.** Analyzing MG requires suitable dynamic models for all components forming the MG. Since the MG components represent new promising resources of energy generation, the thesis develops models that describe their dynamic behaviour. A simple and flexible model for stability studies and online management purposes of the MG is developed in addition to an exhaustive nonparametric model for detailed analysis of the MG. The MG components which have been studied are the Diesel Engine, the Fuel Cell, the Microturbine, the Wind turbine, and the Photovoltaic Cell.
- **Modelling the Diesel Generator cost from industrial data.** In order to find the mathematical formulation describing the relation between the fuel consumption and the power generated of a diesel generator, the diesel fuel consumption data of a 6-kW diesel generator set (Cummins Power) model DNAC 50 Hz is used to model the fuel cost function.
- **Modelling the Wind Turbine generator from industrial data.** A wind turbine model is obtained from a mathematical relation between the wind speed and the output power. A power curve for a wind turbine is determined from a vender's manual, in order to determine a mathematical relationships between the actual power and wind speed.

1.5.2 Problem Model Formulation

- **A novel optimization model is constructed.** This takes into account the start-up cost, available resources, environmental costs, operation and maintenance cost, purchased and sold power, and constraint requirements. An optimal economic generation schedule is established based on the assumption that the MG will serve the electric power needs of its own customers at minimum cost. A central controller controls the scheduling and dispatching of the MG. Optimization is performed for

each unit first. Therefore, all the generator of the MG behaviors are dependent on each other and their functions are coordinated to meet a single economic objective. The economic problem of a MG is a deterministic optimization problem due to the fact that the consumption fuel rate of each generator unit is used to determine an objective function, which forms the total cost of the generation, together with the constraints.

- **A new multiobjective optimization problem is formulated and solved.** This includes minimization of the total power production cost and minimization of the emission level. In the emission model introduced in [15] and [22], a method is proposed to evaluate the parameters of the model using the data available in [27]. Thus, the emissions per day for the diesel engine, fuel cell, and microturbine are estimated, and the characteristics of each generator will be detached accordingly.

1.5.3 Management of Microgrid

- **Applying Game Theory technique to a multiobjective problem of the MG.** One of the contributions in this thesis is a novel procedure to solve the MG management problem based on Game Theory and multiobjective optimization. Two players are assumed to correspond to the two objectives; one represents the operating cost and the other the emission level. While playing the game, each player will try to improve his own condition (that is, to decrease the value of his own objective function).
- **Applying the Mesh Adaptive Direct Search technique to solve the single objective problem of MG.** The recently developed, efficient mesh adaptive direct search (MADS) algorithm is presented and applied. In this thesis, MADS algorithm is used to optimize the MG operating cost function. In comparison with the previously used optimization methods (SQP), a reduction in \$/Day is obtained even if the model is more complicated.
- **Propose three different Scenarios can be found in the MG.** The scenarios proposed are aimed to reflect the physical characteristics found in the MGs, starting with a MG without a battery storage. In the second scenario a battery storage is added with more constraints. Costs are considered such as start-up cost and a number of on and off time of the generators. In the third scenario balancing with the main grid is addressed with the same constraints as in the second scenario.
- **Applying the Mesh Adaptive Direct Search technique to solve the multiobjective optimization problem of the MG (MOMADS).** MOMADS technique is applied to solve the optimization problem when it becomes multiobjective. The proposed method finds the optimal values taking different objectives into account, including the best operating cost, the best emission level and the best compromise between them, as well as the Pareto optimal set depicting the trade-off between the objectives. However, the MOMADS method requires a significantly longer computing time than with the conventional MOSQP.

1.6 Outline of the Thesis

The work in this thesis is organized as follows. In Chapter 1, an introduction and a background of distributed generator units is presented. The main focus in Chapter 2 is on modelling and simulation of the MG components. The MG under consideration includes DG's, FC's, MT's, WT's, PV's, and a battery storage. Investigation on minimizing the operating costs of a MG using MADS, and its performance are discussed in Chapter 3. The objective of Chapter 4 is to investigate the management of the MG, when it has two objective functions, namely minimizing operating costs and emission level. Two different methods, Multiobjective Mesh Adaptive Direct Search (MOMADS) and Multiobjective Sequential Quadratic Programming (MOSQP) are applied. Chapter 5 deals with solving the same problem as in Chapter 4 using Multiobjective Genetic Algorithm (MOGA). Multiobjective Game Theory (MOGT) is introduced in Chapter 6 and its performance for handling the economical and environmental problems of MG are investigated. Finally, conclusions and future considerations are summarized in Chapter 7.

Chapter 2

System Modelling

2.1 Introduction

This chapter discusses modelling of the MG components. For understanding the MG behaviour, each source is modelled individually and then combined together to form a MG. The components modelled are a diesel generator, a fuel cell, a microturbine, a wind turbine, a photovoltaic array, and a battery storage. Particularly, modelling the MG in a steady-state condition and dynamic analysis of it are important. Each component model is first completed individually. Then the models are combined to form a complete model of a MG. The model described will be used for developing optimal online management techniques of the MG.

2.2 Diesel Generator

Diesel Engines, developed more than 100 years ago, were the first among distribution generator technologies. Both Otto (spark ignition, SI) and Diesel cycle (compression ignition, CI) engines have gained widespread acceptance in almost every sector of the economy. Because of their high efficiency and reliability they are used on many scales, ranging from small units of 1 KW to large several tens of MW power plants. Smaller engines are primarily designed for transportation and can usually be converted to power generation with little modification. Large engines are most frequently designed for power generation, mechanical drives, or marine propulsion. Because of sudden changes in load demands by the consumers, it is important that the diesel prime mover has a fast dynamic response and good capabilities of disturbance rejection [28].

The Diesel Engine model gives a description of the fuel consumption rate as a function of speed and mechanical power at the output of the engine, and is usually modeled by a simple first order model relating the fuel consumption (fuel rack position) to the engine mechanical power [29].

The power outputs of the engine and the generator have to be varied with the changing load in order to meet the consumer demands. The task of the governor is to adjust the fuel flow and then regulate the inputs of the engine and generator, and hence provide the required power to meet the change in the load.

2.2.1 Modelling of Diesel Engine

There are many methods already proposed for modelling a diesel generator [5], [29], [30], [31], [32]. From control system point of view, a diesel engine can be considered as a speed-feedback system. After the operator gives a speed command through adjusting the governor setting, the engine governor which is also working as a sensor, will recognize the difference between the actual speed and the desired speed, and regulates the fuel supply to maintain the engine speed within the range.

The model of the fuel actuator system is usually represented as a first order phase-lag network, which is characterized by gain K_2 and time constant τ_2 . Figure 2.1 shows the transfer function (2.1) of the actuator, where K_3 is current driver constant. The output of the actuator is the fuel-flow $\Phi(s)$ and the input current is $I(s)$.

$$\Phi(s) = \frac{K_3 K_2}{(1 + \tau_2 s)} I(s) \quad (2.1)$$

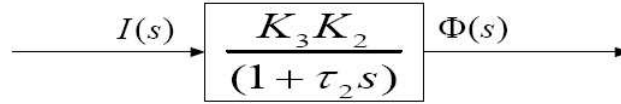


Figure 2.1: The transfer function of the actuator model where K_3 is the current drive constant, current $I(s)$ the input and fuel-flow $\Phi(s)$ the output .

Fuel Flow $\Phi(s)$ is then converted into mechanical torque $T(s)$ after a pure time delay τ_1 and engine torque constant K_1 . This is represented by the transfer function model of equation (2.2) and shown in Figure 2.2.

$$T(s) = \Phi(s) K_1 e^{-\tau_1 s} \quad (2.2)$$

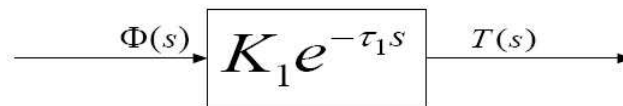


Figure 2.2: The Engine Model.

The governor can be defined as a mechanical or electromechanical device for automatically controlling the speed of an engine by relating the intake of the fuel. Several types of governors exist such as mechanical-hydraulic, direct mechanical, electro-hydraulic, electronic, and microprocessor based [29].

The flywheel represents the complex dynamic effects of the engine inertia, the angular speed of a flywheel ω_w , the viscous friction coefficient ρ , and the loaded alternator. Its model is assumed to have an integrator with flywheel acceleration constant J which serves to filter out a large proportion of the disturbance and noise effects. The noise itself is an inherent property of all internal combustion engines. Reference [30] proposes an integrator to be added between the reference signal r and the engine actuator. It is necessary to eliminate the speed droop in the steady-state operation by raising the order of the whole system as shown in Figure 2.3, where the overall transfer function model of

the diesel engine is presented.

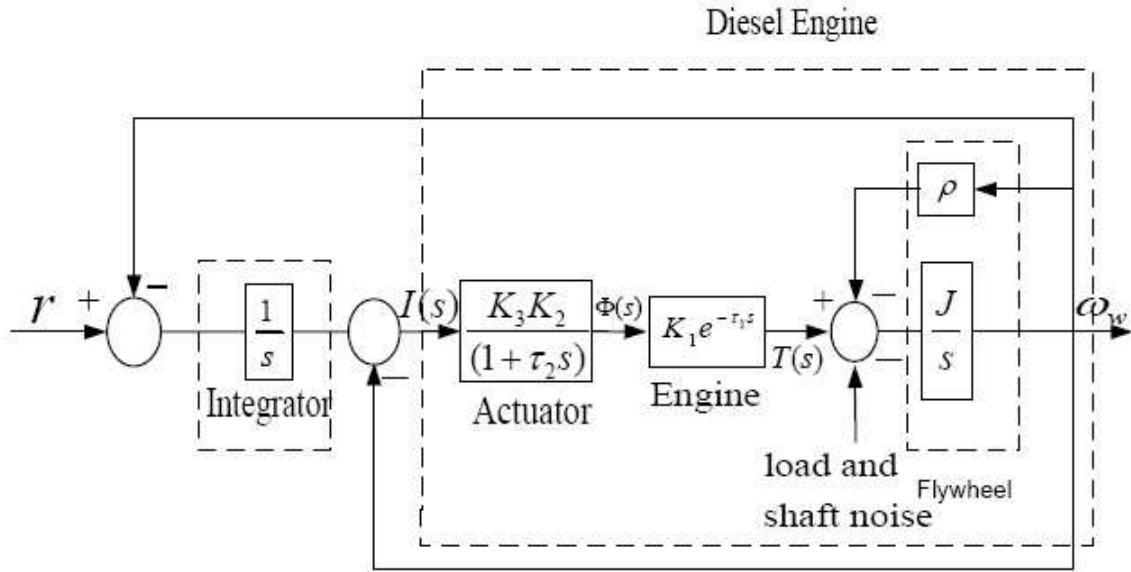


Figure 2.3: The Block diagram of the Diesel Engine System.

The values of K_2 and K_3 can be considered to be constant for a particular engine setup. Gain K_3 is a factor that determines the amount of the mechanical torque obtained per unit of fuel flow. It depends on the operating point of the prime mover. Time constant τ_2 is dependent on the temperature of the oil flowing into the actuator. Both K_2 and τ_2 are variables, but the variation is negligible in a small time interval, [30].

As seen from Figure 2.2 and from references such as [30], [32], [33] and [34], the engine combustion system is commonly represented by the engine torque constant multiplied by a time delay. In a real system, the dead time is mainly comprised of three components:

1. The time from the actuator signal change until fuel is injected to any cylinder. This is called "power stroke delay".
2. The time for the fuel to burn in a cylinder and to produce a torque output, which is similar to the characteristic "combustion delay".
3. The time for a new torque level to produce a sufficient number of cylinders assignable to the prime-mover as a whole. This is an effect of the multi-cylinder nature of the prime-mover.

2.2.2 System Description

From Figure 2.3, the transfer function of the actuator-engine system to be considered is:

$$G(s) = \frac{T(s)}{I(s)} = \frac{K_0}{(1 + \tau_2 s)} e^{-\tau_1 s} \quad (2.3)$$

where the actuator time constant is τ_2 , engine time delay τ_1 , and the process gain $K_0 = K_1 K_2 K_3$. The parameters are usually unknown or time varying.

First order Pade approximation for the time delay term yields [35]:

$$e^{-\tau_1 s} \approx \frac{1 - \tau_1 s/2}{1 + \tau_1 s/2} \quad (2.4)$$

The following simplified transfer function is now obtained from (2.3):

$$G'(s) = \frac{K_0}{(1 + \tau_2 s)} \frac{1 - \tau_1 s/2}{1 + \tau_1 s/2} \quad (2.5)$$

2.2.3 Diesel Generator Costs

Diesel engines are the most common type of MG technology in use today. The traditional roles of diesel generation have been the provision of stand-by power and peak shaving. The fuel cost of a power system can be expressed mainly as a function of its real power output and can be modeled by a quadratic polynomial [36]. The total diesel fuel consumption rate L/h $F_{DG,i}$ can be expressed as:

$$F_{DG,i} = \sum_{i=1}^N a_i + b_i P_{DG,i} + c_i P_{DG,i}^2 \quad (2.6)$$

where N is the number of generators, a_i , b_i , and c_i are the coefficients of the particular generator, $P_{DG,i}$ $i = 1, 2, \dots, N$ is the output power of the diesel generator i in (kW) assumed to be known. The generator cost function is obtained from data points taken during "heat run" tests, when input and output are measured as the unit is slowly varied through its operation region [37].

Typically, the constants a_i , b_i , and c_i are given by the manufacturer. For example, diesel fuel consumption data of a 6-kW diesel generator set (Cummins Power) model DNAC 50 Hz [38] is available in L/h at 1/4, 1/2, 3/4 and full loads. From the data sheet the parameters in (2.6) are: $a_1 = 0.4333$, $b_1 = 0.2333$, and $c_1 = 0.0074$. Figure 2.4 shows the fuel consumption as function of power of the DNAC 50 Hz diesel engine.

2.3 Fuel Cell

Fuel cells generate power through the electrochemical reaction between hydrogen and oxygen. The conversion is highly efficient and leaves only water and heat as by-products, which is the main motivation for the increasing interest in the technology [39]. Fuel Cells offer lower emission and higher efficiency than Diesel Engines but are likely to be too expensive for many applications. The first fuel cell unit was discovered and developed by Sir William Grove 1842 [40] with the use of four primitive cells utilizing hydrogen and oxygen. However, fuel cells were not practically used until 1960's when NASA demonstrated a potential fuel cell application. After such demonstrations, commercial companies became interested in this technology because of its power quality, high efficiency,

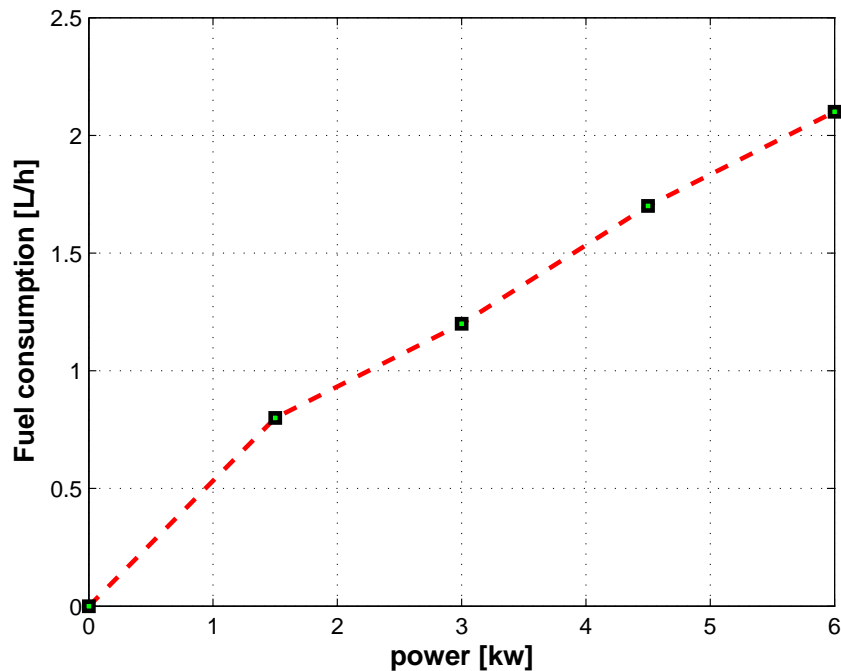


Figure 2.4: Fuel consumption of DNAC 50 Hz diesel engine.

modularity, and environmental benefits.

A fuel cell is an electrochemical energy conversion system, where chemical energy is converted directly into electrical energy and heat. The basic structure of fuel cells consists of a pair of electrodes and an electrolyte. The fuel which is usually hydrogen, is supplied to the anode where the fuel is oxidized, yielding electrons, which move through the external circuit. At the cathode, the oxidant is reduced, consuming electrons from the external circuit. Ions move through the electrolyte to balance the flow of electrons through the external circuit. The anode-cathode reactions and the composition and direction of flow of the mobile ion vary with the type of fuel cell. Figure 2.5 explains the operation principle, cathode reactions, and the mobile ion associated with most common fuel cell types. The

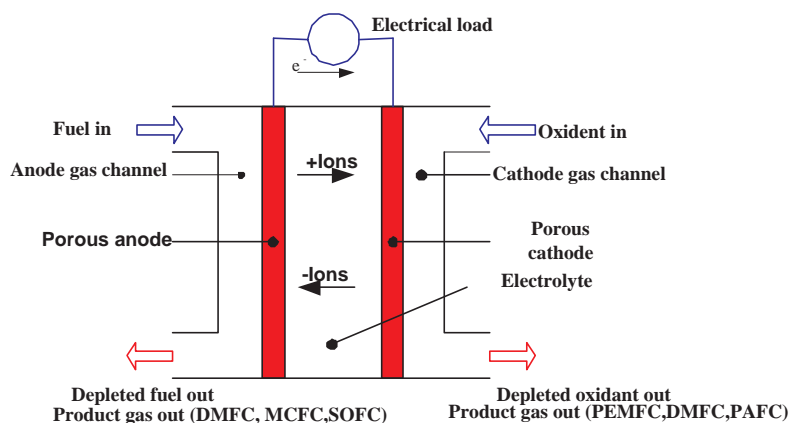


Figure 2.5: Operation principle, cathode reactions, and the mobile ion associated with most common fuel cell types.

reactions of Alkaline Fuel Cell (AFC), Proton Exchange Membrane Fuel Cell (PEMFC), Phosphoric Acid Fuel Cell (PAFC), Molten Carbonate Fuel Cell (MCFC) and Solid Oxide Fuel Cell (SOFC) are summarized in Table 2.1 [39].

Table 2.1: Summary of chemical reactions in different types of fuel cell.

Fuel cell type	Anode reaction	Mobile Ion	Cathode reaction
PEMFC and PAFC	$H_2 \rightarrow 2H^+ + 2e^-$	H^+	$1/2O_2 + 2H^+ + 2e^- \rightarrow H_2O$
AFC	$H_2 \rightarrow 2H^+ + 2e^-$	OH^-	$1/2O_2 + H_2O + 2e^- \rightarrow 2OH^-$
MCFC	$H_2O + CO_3^{2-} \rightarrow H_2O + CO_2 + 2e^-$	CO_3^{2-}	$1/2O_2 + CO_2 + 2e^- \rightarrow CO_3^{2-}$
SOFC	$H_2 + O^{2-} \rightarrow H_2O + 2e^-$	O^{2-}	$1/2O_2 + 2e^- \rightarrow O^{2-}$

where

CO_2 : - carbon dioxide e^- : - electron H_2O :- water CO_3^{2-} : - carbonate ion H_2 : - hydrogen
 OH^- - H^+ :- hydroxy ion H^+ : - hydrogen ion O_2 - oxygen O^{2-} : - oxygen ion

2.3.1 Characteristics

There are four major fuel cell technologies with somewhat different characteristics. The main apparent difference is the electrolyte, which also has far reaching effects on the design and operating characteristics of the fuel cell. In Table 2.2. those four technologies are listed with some key characteristics [41] and [40].

Table 2.2: Major fuel cell technologies.

	PEMFC (PEFC)	PAFC	MCFC	SOFC
Electrolyte	Proton Exchange Membrane	Phosphoric Acid	Molten Carbonate	Solid Oxide
Operating temperature ($^{\circ}C$)	80	200	650	800-1000
Electric efficiency based on natural gas*(%)	30-35	35-40	45-55	45-55

*With hydrogen as fuel the electric efficiency is the same or even higher for low temperature fuel cells, as this is not a Carnot process. The reason for the higher efficiency with higher temperature for natural gas (or any reformed fuel) lies primarily in that fuel processing can be thermally integrated with the fuel cell and to a lesser extent to lower internal electric resistances.

All fuel cells generate a direct current, the voltage depending on cell voltage and the number of cells in series. Furthermore, the voltage varies with the load and also to some extent with time as the fuel cell stack ages. To obtain AC current, the equipment should have power-conditioning equipment to handle DC to AC conversion and current, voltage, and frequency control. Apart from supplying power to the external point of supply,

the fuel cell also has to cover some internal power needs, e.g. pumps, fans, and control system.

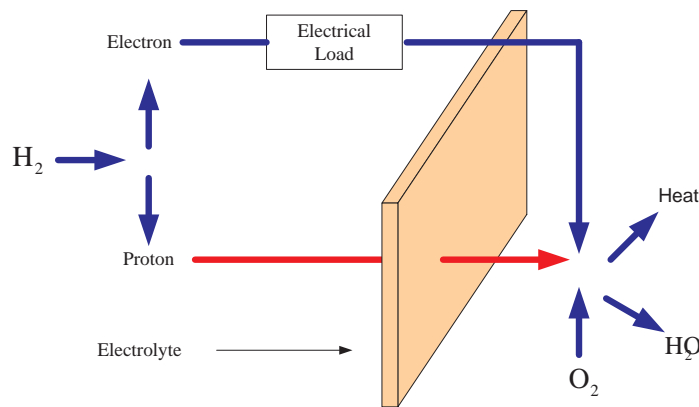
2.3.2 Fuel Cell Workings

The workings of the fuel cells are based on fundamental electrochemical principles [39]. The reaction of hydrogen gas (H_2) and oxygen gas (O_2), to form water, is the form of reaction in the process as presented in [40]:



Fuel cells have an electrolyte between two electrodes. The process occurs naturally and is caused by the fact that the charged particles migrate towards regions of lower electrochemical energy.

The charged particles of hydrogen and oxygen migrate towards each other and connect together since the final product has a lower electrochemical energy [40]. It is essential to separate electrons from protons and to regulate the movement of the electrons. This can be accomplished by separating the hydrogen and oxygen by an electrolyte, which completely insulates electrons and allows protons from the hydrogen atoms to move through. An external path is formed from electrons using an electrical load to generate useful electrical energy [40] as shown in Figure 2.6.



Fuel Cell: How it works

Figure 2.6: Fuel cell. principles of operation.

2.3.3 Modelling of SOFC

Solid Oxide Fuel Cells (SOFC) are particularly attractive because they are the most efficient in terms of fuel input to electricity output. The technology is best applicable in the MG. The high operating temperature produces heat suited well to cogeneration applications. SOFC does not contain noble metals and does not utilize liquid electrolytes which can cause problems and be expensive [42].

The stack model is based on the following assumptions:

1. The gases are ideal.
2. The stack is fed with hydrogen and air. If natural gas instead of hydrogen is used as fuel, the dynamics of the fuel processor must be included in the model, upstream of the hydrogen inlet as a first order transfer function [41]. The transfer function gain should reflect the changes in composition occurring during the process. The effect of the fuel processor in the model will be tested in the future.
3. The channels that transport gases along the electrodes have a fixed volume, but their lengths are small, so that it is only necessary to define one single pressure value in their interior.
4. The exhaust of each channel is via a single orifice. The ratio of pressures between the interior and exterior of the channel is large enough to consider that the orifice is choked.
5. The temperature is stable at all times.
6. The only source of losses is ohmic, as the working conditions of interest are not close to the upper and lower extremes of current.
7. The Nernst's equation can be applied.

The change in concentration of each species that appears in the SOFC chemical reactions can be written generally in terms of input and output flows into a control volume as well as net generation due to the material balance equation:

$$\left(\frac{P_r V_o}{R_{gass} T}\right) \dot{x} = N_i^{in} - N_i^0 + N_i^r \quad (2.8)$$

where V_o is the cell volume, N_i^{in} , N_i^0 are the flow rates (mole/s) of the i th reactant at the cell input and output (exit), respectively, N_i^r is the reaction rate (mole/s) of the i th reactant. P_r is the cell pressure (atm), T is the cell temperature in $^{\circ}K$, and R_{gass} is the gas constant (8.31 J/mole $^{\circ}K$).

2.3.4 Characterization of the exhaust of the channels

According to [43], an orifice that can be considered choked, when fed with a mixture of gases of average molar mass M [kg/kmol] and similar specific heat ratios, at a constant temperature, assumes the following form:

$$\frac{W}{P_{ru}} = K \sqrt{M} \quad (2.9)$$

where, W is the mass flow [kg/s], K is the valve constant, mainly depending on the area of the orifice $\left[\frac{\sqrt{kmol.Kg}}{atm.s}\right]$, and P_{ru} is the pressure upstream (inside the channel) [atm].

For the anode, the concept of fuel utilization U_f can be introduced, as the ratio between the fuel flow that reacts and the fuel flow injected to the stack. U_f is also a way to express the water molar fraction at the exhaust. According to this definition, equation (2.9) can be written as:

$$\frac{W_{an}}{P_{an}} = K_{an} \sqrt{(1 - U_f)M_{H_2} + U_f M_{H_2O}} \quad (2.10)$$

where W_{an} is the mass flow through the anode valve [kg/s], K_{an} is the anode valve constant, $\left[\frac{\sqrt{\text{kmol.Kg}}}{\text{atm.s}}\right]$, M_{H_2} , M_{H_2O} are the molecular masses of hydrogen and water, respectively [kg/kmol], and P_{an} is the pressure inside the anode channel [atm].

Assuming that the molar flow of any gas through the valve is proportional to its partial pressure inside the channel, then according to [43]:

$$\frac{q_{H_2}}{P_{H_2}} = \frac{K_{an}}{\sqrt{M_{H_2}}} = K_{H_2} \quad (2.11)$$

$$\frac{q_{H_2O}}{P_{H_2O}} = \frac{K_{an}}{\sqrt{M_{H_2O}}} = K_{H_2O} \quad (2.12)$$

where q_{H_2O} and q_{H_2} are the molar flows of water and hydrogen, respectively, through the anode valve [kmol/s]. P_{H_2O} and P_{H_2} are the partial pressures of water and hydrogen, respectively [atm]. K_{H_2O} and K_{H_2} are the valve molar constants for water and hydrogen, respectively $\left[\frac{\text{kmol}}{\text{s.atm}}\right]$.

Reference [43] introduces the following expression:

$$\frac{W}{P_{an}} = K_{an} \cdot \left[(1 - U_f) \sqrt{M_{H_2}} + U_f \sqrt{M_{H_2O}} \right] \quad (2.13)$$

Comparison of (2.10) and (2.13) indicates that for $U_f > 70\%$ the error is less than 7%. It is possible to redefine slightly (2.11) and (2.12) so that the percentage error is even lower. The same study for the cathode shows that the error in that valve is even lower, because of the similar molecular masses of oxygen and nitrogen.

2.3.5 Calculation of the partial pressures

Every individual gas will be considered separately, and the perfect gas equation will be applied to it. We will take the hydrogen as an example:

$$P_{H_2} V_{an} = n_{H_2} R_{gass} T \quad (2.14)$$

where V_{an} is the volume of the anode, n_{H_2} is the number of hydrogen moles in the anode channel, R_{gass} is the universal gas constant $\left[\frac{\text{L.atm}}{\text{kmol.K}}\right]$, T is the absolute temperature [K].

By isolating the pressure and taking the derivative of the previous equation, the rate of

change of the partial pressures of hydrogen is in the form:

$$\frac{d}{dt}P_{H_2} = \frac{R_{gass}T}{V_{an}}q_{H_2} \quad (2.15)$$

where, q_{H_2} is the time derivative of n_{H_2} , and represents the hydrogen molar flow q_{H_2} [kmol/s].

There are three relevant contributions to the hydrogen molar flow q_{H_2} : input flow $q_{H_2}^{in}$, the flow $q_{H_2}^r$ that takes part in the reaction and output flow $q_{H_2}^{out}$ [43], [44]. Therefore (2.15) can be expressed as:

$$\frac{d}{dt}P_{H_2} = \frac{R_{gass}T}{V_{an}}(q_{H_2}^{in} - q_{H_2}^{out} - q_{H_2}^r) \quad (2.16)$$

The molar flow of hydrogen $q_{H_2}^r$ that reacts can be calculated according to the basic electrochemical relationship as:

$$q_{H_2}^r = \frac{N_0 I^r}{2F} = 2K_r I^r \quad (2.17)$$

where N_0 is a number of cells connected in series in the stack, F is the Faraday's constant [C/kmol], I^r is the stack current [A] (note that r is a superscript, not power), and K_r is a constant defined for modelling purposes [$\frac{kmol}{s.A}$].

Substituting equation (2.17) into (2.16):

$$\frac{d}{dt}P_{H_2} = \frac{R_{gass}T}{V_{an}}(q_{H_2}^{in} - q_{H_2}^{out} - 2K_r I^r) \quad (2.18)$$

Substituting the output flow of equation (2.11) into (2.18), taking Laplace transform in both sides, and solving for the hydrogen partial pressure results in:

$$sP_{H_2} = \frac{R_{gass}T}{V_{an}}(q_{H_2}^{in} - K_{H_2}P_{H_2} - 2K_r I^r) \quad (2.19)$$

where all the variables are in s-domain. After some algebraic manipulation in (2.19)

$$P_{H_2} = \frac{1/K_{H_2}}{1 + s\tau_{H_2}}(q_{H_2}^{in} - 2K_r I^r) \quad (2.20)$$

where τ_{H_2} , expressed in seconds, is the time constant of the system associated with the hydrogen flow. It is a function of temperature and has the form:

$$\tau_{H_2} = \frac{V_{an}}{K_{H_2}R_{gass}T} \quad (2.21)$$

For calculating the stack voltage, Nernst's equation and Ohm's law (to consider ohmic losses) are applied. The stack output voltage V^r can be represented by the following

expression:

$$V^r = N_0 \left(E_0 + \frac{R_{gass}T}{2F} \left[\ln \frac{P_{H_2} P_{O_2}^{0.5}}{P_{H_2O}} \right] \right) - r_{loss} I^r \quad (2.22)$$

where E_0 is the voltage associated with the reaction free energy [V]. R_{gass} is the gas constant, but care should be taken with the system unit [$\frac{J}{kmol.K}$] [43]. r_{loss} describes the ohmic losses of the stack [Ω].

The above equations are provided by [43] from the basic SOFC power section dynamic model used for performance analysis during normal operation. In [45], the SOFC power generation is modelled by adding the control strategy of the fuel cell system, models of fuel processor, and the power section.

Based on [43] and the above discussions, the dynamic model of the SOFC system which is proposed in [45] is summarized in (2.23)-(2.27). The block diagram of the system is given in Figure 2.7.

$$\begin{aligned} \frac{dI^r}{dt} &= \frac{1}{T_e} [-I^r + I_{ref}] \\ \frac{dq_{H_2}^{in}}{dt} &= \frac{1}{T_f} \left[-q_{H_2}^{in} + \frac{2K_r}{U_{opt}} I^r \right] \\ \frac{dP_{H_2}}{dt} &= \frac{1}{\tau_{H_2}} \left[-P_{H_2} + \frac{1}{K_{H_2}} [q_{H_2}^{in} - 2K_r I^r] \right] \\ \frac{dP_{H_2O}}{dt} &= \frac{1}{\tau_{H_2O}} \left[-P_{H_2O} + \frac{2K_r}{K_{H_2O}} I^r \right] \\ \frac{dP_{O_2}}{dt} &= \frac{1}{\tau_{O_2}} \left[-P_{O_2} + \frac{1}{K_{O_2}} \left[\frac{1}{r_{HO}} q_{H_2}^{in} - K_r I^r \right] \right] \end{aligned} \quad (2.23)$$

$$I_{ref} = \begin{cases} q_{H_2}^{in} \frac{U_{max}}{2K_r}, & \text{if } \tilde{I} > q_{H_2}^{in} \frac{U_{max}}{2K_r} \\ q_{H_2}^{in} \frac{U_{min}}{2K_r}, & \text{if } \tilde{I} < q_{H_2}^{in} \frac{U_{min}}{2K_r} \\ \tilde{I} = P_{ref}/V^{in}, & \text{otherwise} \end{cases} \quad (2.24)$$

$$\tilde{I} = \frac{1}{V_{in}} (P_{ref} - \Delta P) \quad (2.25)$$

$$V^r = N_0 \left(E_0 + \frac{R_{gass}T}{2F} \left[\ln \frac{P_{H_2} P_{O_2}^{0.5}}{P_{H_2O}} \right] \right) - r I^r \quad (2.26)$$

The active (DC) power produced by the fuel cell is then given by the following relation:

$$P_e = V^r I^r \quad (2.27)$$

where I^r is the fuel cell stack current; V^r is the DC voltage across the stack of the fuel cells governed by the Nernst equation, $q_{H_2}^{in}$ stands for the hydrogen input flow; and P_{H_2} , P_{O_2} , P_{H_2O} denote the partial pressures of hydrogen, oxygen, and water, respectively. The time constants T_e , T_f , τ_{H_2} , τ_{H_2O} , τ_{O_2} , designate the electrical response time of the fuel cell, fuel processor response time, response times of hydrogen, water, and oxygen flows, respectively. Constants K_{H_2} , K_{H_2O} , and K_{O_2} , denote the valve molar constants for hydrogen, water, and oxygen. The auxiliary constants U_{opt} , U_{max} , and U_{min} stand for the optimal, maximum, and minimum fuel utilization, respectively. Finally, $K_r = N_0/(4F)$.

The numerical values of the aforementioned constants can be found in [43], [45] and appendix B.

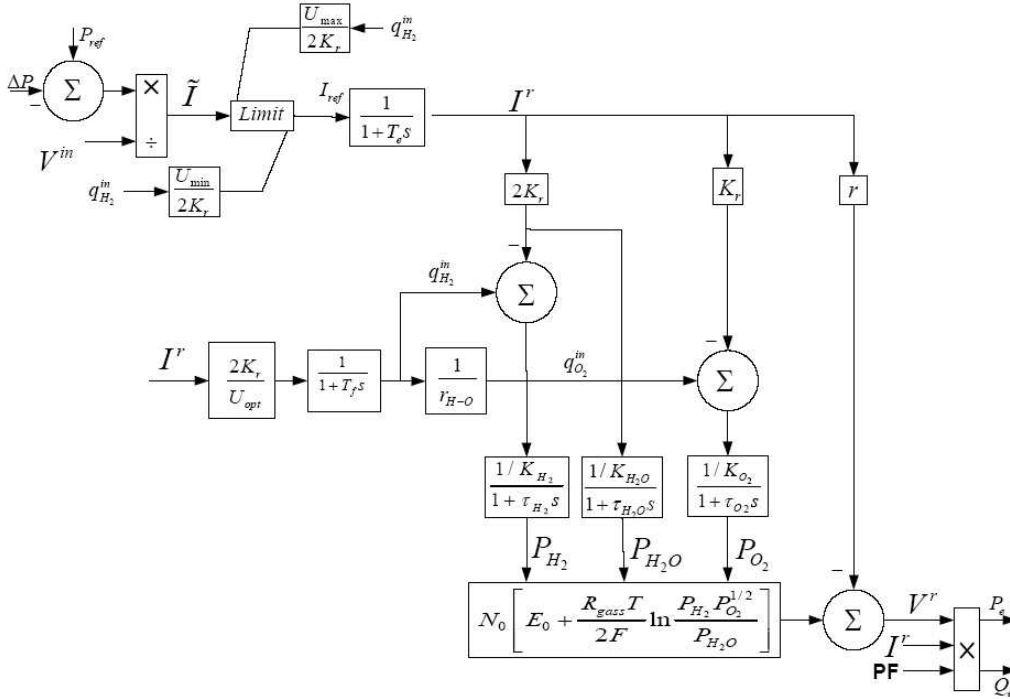


Figure 2.7: SOFC system dynamic model.

2.3.6 Simulation Results

In this work, it is assumed that the SOFC fuel system is a stand-alone system and it is operating with a constant rated voltage 1.0 p.u. and power demand 0.7 p.u. The other parameters are the same as in [45]. Figure 2.8 shows a dynamic step response of a SOFC fuel cell system, where the output power started to increase after 2 to 3 seconds. The step increase of the demand power is related to the fast electrical response of the fuel cell. After that, the output power increased slowly until it reached the demand power. This is due to the slow chemical response time of the fuel processor.

Figure 2.9 illustrates the response of the fuel cell pressure difference between hydrogen and oxygen. This difference increases to the peak value of 3.5 kPa, which is less than the maximum safety pressure difference 8 kPa. It can return to the normal operating pressure difference value around 0 kPa.

In Figure 2.10 the fuel utilization response is presented. Due to the increase in the power demand, the fuel utilization increases to the maximum fuel utilization U_{max} in about 5 s. After staying at U_{max} for about 29 s, it decreases to optimal fuel utilization U_{opt} . The fuel is decreased to its value before the increase in power because of slow chemical reaction of the fuel cell.

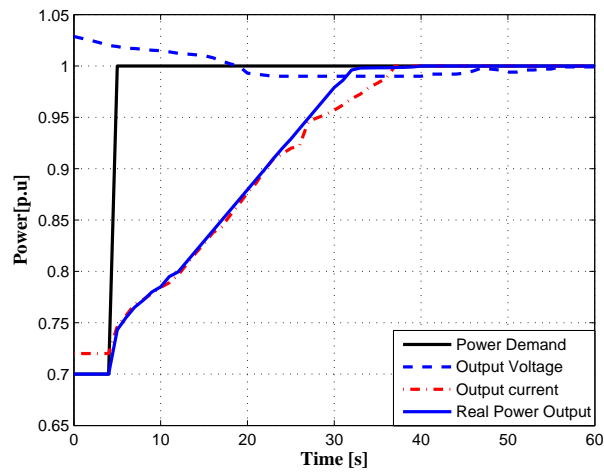


Figure 2.8: Responses output voltage, output current, real power output due to the power demand input.

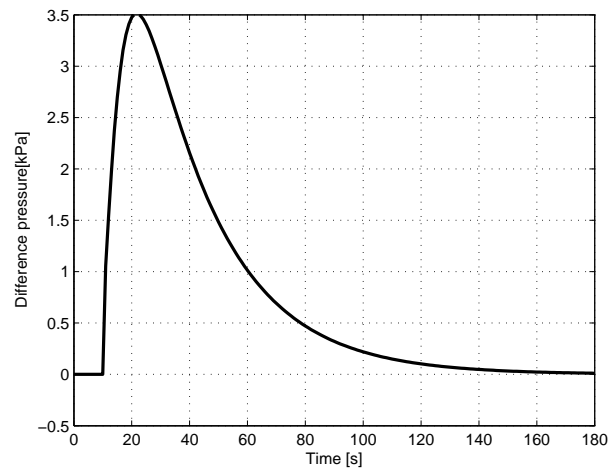


Figure 2.9: Response of pressure difference between hydrogen and oxygen.

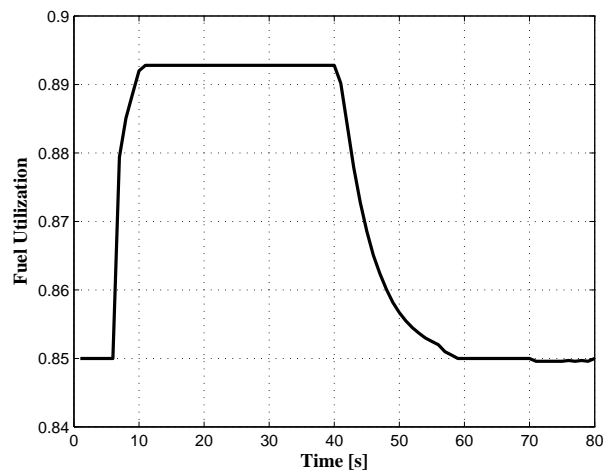


Figure 2.10: Response of Fuel Utilization.

2.3.7 Fuel Cost of Fuel Cell

Fuel cells operate at electrical efficiencies around 40 to 60 percent lower than the heating value (LHV) of the consumed fuel, and up to 85 percent in CHP applications. The fuel cell's efficiency is independent of its capacity and these units may be combined into "stacks" to increase the power output.

The efficiency of the FC depends on the operating point. It refers to the ratio of the stack output power to the input energy content in the natural gas. It is normally calculated as the ratio of the actual operating voltage of a single cell to the reversible potential (1.482V) [46]. The overall unit efficiency is the efficiency of the entire system including auxiliary devices. Figure 2.11 shows typical efficiency curves of the Protone Exchange Membrane (PEM) fuel cell including the cell and overall efficiencies [46] and [47].

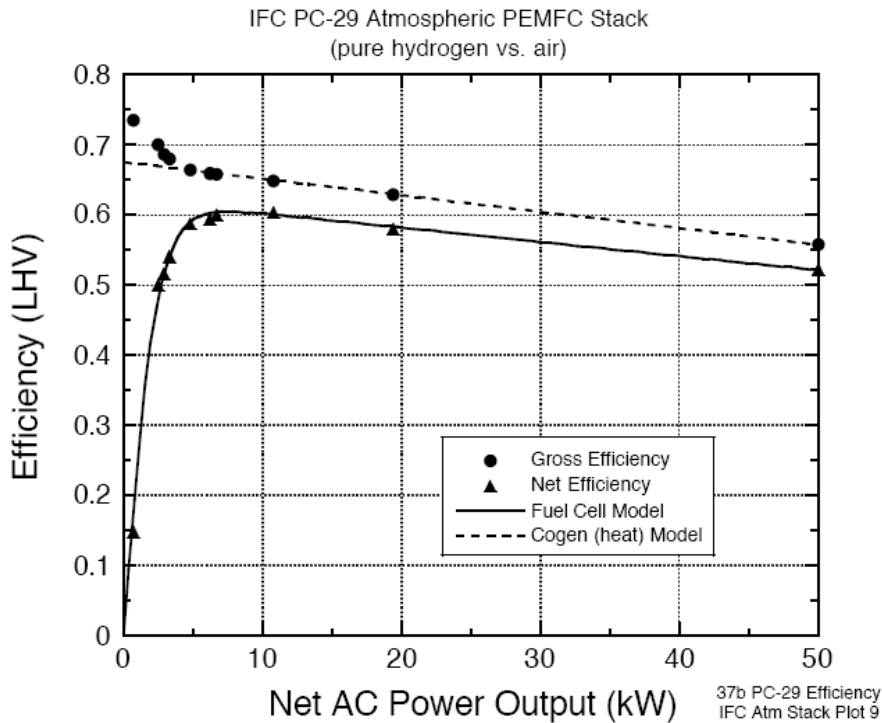


Figure 2.11: Assumed efficiency curve for 50 kW PEMFC stack based on IFC PC-29.

Furthermore, the efficiency of any fuel cell is the ratio between the electrical power output and the fuel input, both of which must be in the same units (W) [46], [21]:

The fuel cost for the fuel cell is calculated as follows:

$$C_{FC} = C_{nl} \sum_J \frac{P_J}{\eta_J} \quad (2.28)$$

where

C_{nl} is the natural gas price to supply the fuel cell,

P_J is the net electrical power produced at interval J ,

η_J is the cell efficiency at interval J .

The power required for auxiliary devices is almost constant regardless of the supplied

power. Therefore, it is assumed as 5% of the unit maximum capacity [21]. To model the technical performance of PEM fuel cell, a typical efficiency curve is used to develop the cell efficiency as a function of the electrical power and used in equation (2.28) [21].

2.4 Microturbines

Microturbines (MTs) are small high-speed gas turbines powered generators ranging in size from 25 to 500kW [48]. The operation principle of the MTs follows the same principles of conventional gas turbine depending on Brayton (constant pressure) cycle [48], [49]. Small gas turbine engines were initially developed by Alison in the 1960s for ground transportation [49]. A microturbine provides input mechanical energy for the MT generator system, which is converted by the generator to electrical energy. The generator nominal frequency is in the range of 1.4-4 kHz. This frequency is transformed to the desired power frequency of 50/60 Hz by a converter. The electrical energy, passing through the transformer, is delivered to the distribution system and the local load. The transformer boosts the converter output voltage up to the voltage level of the distribution system. The components of the MT generator system are described in detail in the following subsections [50].

2.4.1 Construction of Microturbines

The components of a MT are shown in Figure 2.12. The main components include a gas turbine and recuperator, electrical system, an exhaust gas heat exchanger, supervision and control system, and a gas compressor. In [51] the basics of how microturbine works is described. The steps are as follows: first fresh air is drawn into to the compressor. The compressor increases the pressure of the fresh air depending on its size and construction. Then, the high-pressure air and fuel are mixed and burnt in the combustion chamber at a constant pressure. The very hot flue gas enters the turbine and produces mechanical energy forcing the turbine to rotate. The flue gas expands to lower pressure and larger volume during this procedure. The exhaust gas is released to the surroundings. It is called an open cycle because there are mass flows in and out of the process.

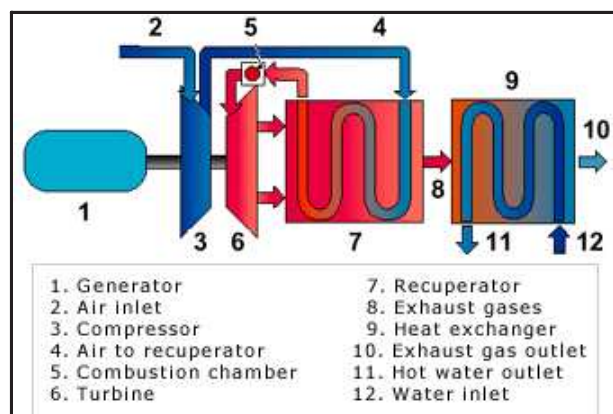


Figure 2.12: Principle components of micro turbine unit(www.turbec.com).

2.4.2 Microturbine Modelling

A micro turbine is a high frequency AC source the output of which need to be rectified. The DC voltage needs to be interfaced to the network using a voltage source inverter. The slow response requires either a DC bus or an AC system storage to insure load tracking. Figure 2.13 illustrates the outline of a micro turbine. The micro turbine requires a power electronic circuit for interfacing with the AC load. This interface consists of an AC to DC rectifier, a DC bus with capacitor and a DC to AC inverter.

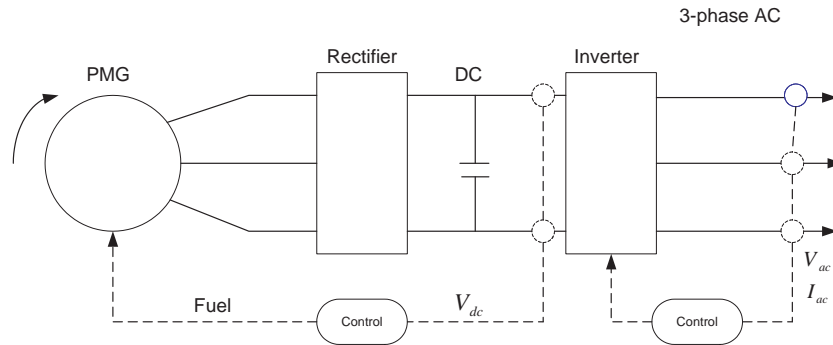


Figure 2.13: Outline of a micro turbine generator.

Figure 2.14 shows the equivalent circuit of the generator and rectifier which can be modelled as a 3-phase, full wave, diode bridge rectifier with the AC source which is assumed to be a permanent magnet generator.

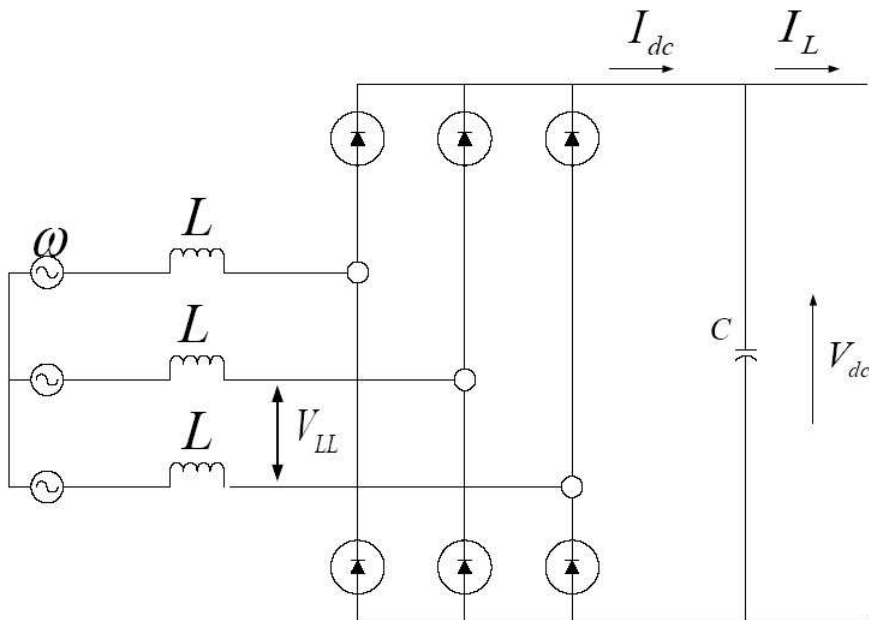


Figure 2.14: The equivalent circuit.

The no load (Ideal) case is considered first. The voltage induced on the generator terminal V_{LL} can be expressed then as:

$$V_{LL} = K_v \omega \sin(\omega t) = K_v \omega \text{Im} \{ e^{j\omega t} \} \quad (2.29)$$

where K_v is the voltage constant and ω is the electrical angular frequency. Since most microturbines use 2 pole PMG, the electrical and mechanical angular frequencies are equal [52]. The output DC voltage is given by:

$$V_{dc} = \frac{3}{\pi} |V_{LL}| - \frac{3\omega L}{\pi} I_{dc} \quad (2.30)$$

Substituting (2.29) into (2.30) we have:

$$V_{dc} = \frac{3}{\pi} K_v \omega - \frac{3}{\pi} \omega L I_{dc} \quad (2.31)$$

This can be written as:

$$\frac{3}{\pi} K_v \omega = V_{dc} + \frac{3}{\pi} \omega L I_{dc} \quad (2.32)$$

Define the no load DC voltage E_g by:

$$E_g = K_e \omega = \frac{3K_v}{\pi} \omega \quad (2.33)$$

where $K_e = \frac{3K_v}{\pi} \{V/(rad/sec)\}$.

Then (2.32) can be expressed as:

$$E_g = V_{dc} + K_x \omega I_{dc} \quad (2.34)$$

where $K_x = \frac{3L}{\pi} \{\Omega/(rad/sec)\}$

Equation (2.32) describes the electromechanical nature of the system. Therefore, if the system has no losses, the input power P_m can be expressed as a function of I_{dc} :

$$P_m = V_{dc} I_{dc} \quad (2.35)$$

Using equation (2.33) and (2.34) this becomes:

$$P_m = K_e \omega I_{dc} - K_x \omega I_{dc}^2 \quad (2.36)$$

The mechanical shaft torque for the no loss system T_m is expressed as:

$$T_m = \frac{P_m}{\omega} = K_e I_{dc} - K_x I_{dc}^2 \quad (2.37)$$

The mechanical part of the system is represented by:

$$\frac{d\omega}{dt} = \frac{1}{J} (T_m - T_t) \quad (2.38)$$

where J is the inertia of the shaft, T_m is the mechanical torque, T_t is the load torque.

Additionally, the DC voltage V_{dc} can also be expressed as:

$$V_{dc} = \frac{1}{C} \int (I_{dc} - I_L) dt \quad (2.39)$$

The relations in equations (2.31) and (2.39) determine the load current I_L and the final output power. Finally from all of the above equations the block diagram of an MT

generator model is described in Figure 2.15:

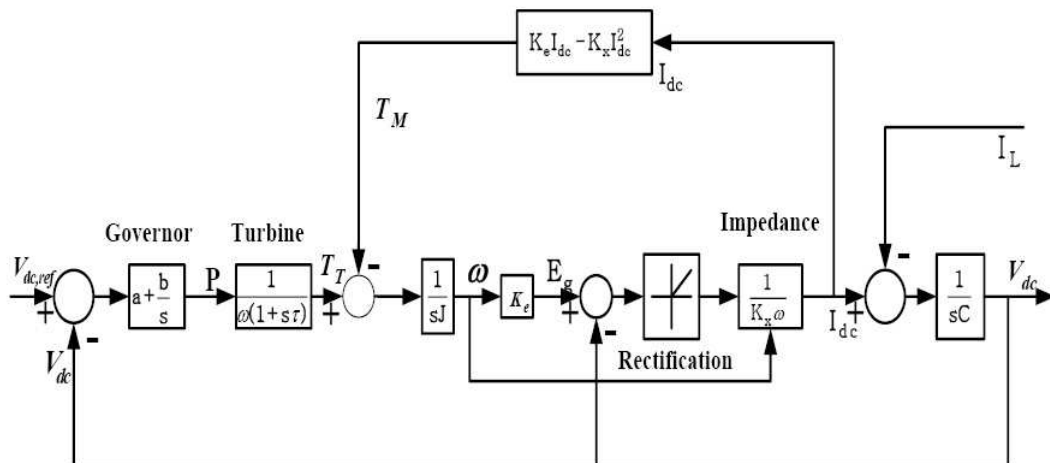


Figure 2.15: The micro turbine generator model.

2.4.3 Simulation Results

The turbine generator tested in simulations was a 75-kW Parallon micro-turbine made by Honeywell [52]. The power reference signal consists of negative power steps of 15 kW lasting 30 s starting from 75 kW, stepping down to 0 kW and then stepping back up to 75 kW, as presented in Figure 2.16. The microturbine system response to this power command is displayed in Figures 2.17-2.20. Figure 2.17 shows the output power of the system; Figure 2.18 the shaft speed; Figure 2.19 the DC link voltage; and Figure 2.20 the rotor speed.

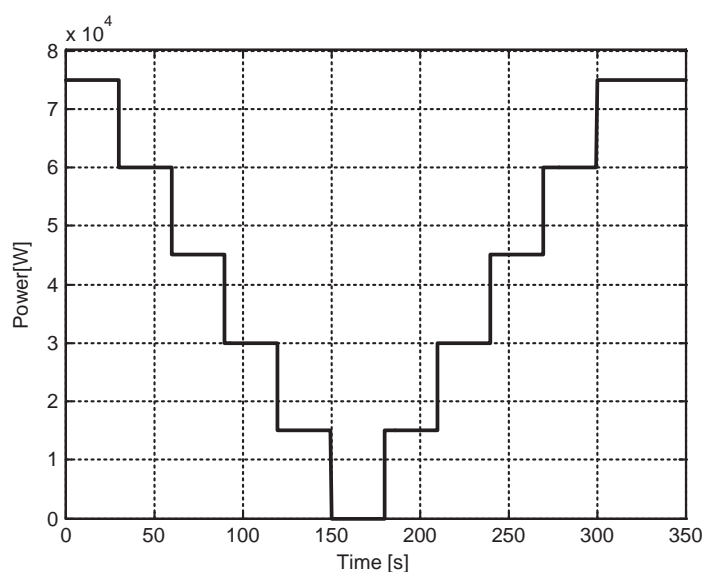


Figure 2.16: Power command to the microturbine system.

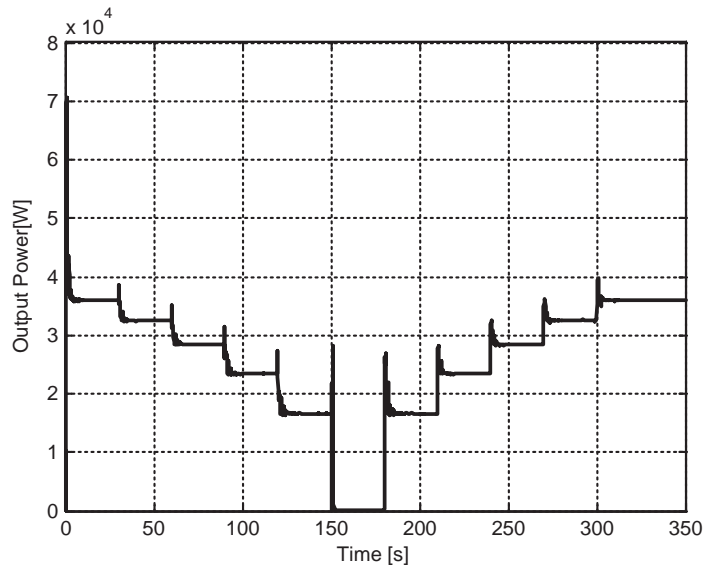


Figure 2.17: The output power of the microturbine P.

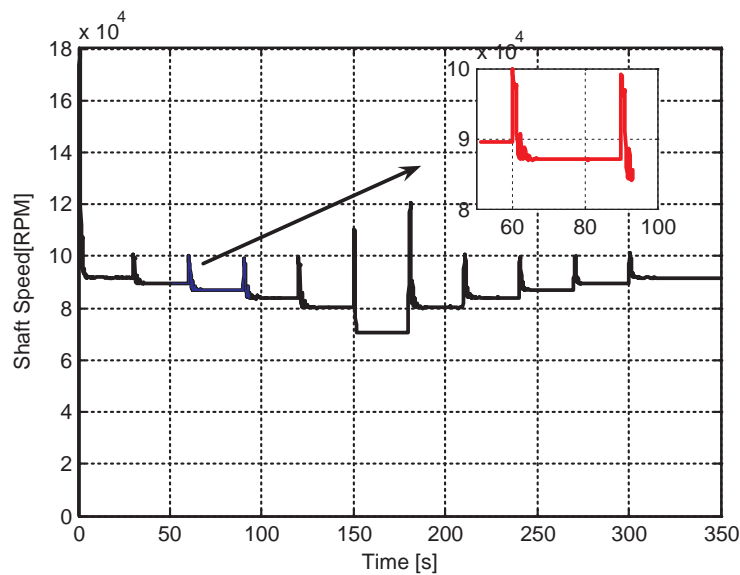


Figure 2.18: Shaft speed of the microturbine model ω . The red curve gives a detailed curve between 50-100 s.

However, there are some responses which do not follow the reference trajectories, such as the rotor speed at higher power levels and the DC link voltage steady state value for mid-level output power. It is believed that a better tuned controller, would result in improved results. More complex controllers could also be added to improve the response.

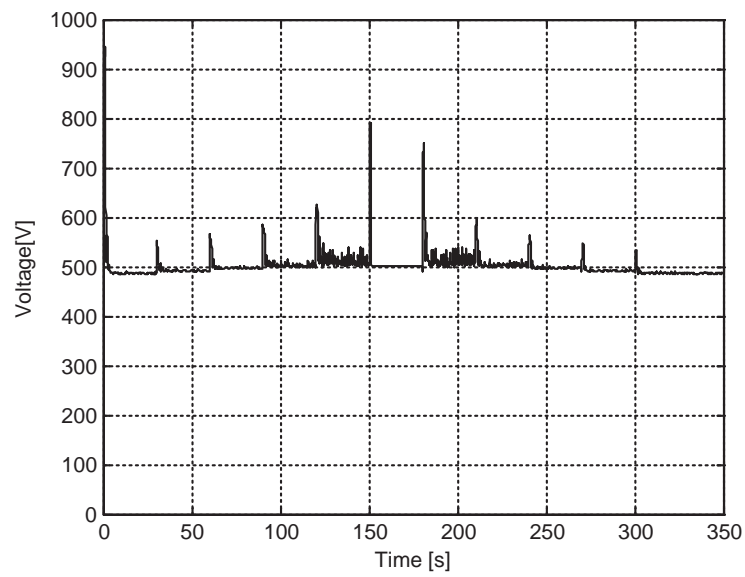


Figure 2.19: DC link Voltage of the microturbine model V_{DC} .

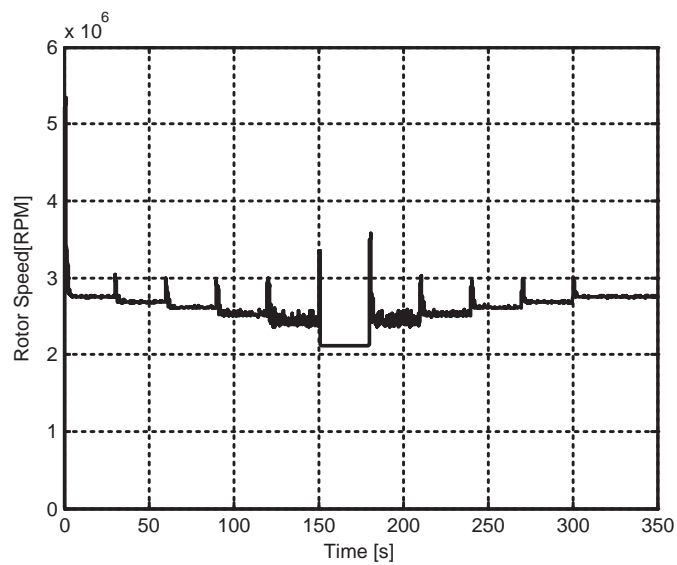


Figure 2.20: Rotor Speed of the microturbine model.

2.4.4 Microturbine Fuel Cost

Microturbines use a simple design with few moving parts to improve the reliability and reduce the maintenance costs. This design is with only one shaft and attached compressor, turbine, and permanent-magnet generator spinning at high rotational speed (up to 100kr/min) on air bearings. MTs can burn a variety of fuels including natural gas, gasoline, diesel, alcohol, and propane.

Microturbine models are similar to those of fuel cells [53], [54]. However, the parameters and curves are modified to properly describe the performance of a MT unit. The total efficiency of the microturbine can be written as:

$$\eta_l = \frac{P_{el} + P_{th,rec}}{m_f * LHV_f} \quad (2.40)$$

where

P_{el} is the net electrical output power,

$P_{th,rec}$ is the thermal power recovered (kW),

LHV_f is the fuel lower heating rate (kJ/kgf),

m_f is the mass flow rate of the fuel(kg/s).

Unlike the fuel cell, the efficiency of the MT increases with the increase of the supplied power. The MT fuel cost is as follows:

$$C_{MT} = C_{nl} \sum_J \frac{P_J}{\eta_{lJ}} \quad (2.41)$$

where

C_{nl} is the natural gas price to supply the MT,

P_J is the net electrical power produced at interval J ,

η_{lJ} is the cell efficiency at interval J .

2.5 Wind Turbine

Wind turbines are packaged systems that include a rotor, a generator, turbine blades, and a drive or a coupling device. As wind blows through the blades, the air exerts aerodynamic forces that cause the blades to turn the rotor. As the rotor turns, its speed is altered to match the operating speed of the generator. Most systems have a gearbox and a generator in a single unit behind the turbine blades. As with photovoltaic (PV) systems, the output of most wind generators is processed by an inverter that changes the electricity from DC to AC so that the electricity can be used.

2.5.1 Wind Turbine Generating System

The working principles of the wind turbine can be described in two processes, that are carried out by its main components: the rotor which extracts kinetic energy from the wind passing it and converts it into mechanical torque and the generating system, which converts this torque into electricity. Figure 2.21 illustrates the working principles of a wind turbine.

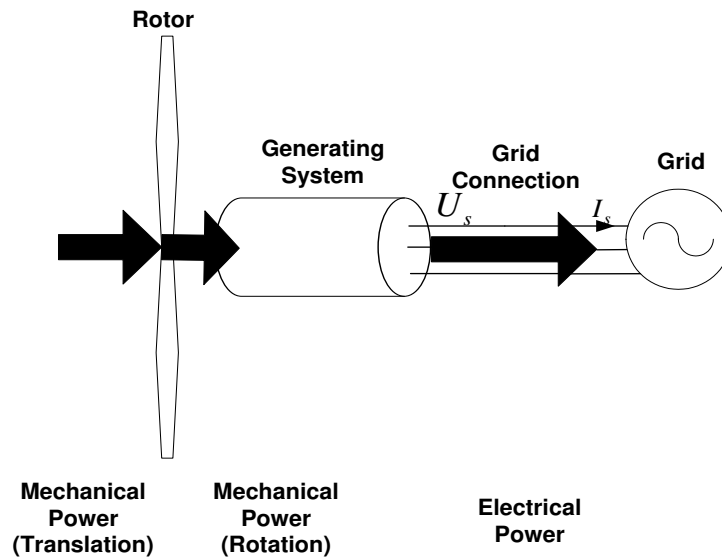


Figure 2.21: General working principle of wind power generation.

Basically, a wind turbine can be equipped with any type of a three phase generator. Several generator types may be used in wind turbines [55], but here three types of wind turbine generators are discussed:

- Squirrel cage induction generators,
- Doubly fed (wound rotor) induction generators,
- Direct drive synchronous generators.

In the next subsection the Doubly fed (wound rotor) induction generators are described:

2.5.2 Doubly Fed (Wound Rotor) Induction Generator and Direct Drive Synchronous Generator

Figure 2.22 shows a direct synchronous generator and a doubly fed (wound rotor) induction generator. They are used in variable speed turbines. With these it is possible to increase the energy captured by the aerodynamic rotor by maintaining the optimum power coefficient over a wide range of wind speeds [55]. However it is then necessary to decouple the speed of the rotor from the frequency of the grid through some form of power electronic converters. In the doubly fed induction generator, a back-to-back

voltage source converter feeds the three phase rotor winding. In this way, the mechanical and electrical rotor frequencies are decoupled and the electrical stator and rotor frequency can be matched, independently of the mechanical rotor speed. In the direct drive synchronous generator, the generator is completely decoupled from the grid by a power electronics converter. The grid side of this converter is a voltage source converter, i.e. an IGBT (Insulated Gate Bipolar Transistor) bridge. The generator side can either be a voltage source converter or a diode rectifier. The generator is excited using either an excitation winding or permanent magnets.

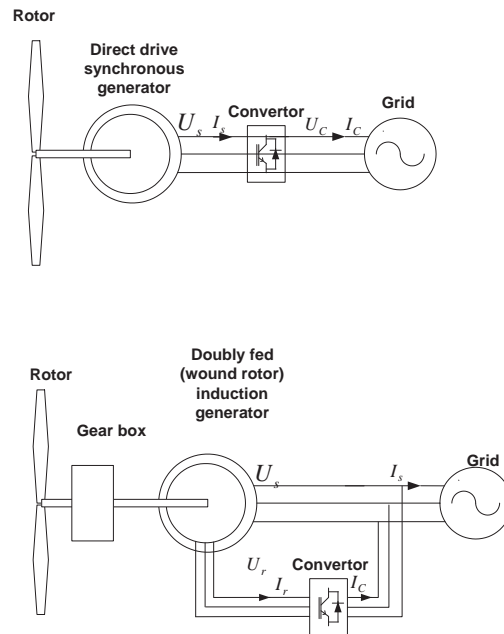


Figure 2.22: Generating systems used in wind turbines: direct synchronous generator (above) and doubly fed (wound rotor) induction generator (below).

2.5.3 Wind Turbine Modelling

In this section, an overview of the developments in wind turbine modelling will be presented. The first wind turbines were based on a direct grid coupled synchronous generator with pitch controlled rotor blades to limit the mechanical power in high wind speeds. Therefore, the first modelling efforts were devoted to this wind turbine concept [56], [55].

The directly grid coupled synchronous generator was followed by a directly grid coupled asynchronous squirrel cage induction generator. This type of a generator has a more favorable torque versus speed characteristic than the synchronous generator, thus reducing the mechanical loads and it is also cheaper. This concept is still applied nowadays by some manufacturers. To limit the power extracted from the wind at high wind speeds, either pitch control or stall control can be applied. Many papers on modelling of a wind turbine with a directly grid coupled squirrel cage induction generator can be found in the literature, both in combination with pitch control and with stall control of the mechanical power, e.g. [56], [57],[58] and [59].

Nowadays, a more modern variable speed wind turbine with a doubly fed induction generator has replaced the conventional constant speed wind turbine with a directly grid

coupled squirrel cage induction generator. The manufacturers have also started to apply a direct drive synchronous generator grid coupled through a power electronic converter of the full generator rating. Therefore, modelling efforts have been given to these wind turbine concepts as well. Because the variable speed wind turbines are complicated systems, most papers addressing their modelling only cover one subsystem, such as the electromechanical conversion system, the drive train, the control of the generator currents and the DC link voltage or the rotor speed controller, e.g. [60], [61].

As the power developed is proportional to the cube of the wind speed it is obviously important to locate any electricity generating turbines in areas of high mean annual wind speed, and the available wind resource is an important factor in determining where the wind farms are sited [1]. Often the areas of high wind speed will be away from the habitation and the associated well-developed electrical distribution network, leading to a requirement for careful consideration of the integration of wind turbines to relatively weak electrical distribution networks. The difference in the density of the working fluid (water and air) illustrates clearly why a wind turbine rotor of a given rating is much larger in size than a hydro-turbine [1].

2.5.4 Rotor Equation

A wind turbine operates by extracting kinetic energy from the wind passing through its rotor. The power developed by a wind turbine is given by [56]:

$$P = \frac{1}{2} C_p \vartheta V_w^3 A \quad (2.42)$$

where

P power (W),

C_p power coefficient,

V_w Wind velocity (m/s),

A swept area of rotor disc (m^2),

ϑ density of air ($1.225 \text{ kg}/m^3$).

The force extracted on the rotor is proportional to the square of the wind speed and so the wind turbine must be designed to withstand large forces during storms. Most of the modern designs are three-bladed horizontal-axis rotors as this gives a good value of peak C_p together with an aesthetically pleasing design [1].

The power coefficient C_p is a measure of how much of energy in the wind is extracted by the turbine. It varies with the rotor design and the relative speed of the rotor and wind (known as the tip speed ratio) to give a maximum practical value of approximately 0.4 [1]. The power coefficient C_p is a function of the tip speed ratio λ and the pitch angle β , which will be investigated further. The calculation of the performance coefficient requires the use of blade element theory [62], [55]. As this needs knowledge of aerodynamics and the computations are rather complicated, numerical approximations have been developed

[62]. Here the following function will be used:

$$C_p(\lambda, \beta) = 0.5176 \left(\frac{116}{\lambda_i} - 0.4\beta - 5 \right) e^{-\frac{21}{\lambda_i}} + 0.0068\lambda \quad (2.43)$$

where

$$\frac{1}{\lambda_i} = \frac{1}{\lambda + 0.08\beta} - \frac{0.035}{\beta^3 + 1} \quad (2.44)$$

Figure 2.23 shows $C_p(\lambda, \theta)$ versus λ characteristics for various values of β . Using the actual values of the wind and rotor speed, which determine λ , and the pitch angle, the mechanical power extracted from the wind can be calculated from equations (2.42)-(2.44). The maximum value of C_p ($c_{pmax}=0.48$) is achieved for $\beta = 0^\circ$ and for $\lambda = 8.1$. This particular value of λ is defined as the nominal value (λ_{nom}).

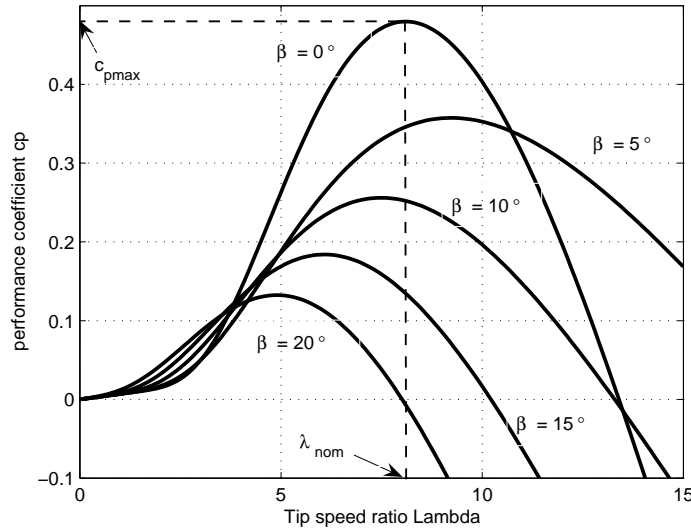


Figure 2.23: Performance coefficient C_p as a function of the tip speed ratio λ with pitch angle β as a parameter.

2.5.5 Generator Equation

Generator is device converting mechanical energy into electricity, so it is important to the whole system. The equation describing the doubly fed induction machine can be found in [60]. When modelling the doubly fed induction generator, the generator convention will be used, which means that the currents are outputs instead of inputs and the real power and reactive power have positive signs when they are fed into the grid. Using the generator convention, the following set of equations is obtained [62], [56]:

$$\begin{aligned} v_{ds} &= -R_s i_{ds} - \omega_s \psi_{qs} + \frac{d\psi_{ds}}{dt} \\ v_{qs} &= -R_s i_{qs} + \omega_s \psi_{ds} + \frac{d\psi_{qs}}{dt} \\ v_{dr} &= -R_r i_{dr} - r_s \omega_s \psi_{qr} + \frac{d\psi_{dr}}{dt} \\ v_{qr} &= -R_r i_{qr} + r_s \omega_s \psi_{dr} + \frac{d\psi_{qr}}{dt} \end{aligned} \quad (2.45)$$

where

- v is the voltage in [V],
- i is the current in [A],
- R_r, R_s are the rotor and stator resistances in [Ω] respectively,
- ω_s is the stator electrical frequency in [rad/s],
- ψ is the flux linkage in [Vs],
- r_s is the rotor slip.

Subscripts d and q are direct and quadrature axis components respectively; subscripts s and r indicate the stator and the rotor quantities. All the quantities in equation (2.45) are functions of time. The d-q reference frame is rotating at synchronous speed with the q-axis 90° ahead of the d-axis. The position of the d-axis coincides with the maximum of the stator flux, which means that v_{qs} equals the terminal voltage e_t and v_{ds} equals to zero. The flux linkages can be calculated using the following set of equations in per unit [56].

$$\begin{aligned}\psi_{ds} &= -(L_s + L_m)i_{ds} - L_m i_{dr} \\ \psi_{qs} &= -(L_s + L_m)i_{qs} - L_m i_{qr} \\ \psi_{dr} &= -(L_r + L_m)i_{dr} - L_m i_{ds} \\ \psi_{qr} &= -(L_r + L_m)i_{qr} - L_m i_{qs}\end{aligned}\tag{2.46}$$

where L_m is the mutual inductance and L_s and L_r are the stator and rotor leakage inductances, respectively. In equation (2.46) the generator convention is used again. The rotor slip is defined as [56]:

$$r_s = \frac{\omega_s - \frac{p}{2}\omega_m}{\omega_s}\tag{2.47}$$

where p is the number of poles and ω_m is the mechanical frequency of the generator in [rad/s].

From equations (2.45), (2.46), we can derive the voltage-current relationships of the doubly fed induction generator.

Reference [56] proposes that the rotor and stator transients, represented by the last term in equation (2.45) are to be neglected. Substituting (2.46) in to (2.45) results in:

$$\begin{aligned}v_{ds} &= -R_s i_{ds} + \omega_s((L_s + L_m)i_{qs} + L_m i_{dr}) \\ v_{qs} &= -R_s i_{qs} - \omega_s((L_s + L_m)i_{ds} + L_m i_{dr}) \\ v_{dr} &= -R_r i_{dr} + r_s \omega_s((L_r + L_m)i_{qr} + L_m i_{qs}) \\ v_{qr} &= -R_r i_{qr} + r_s s \omega_s((L_r + L_m)i_{dr} + L_m i_{ds})\end{aligned}\tag{2.48}$$

The active power P and reactive power Q generated by the generator can be written as:

$$\begin{aligned}P &= v_{ds}i_{ds} + v_{qs}i_{qs} + v_{dr}i_{dr} + v_{qr}i_{qr} \\ Q &= v_{ds}i_{ds} - v_{qs}i_{qs} + v_{dr}i_{dr} - v_{qr}i_{qr}\end{aligned}\tag{2.49}$$

From these equations, it can be concluded that the reactive power Q is not necessarily equal to the generated reactive power fed into the grid. Equations (2.48) and (2.49) describe the electrical part the generator. However, also the mechanical part must be taken

into account in the dynamical model. The following expression gives the electromechanical torque developed by the generator:

$$T_e = \Psi_{dr}i_{qr} - \Psi_{qr}i_{dr} \quad (2.50)$$

The changes in generator speed that result from a difference in electrical and mechanical torque can be calculated using the generator equation of motion in which H_m is the equivalent inertia constant of the generator rotor [s] and T_m is the mechanical torque [p.u.].

$$\frac{d\omega_m}{dt} = \frac{1}{2H_m}(T_m - T_e) \quad (2.51)$$

Figure 2.24 shows the speed-power turbine curve which reflects both the aerodynamic power and the generated power. At low wind speeds, the output power is too low to be exploited. Normally turbines are started when the wind speed exceeds 3-4 m/s. We can see also that the wind turbine started at 5 m/s and the output power increases with the cube of the wind speed until the rated wind speed is reached.

At wind speeds from 12 m/s to 25 m/s the power is limited to the rated power of the wind turbines by means of stall-regulation or pitch-control. At wind speeds over 25 m/s wind turbines are normally stopped to avoid high mechanical loads. The wind speed at which the wind turbines are stopped is called cut-out speed.

The power is controlled in order to follow a pre-defined power-speed characteristic, named tracking characteristic. The tracking characteristic is defined by four points: A, B, C and D. From zero speed to speed of point A the reference power is zero. Between point A and point B the tracking characteristic is a straight line, the speed of point B must be greater than the speed of point A. Between point B and point C the tracking characteristic is the locus of the maximum power of the turbine (maxima of the turbine power vs turbine speed curves). The tracking characteristic is a straight line from point C and point D. The power at point D is one per unit (1 pu) and the speed of the point D must be greater than the speed of point C. Beyond point D the reference power is a constant equal to one per unit (1 pu).

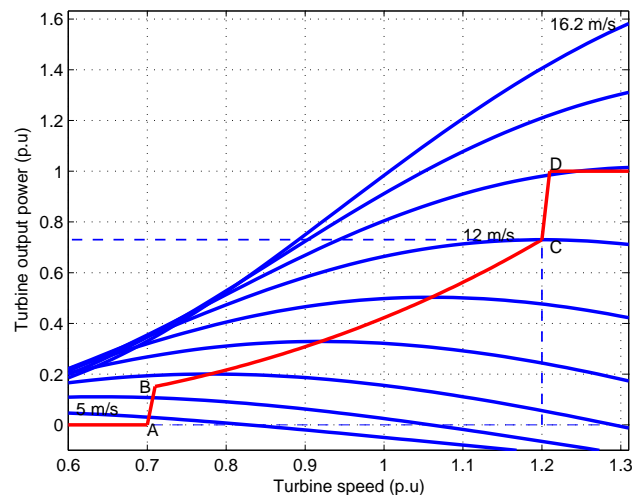


Figure 2.24: Power curve of wind turbine.

2.5.6 Simulation Results

In this section, the behavior of the wind turbine is examined when the wind speed changes. The speed is first constant 8 (m/s), then at time 5 seconds a ramp is introduced lasting until 11 seconds and then constant speed of 14 (m/s) follows, as illustrated in Figure 2.25. Figure 2.26 shows the corresponding generated active power P . This power starts increasing smoothly (together with the turbine speed) to reach its rated value of 1.5 MW in approximately 19 s. The response of the reactive power due to a change in the wind speed is shown in Figure 2.27. It can be seen that at nominal power, the wind turbine absorbs 0.11 Mvar (generated $Q = -0.11$ Mvar).

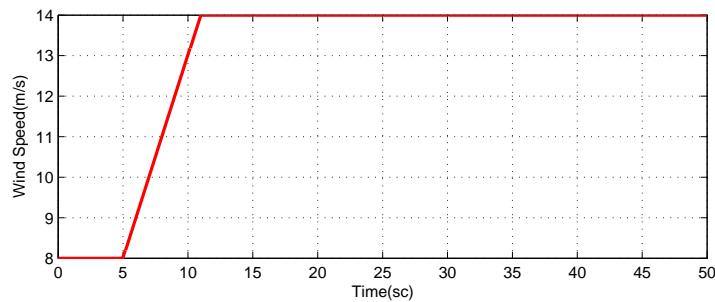


Figure 2.25: Wind Speed.

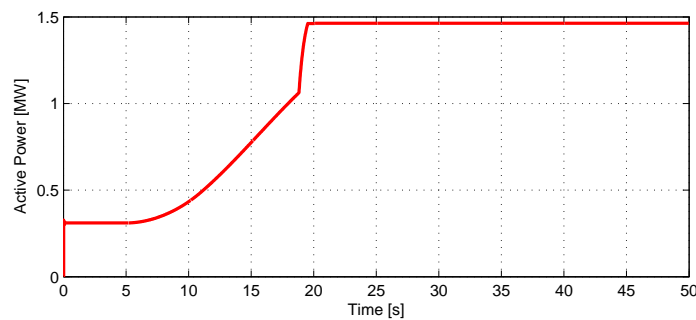


Figure 2.26: Generated active power P .

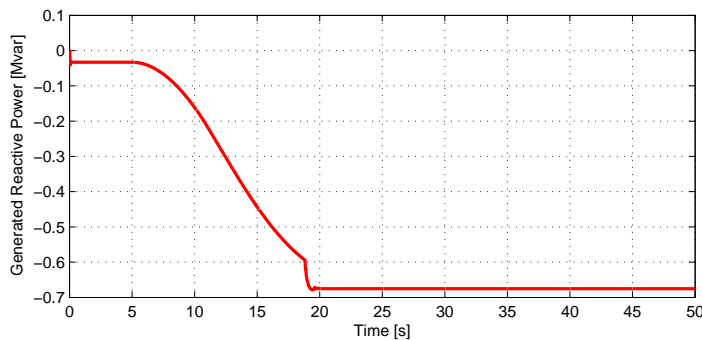


Figure 2.27: Generated reactive power Q .

Figure 2.28 shows the pitch angle response due to the change in the wind speed. In this figure, it is clear that, initially, the pitch angle of the turbine blades is zero degrees and the turbine operating point follows the red curve of the turbine power characteristic

up to point D shown in Figure 2.24. Then the pitch angle is increased from 0 deg to 0.078 deg in order to limit the mechanical power. In Figure 2.29 the turbine speed is increased when the wind speed increased from 0.8 pu to 1.21 pu.

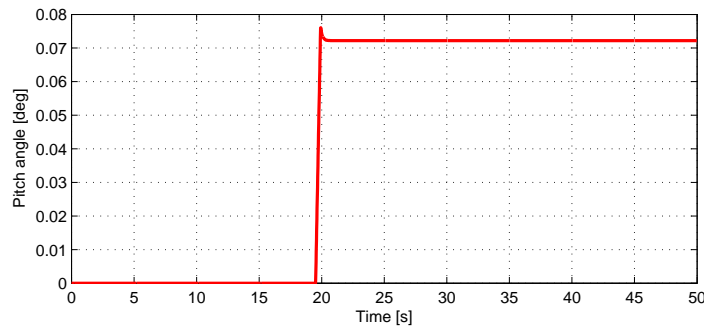


Figure 2.28: Pitch Angle.

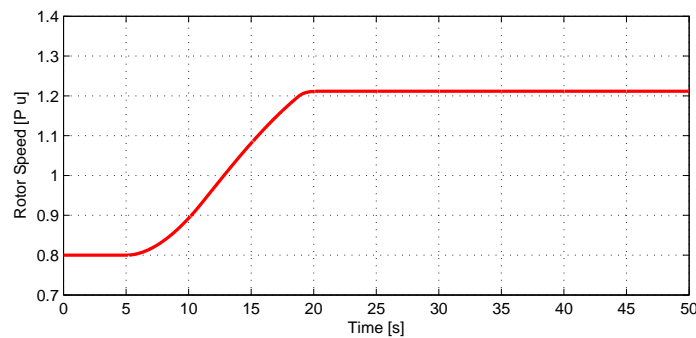


Figure 2.29: Rotor Speed.

To simulate the wind turbine responses for different values of wind speed, the initial wind speed is below the nominal wind speed which is assumed to be 14 m/s. After 7 seconds, a wind speed ramp starts which leads to an increase in the average wind speed in 30 seconds. After 10 seconds a wind gust with an amplitude of -3 m/s and duration of 10 seconds occurs [63]. The results are illustrated in Figures 2.30-2.32. At 20 s, the nominal power of the wind turbine is reached because the pitch angle controller is not used which can prevent the rotor overspeeding.

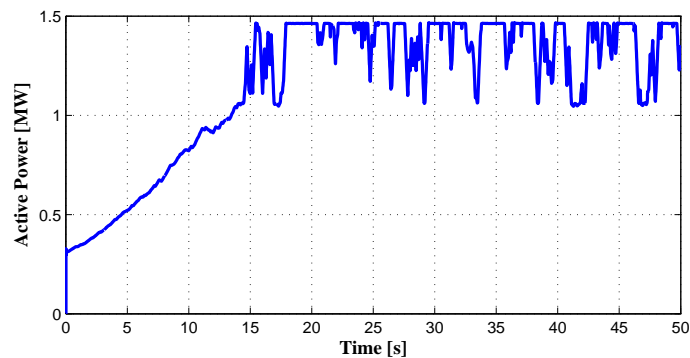


Figure 2.30: Generated active power due to different values of wind speed.

The next step is to simulate the responses of the wind turbine when the input is a mea-

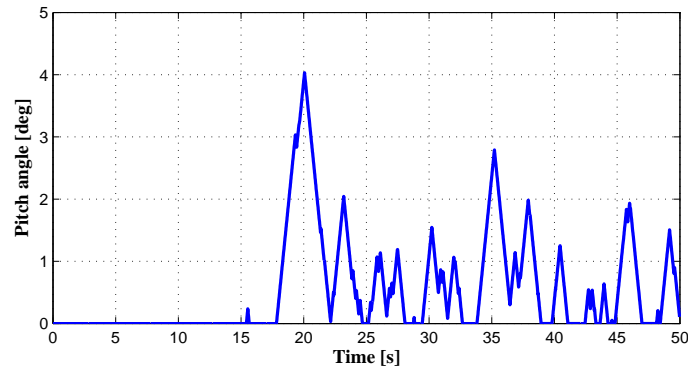


Figure 2.31: Pitch Angle due to different values of wind speed.

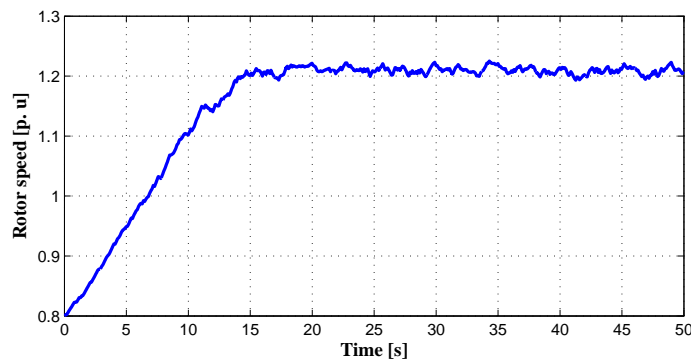


Figure 2.32: Rotor Speed due to different values of wind speed.

sured wind sequence. Figures 2.34-2.36 show the responses of the active power, the pitch angle, and the rotor speed due to the input measured wind speed shown in Figure 2.33. The wind speed measurements were downloaded from "Database of Wind Characteristics" [64].

By comparing the responses attained using the simulated and measured inputs, wind speed curves have almost the same range fluctuations of the output power. The range of the response of the rotor speed fluctuations are also similar. The behavior of the response of the pitch angle is different because there is no pitch controller in the design model.

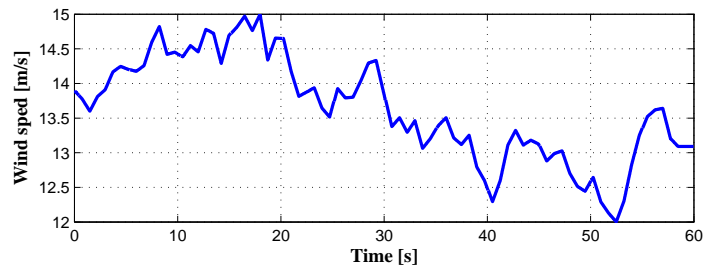


Figure 2.33: Measured sequence of wind speed.

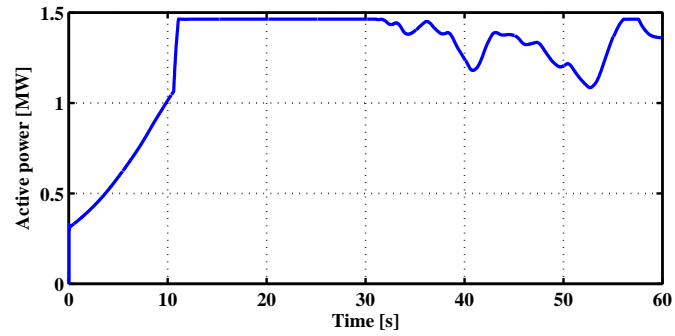


Figure 2.34: Response of the generated active power due to the measured sequence wind speed input.

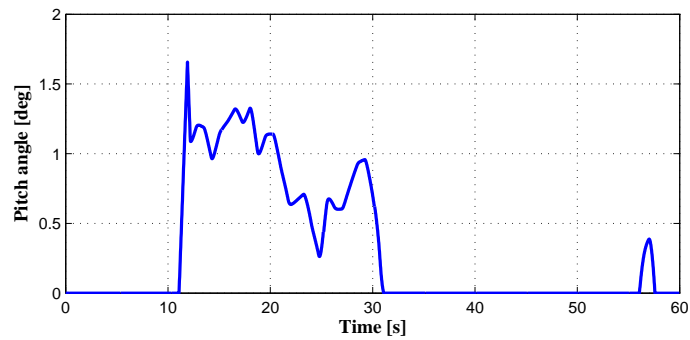


Figure 2.35: Response of the pitch angle due to measured sequence wind speed input.

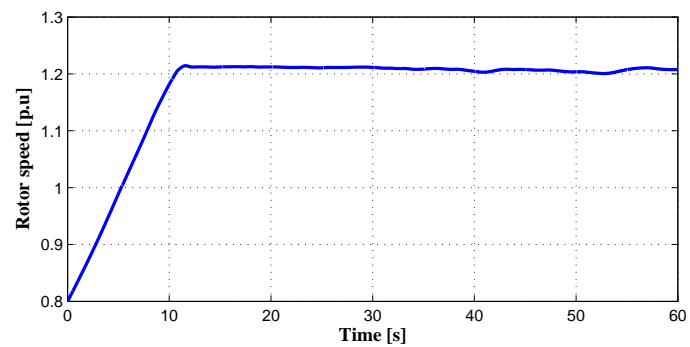


Figure 2.36: Response of the rotor speed due to measured sequence wind speed input.

2.5.7 Wind turbine optimization model

In the design of a wind turbine model, two important factors are considered; the availability of the wind and the power curve of the wind turbine itself. The available wind generator output, is a function of the wind velocity. In order to model the performance of the wind turbine, the power curve of the wind turbine must be obtained. The following is the model used to calculate the output power generated by the wind turbine generator [65],[66]:

$$\begin{cases} P_{WT} = 0, & V_{ac} < V_{ci} \\ P_{WT} = aV_{ac}^2 + bV_{ac} + c, & V_{ci} \leq V_{ac} < V_r \\ P_{WT,r} = 130, & V_r \leq V_{ac} < V_{co} \end{cases} \quad (2.52)$$

where $P_{WT,r}$, V_{ci} , and V_{co} are the rated power, cut-in and cut-out wind speed, respectively. Furthermore, V_r and V_{ac} are the rated and actual wind speed, respectively. For modelling the performance of a wind turbine, the mathematical equation of the power curve of a wind turbine must be obtained.

In a typical design of a wind turbine, the turbine does not generate power after its cut-off speed V_{co} . As we will use the AIR403 wind turbine model [67], it is stated in the manual that it uses a unique rotor blade that twists the blade and stalls the rotor when the cut-off speed is reached. According to the data from the manufacturer, the turbine output $P_{WT,r}$ is roughly 130 W if the wind speed is greater than approximately 18 m/s [67], [68]. One specific example of the generated power as a function of the wind speed is shown in Figure 2.37. In this figure, the AIR403 power curve is modeled, according to equation (2.52), where the actual power curve is obtained from the owner's manual. The parameters in the model of the power curve are as follows:

$a = 3.4$; $b = -12$; $c = 9.2$; $P_{WT,r} = 130$ watt; $V_{ci} = 3.5$ m/s; $V_{co} = 18$ m/s; $V_r = 17.5$ m/s.

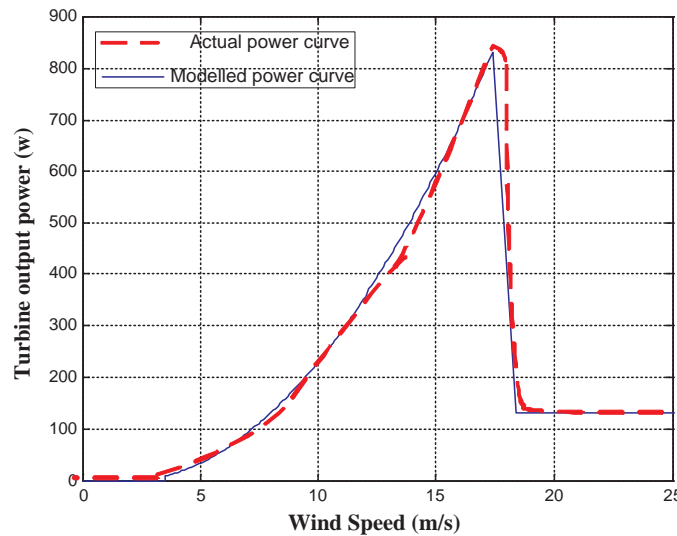


Figure 2.37: The actual and modeled power curve of AIR403.

2.6 Photovoltaic

The photovoltaics (PVs) are an attractive source of renewable energy for distributed urban power generation due to their relatively small size and noiseless operation. Their applications are expected to significantly increase all over the world. PV generating technologies have the advantage that more units can be added to meet the load increase demand [1] and [7].

Major advantages of the photovoltaic power are [69]:

- Short lead time to design, install, and start up a new plant.
- Highly modular structure, hence the plant economy is not a strong function of size.
- Power output matches very well with peak load demands.
- Static structure with no moving parts and hence, no noise.
- High power capability per unit of weight.
- Longer life with little maintenance because no moving parts exist.
- Highly mobile and portable because of light weight.

Photovoltaic cells can be divided into four groups: crystalline cells, thin-film cells, dye-sensitised solar cells (DYSC or Grätzel-cell) and multilayer cells. The latter can also be considered as several layers of thin-film PV cells. The different types are described in [70].

Figure 2.38 shows the schematic diagram of an inverter for a small PV grid connected system. The inverter typically consists of the following items:

- Maximum power point tracking (MPPT) circuit.
- Energy storage element, usually a capacitor.
- A DC converter to increase the voltage.
- An AC inverter stage.
- A Isolation transformer to ensure that DC is not injected into the network.
- Output filter to restrict the harmonic currents passed into the network.

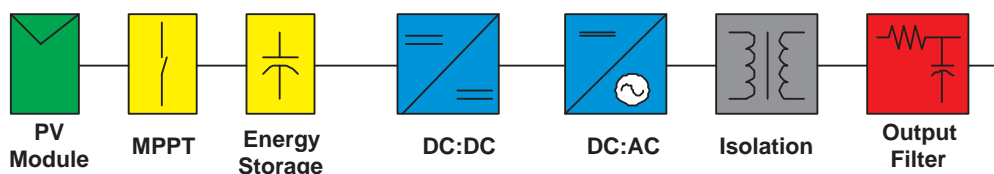


Figure 2.38: Schematic diagram of small PV inverter for grid connected operation.

2.6.1 Modelling

An initial understanding of the performance of a solar cell may be obtained by considering it as a diode. The light energy, which is in the form of photons with the appropriate energy level, falls on the cell and generates electron-hole pairs. The electrons and holes are separated by the electric field established at the junction of the diode and are then driven around an external circuit by this junction potential. There are losses associated with the series and shunt resistance of the cell as well as leakage of some of the current back across the p-n junction. This leads to the equivalent circuit shown in Figure 2.39 [1], [71].

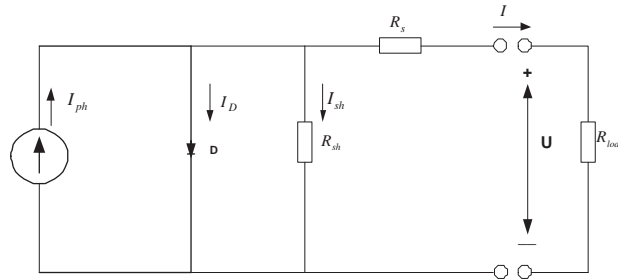


Figure 2.39: Equivalent circuit of a PV module.

The PV cell can be modeled as a diode in parallel with a constant current source and a shunt resistor. These three components are in series with the series resistor. The output-terminal current I is equal to the light-generated current I_{ph} , with subtracted diode-current I_D and the shunt-leakage current I_{sh} .

$$I = I_{ph} - I_D - I_{sh} \quad (2.53)$$

The series resistance R_s represents the internal resistance of the current flow, and it depends on the p-n junction depth, the impurities and the contact resistance. The shunt resistance R_{sh} is inversely related to the leakage current to the ground. In an ideal PV cell, $R_s = 0$ (no series loss), and $R_{sh} = \infty \Omega$ (no leakage to ground). The PV cell conversion efficiency is sensitive to small variations in R_s , but is insensitive to variations in R_{sh} . A small increase in R_s can decrease the PV output significantly. In the equivalent circuit, the current delivered to the external load equals the current I_{ph} generated by the illumination, less than the diode current I_D and the ground-shunt current I_{sh} . The open circuit voltage U_{oc} of the cell is obtained when the load current is zero, i.e., when $I_{sh} = 0$ and is given as:

$$U_{oc} = U + IR_s \quad (2.54)$$

where U is the terminal voltage of the cell [V].

The diode current I_D is given by the classical diode current expression [69]:

$$I_D = I_d \left[\frac{qU_{oc}}{A_{cf}K_B T} - 1 \right] \quad (2.55)$$

where

- I_d the saturation current of the diode,
 q electron charge = $1.6 * 10^{-19}$ Coulombs,
 A_{cf} curve fitting constant,
 K_B Boltzmann constant = $1.38 * 10^{-23}$ Joule/°KT
 T temperature [°K].

The output current is given by the expression [72]:

$$I = I_{ph} - I_{os} \left\{ \exp \left[\frac{qU_{oc}}{A_{cf}K_B T} \right] - 1 \right\} - \frac{U_{oc}}{R_{sh}} \quad (2.56)$$

where

$$I_{ph} = \frac{G}{100} [I_{SCR} + K_I(T - 25)] \quad (2.57)$$

$$I_{os} = I_{or} \left(\frac{T}{T_r} \right)^3 \exp \left[\frac{qE_{GO}}{BK_B} \left(\frac{1}{T_r} - \frac{1}{T} \right) \right] \quad (2.58)$$

and

- I, U cell output current and voltage,
 I_{os} cell reverse saturation current,
 B ideality factor of p-n junction,
 K_I short circuit current temperature coefficient at
 $I_{SCR}, K_I = 0.0017 \text{ A/}^\circ\text{C}$,
 G solar irradiation in W/m^2 ,
 I_{SCR} short circuit current at
 25°C and 1000W/m^2 ,
 I_{ph} light generated current
 E_{GO} band gap for silicon,
 T_r reference temperature, $T_r = 301.18^\circ\text{K}$,
 I_{or} cell saturation current at T_r ,
 R_{sh} shunt resistance,
 R_s series resistance.

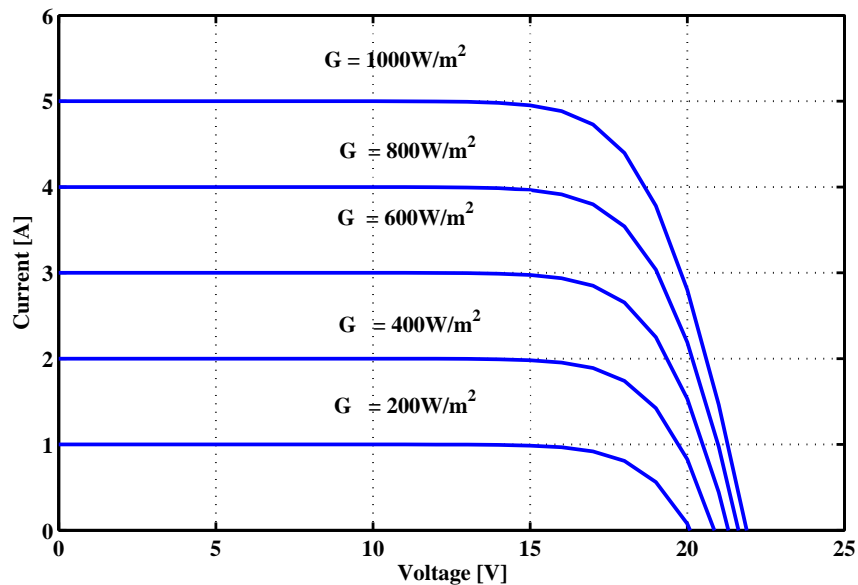
I_{SCR} , the current at maximum power point (I_{mpp}), the voltage at maximum power point (V_{mpp}), and the open circuit voltage of the cell U_{oc} , are given by the manufacturers. Table 2.3 illustrates the Standard Test Condition (STC) of AM1.5, 1000W/m^2 and 25°C , also the data for 80W PHOTOWATT which are used in the simulation study of [73]

2.6.2 Simulation Results

The I-U and P-U characteristics for various irradiance at fixed temperature ($T = 25^\circ\text{C}$), obtained from the model are shown in Figures 2.40 and 2.41, respectively.

Table 2.3: Parameters for 80W PHOTOWATT panel PWZ750 at STC.

Parameter	Value
Maximum Power Point, (P_{mpp})	80W
Minimum Power Point, (P_{minpp})	75.1W
Current at MPP, (I_{mpp})	4.6A
Voltage at MPP, (V_{mpp})	17.3V
Short Circuit Current, (I_{SCR})	5A
Open Circuit Voltage, (U_{oc})	21.9V
Short circuit current temperature coefficient, α_{scT}	$1.57mA/^{\circ}C$
Open circuit voltage temperature coefficient, β_{ocT}	$-78.2mV/^{\circ}C$
NOCT (Normal Operating Cell Temperature)	$45^{\circ}C$
Insolation, $G=0.8W/m^2$, $T_a=20^{\circ}C$, wind speed=1m/s	

Figure 2.40: I-U characteristic for a PV cell at a constant temperature of $25^{\circ}C$

Figures 2.42 and 2.43 show the I-U and P-U characteristics respectively, for different values of temperature and fixed irradiance of $1000W/m^2$.

From these figures, the upper curve shows that the open-circuit voltage of the cell is about 22 Volt, when the irradiation is $1000W/m^2$, which corresponds approximately to a cloud-free, sunny day. As the load (current) of the cell increases, the voltage decreases and at short-circuit (voltage = 0) the current is approximately 5 A. At open circuit and at short-circuit, no power is produced. At a point called the maximum power point (MPP), maximum power is gained from the PV-cell. To visualize this, a rectangle can be drawn from a point on the curve to the x and y-axis. For the point where this rectangle has the largest area, the maximum power is generated. At a lower irradiation, the short-circuit current decreases approximately linearly with irradiation. The open circuit voltage does not decrease as much until a very low irradiation. However, the open circuit voltage is much more affected by the temperature of the PV-cell. At a higher temperature, the open circuit voltage decreases. The phenomenon has quite large an impact and it decreases the

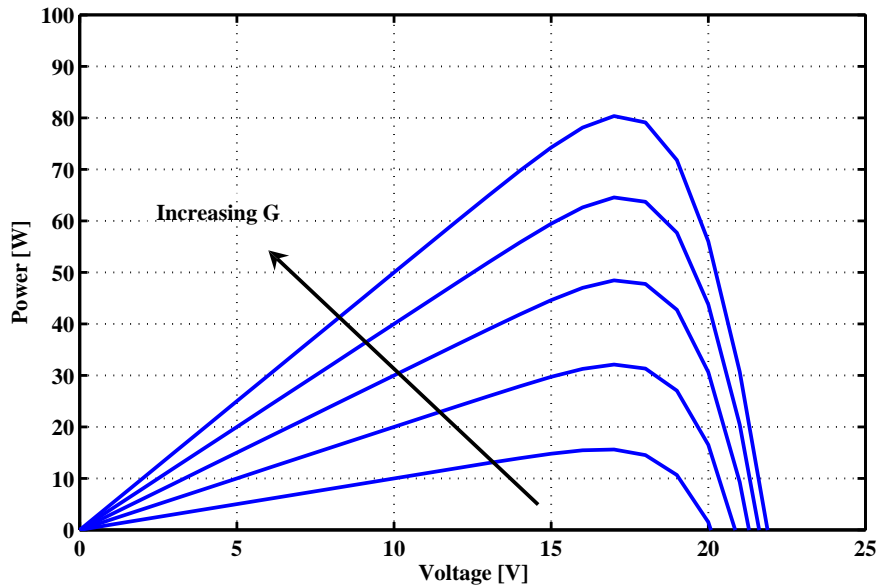


Figure 2.41: P-U characteristic for a PV cell at a constant temperature of 25°C

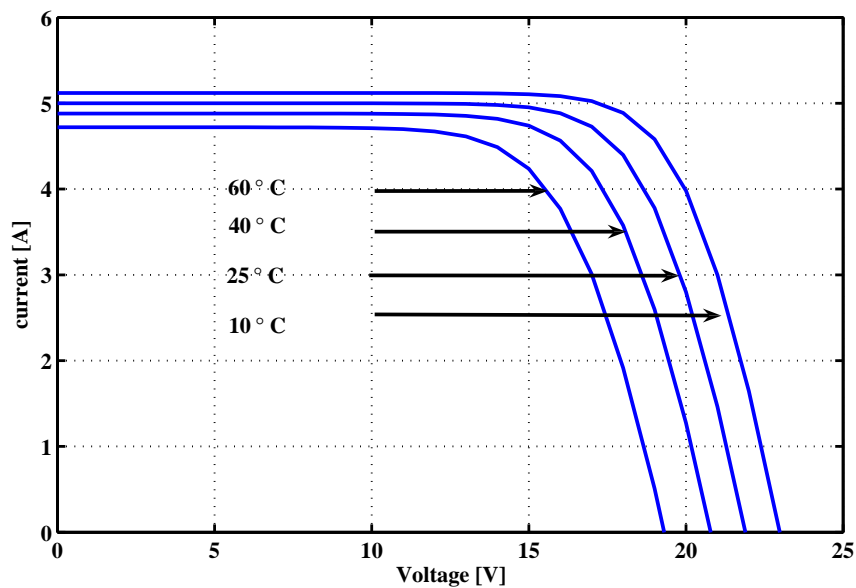


Figure 2.42: I-U characteristic for a PV cell at constant $G = 1000\text{W}/\text{m}^2$

output power by approximately 15 % at a temperature increase from 25°C to 60°C . The effect of irradiance and cell temperature on I-U characteristic curve is shown in Figures 2.42 and 2.43. Figure 2.42 shows that the maximum power output varies almost linearly with the irradiance. Figure 2.43 shows that the maximum output power from the PV decreases as the temperature increases.

2.6.3 PV optimization model

Photovoltaic generations are systems which convert the sunlight directly to electricity. PV technology is well established and widely used for power supplies to remote sites from

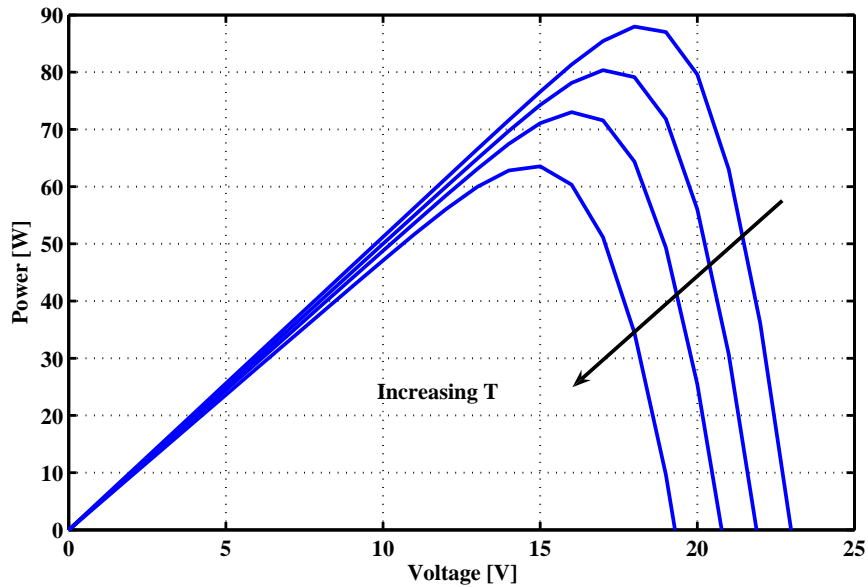


Figure 2.43: P-U characteristic for a PV cell at constant $G= 1000W/m^2$

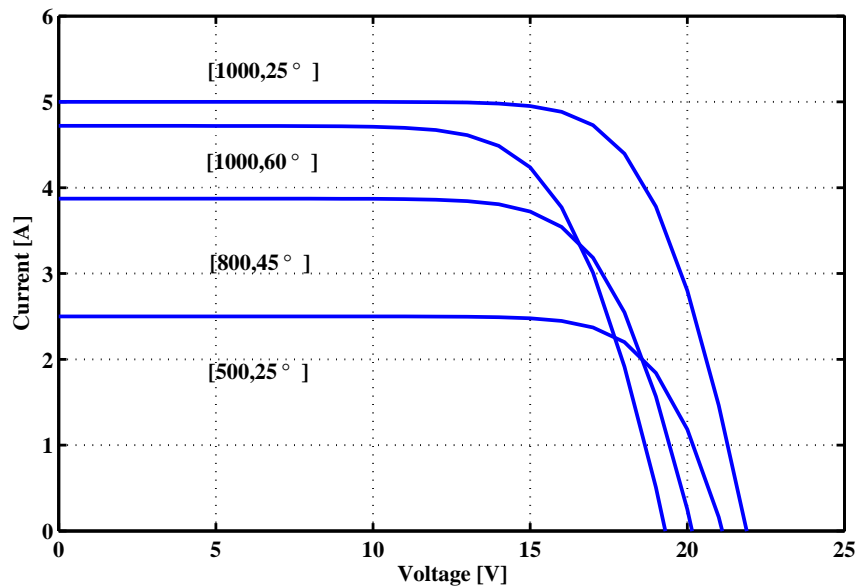


Figure 2.44: I-U characteristic of PV for some set of G and T

the distribution network [1]. The characteristics of the PV in operating conditions that differ from the standard condition ($1000 W/m^2, 25^\circ C$ cell temperature), the influences of the solar irradiance and ambient temperature on PV characteristics are modeled. The effect of solar intensity is modelled by considering the power output of the module to be proportional to the irradiance [74],[75]. The PV Modules are treated at Standard Test Condition (STC). The output power of the module for can be calculated using equation (2.59):

$$P_{PV} = P_{STC} \frac{G_{ING}}{G_{STC}} (1 + k(T_c - T_r)) \quad (2.59)$$

where

P_{PV}	The output power of the module at Irradiance G_{ING} ,
P_{STC}	The Module maximum power at STC,
G_{ING}	Incident Irradiance,
G_{STC}	Irradiance at STC $1000 W/m^2$,
k	Temperature coefficient of power,
T_c	The cell temperature.
T_r	The reference temperature.

In computing the different modules, the Standard Rating System used is a peak power value given by the manufacturers. This is based on the module maximum power output at (STC), which means that under 5.11 PHS the output of the modules per day will be 5.11 times their rating, where SOLAREX MSX-83 modules are used in this study. Their output characteristics are: peak power = $83W$, voltage at peak power = $17.1V$, current at peak power = $4.84A$, short circuit current = $5.27A$, and open circuit voltage = $21.2V$ at STC.

2.7 Battery Storage optimization model

Battery banks are electrochemical devices that store energy from other AC or DC sources for later use. The power from the battery is needed whenever the microsources are insufficient to supply the load, or when both the microsources and the main grid fail to meet the total load demand. On the other hand, energy is stored whenever the supply from the microsources exceeds the load demand.

The following assumptions are used to model the battery bank: The charge and discharge current are limited at 10 % of battery AH capacity (the storage capacity of a battery is measured in terms of its ampere-hour (AH) capacity [76] [68]). The round-trip efficiency is 95 %.

Because it is impossible for an energy storage device to contain negative energy, the maximum state of charge (SOC_{max}) and the minimum state of charge (SOC_{min}) of the battery are 100 % and 20 % of its AH capacity, respectively. When determining the state of charge for an energy storage device, two constraint equations must be satisfied at all times [68]. The maximum allowable charge and discharge current must be to be less than 10% of the battery AH capacity and are given by the following equations, respectively.

$$P_+ \leq (0.1 \times V_{sys} \times U_{batt}) / \Delta_t \quad (2.60)$$

$$P_- \leq (0.1 \times V_{sys} \times U_{batt}) / \Delta_t \quad (2.61)$$

where the parameter V_{sys} is the system voltage at the DC bus, Δ_t is time in hours, and the parameter U_{batt} is the battery capacity in AH. The state of charge (SOC) of the battery can be obtained by monitoring the charge P_+ and discharge P_- power of the battery, and

is given by the following equation:

$$SOC = SOC_{\max} - P_- + P_+ \quad (2.62)$$

It is important that the SOC of the battery prevents the battery from overcharging or undercharging. The associated constraints can be formulated by comparing the battery SOC at any hour Δ_t with the battery SOC_{\min} and the battery SOC_{\max} , as depicted in (2.63). This study assumes that the initial SOC of the battery is equal to 100% in the beginning of the simulation.

The constraints on battery SOC are:

$$SOC_{\min} \leq SOC \leq SOC_{\max} \quad (2.63)$$

Finally, in order for the system with battery to be sustained over a long period of time, the battery SOC at the end must be greater than a given percentage of its SOC_{\max} . This study assumes the percentage to be 90%.

2.8 Conclusions

To analyze the dynamic performance of MGs, proper dynamic models are required for different investigation purposes. Therefore, component models, which reflect the physical processes within MGs components, are modeled to simulate the dynamics of MGs for steady-state studies and online management purposes. In this Chapter, modelling of components of a MG system has been successfully done. Models, which allow the investigation of the individual power sources behaviour, have been developed. Testing was also a significant part of this chapter. In the following Chapters further development will be carried out on the system, with the goal that MGs will be able to generate power in an economical and efficient way by reducing the costs and the emission. Although certain commercial components were specifically chosen, the models are easily generalizable to other, similar components.

Chapter 3

Online Optimal Management of MicroGrid using Mesh Adaptive Direct Search (MADS)

3.1 Introduction

This chapter presents a generalized formulation to determine the optimal operating strategy and cost optimization scheme for a MicroGrid. The proposed cost function takes into consideration the costs of the emissions NO_x , SO_2 , and CO_2 , start-up costs, as well as the operation and maintenance costs. Also, the daily income and outcome is added from the sales or purchased power. The optimization is aimed at minimizing the cost function of the system while constraining it to meet the customer demand and safety of the system. For purpose of comparison, two different techniques are applied to solve the proposed optimization problem. The first technique is Sequential Quadratic Programming (SQP), while the second one is the Mesh Adaptive Direct Search (MADS) method.

MADS is a generalization of the pattern search algorithm. These methods are intended for black box optimization problem. They are derivative-free methods in the sense that they do not compute nor even attempt to evaluate derivatives. There is a wide range of interesting applications of pattern search and MADS methods [77, 78, 79, 80]. In this work, (MADS) reported in [24] is applied to the optimization management problem of a MG.

The chapter is divided as follows. An overview of the optimization problem is provided in Section 3.2. Section 3.3 contains a brief description of MADS method. Section 3.4 outlines the optimization model process. Section 3.5 presents the proposed objective functions for online management of a MG with the three scenarios applied. In section 3.6, the golden search method is applied to see the minimization of the three cost functions of MT, FC and DG individually. Section 3.7 summarizes the key characteristics of the implemented strategy. Section 3.8 discusses the results obtained for this specific problem. In Section 3.9, the conclusions and the performance of the algorithms are presented.

3.2 Optimization Overview

A General optimization Problem (GP) is given as:

$$\begin{aligned}
 & \underset{\mathbf{P} \in \mathbb{R}^n}{\text{minimize}} && f(\mathbf{P}) \\
 & \text{subject to} && \\
 & G_i(\mathbf{P}) = 0, && i = 1, \dots, m_e \\
 & G_i(\mathbf{P}) \leq 0, && i = m_e + 1, \dots, m \\
 & \mathbf{P}_l \leq \mathbf{P} \leq \mathbf{P}_u
 \end{aligned} \tag{3.1}$$

where \mathbf{P} is an n dimensional vector of design parameters, $f(\mathbf{P})$ is the objective function, $f : \mathbb{R}^n \rightarrow \mathbb{R}$, and the vector function $\mathbf{G} : \mathbb{R}^n \rightarrow \mathbb{R}^m$ returns a vector of length m containing the values of the equality and inequality constraints evaluated at \mathbf{P} .

Optimization techniques are used to find the design parameters vector,

$\mathbf{P} = (P_1, P_2, \dots, P_n)$, that can in some way be defined as optimal. In a simple case this might be the minimization or maximization of some system characteristic that is dependent on \mathbf{P} . In a more advanced formulation the objective function, $f(\mathbf{P})$, to be minimized or maximized, might be subject to constraints in the form of equality constraints, $G_i(\mathbf{P}) = 0$ ($i = 1, \dots, m_e$); inequality constraints, $G_i(\mathbf{P}) \leq 0$ ($i = m_e + 1, \dots, m$); and/or parameter bounds, $\mathbf{P}_l, \mathbf{P}_u$.

3.3 Direct Search

Direct search algorithms can be used for problems that are difficult to be solved with traditional optimization techniques, including problems that are not well defined or are difficult to model mathematically. They can be also used when the objective function is discontinuous, highly nonlinear, stochastic, or has unreliable or undefined derivatives.

In general, direct search algorithms are called the generalized pattern search (GPS) algorithms or the MADS algorithms. Both are pattern search algorithms that compute a sequence of points that get closer and closer to the optimal point. At each step, the algorithm searches a set of points, called a mesh, around the current point (the point computed at the previous step of the algorithm). The mesh is formed by adding the current point to a scalar multiple of a set of vectors called a pattern. If the pattern search algorithm finds a point in the mesh that improves the objective function at the current point, the new point becomes the current point at the next step of the algorithm.

MADS algorithms are a modification of the GPS algorithm. The algorithms differ in how the set of points forming the mesh is computed. The GPS algorithm uses fixed direction vectors, whereas the MADS algorithms use a random selection of vectors to define the mesh.

3.3.1 The MADS algorithm

The MADS class of algorithms, introduced in [24], is designed for nonsmooth optimization problems. The convergence analysis of MADS ensured necessary optimality conditions of the first [24] and second [81] orders under certain assumptions.

A general optimization problem (3.1) may be stated as,

$$\min_{\mathbf{P} \in X} CF(\mathbf{P}) \quad (3.2)$$

$$X = \{\mathbf{P} \in \mathbb{R}^n \mid G_i(\mathbf{P}) \leq 0, i = 1, 2, \dots, m, \mathbf{P}_l \leq \mathbf{P} \leq \mathbf{P}_u\} \quad (3.3)$$

where, $CF : \mathbb{R}^n \rightarrow \mathbb{R} \cup \{+\infty\}$, $\mathbf{G} : \mathbb{R}^n \rightarrow \mathbb{R}^m$, and $\mathbf{P}_l \in (\{-\infty\} \cup \mathbb{R})^n$ and $\mathbf{P}_u \in (\mathbb{R} \cup \{+\infty\})^n$. Each iteration k of the MADS algorithm is characterized by two steps. First, an optional search step over the space of variables is carried out, as long as it is a finite process and all trial points lie on a mesh. If no better point is found or no global search is used, the algorithm goes to a mandatory local exploration step (mandatory because it ensures convergence). Second is the poll step, at most $2n$ trial mesh points near the incumbent solution are selected (the poll set) and evaluated. If no better neighbor is found, the mesh is refined.

If an improved mesh point $\mathbf{P}_{k+1} \in X$ is found, the mesh is kept the same or coarsened, and then \mathbf{P}_{k+1} is the next incumbent. The exploration directions vary at each iteration, and become dense with probability 1. This is the main difference between the pattern search and MADS algorithms. General constraints are handled with a barrier approach, which redefines the objective as in the equation below.

$$CF_X = \begin{cases} CF(\mathbf{P}) & \text{if } \mathbf{P} \in X \\ +\infty & \text{otherwise} \end{cases} \quad (3.4)$$

Then, MADS is applied to the unconstrained barrier problem

$$\min_{\mathbf{P}} CF_X(\mathbf{P}) \quad (3.5)$$

The feasible region X can be nonlinear, non-convex, non-differentiable, or disjoint. There are no hypotheses made on the domain, except that the initial point must be feasible. The convergence results depend on the local smoothness of CF (and not CF_X , which is obviously discontinuous on the boundary of X). They also depend on the tangent cone at the limit point produced by the algorithm.

3.3.2 Description of MADS algorithm

A general and flexible algorithmic framework for MADS was proposed in [24]. This general framework is then specialized to a specific algorithmic implementation. The main steps of the algorithm are summarized as follows, and in more details in the Appendix A.

- *Initialization*

The user defines the starting point and the initial mesh size.

The algorithm initializes other parameters for subsequent steps.

- *Quest for an improved mesh point*

Global search (optional): evaluation of CF over a finite subset of points defined by

the mesh;

Local poll (mandatory): definition of a poll set and evaluation of CF over points in that set.

- *Parameters update*

Parameters are updated.

- *Termination*

If some stopping criterion is reached, stop; if not, go back to step 2.

3.4 Optimization Model

The power optimization model is formulated as follows. The output of this model is the optimal configuration of a MG taking into account the technical performance of supply options, locally available energy resources, load demand characteristics, environmental costs, start-up costs, daily purchased-sold power tariffs, and operating and maintenance costs.

Figure 3.1 illustrates the optimization model, where its inputs are:

- The power demand by the load.
- Data about locally available energy resources: These include solar irradiation data (W/m^2), temperature ($^{\circ}C$), wind speed (m/s), as well as cost of fuels (\$/liter) for the DG and natural gas price for supplying the FC and MT (\$/kW).
- Daily purchased and sold power tariffs in (\$/kWh).
- Start-up costs in (\$/h).
- Technical and economic performance of supply options: These characteristics include, for example, rated power for PV, power curve for WT, fuel consumption characteristics of DG, MT and FC.
- Operating and maintenance costs and emission factors: Operating and maintenance costs must be given (\$/h) for all emissions; emission factors must be given in kg/h for DG, FC, and MT

3.5 Proposed Objective Functions

A major concern in the design of an electrical system that utilizes MG sources is the accurate selection of output power. The power economically satisfies the load demand, while taking into account the environmental externality costs by minimizing the emissions of oxides of nitrogen (NO_x), sulfur oxides (SO₂), and carbon oxides (CO₂). In this section, different scenarios of the MG operation are considered. These scenarios are:

Scenario 1: The MG is considered to be working in an islanding condition with no battery storage in the MG, with power balance and power generation constraints.

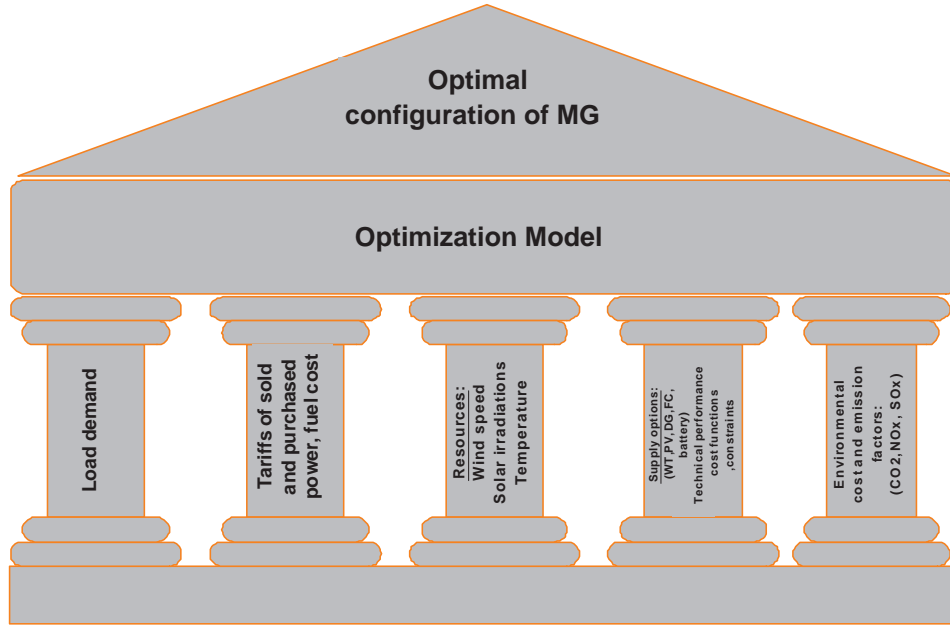


Figure 3.1: The Optimization Model.

Scenario 2: Again the islanding condition is considered, with a battery storage. Furthermore, more constraints are added to reflect some of the behavior which can be found in the MG.

Scenario 3: The MG is considered to be connected to the upper grid, taking into account the battery storage and the constraints in the pervious two Scenarios. The following subsections describe how these Scenarios are implemented in detail.

In power balance constraints, the line loss is not considered here as it is quite small and could be neglected.

3.5.1 Scenario 1

The proposed cost function for a MG serving an isolated load demand is given in the following form [82]:

$$CF(\mathbf{P}) = \sum_{i=1}^N (C_i \times F_i(P_i) + OM_i(P_i)) + \sum_{i=1}^N \sum_{k=1}^M \alpha_k (EF_{ik} P_i) \quad (3.6)$$

where

C_i	Fuel costs of generating unit i ,
$F_i(P_i)$	Fuel consumption rate of generator unit i .
$OM_i(P_i)$	Operation and maintenance cost of generating unit i ,
P_i	Decision variables, representing the power output from generating unit i ,
$\mathbf{P} = (P_1, P_2, \dots, P_N)$	Decision variable vector,
α_k	Externality costs of emission type k ,
EF_{ik}	Emission factor of generating unit i and emission type k ,
N	Number of generating units i ,
M	Emission types (NOx or CO ₂ or SO ₂).

The solution of the optimization procedure produces the optimal decision variables:

$$\{P_i = P_{FC_i}, P_j = P_{MT_j}, P_k = P_{DG_k} : i = 1, \dots, N_1; j = N + 1, \dots, N_2; k = N_2 + 1, \dots, N\}.$$

where

P_{FC_i} : Output power of fuel cell i [kW], $i = 1, \dots, N_1$,

P_{MT_j} : Output power of microturbine j [kW], $j = N + 1, \dots, N_2$

P_{DG_k} : Output power of diesel generator k [kW], $k = N_2 + 1, \dots, N$

In equation (3.6), the expressions for different $F_i(P_i)$'s are found in equations (2.6), (2.28) and (2.41). Expression for $OM_i(P_i)$ is given in equation (3.13).

Objective Constraints:

Power balance constraints: The total power generation must cover the total load demand. Hence

$$\sum_{i=1}^N P_i = P_L - P_{PV} - P_{WT} \quad (3.7)$$

where

$\sum P_i$ Total power generation [kW],

P_L Power demanded by the load [kW],

P_{PV} Output power of the photovoltaic [kW],

P_{WT} Output power of the wind turbine [kW].

Generation capacity constraints: For stable operation, real power output of each power generator is restricted by lower and upper limits as follows:

$$P_i^{\min} \leq P_i \leq P_i^{\max}, \quad \forall i = 1, \dots, N \quad (3.8)$$

where

P_i^{\min} Minimum operating power of unit i ,

P_i^{\max} Maximum operating power of unit i .

3.5.2 Scenario 2

In this Scenario a battery storage is added to the system and more constraints are considered in the objective function to obtain a more realistic model. The total power generation to cover the total load demand becomes [83]:

$$\sum_{i=1}^N P_i = P_L - P_{PV} - P_{WT} - P_{batt} \quad (3.9)$$

where:

$\sum P_i$ Total power generation [kW],

P_L Power demanded by the load [kW],

P_{PV} Output power of the photovoltaic [kW],

P_{WT} Output power of the wind turbine [kW],

P_{batt} Output power of the battery [kW].

Where the start-up cost and the max and min stop time constraints are included, the

cost function will take the form:

$$CF(\mathbf{P}) = \sum_{i=1}^N (C_i \times F_i(P_i) + OM_i(P_i) + STC_i) + \sum_{i=1}^N \sum_{k=1}^M \alpha_k (EF_{ik} P_i) \quad (3.10)$$

where

STC_i is the start-up cost in \$/h given in equation (3.12). Each generating unit has a minimum up/down time limit (MUT/MDT). Once the generating unit is switched on, it has to operate continuously for a certain minimum time before switching it off again. On the other hand, a certain stop time has to be terminated before starting the unit. A violation of such constraints can cause shortness in the life-time of the unit. These constraints are formulated as continuous run/stop time constraints as follows [84]:

$$\begin{cases} (T_{t-1,i}^{on} - MUT_i)(u_{t-1,i} - u_{t,i}) \geq 0 \\ (T_{t-1,i}^{off} - MDT_i)(u_{t,i} - u_{t-1,i}) \geq 0 \end{cases} \quad (3.11)$$

$T_{t-1,i}^{off}/T_{t-1,i}^{on}$ is the unit off/on time, while $u_{t,i}$ denotes the unit off/on $[0, 1]$ status.

The generator start-up cost depends on the time the unit has been off prior to a start-up. The start-up cost in any given time interval can be represented by an exponential cost curve:

$$STC_i = \sigma_i + \delta_i \left[1 - \exp\left(\frac{-T_{off,i}}{\tau_i}\right) \right] \quad (3.12)$$

where, σ_i is the hot start-up cost, δ_i the cold start-up cost, τ_i the unit cooling time constant and $-T_{off,i}$ is the time a unit has been off.

The operating and maintenance costs refer to the electricity output [7]. They are assumed to be proportional with the produced power and therefore the total costs are:

$$OM = \sum_{i=1}^N OM_i(P_i) = \sum_{i=1}^N K_{OM_i} P_i \quad (3.13)$$

where the proportionally constant is K_{OM_i} for each generating unit. The values of K_{OM} for different types of generation units are as follows [85]: $K_{OM_1} = K_{OM}(DG) = 0.01258$ \$/kWh, $K_{OM_2} = K_{OM}(FC) = 0.00419$ \$/kWh and $K_{OM_3} = K_{OM}(MT) = 0.00587$ \$/kWh.

For a stable operation of the MG, a number of the starts and stops ($\varepsilon_{start-stop}$) should not exceed a certain number (N_{max}).

$$\varepsilon_{start-stop} \leq N_{max} \quad (3.14)$$

3.5.3 Scenario 3

As shown in Figure 1.1, the main utility balances the difference between the load demand and the generated output power from the microsources. Therefore, there is a cost to be paid for the purchased power whenever the generated power is insufficient to cover the

Table 3.1: Externality costs and emission factors for NO_x, SO₂, and CO₂.

Emission Type	Externality costs	Emission factors	Emission factors	Emission factors
	\$/lb	for DG lb/MWh	for FC lb/MWh	for MT lb/MWh
NO _x	4.2	21.8	0.03	0.44
SO ₂	0.99	0.454	0.006	0.008
CO ₂	0.014	1.432	1.078	1.596

load demand. On the other hand, there is income due to the sold power when the power generated is more than the load demand but the price of the sold power is lower than the purchased power tariff. It is possible that there will be no sold power at all. Therefore, to model the purchased and sold power, two different conditions are considered. These conditions are defined in the form [21]:

$$\begin{aligned} DCPE_i &= C_p \times \max(P_L - \sum P_i, 0) \\ IPSE_i &= C_s \times \max(\sum P_i - P_L, 0) \end{aligned} \quad (3.15)$$

where C_p and C_s are the tariffs of the purchased and sold power respectively in (\$/kWh). Then the cost function takes the form:

$$CF(\mathbf{P}) = \sum_{i=1}^N (C_i \times F_i(P_i) + OM_i(P_i) + STC_i + DCPE_i - IPSE_i) + \sum_{i=1}^N \sum_{k=1}^M \alpha_k (EF_{ij} P_i) \quad (3.16)$$

where

$DCPE_i$ Daily purchased electricity if the load demand exceeds the generated power in \$/h,

$IPSE_i$ Daily income for sold electricity if the output generated power exceeds the load demand in \$/h.

This Chapter considers the effect of the environmental externalities, including NO_x, SO₂ and CO₂, on the per \$/h cost of power supply solutions. The total discounted cost of environmental externalities is calculated by multiplying the estimated discounted externality cost by the emission factor of each power generating technology, and by the total power generated by microsourses. Externality costs and emission factors of the DG, FC, and MT used in this Chapter are stated in [27], [86], [87] and summarized in Table 3.1.

3.6 Golden Search

This method is applicable to an unconstrained minimization problem such that the solution interval $[P_{min}, P_{max}]$ for each generation unit is known and the objective function $CF(\mathbf{P})$ is unimodal within the interval; that is, the sign of its derivative CF' changes at most once in $[P_{min}, P_{max}]$ so that $CF(\mathbf{P})$ decreases/increases monotonically for $[P_{min}, P^o]/[P^o, P_{max}]$, where P^o is the solution that we are looking for. The so-called golden search procedure is summarized in [35] as:

- Step 1. Pick two points c and d , $c = P_{\min} + (1 - r)h$ and $d = P_{\min} + rh$, inside the interval $[P_{\min}, P_{\max}]$, where $r = (\sqrt{5} - 1)/2$ and $h = P_{\max} - P_{\min}$.
- Step 2. If the values of $CF(\mathbf{P})$ at the two points are almost equal [i.e., $CF(\mathbf{P}_{\min}) \approx CF(\mathbf{P}_{\max})$] and the width of the interval is sufficiently small (i.e., $h \approx 0$), then stop the iteration to exit the loop and declare $P^o = c$ or $P^o = d$ depending on whether $CF(c) < CF(d)$ or not. Otherwise, go to Step 3.
- Step 3. If $CF(c) < CF(d)$, let the new upper bound of the interval $\mathbf{P}_{\max} \leftarrow d$; otherwise, let the new lower bound of the interval $\mathbf{P}_{\min} \leftarrow c$. Then, go to Step 1.

In order to explore the minimum costs of the DG, FC, and MT, golden search technique is used for all the three cost functions individually. Figure 3.2 shows the minimization of the costs of the three cost functions. It is noticeable that the DG has the highest cost, whereas the MT has the lowest cost. The lower and upper bounds for each generator unit were as follows:

DG: $P_{\min} = 0$ Kw, $P_{\max} = 7$ Kw.

MT : $P_{\min} = 0$ kW, $P_{\max} = 4$ Kw.

FC: $P_{\min} = 0$ Kw, $P_{\max} = 4$ Kw.

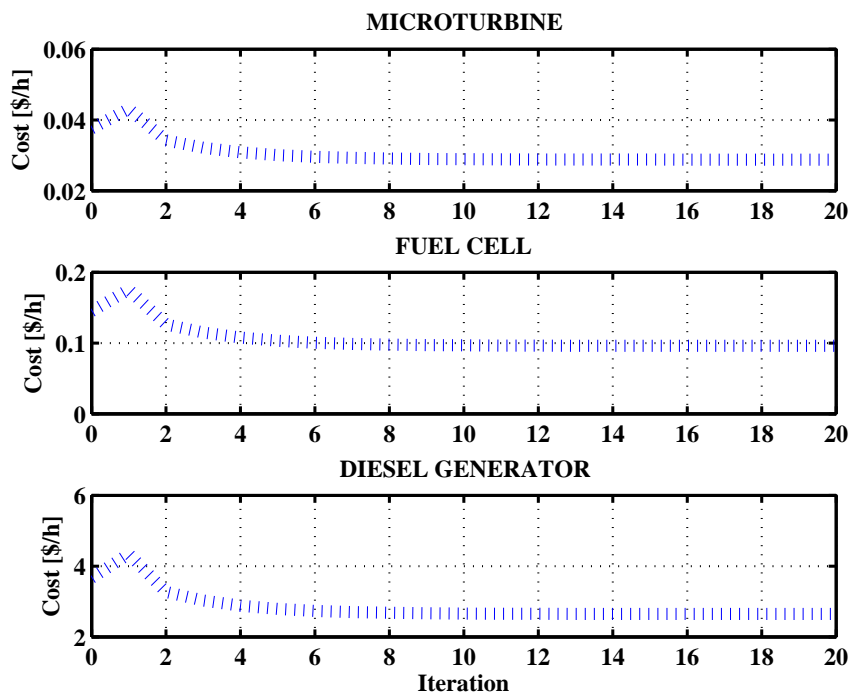


Figure 3.2: Minimization of the MT, FC, and DG costs.

3.7 Implementation of the Optimization Algorithm

When designing MGs, several goals could be set, including reduction in emissions and generation costs. To achieve this, it is important to highlight all factors influencing the main goal. The following items summarize the key characteristics of the implemented strategy:

- Power output of WT is calculated according to equation (2.52) with measured wind speed data depicted in Figure 3.3.
- Power output of PV is calculated according to equation (2.59) with measured temperature and solar radiation data as shown in Figures 3.4 and 3.5, respectively .
- It is assumed that WT and PV deliver free cost power (in terms of running as well emission free). The output powers are then treated as negative loads.
- The power from the battery is needed whenever the PV, WT are insufficient to serve the load , meanwhile the charge and discharge of the battery is monitoring.
- Calculate the unmet load that can not served by WT,MT and battery storage.
- Choose serving the load by other sources (FC or MT or DG) according to the objective functions.
- If the output power is not enough then purchase power from the main gird, and if the output power is more then the load demand sell the exceed power to the main grid

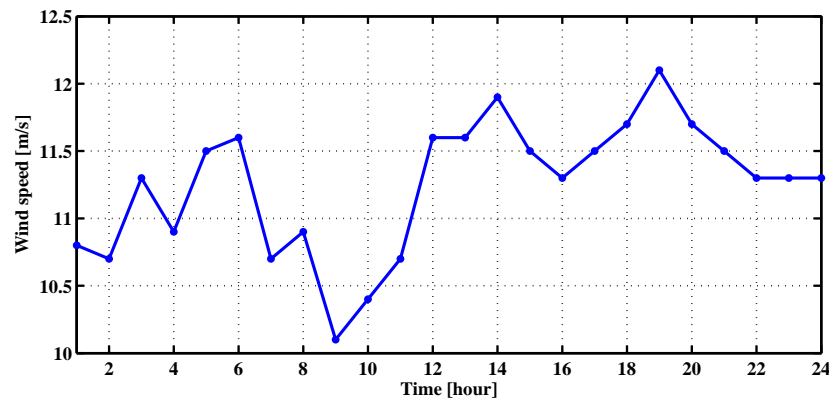


Figure 3.3: The input wind speed to the model.

3.8 Results and Discussions

The optimization model described in Section 3.4 is applied where the load demand is shown in Figure 3.6 which is rescaled from [88] and [89]. The load varying between 4 kW to 14 kW. The available power from the PV and the wind generators are used first. The result obtained by applying the three Scenarios are given next:

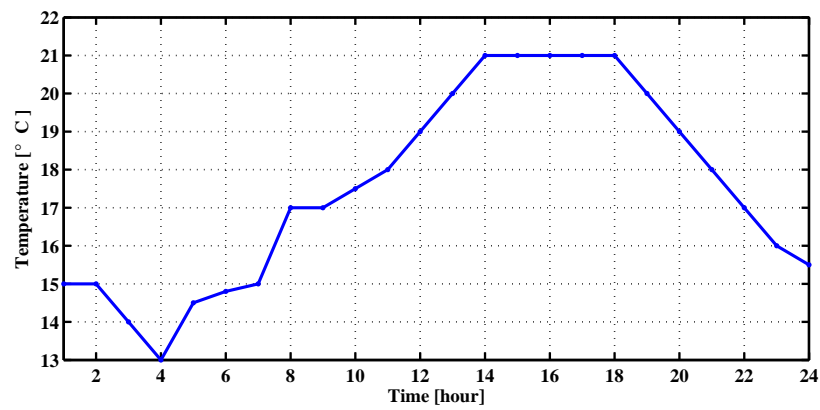


Figure 3.4: The input temperature data to the model.

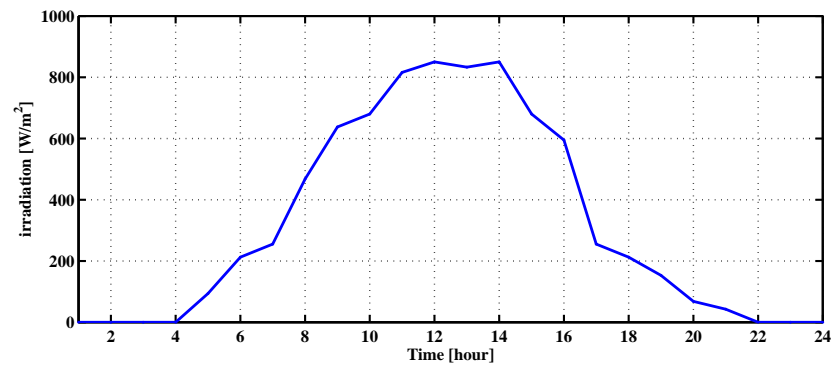


Figure 3.5: The input irradiation data to the model.

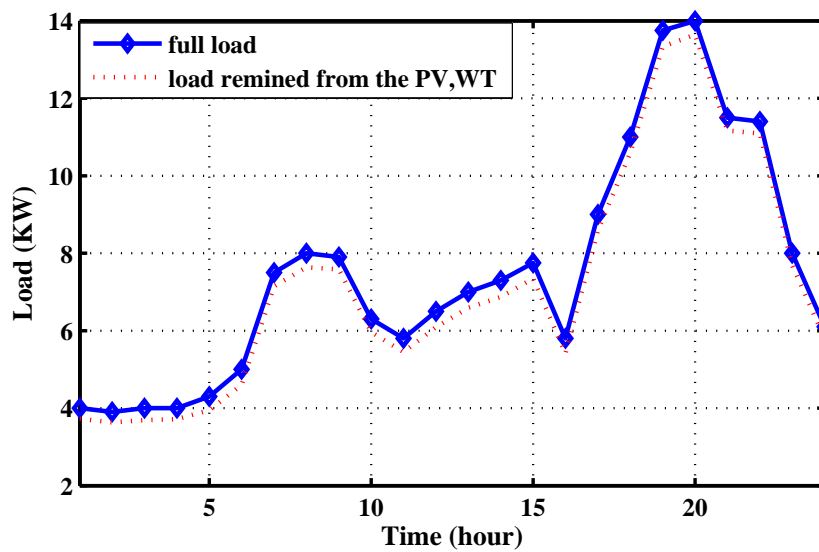


Figure 3.6: Hourly load.

3.8.1 Scenario 1

Table 3.2, Figures 3.7 and 3.8 show the optimal setting and the total cost of the MG per day for Scenario 1 in both methods (SQP and MADS). These curves are plotted against time. It is observed from the figures that the load demand is satisfied with the three available sources, and the DG is the last preferable source as it has the highest operating cost. In

Table 3.2: Total Optimal Generation and Total Cost of the MG Scenario 1

Total load Demand (kW/Day)	Optimal Generation (kW/Day)		Total Cost (\$/Day)	
	SQP	MADS	SQP	MADS
171.2924	171.2924	171.2928	28.6813	28.7460

Table 3.2 the total cost of the MG found using the MADS technique is \$ 28.7460 , which is almost the same as for the SQP technique \$ 28.6813. This is a very small difference as seen in Fig 3.9. Figures 3.10 to 3.12 show the contribution of the fuel cost, operation and maintenance cost, and the emission cost to the total cost. It can be seen that the fuel cost assumes major part of the total cost.

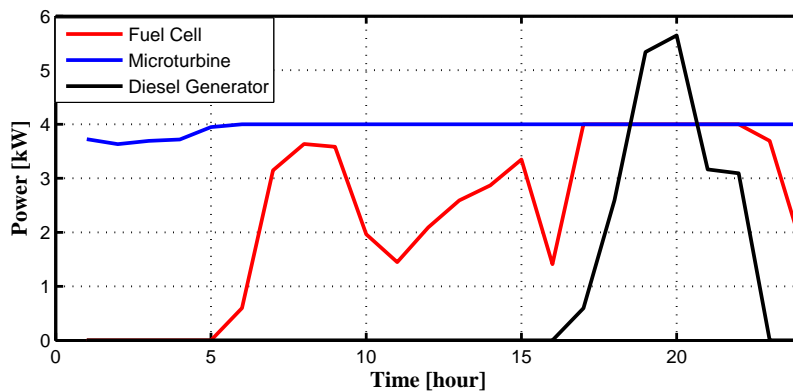


Figure 3.7: The hourly power curves using SQP scenario 1.

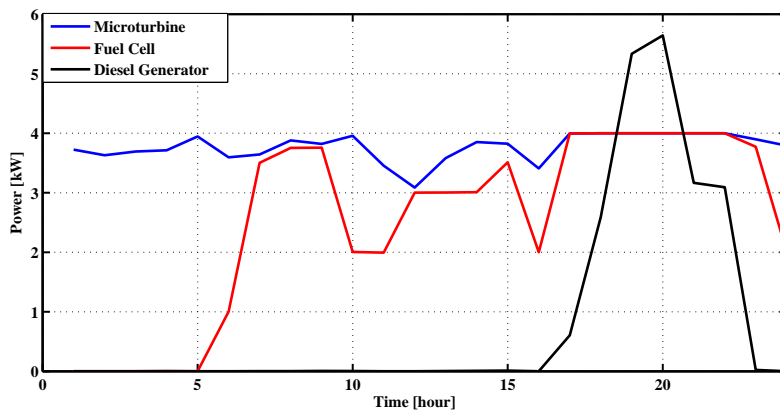


Figure 3.8: The hourly power curves using MADS scenario 1.

Due to low operating cost of MT, it is noticeable that the MT supplies its maximum or near maximum power for prolonged periods within the day. Therefore, it is adequate to

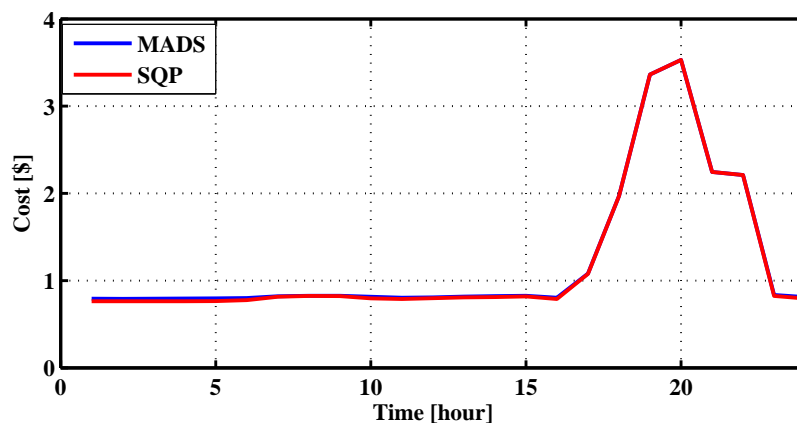


Figure 3.9: Hourly total cost of the microgrid using 2 different technique scenario 1.

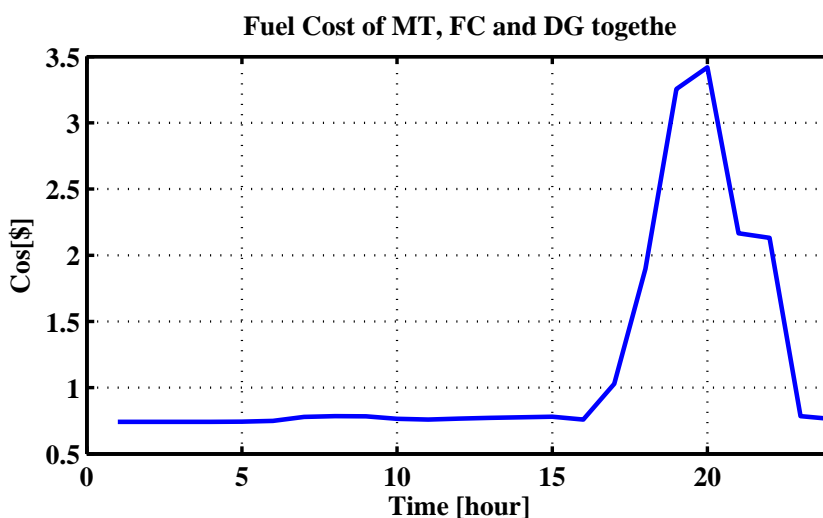


Figure 3.10: Hourly fuel costs of the microgrid scenario 1.

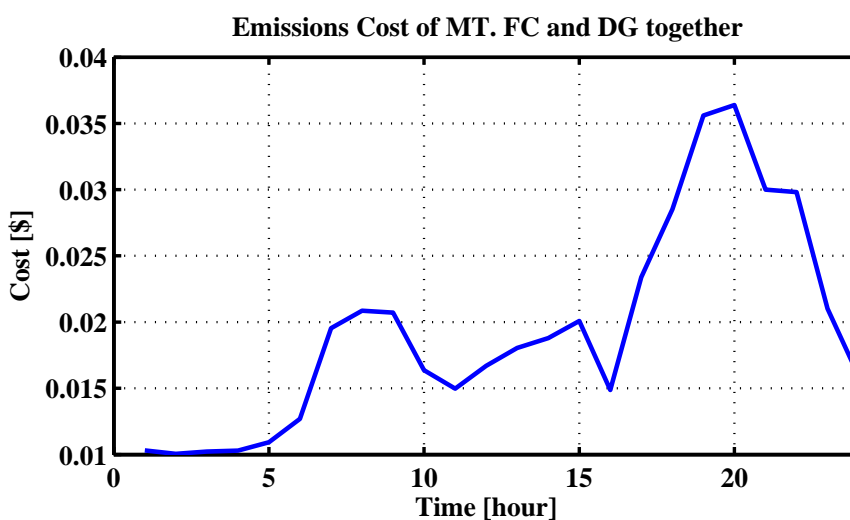


Figure 3.11: Hourly emission costs of the microgrid scenario 1.

investigate whether the utilization of smaller identical units with total equivalent capacity would be more economical regarding the operating costs. In this case, one unit is used when low power is to be supplied and the other units are added when required.

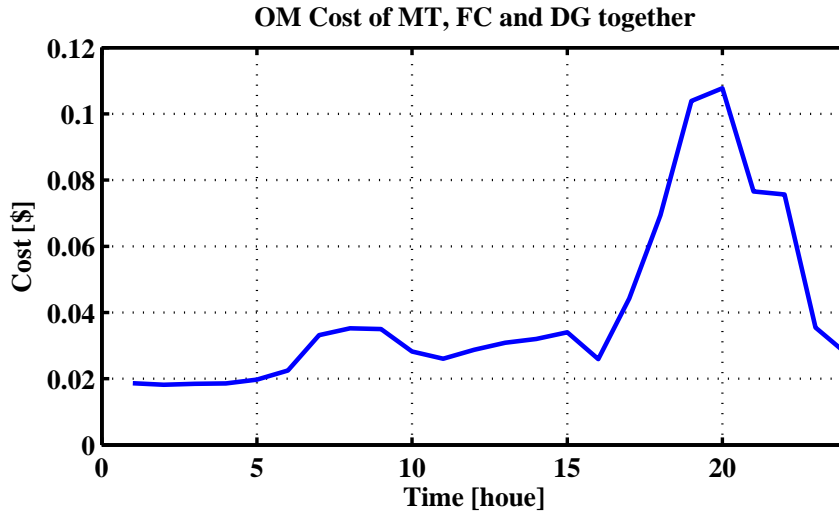


Figure 3.12: Hourly OM cost of the microgrid scenario 1.

A combined algorithm of the two techniques can be used together, as MADS alone was not sufficient to find the minimum. The idea is to use the SQP method first. The optimal generation variable is used then as a starting point to search for optimal solution with MADS method. After applying the proposed procedure, the same results are reached as obtained with SQP.

3.8.2 Scenario 2

In this Scenario, the results are different as more constraints and a battery storage are added to the MG system. From the results obtained, it can be seen that the algorithms acted very well in meeting the load demand but they had a different distribution of the power on the sources. Furthermore, the effect of the battery is very small as just one battery unit (PVX-340 battery,33AH, 12 v) is used in the system. The controller of the SOC met the design requirement desired, in which the battery has to be fully charged at the end of the day.

The results illustrated in Table 3.3, Figures 3.13 and 3.14 show that the MADS optimization technique has made as good a selection of the power of the microsources as the SQP to meet the changes in the load in minimum cost. The total cost per day is shown in Fig 3.15 and Table 3.3. It can be seen that the total cost is 47.7148 \$ using the SQP, while it is decreased to 44.6829 \$ using the MADS method. It is also noticed that the repeti-

Table 3.3: Total Optimal Generation and Total Cost of the MG Scenario 2

Total load Demand (kW/Day)	Optimal Generation (kW/Day)		Total Cost (\$/Day)	
	SQP	MADS	SQP	MADS
171.4009	171.4009	171.4013	47.7148	44.6829

tive start/stop cycles of each microsource causes a higher daily operating cost compared to Scenario 1. This is also due to the associated start-up cost STC. The priority is always given to the lowest operating cost of continuous running or, in a few cases, for the complete shut down of the highest costs. In MADS, the optimal scenario is to run

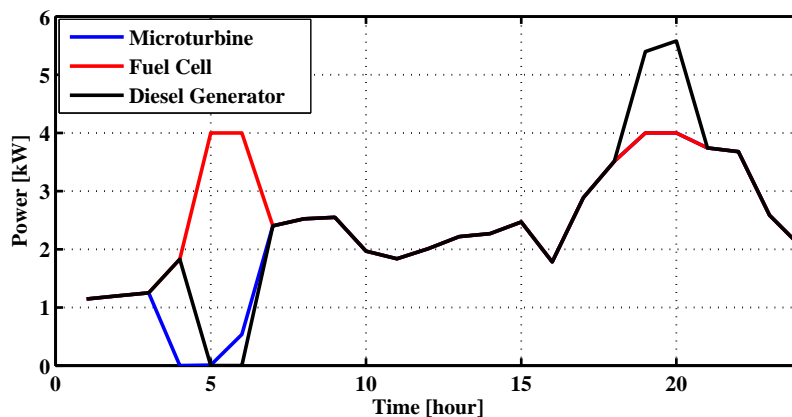


Figure 3.13: The hourly power curves using SQP Scenario 2.

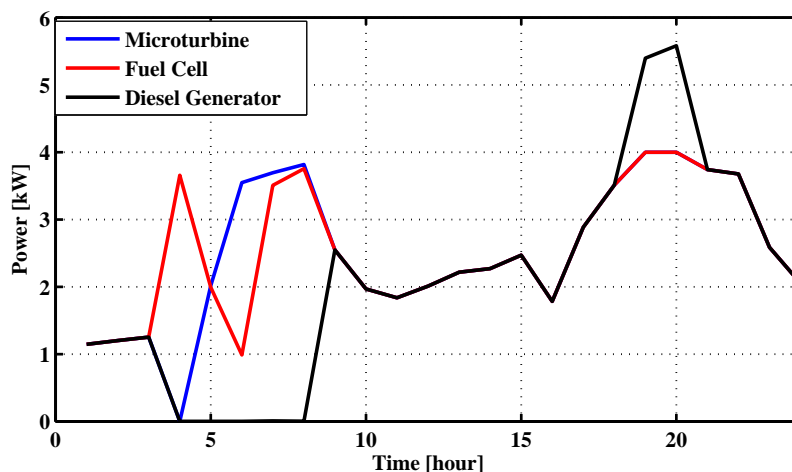


Figure 3.14: The hourly power curves using MADS Scenario 2.

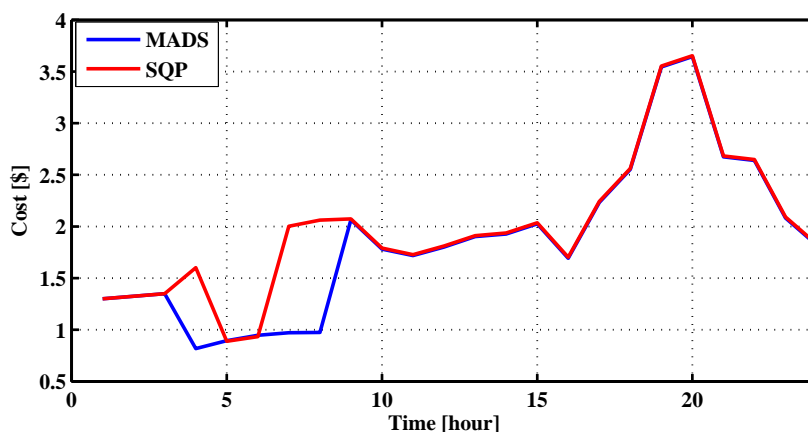


Figure 3.15: Hourly total cost of the microgrid using 2 different technique Scenario 2.

MT continuously for a certain time period and then to switch it off for a short time as shown in Figure 3.14. On the other hand, the DG is kept off for a longer time and is only switched on when the peak load occurs (Fig. 3.6) . Therefore, the constraint, which limits the start/stop cycles below a certain number as in equation (3.14), is always inactive since this situation cannot be avoided in the case of MT.

3.8.3 Scenario 3

Figures 3.16-3.19 show the effect of varying sold tariffs on the operation of the MG for the applied load demand of both algorithms. Let the sold tariff be \$ 0.0/kWh in Case 1 and 0.12/kWh in Case 2, while the purchased tariff is kept constant at \$ 0.16/kWh for both cases. Again the same optimization methods (SQP and MADS) are applied. Furthermore, Figures 3.20 and 3.21 show the sold and purchased power of the two cases above of the MG when the SQP and MADS methods are used.

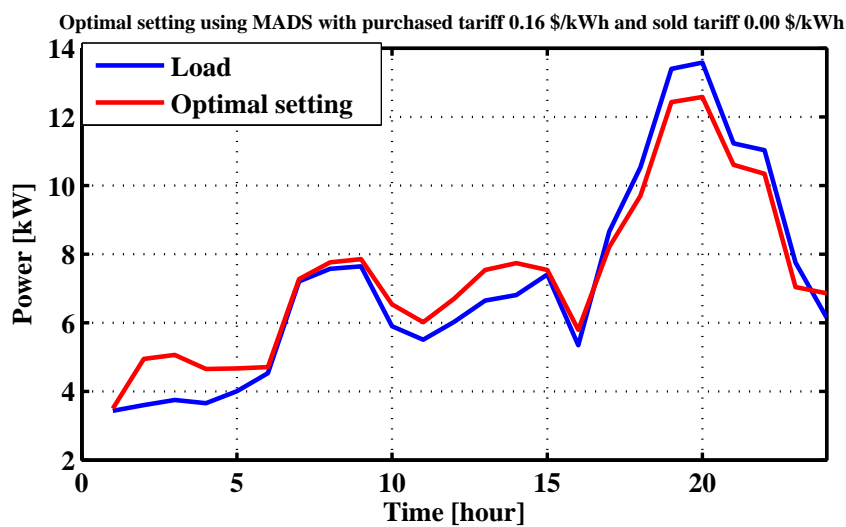


Figure 3.16: Effect of sold power tariff on the MG optimal operation Scenario 3.

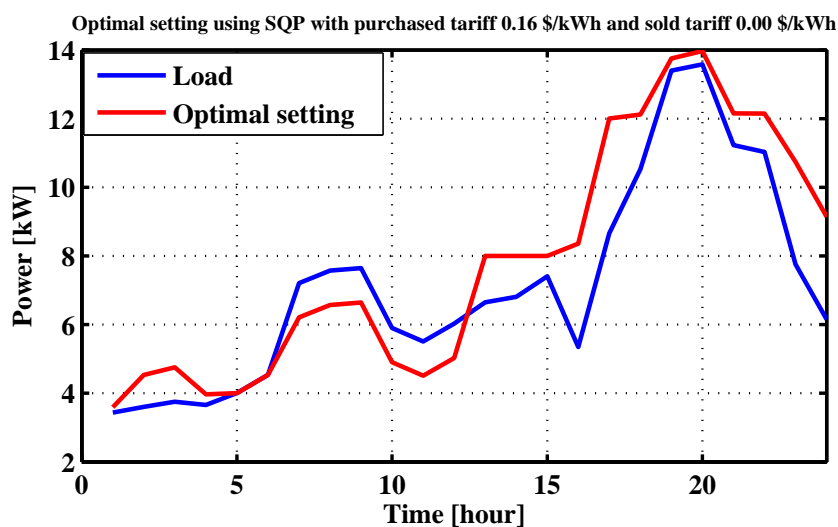


Figure 3.17: Effect of sold power tariff on the MG optimal operation Scenario 3.

In the first case, Figure 3.20 shows that no power is sold back to the main grid. In the second case with SQP, the MG produces more power to cover the load and the excess power is sold back for \$ 0.12/kWh. In Figures 3.21 and 3.23 MADS is applied to the same

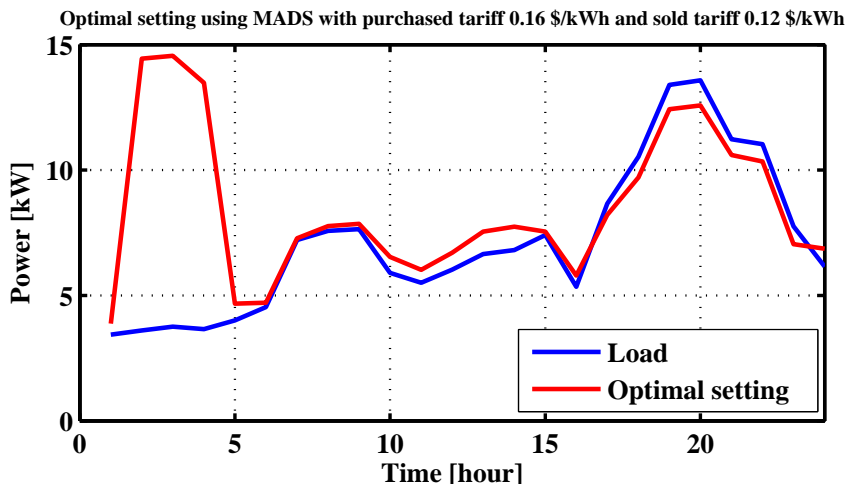


Figure 3.18: Effect of sold power tariff on the MG optimal operation Scenario 3.

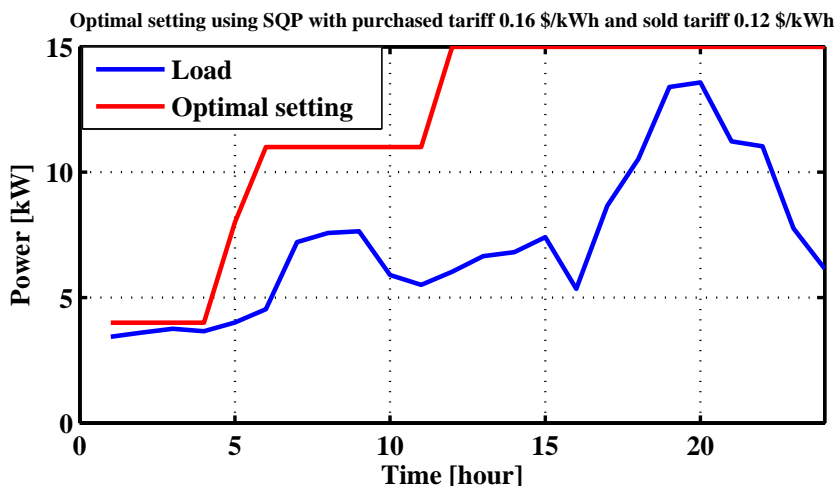


Figure 3.19: Effect of sold power tariff on the MG optimal operation Scenario 3.

optimization problem. It can be seen that the effect of changing the sold tariffs is very clear compared to the SQP method.

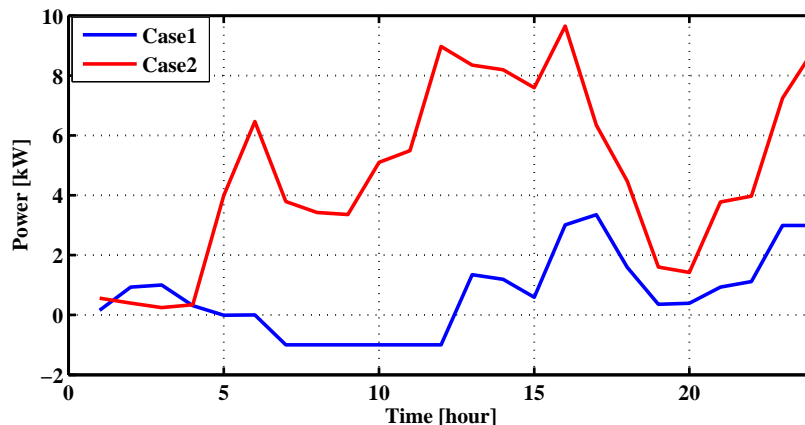


Figure 3.20: Sold and purchased power using SQP method and Scenario 3.

Figure 3.22 illustrates the total cost in the two cases using the SQP method. It is quite evident that the algorithm failed to meet reducing the cost as the selected power option

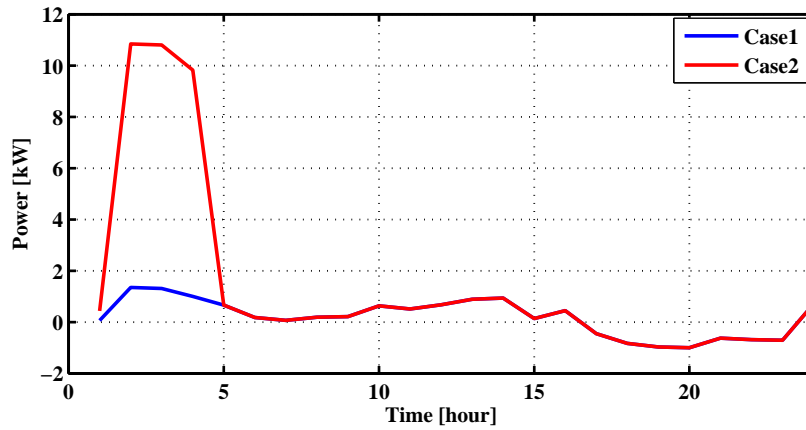


Figure 3.21: Sold and purchased power using MADS method and Scenario 3.

was at maximum. The total cost was 80.8576 \$ in Case 1 and 120.8424 \$ in case 2. The total cost of the MG using MADS method for Case 1 and Case 2 is shown in Fig 3.23. In Case 1 the total cost is 79.0752 \$ while in Case 2 it is 83.9106 \$ which is less than in Scenario 2. Using the MADS method, the total cost is reduced compared to the SQP method.

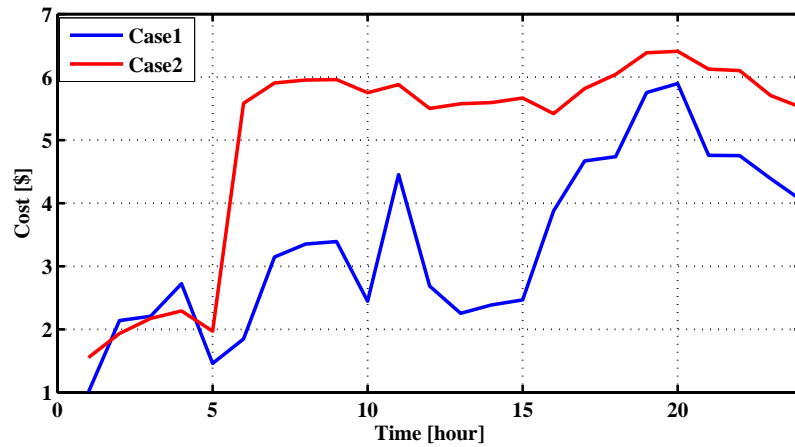


Figure 3.22: Cost per day using SQP method and Scenario 3.

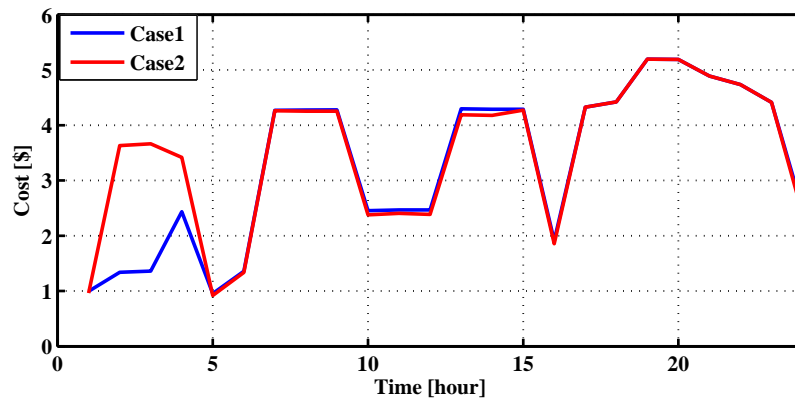


Figure 3.23: Cost per day MADS method and Scenario 3.

Figures 3.24 to 3.27 show the effect of varying purchase tariffs on the operation of the MG with purchase tariff \$ 0.12/kWh in Case 3 and 0.16/kWh in Case 4, while the sold tariff is kept constant at \$ 0.07/kWh for both cases.

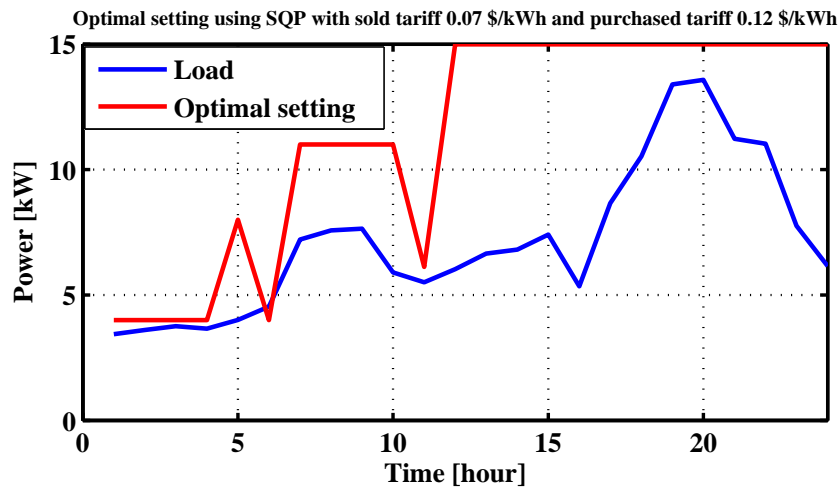


Figure 3.24: Effect of purchased power tariff on the MG optimal operation Scenario 3

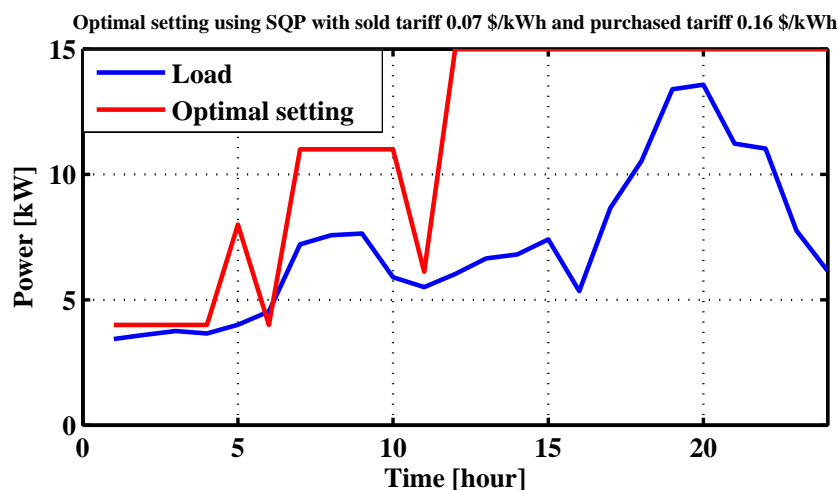


Figure 3.25: Effect of purchased power tariff on the MG optimal operation Scenario 3

Figures 3.28 and 3.29 show the effect of changing the purchased tariffs on the sold and purchased power as well the effect on the total cost per day. The MADS algorithm has a better output for minimizing the total cost, with a better of compromise between the sold and purchased power.

Table 3.4 summarizes the four cases applied in Scenario 3. It can be seen that in the last two cases when the purchase tariffs are changed and the sold tariffs are kept constant, this has no effect on the optimal setting of the MG when MADS method is applied. The same situation occurs when the SQP is applied to the problem. However, using SQP results in a higher cost compared to MADS method.

The proposed approach is general in the sense that multiple fuels, multiple pollutants and a highly non-linear cost function can be dealt with. The effectiveness of the approach has been demonstrated in all three different scenarios.

The total electrical output power from the three microsources together for MADS is simi-

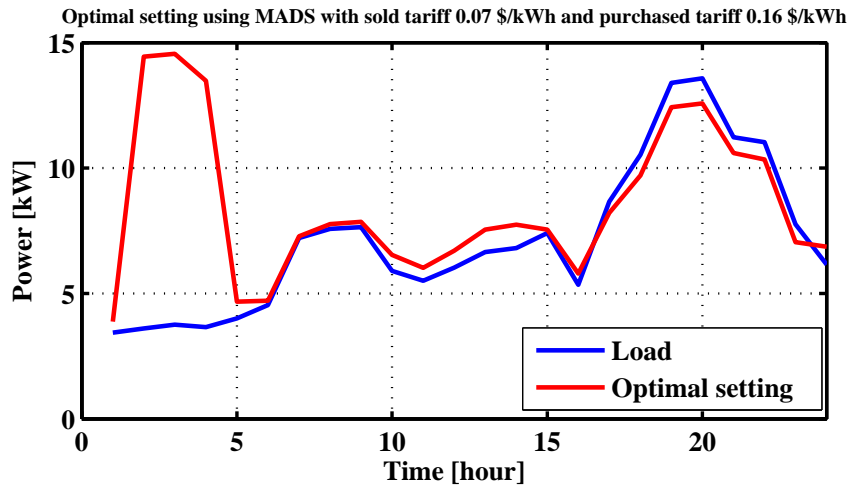


Figure 3.26: Effect of purchased power tariffs on the MG optimal operation Scenario 3

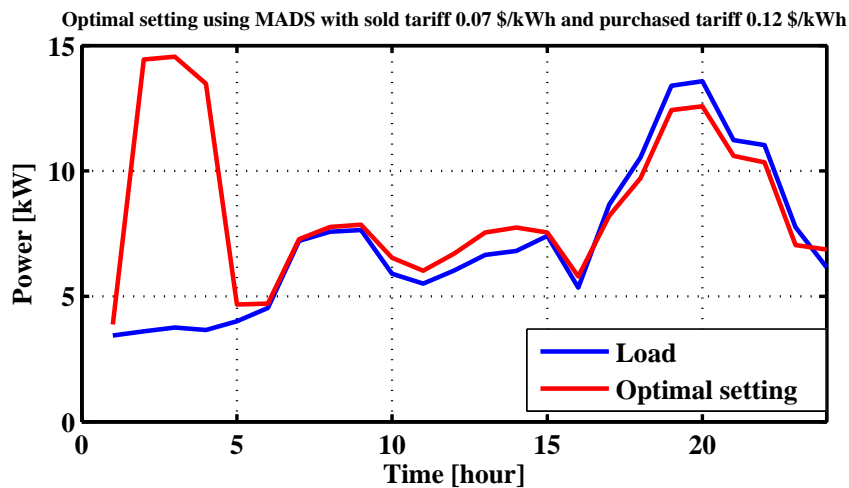


Figure 3.27: Effect of purchased power tariff on the MG optimal operation Scenario 3

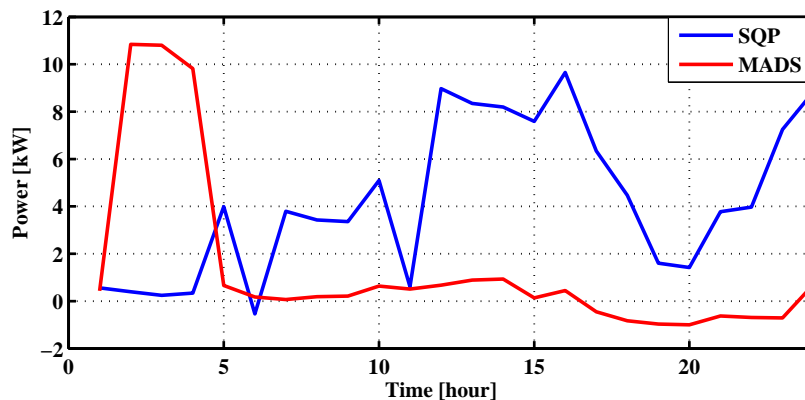


Figure 3.28: Sold and purchased power using SQP and MADS methods and Scenario 3.

lar in the last three cases. However, the contributions from individual units vary depending on the load, the operating tariffs and the operating cost of each one. In some cases, one or two units are not used for a long time. In other cases, one or two units are used only for short periods, particularly at peak-load time, as shown in Figures 3.24 to 3.27. Switching on one or two units increases the total operating cost as a result of the start-up

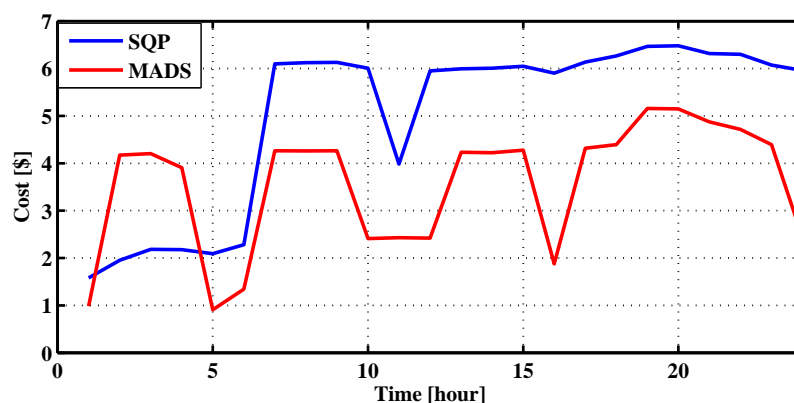


Figure 3.29: Total cost per day using SQP, MADS methods and scenario 3.

Table 3.4: Total Optimal Generation and Total Cost of the MG Scenario 3

	P_L (kW/Day)	C_p (\$/kWh)	C_s (\$/kWh)	Total Cost (\$/Day)		Optimal Generation (kW/Day)	
				SQP	MADS	SQP	MADS
Case 1	171.4009	0.16	0.00	80.8576	79.0752	187.6473	176.1020
Case 2	171.4009	0.16	0.12	120.8424	83.9106	285.0000	204.2817
Case 3	171.4009	0.12	0.07	120.5106	85.6072	273.1226	204.2817
Case 4	171.4009	0.16	0.07	120.5220	85.7750	273.1226	204.2817

costs. In addition, utilization of three units in parallel results in operating the units at lower efficiencies compared to a single unit since they generate a higher percentage of power based on their ratings. The result from MADS in Scenario 3 reflects the high accuracy of finding the minimum and ensures the efficient capability of the MADS to extract the features of the optimal performance.

The MADS outputs show good performance to meet the load demand, which demonstrates the capability of the MADS and the effectiveness of the presented approach. It is expected that using more constraints such as the starting cost leads to a significant increase in the operating cost compared to Scenario 1.

The average optimal daily operating cost using MADS is about 83.5920\$/day depending on the four cases in Scenario 3. This value increases to 110.6832 \$/day if the SQP method is used. These results reflect the success of the MADS to capture the optimal behavior of the MG with high accuracy even with new four different cases. Table 3.4 compares the total daily operating costs when the MADS is used to minimize the total cost of the MG with the SQP considering the optimal settings for the four investigated cases.

Generally, the MADS approach can be applied to provide a simple and effective optimization technique for MG management and also other distributed generation sources in the online mode with a high accuracy.

3.9 Conclusions.

The optimization problem includes a variety of energy sources that are likely to be found in a MG: a fuel cell, a diesel generator, a microturbine, a photovoltaic cell, and a wind generators. Constraint functions are added to the optimization problem to reflect some of the additional considerations which are often found in a small-scale generation system. From the results obtained, it is clear that the optimization works very well and assigns optimal power to the generators after taking into account the cost function for each of them. The effectiveness of the suggested approach is confirmed through the agreement between the optimized settings and the output from the algorithm. The responses are effected by several variables including weather conditions, emissions operation and maintenance costs, sold and purchased tariffs, and of course, the actual power demand.

The results show the capability of the proposed system model and the proposed algorithm to achieve both reduction in the operating costs and meeting the load demand. The proposed procedure can be implemented with different loads and for periods more than one day. From the results obtained it is noticeable that the effect of changing the sold tariffs results in different optimal settings of the MG depending on the optimization technique. It is clear that the sold tariffs have more effect on the SQP method, and a smaller effect on the MADS method. Both optimization techniques made a good selection to meet the load demand. Furthermore, some constraints were found not to be active when MADS method is applied. The total cost per day was the lowest when the MADS is used in all cases.

Chapter 4

MicroGrid Online Management Using Multiobjective Optimization

4.1 Introduction

This chapter presents a generalized formulation to determine the optimal operating strategy and cost optimization scheme as well as the reduction of emissions for a MG. Multiobjective (MO) optimization is applied to the environmental/economic problem of the MG. The proposed problem is formulated as a nonlinear constrained MO optimization problem. Prior to the optimization, system model components from real industrial data are constructed. The model takes into consideration the operation and maintenance costs as well as the emission reduction of NO_x , SO_2 , and CO_2 . The optimization is aimed at minimizing the cost function of the system while constraining it to meet the customer demand and safety of the system. The results ensure the efficiency of the proposed approach to satisfy the load and to reduce the cost and the emissions in one single run.

Multiobjective (MO) optimization has a very wide range of successful applications in engineering and economics. Such applications can be found in optimal control systems [90], chemical engineering [91], engineering design [92], and communication [93]. The MO optimization is applied to find the optimal solution which is a compromise between multiple and contradicting objectives. In MO optimization we are mostly interested in the Pareto optimal set which contains all non-inferior solutions. The decision maker can then select the most preferred solution out of the Pareto optimal set. The weighted sum method is applied in this Chapter. Furthermore, the weighted sum is a simple and straightforward method to handle the MO optimization problems.

Solving the environmental/economic problem in the power generation has received considerable attention. An excellent overview on commonly used environmental/economic algorithms can be found in [15]. The environmental/economic problems have been effectively solved by goal programming [16], classical technique [17], and fuzzy satisfaction-maximizing approach [18]. The computing speed of these approaches limits their applicability in online applications. The goal here is to develop methods that improve the online applicability and efficiency.

The proposed optimization method is compared with the results obtained in [94, 95, 96]. It incorporates an explicit cost minimization criterion applied to the MG architecture as well as minimizing the emission. The formulation in this work seeks the most optimal environmental/economical generation to satisfy the load demand and the constraints. The problem is decomposed into two stages starting by building the system model. The next stage is the application of the algorithm developed. The algorithm consists of determining at each iteration the optimal use of the resources available, such as wind speed, temperature, and irradiation as they are the inputs to the model. If the produced power from the wind turbine and the photovoltaic cell is less than the load demand, then the algorithm goes to the next stage which is the use of the other alternative sources according to the load and the objective function of each one.

The second objective of this Chapter deals with solving the optimization problem considering several scenarios to explore the benefits of having optimal management of the MG. The study is based on minimizing the running costs and reducing the emissions. This is extended to cover a load demand scenario in the MG. It will be shown that by developing a good system model, the proposed problem is accurately and efficiently solved using optimization techniques.

The power optimization model is shown in Figure 4.1 highlighting the following points. The output is the optimal configuration of a MG that takes into account technical performance of supply options, locally available energy resources, demand characteristics, and environmental level. Small-scale power generating technologies under consideration include PV, WT, DG, and FC.

To run the model, the following items have to be defined:

- The power demand by the load.
- Locally available energy information: This includes solar irradiation data (W/m^2), temperature ($^{\circ}C$), wind speed (m/s), as well as cost of fuels (\$/liter) for the DG and natural gas price for supplying the FC and MT (\$/kWh).
- Daily purchased and sold power tariffs in (\$/kWh).
- Start-up costs in (\$/h).
- Technical and economic performance of supply options: These characteristics include, for example, rated power for PV, power curve for WT, fuel consumption characteristics DG and FC.
- Operating and maintenance costs and the total emission: Operating and maintenance costs must be given (\$/h) for DG, FC, and MT.
- Emission level must be given in kg/h for DG, FC, and MT.

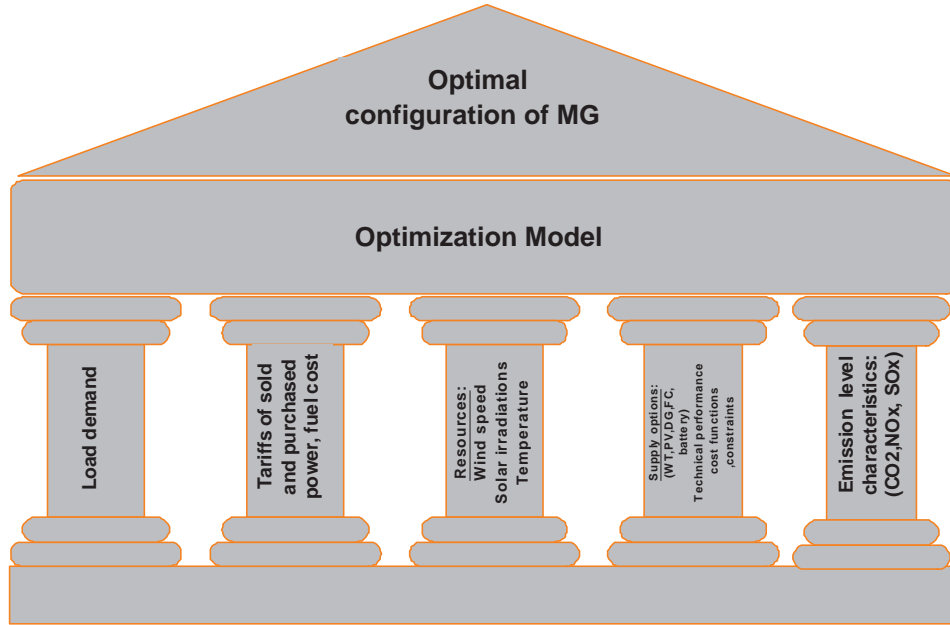


Figure 4.1: Optimization algorithm Model.

4.2 Optimization Problem

4.2.1 Proposed Objective Function

The major concern in the design of an electrical system that utilizes MG sources is the accurate selection of output power that can economically satisfy the load demand, while minimizing the emissions. Hence, the system requirements are determined subject to:

1. Minimizing the operation costs (\$/h).
2. Minimizing the emission (kg/h).
3. Ensuring that the load is served according to given constraints.

4.2.2 Operating Cost

The same Scenarios as formed in Chapter 3 are also considered here. However, the only difference in the operating cost function is that there is no emission cost. As the problem is treated as multiobjective, the emissions are computed separately as emission level. The three different scenarios are modified as follows:

Scenario 1

The purpose of the cost function is to optimize the operation cost $CF(\mathbf{P})$ of the MG in \$/h as follows:

$$CF(\mathbf{P}) = \sum_{i=1}^N (C_i \times F_i(P_i) + OM_i(P_i)) \quad (4.1)$$

where the same notation as in (3.6) is used.

The solution of the optimization procedure produces the optimal decision variables:

$\{P_i = P_{FC_i}, P_j = P_{MT_j}, P_k = P_{DG_k}: i = 1, \dots, N_1; j = N + 1, \dots, N_2; k = N_2 + 1, \dots, N\}$.

\mathbf{P} is N vector of the generators active power and is defined as $\mathbf{P} = (P_1, P_2, \dots, P_N)$

The operating and maintenance costs of the generating unit OM_i have the same form as in (3.13). Furthermore, the values of K_{OM_i} are as in Chapter 3.

Objective Constraints:

Power balance constraints are described by (3.7) and the generation capacity constraints are given in (3.8).

Scenario 2

The total power generation to cover the total load demand is given in(3.9). Considering the start-up cost (3.12), the cost function assumes the form:

$$CF(\mathbf{P}) = \sum_{i=1}^N (C_i \times F_i(P_i) + OM_i(P_i) + STC_i) \quad (4.2)$$

and the maximum and minimum stop time constraints are described by (3.11). A number of starts and stops ($\varepsilon_{start-stop}$) are given in (3.14) and the generation capacity and power balance constraints are also considered in this scenario.

Scenario 3

As in Fig 1.1, the main utility balances the difference between the load demand and the generated output power from the microsources. Then the cost function takes the form:

$$CF(\mathbf{P}) = \sum_{i=1}^N (C_i \times F_i(P_i) + OM_i(P_i) + STC_i + DCPE_i - IPSE_i) \quad (4.3)$$

where

$DCPE_i$ Daily purchased electricity of unit i if the load demand exceeds the generated power in $\$/h$.

$IPSE_i$ Daily income for sold electricity of unit i if the output generated power exceeds the load demand in $\$/h$.

The constraints of Scenario 2 apply also here.

4.2.3 Emission Level

The atmospheric pollutants such as sulphur oxides (SO_2), carbon oxides (CO_2), and nitrogen oxides (NOx) caused by fossil-fueled thermal units can be modeled separately. However, for comparison purposes, the total ton/h emission of these pollutants can be expressed as [22]:

$$E(\mathbf{P}) = \sum_{i=1}^N 10^{-2}(\alpha_i + \beta_i P_i + \gamma_i P_i^2) + \zeta_i \exp(\lambda_i P_i) \quad (4.4)$$

where $\alpha_i, \beta_i, \gamma_i, \zeta,$ and λ_i are nonnegative coefficients related to the i^{th} generator emission characteristics.

In the emission model introduced in [15], [22], an approach is proposed to evaluate the parameters $\alpha, \beta, \gamma, \zeta,$ and λ using the data available in [27]. Thus, the emissions per day

for the diesel engine, fuel cell, and microturbine are estimated, and the characteristics of each generator will be accordingly determined.

4.3 Implementation of the Algorithm

When designing MGs, several goals should be set including reduction in emissions and generation cost. To achieve this, it is important to highlight all factors influencing the main goal. Figure 4.2 summarizes the key characteristics of the implemented strategy as illustrated in the following items:

- Power output of WT is calculated according to the relation between the wind speed and the output power.
- Power output of PV is calculated according to the effect of the temperature and the solar radiation that are different from the standard test condition.
- Since the WT and PV deliver free cost power (in terms of running as well the emission free), the output power is treated as a negative load, so the load which is the difference between the actual and microsource output can be determined if the output from PV and WT is smaller than the load demand.
- The power from the battery is needed whenever the PV, WT are insufficient to serve the load, meanwhile the charge and discharge of the battery is monitoring.
- Calculate the unmet load that can not served by WT, MT and battery storage.
- Choose serving the load by other sources (FC or MT or DG) according to the objective functions.
- If the output power is not enough then purchase power from the main grid, and if the output power is more than the load demand sell the exceed power to the main grid

4.4 Multiobjective optimization problem

Multiobjective optimization is a method to find the best solution between different objectives, usually conflicting objectives. In the MO optimization problem, there is a vector of objective functions. Each objective function is a function of the decision (variable) vector [97], [90]. A general multiobjective mathematical formulation is expressed as:

$$\begin{aligned} & \min \{f_1(\mathbf{x}), f_2(\mathbf{x}), \dots, f_k(\mathbf{x})\} \\ & \text{subject to } \mathbf{x} \in S \end{aligned} \tag{4.5}$$

where k is the number of the objective functions f_i ($i \geq 2$), $f_i : \mathbb{R}^n \rightarrow \mathbb{R}$ $i = 1, \dots, k$. The vector of objective functions is denoted by $\mathbf{F}(\mathbf{x}) = (f_1(\mathbf{x}), f_2(\mathbf{x}), \dots, f_k(\mathbf{x}))^T$. The decision variable vector $\mathbf{x} = (x_1, x_2, \dots, x_n)^T$ belongs to a (nonempty) feasible region (set) S , which is a subset of the decision variable space \mathbb{R}^n . The abbreviation $\min \{.\}$ means that all the

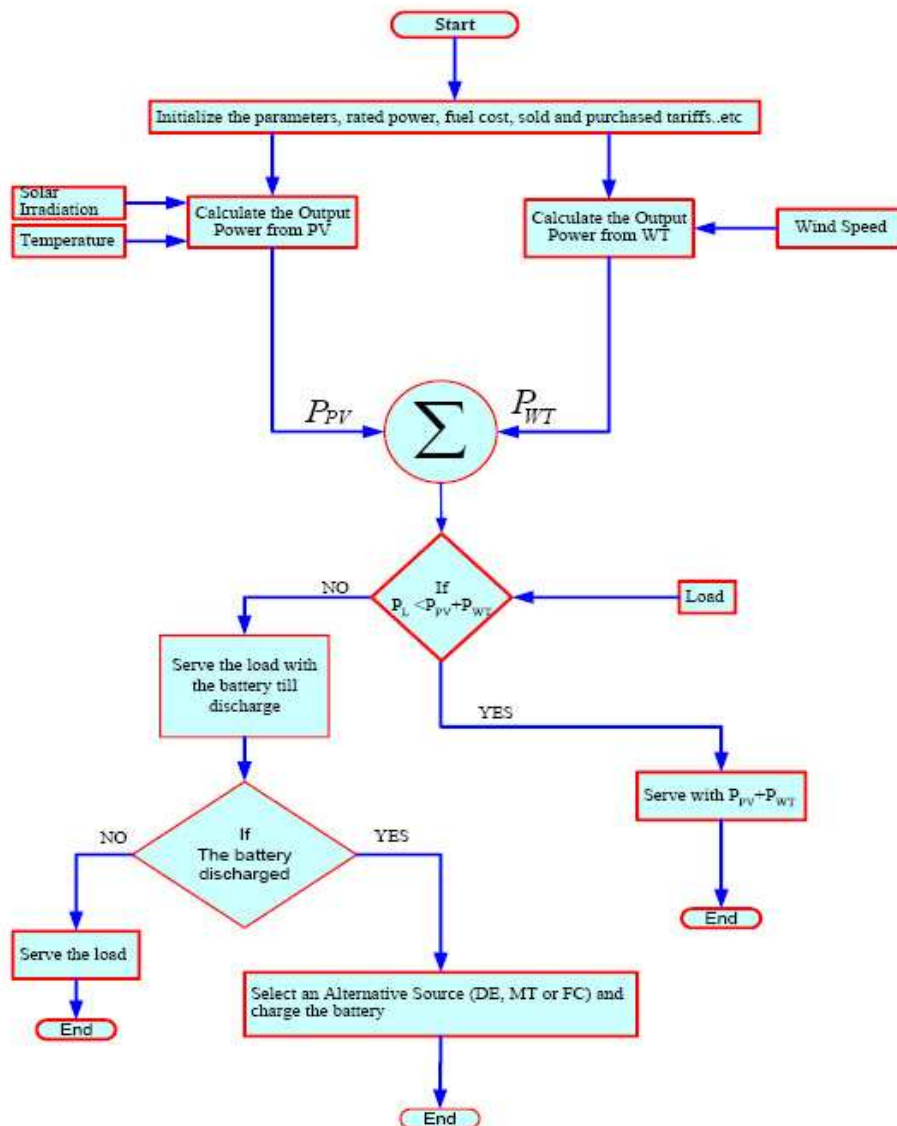


Figure 4.2: Implementation of the algorithm flow chart.

objectives are to be minimized simultaneously. Usually the objectives are at least partially conflicting and possibly incommensurable. This generally means that there is no single vector x , which can minimize all the objectives simultaneously. Otherwise, there is no need to consider multiple objectives. Because of this, MO optimization is used to search for efficient solutions that can best compromise between the different objectives. Such solutions are called non-dominated or Pareto optimal solutions.

If the final solution is selected from a set of Pareto optimal solutions, there would not exist any solutions that are better in all attributes. It is clear that any final design solution should preferably be a member of the Pareto optimal set. If the solution is not in the Pareto optimal set, it could be improved without degeneration in any of the objectives, and thus it is not a rational choice. This is true as long as the selection is only done based on the objectives. Pareto optimal solutions are also known as non-dominated or efficient solutions.

Definition [97]

A decision vector $\mathbf{x}^* \in S$ is Pareto optimal if no another decision vector does exist $\mathbf{x} \in S$ such that $f_i(\mathbf{x}) \leq f_i(\mathbf{x}^*)$ for all $i = 1, 2, \dots, k$ and $f_j(\mathbf{x}) < f_j(\mathbf{x}^*)$ for at least one index j . There are usually a lot (infinite number) of Pareto optimal solutions. The Pareto optimal set is the set of all possible Pareto optimal solutions. This set can be nonconvex and non-connected.

After the generation of the Pareto set, one solution of this set is the aim. This solution is selected by the decision maker. There are different techniques to solve the MO optimization problems. One way to solve this kind of problems is to use softcomputing methods such as genetic algorithms. This thesis concentrates on the analytical solutions of the MO optimization problems. One of the techniques to solve the MO optimization problem is to convert it to a single objective optimization problem as in the Weighting Method [97].

4.4.1 Weighted Sum

The weighted sum method is one of the most common methods for solving MO optimization. The idea is to associate each objective with a weighting coefficient and minimize the weighted sum of the objectives. In this way, the multiobjective functions are transformed into a single objective function.

The weighting method transforms (4.5) into the following scalar objective optimization problem:

$$\begin{aligned} \text{Min} \quad & \sum_{i=1}^k w_i f_i(\mathbf{x}) \\ & \text{subject to } \mathbf{x} \in S \end{aligned} \quad (4.6)$$

where f_i 's are as in (4.5) and the weighted coefficients w_i are real numbers such that $w_i \geq 0$ for all $i = 1, \dots, k$. It is usually supposed that the weights are normalized, that is, $\sum_{i=1}^k w_i = 1$. The multiobjective problem can be solved e.g. using MADS.

Mathematically, the environmental/economic for MG problem is formulated as follows: Find the output generator power vector $\mathbf{P} = (P_1, P_2, \dots, P_N)$ that minimizes the function:

$$\mathbf{F}(\mathbf{P}) = \{CF(\mathbf{P}), E(\mathbf{P})\} \quad (4.7)$$

subject to

$$h_i(\mathbf{P}) = 0 \quad i = 1, \dots, q \quad (4.8)$$

$$g_j(\mathbf{P}) \leq 0 \quad j = 1, \dots, p \quad (4.9)$$

$$P_i^{\min} \leq P_i \leq P_i^{\max}, \quad \forall i = 1, \dots, N \quad (4.10)$$

where the number of the objective functions = 2, $\mathbf{F}(\mathbf{P}) : \mathbb{R}^n \rightarrow \mathbb{R}^2$. The vector of objective functions is denoted by $\mathbf{F}(\mathbf{P}) = (F(P_1), F(P_2))^T$.

The decision variable vector $\mathbf{P} = (P_1, P_2, \dots, P_N)$ consists of all the design variables in the problem which may be bounded.

The collection of the equality constraints, $\mathbf{H}(\mathbf{P}) = (h_1(\mathbf{P}_i), h_2(\mathbf{P}_i), \dots, h_q(\mathbf{P}_i))^T$, is an equality constraint vector. The inequality constraint vector is $\mathbf{G}(\mathbf{P}) = (g_1(\mathbf{P}_i), g_2(\mathbf{P}_i), \dots, g_p(\mathbf{P}_i))^T$ and it is less or equal to zero. The elements of vector \mathbf{P} may be constrained by P_i^{\min} and P_i^{\max} .

From the definition of multi-objective problems, a non-dominated solution is a feasible solution; at least one of the objective values is better than the corresponding objective of all the other feasible solutions. The non-dominated solutions are those from which the multi-objective decision algorithm attempts to select the best compromise solution according to the preferences of the decision makers. Consequently, the two objectives of all the non-dominated solutions are located along the left and lower boundaries of the feasible domain as minimization is desired.

Based on the proposed modelling concept, the three considered Scenarios can be summarized as follows:

Scenario 1

$$CF(\mathbf{P}) = \sum_{i=1}^N (C_i \times F_i(P_i) + OM_i(P_i)) \quad (4.11)$$

subject to:

$$\sum_{i=1}^N P_i - P_L + (P_{PV} + P_{WT}) = 0 \quad (4.12)$$

$$P_i^{\min} \leq P_i \leq P_i^{\max}, \quad \forall_i = 1, \dots, N \quad (4.13)$$

Scenario 2

$$CF(\mathbf{P}) = \sum_{i=1}^N (C_i \times F_i(P_i) + OM_i(P_i) + STC_i) \quad (4.14)$$

subject to:

$$\sum_{i=1}^N P_i = P_L - P_{PV} - P_{WT} - P_{batt} \quad (4.15)$$

$$\begin{cases} (T_{t-1,i}^{on} - MUT_i)(u_{t-1,i} - u_{t,i}) \geq 0 \\ (T_{t-1,i}^{off} - MDT_i)(u_{t,i} - u_{t-1,i}) \geq 0 \end{cases} \quad (4.16)$$

$$\varepsilon_{start-stop} \leq N_{\max} \quad (4.17)$$

Scenario 3

$$CF(\mathbf{P}) = \sum_{i=1}^N (C_i \times F_i(P_i) + OM_i(P_i) + STC_i + DCPE_i - IPSE_i) \quad (4.18)$$

subject to the same constraints as in Scenario 2.

Emission Level

$$E(\mathbf{P}) = \sum_{i=1}^N 10^{-2}(\alpha_i + \beta_i P_i + \gamma_i P_i^2) + \zeta_i \exp(\lambda_i P_i) \quad (4.19)$$

4.5 Results and Discussion

At first, the optimization model is applied to the load shown in Figure 4.3 which is rescaled from [88] and [89]. The load demand varies from 4 kW to 14 kW. The available power from the PV and the WT are used first. The result obtained from applying the three Scenarios are discussed next:

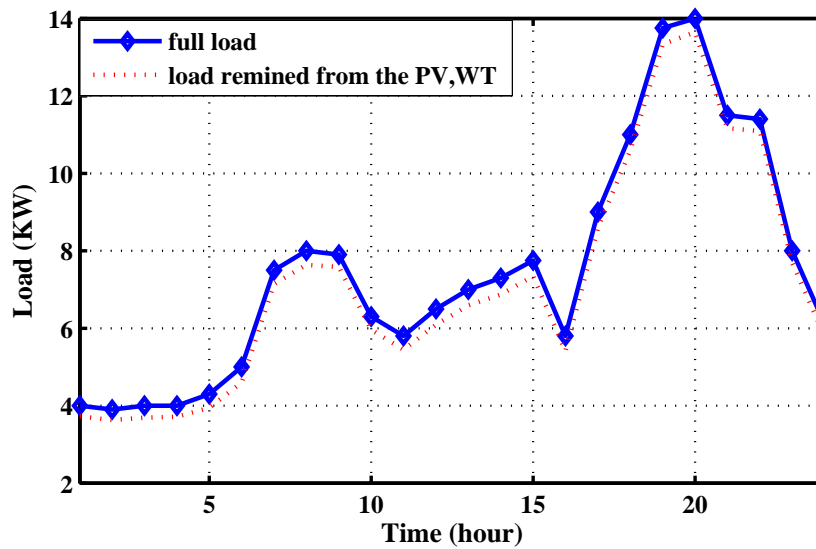


Figure 4.3: Hourly load.

4.5.1 Scenario 1

In order to explore the extreme points of the trade-off surface, operational cost and emission objectives are optimized individually using two different techniques. They are Multiobjective Sequential Quadratic Programming (MOSQP) and Multiobjective Adaptive Direct Search (MOMADS). In Case 1, the cost objective function is optimized and in Case 2, the emission objective function is optimized.

The best results of cost and emission functions, when optimized individually with the two techniques, are given in Table 4.1. Convergence of the operation cost and emission objectives using MOSQP and MOMADS are shown in Figure 4.4. It should be noted that the figure is plotted by selecting an arbitrary one hour load sample from the 24 hour data samples. On the other hand the Table 4.1 shows the total by summing the values over one day.

Then the problem is solved as a MO optimization problem where both operation cost and emissions are optimized simultaneously. Considering the diversity of the Pareto optimal set over the trade-off surface, the trade-off relation can be obtained by minimizing the function [15]:

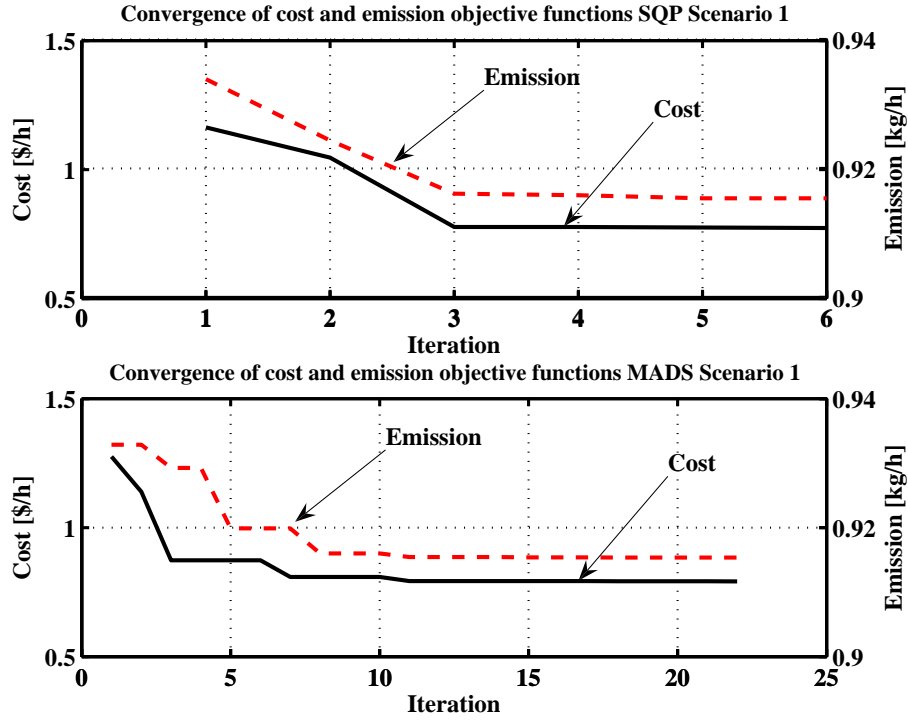


Figure 4.4: Convergence of the operating cost and emission objective functions using MOSQP and MOMADS Scenario 1.

Table 4.1: The objective functions when optimized individually: Scenario 1

	P_L (kW/Day)	Total Emission (kg/Day)		Total Cost (\$/Day)		Optimal Generation (kW/Day)	
		MOSQP	MOMADS	MOSQP	MOMADS	MOSQP	MOMADS
Case 1	171.2924	104.2151	88.8812	28.6813	31.6402	171.2924	171.2928
Case 2	171.2924	50.5100	49.6815	68.0909	69.0050	171.2924	171.2928

$$C(\mathbf{P}) = wCF(\mathbf{P}) + (1 - w)E(\mathbf{P}) \tag{4.20}$$

subject to power balance, and upper and lower limits on the generation. Here $w \in [0, 1]$. Value $w = 1.0$ implies minimum operating cost and full emissions. We obtain the optimum solution of the operating cost objective. The importance of the emission objective increases when w decreases. Then the optimum solution will move toward the optimal emission objective value $w = 0.0$, which implies minimum emission with no attention being paid to operating costs. The optimum solution of the emission objective is now obtained. Function C is minimized for successive values of w to cover the entire range from 0 to 1, the two objectives are given the same weights. For non-dominated solution points, an improvement in one objective requires degradation of the other objective. The proposed model is highly nonlinear. Since each generator has different behavior that influences the operating cost, the solutions are diverse and acceptably distributed over the trade-off curve.

Figures 4.5 and 4.6 show the relationship (trade-off curves) of the operating costs and emissions level objectives of the non-dominated solutions obtained by the MO optimization. The operating costs of the non-dominated solutions appear to be inversely pro-

portional to their emissions. It can be seen that the Pareto optimal set has a number of non-dominated solutions. Out of them, two nondominated solutions that represent the best cost and best emission can be chosen.

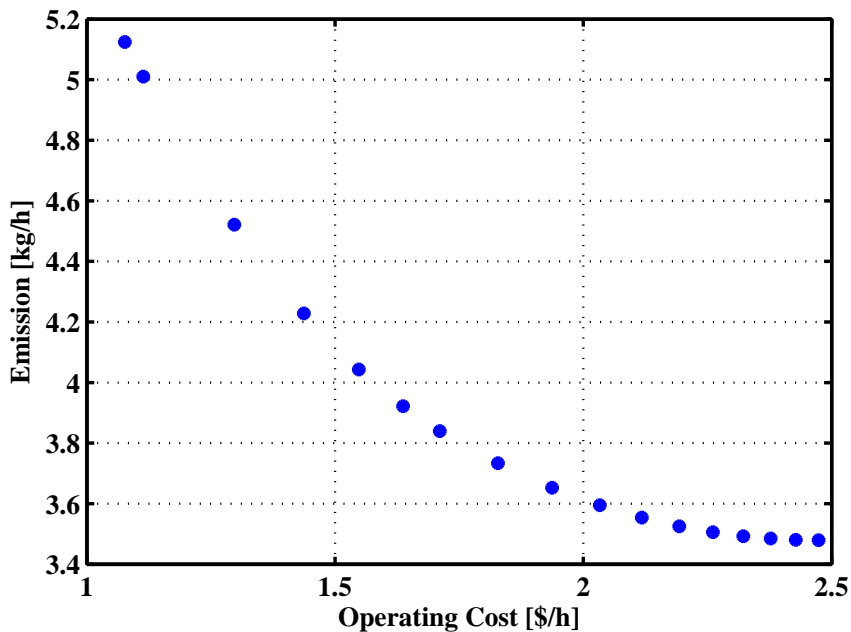


Figure 4.5: Trade- off in operating cost and emission using MOSQP Scenario 1.

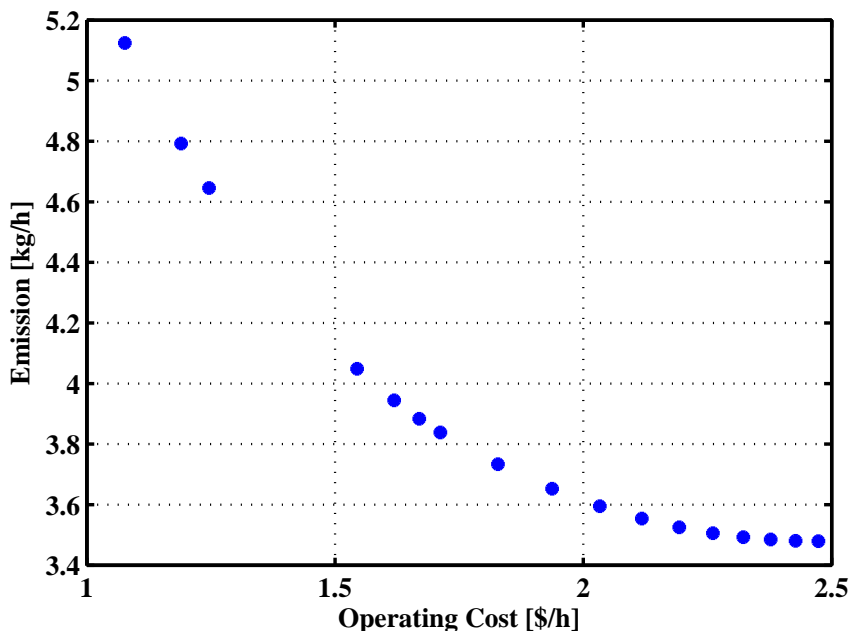


Figure 4.6: Trade- off in operating cost and emission using MOMADS Scenario 1.

The best selection of the power generators of the MG using MOSQP and MOMADS are given in Table 4.2. Both techniques produce nearly the same results while solving the MO problem. Furthermore, this ensures that the proposed approach is capable of exploring more efficient and noninferior solutions of multiobjective optimization problem of MG.

Table 4.2: The best selection per day of the power generators of the MG using MO: Scenario 1

	P_L (kW/Day)	Optimal Generation (kW/Day)	Total Cost (\$/Day)	Total Emission (kg/Day)
MOSQP	171.2924	171.2924	36.2344	74.4566
MOMADS	171.2924	171.2928	35.9737	74.8105

The set of power curves found by the MOSQP and MOMADS optimization algorithms are shown in Figures 4.7 and 4.8, respectively. These figures confirm that when the load demand is low, the best choice in terms of cost is to switch off the diesel generator and start to use the output power from the MT. The second best choice is the use of the fuel cell. When the load is high at the peak time, the diesel generator is switched on and its extra power is used to serve the load.

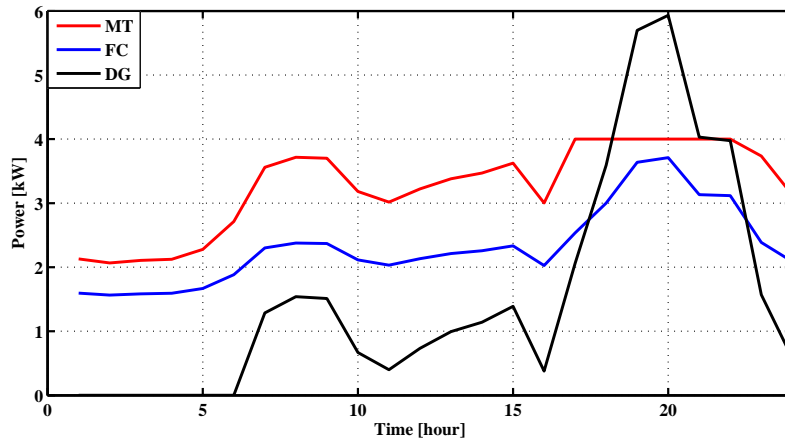


Figure 4.7: The hourly power curves generated by different energy resource using MOSQP Scenario 1.

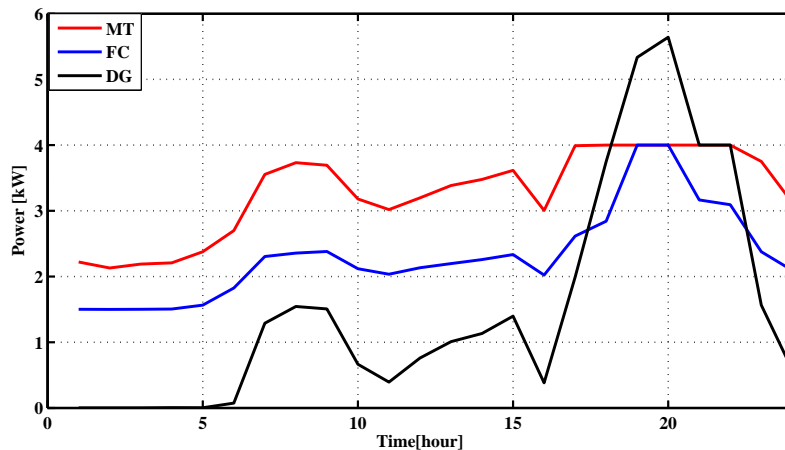


Figure 4.8: The hourly power curves generated by different energy resource using MOMADS Scenario 1.

Table 4.2 and Figures 4.7 and 4.8 confirm that the MO optimization technique has made reasonable selections for the whole day. The selections for the rest of the electricity demand are as straightforward. The DG is the least preferred generator, because of its higher cost and emissions, compared with the others. It is used only when there are no

other generation options available.

Figures 4.9 and 4.10 illustrate the hourly cost and the hourly emissions using MOSQP and MOMADS. In both figures, the cost and emission are high during the peak time and the DG is fully on.

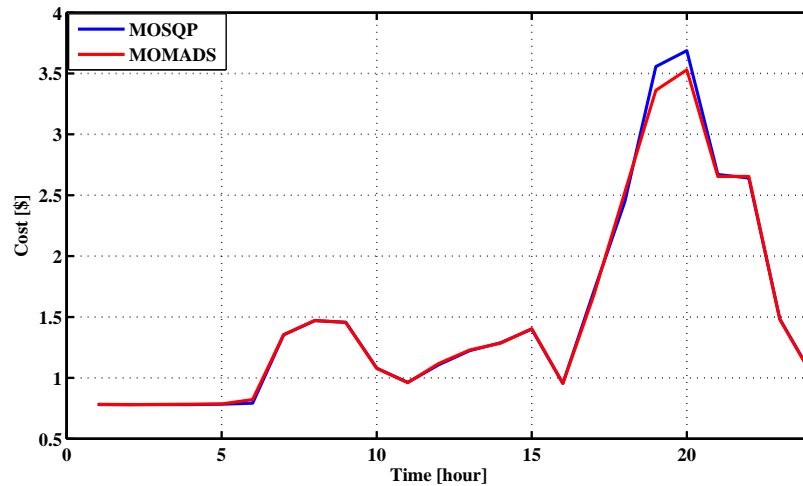


Figure 4.9: Hourly operating cost using the MOSQP and MOMADS Scenario 1.

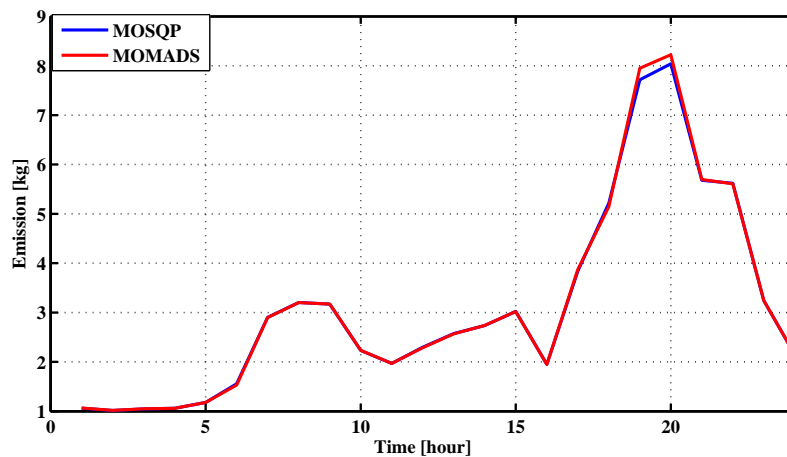


Figure 4.10: Hourly emission using the MOSQP and MOMADS Scenario 1.

4.5.2 Scenario 2

Following the same procedure to explore the extreme points of the trade-off surface, the same two different cases covered in Scenario 1 are considered again. Table 4.3 shows the best results when the operational cost and emission objectives are optimized individually. The result obtained is different than the result in Table 3.3, because they have different settings in the constraints 4.16 and 4.17.

Convergence of operation cost and emission objectives at different times of the day are shown in Figure 4.11. It is noticeable that there is some difference between the two algorithms when the objectives are optimized individually, unlike in Scenario 1.

Table 4.3: The objective functions when optimized individually: Scenario 2

	P_L (kW/Day)	Total Emission (kg/Day)		Total Cost (\$/Day)		Optimal Generation (kW/Day)	
		MOSQP	MOMADS	MOSQP	MOMADS	MOSQP	MOMADS
Case 1	171.4009	95.0842	84.4096	52.0362	54.5920	171.4009	171.4013
Case 2	171.4009	68.2011	68.2014	51.8436	51.8281	171.4009	171.4009

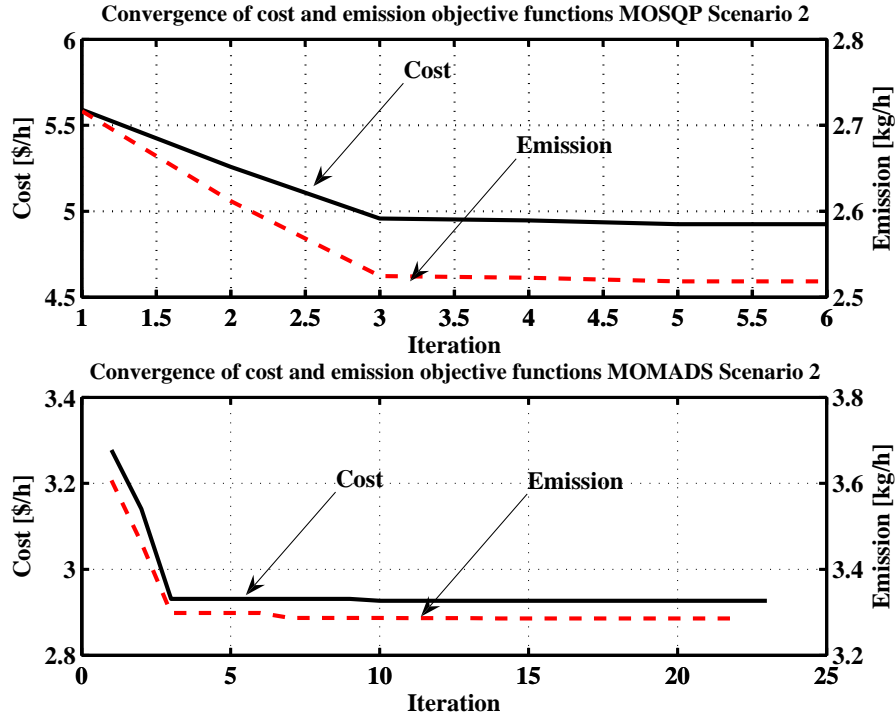


Figure 4.11: Convergence of operating cost and emission objective functions using MOSQP and MOMADS Scenario 2.

Figures 4.12 and 4.13 show the output power of the MG in Cases 1 and 2 using MOMADS method. These figures show that the constraints (4.16) and (4.17) have no effect on Case 2 where the emission objective is optimized individually. The figures clarify why case 2 gives better cost values than Case 1.

Figures 4.14 and 4.15 illustrate the hourly operating costs and emissions using the MOSQP and MOMADS techniques. Both hourly operating costs and emissions are high when the generators are on and the load is high.

The Pareto-optimal front of MOSQP is depicted in Figure 4.16. The distribution of the non-dominated solutions in the Pareto-optimal front using the proposed MOMADS is shown in Figure 4.17. It is evident that the solutions are diverse and well distributed over the trade-off curve. Comparison of Figures 4.16 and 4.17 showed that the non-dominated solutions of both approaches have good diversity characteristics and better non-dominated solutions.

The set of power curves found by the two optimization algorithms are shown in Figures 4.18 and 4.19. It is observed in these figures that when the battery reaches the SOC minimum limit, it is considered as a load (when battery power is negative in the figures). The other sources are then used to charge the battery and serve the load. Table 4.4 with

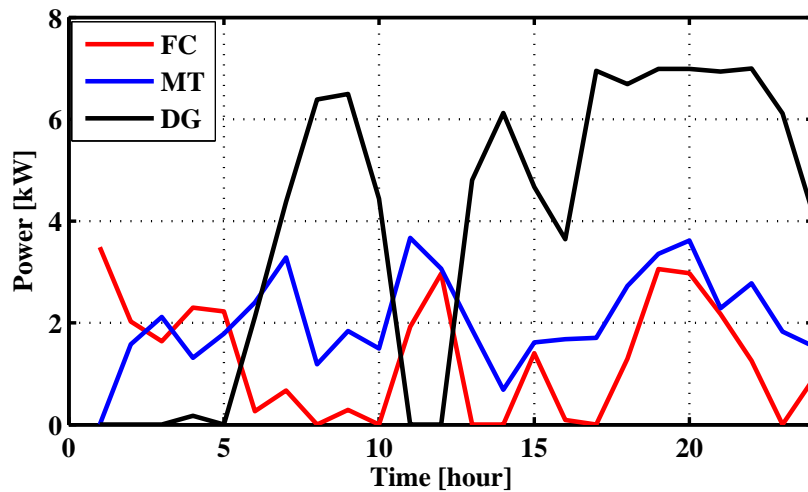


Figure 4.12: Power Generation distribution case 1 using MOMADS Scenario 2.

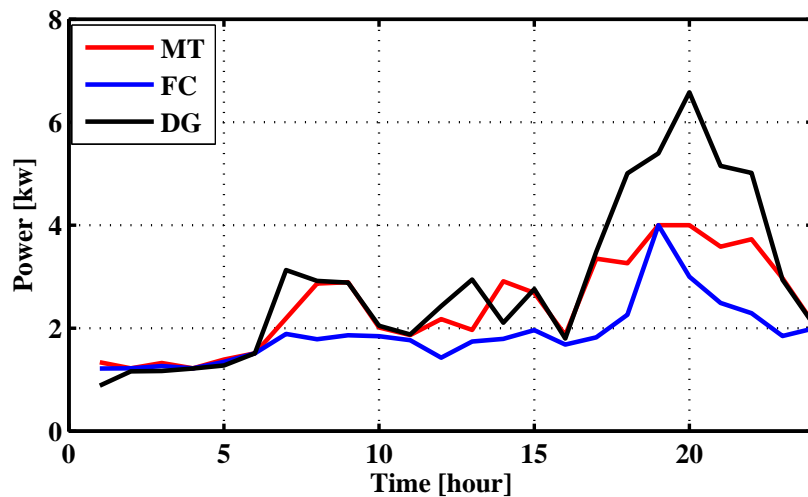


Figure 4.13: Power Generation distribution case 2 using MOMADS Scenario 2.

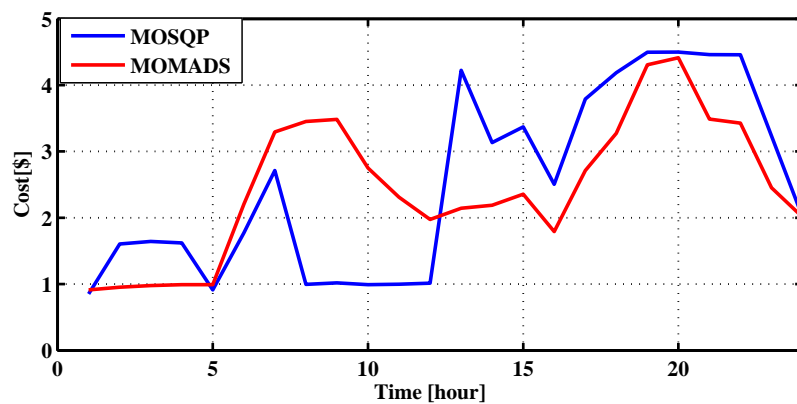


Figure 4.14: Hourly operating cost using the MOSQP and MOMADS Scenario 2.

Figures 4.18 and 4.19 confirm that the MO optimization technique has made reasonable selections in the total cost and emissions per day compared with the result in Table 4.3. The selections were not so straightforward, because of the existing start-stop time limit

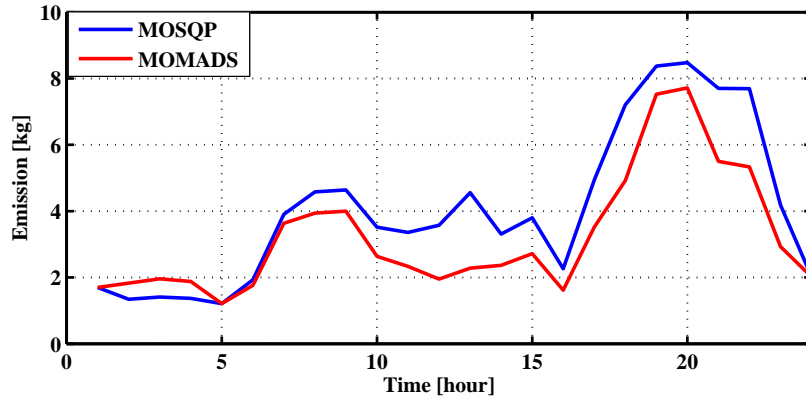


Figure 4.15: Hourly emission using the MOSQP and MOMADS Scenario 2.

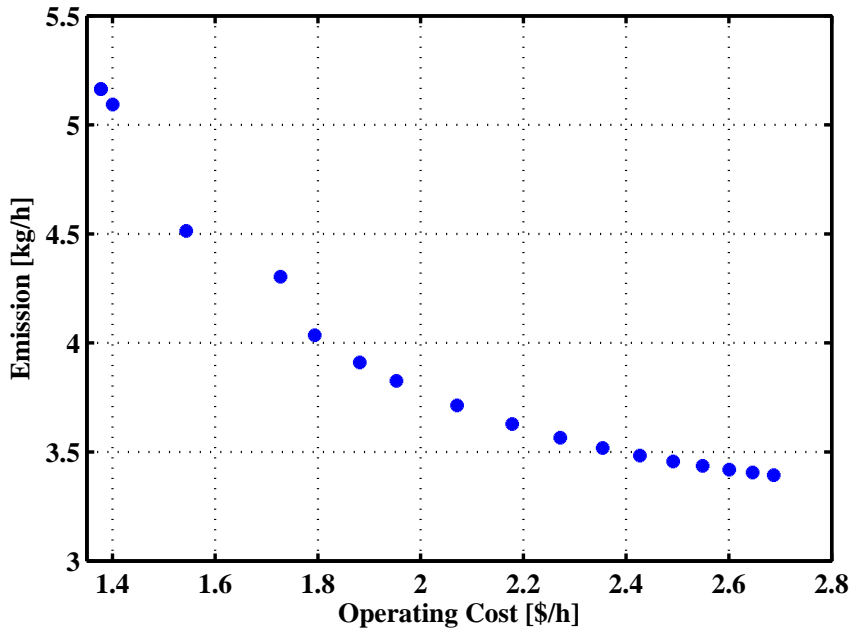


Figure 4.16: Trade- off in operating cost and emission using MOSQP Scenario 2.

constraints which have a big effect on the performance of the algorithm. It finally confirms that the load is perfectly served.

Table 4.4: The best selection per day of the power generators of the MG using MO: Scenario 2

	P_L (kW/Day)	Optimal Generation (kW/Day)	Total Cost (\$/Day)	Total Emission (kg/Day)
MOSQP	171.4009	171.4016	60.4935	97.0396
MOMADS	171.4009	171.4009	58.8531	77.2721

The load demand is served with the battery storage and at the same time the SOC is monitored. At the end of the simulation the battery should be fully charged. The battery capacity is not large enough to supply the load for the whole time. The charged values of the battery power are added to the power demand. The algorithm then calculates the needed power to charge the battery and serve the load.

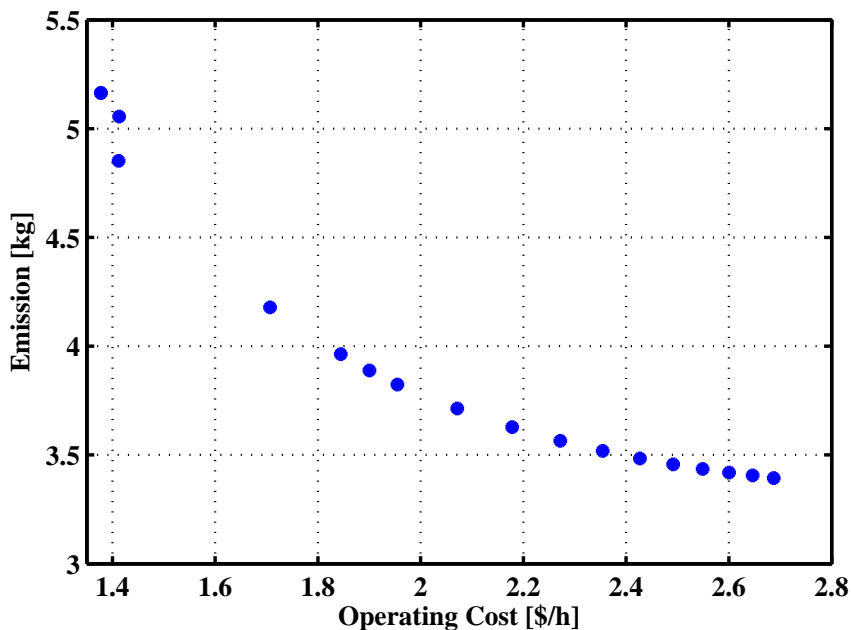


Figure 4.17: Trade- off in operating cost and emission using MOMADS Scenario 2.

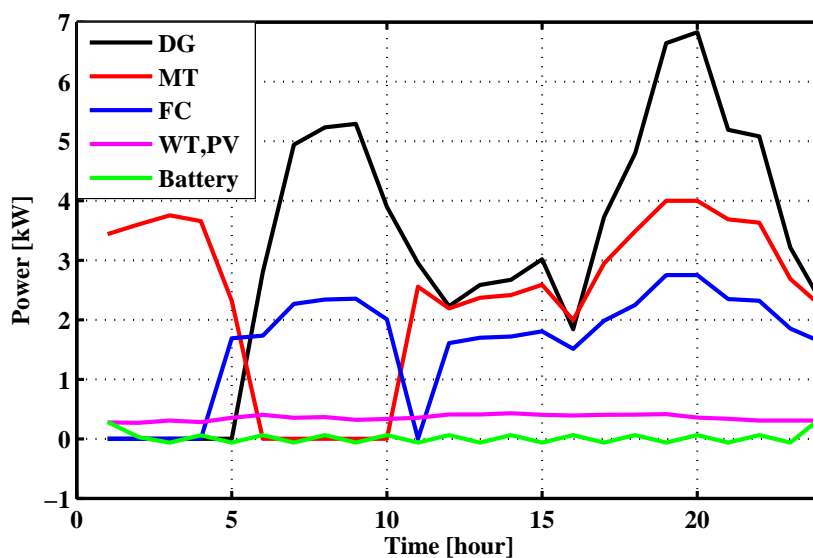


Figure 4.18: The hourly power curves generated by different energy resource using MOMADS Scenario 2.

4.5.3 Scenario 3

The best results of the cost and emission functions, when optimized individually, are given in Table 4.5. Convergence of operation cost and emission objectives for both approaches, when the purchased tariff is 0.12 \$/kWh and the sold tariff 0.07 \$/kWh, is as shown in Figure. 4.20.

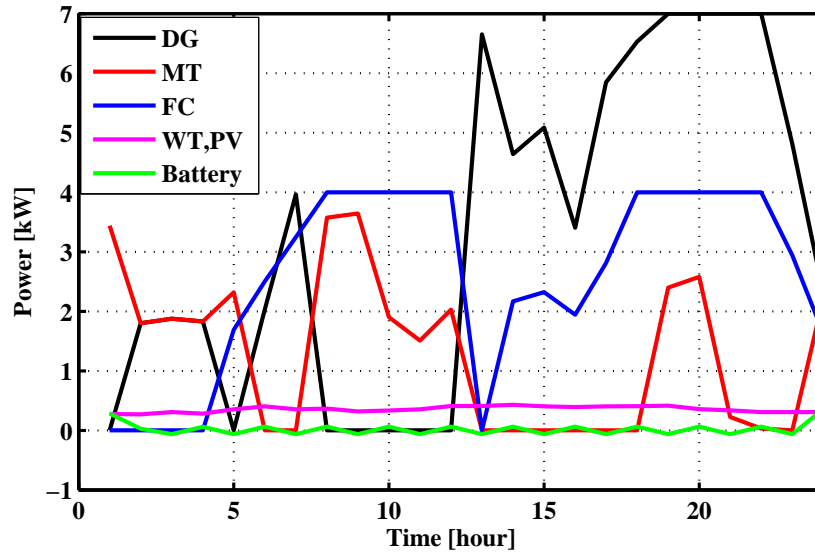


Figure 4.19: The hourly power curves generated by different energy resource using MOSQP Scenario 2.

Table 4.5: The objective functions when optimized individually: Scenario 3

	P_L (kW/Day)	T E(kg/Day)		T C(\$/Day)		O G (kW/Day)		S P (kW/Day)		P P (kW/Day)	
		MOSQP	MOMADS	MOSQP	MOMADS	MOSQP	MOMADS	MOSQP	MOMADS	MOSQP	MOMADS
Case 1	171.4009	149.9198	68.6616	76.1973	61.3615	241.9197	144.3805	70.5188	17.8455	14.8635	27.0204
Case 2	171.4009	12.3885	13.0826	124.6914	113.7293	36.0860	42.5693	00.0000	00.0000	135.3149	128.8316

where

- TE Total Emissions.
- TC Total Operating Cost .
- OG Total Optimal Generated Power .
- SP Total Sold Power.
- PP Total Purchased Power.

Figures 4.21 and 4.22 illustrate the hourly operating costs and emissions for the two proposed techniques. Constraints (4.16) and (4.17) behave differently compared to the previous scenarios. However, the costs and emissions are high when the generators are on and the load is high.

Figures 4.23-4.26 show the relationship (trade-off curves) of the operating cost and emission objectives of the non-dominated solutions obtained by MOSQP and MOMADS approaches for different purchased and sold tariffs. Considering the definition of the multi-objective problems, a non-dominated solution becomes a feasible solution. Then at least one of the objective values is better than the corresponding objective of all the other feasible solutions. The non-dominated solutions are those from which the multi-objective decision algorithm attempts to select the best compromise solution according to the preferences of the decision makers. Consequently, the two objectives of all the non-dominated solutions are located along the left and lower boundaries of the feasible domain as minimization is desired.

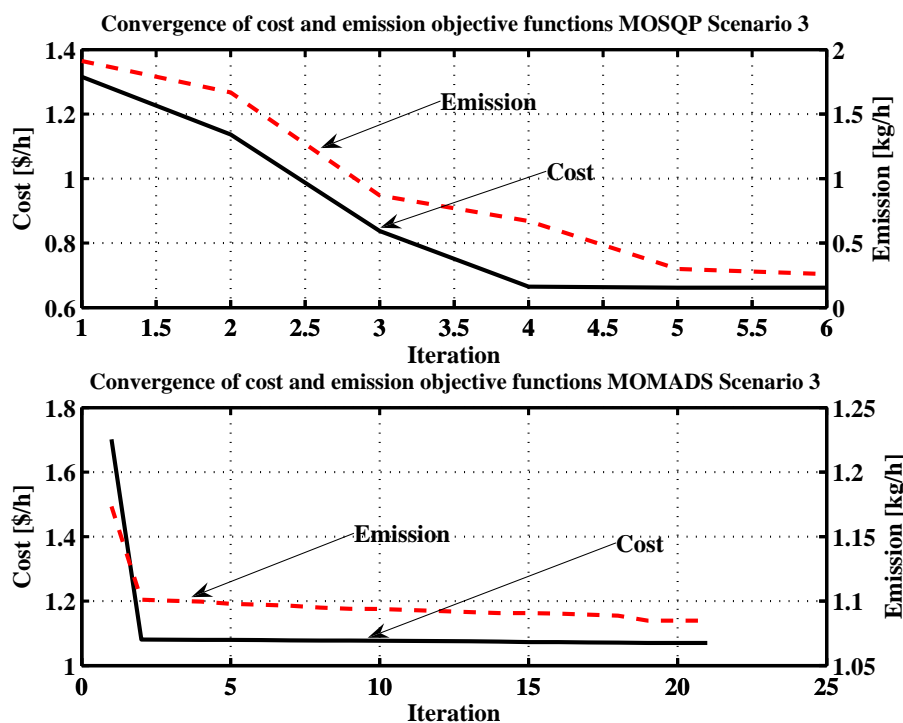


Figure 4.20: Convergence of operating cost and emission objective functions using MOSQP and MOMADS Scenario 3.

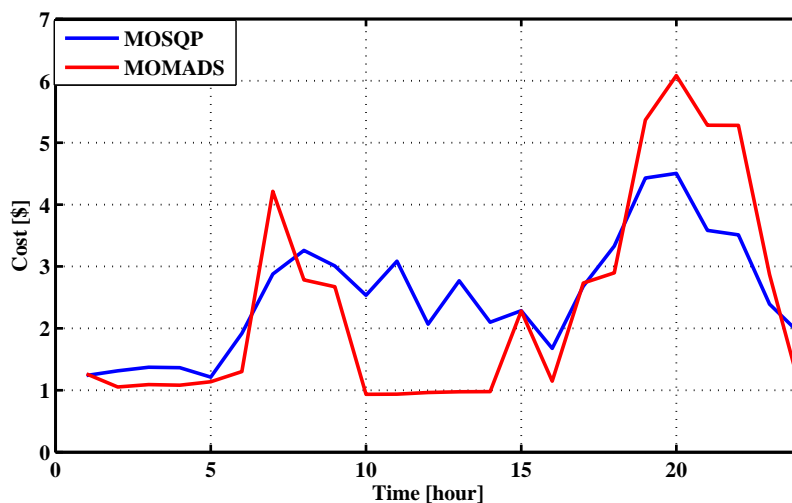


Figure 4.21: Hourly operating cost using the MOSQP and MOMADS Scenario 3.

The operating costs of the non-dominated solutions thus appear to be inversely proportional to their emissions, as illustrated in Figures 4.23-4.26. Table 4.6 and Figures 4.27 and 4.28 show the effect of changing the purchased and sold tariffs on the optimal setting of the MG. There are all together four cases. In case 1, the effect of the changing the purchased tariffs is studied. The sold power is first 0.04 \$/kWh and the purchased tariff is 0.1 \$/kWh. In Case 2 the value of the purchased tariff is increased to 0.16 \$/kWh and the sold one is the same as in Case 1. During changing the purchased tariff values, it was noticed that when the tariff is low, it was preferable to buy as much power from the main grid as possible. However, when the tariffs were higher, it was more economical to gen-

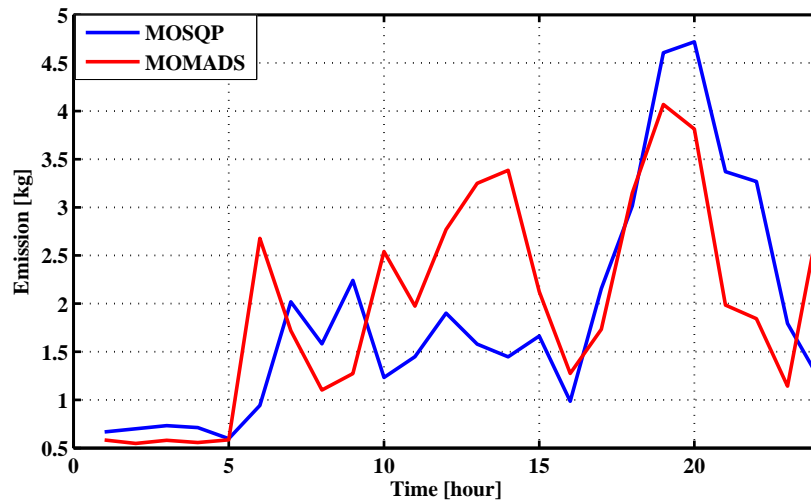


Figure 4.22: Hourly emission using the MOSQP and MOMADS Scenario 3.

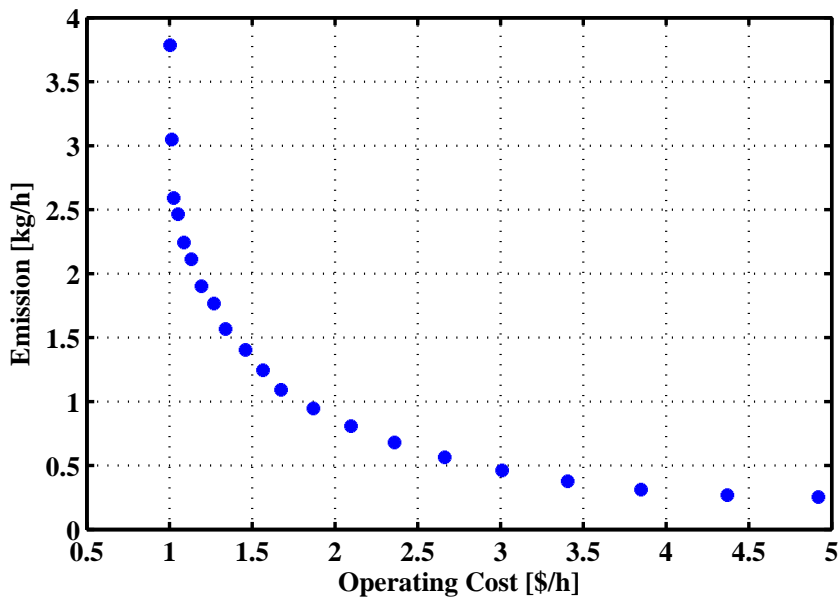


Figure 4.23: Trade-off in operating cost and emission using MOSQP at Scenario 3 and for $P = 0.12$ and $S = 0$.

erate the required power from the MG according to MOSQP and MOMADS approaches. In Cases 3 and 4, the purchase power tariff is kept constant at 0.12 \$/kWh, while the sold tariff was 0.0 \$/kWh in Case 3 and 0.04 \$/kWh in Case 4. It is noticeable that the MG generates more power when increasing the sold tariffs and when applying MOMADS optimization algorithm. In MOSQP, changing of the sold tariffs has no effect for such a small change. MOSQP only reacts if the change is much larger. This leads to conclude that the MOMADS is more efficient if there is a change in the sold tariffs even if the change is very small. The higher values of the sold power tariff gives the possibility to produce more power to meet the load demand in MOMADS.

Table 4.7 illustrates the cost savings and emission reductions of the MG using different cases and compares them with the proposed MOMADS technique. The results obtained

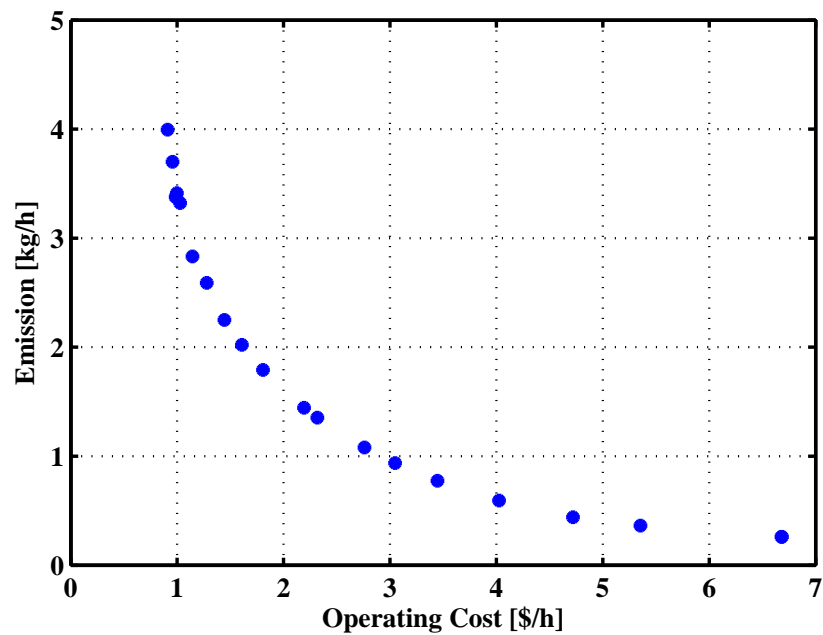


Figure 4.24: Trade-off in operating cost and emission using MOMADS at Scenario 3 and for $P = 0.12$ and $S = 0$.

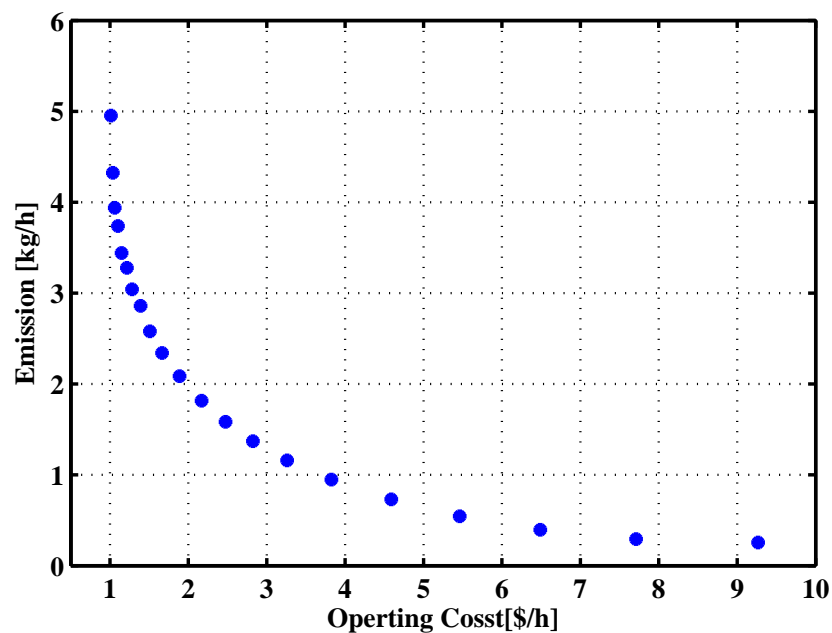


Figure 4.25: Trade-off in operating cost and emission using MOSQP at Scenario 3 and for $P = 0.16$ and $S = 0.1$.

using the proposed technique to minimize the total cost and total emissions are compared with conventional strategies. In the first case the DG, FC, and MT operate at their rated power for the whole day (Case A). In the second case costs are optimized individually (Case B). In the third scenario emissions objective function is optimized individually (Case C).

Case A gives a higher operating cost and higher emissions than other settings which indicates that it is not relevant. Larger generating power, larger costs and emissions are

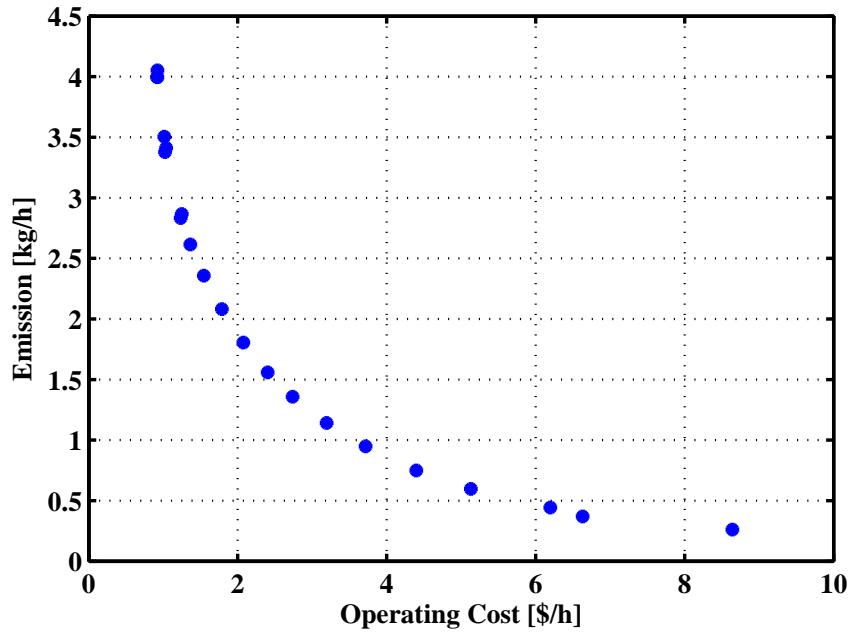


Figure 4.26: Trade- off in operating cost and emission using MOMADS at Scenario 3 and for P = 0.16 and S= 0.1

Table 4.6: The effect of the Purchased and Sold tariffs on the optimal Generation: Scenario 3

	Load (kW/Day)	Optimal Generation (kW/Day)		Total Cost(\$/Day)		Total Emission(kg/Day)	
		MOSQP	MOMADS	MOSQP	MOMADS	MOSQP	MOMADS
Case 1	171.4009	112.5081	110.7196	58.5862	51.0058	40.3235	47.3697
Case 2	171.4009	127.1114	112.4749	61.3490	64.5349	49.4893	47.1226
Case 3	171.4009	117.7365	111.2769	60.4168	56.3351	44.6083	47.5260
Case 4	171.4009	117.7365	111.2769	60.4168	56.3351	44.6083	47.5260

attained. In Case B, the cost is somewhat reduced, while the emissions increase. In the third case, the cost increased while the emissions decreased and the optimal choice was to purchase more power from the main grid.

For achieving the completeness and checking the effectiveness of the proposed cost function and proposed solution, the problem is treated as a single objective optimization problem: [22] (case D):

$$\underset{\mathbf{P}}{\text{Minimize}} \quad \omega CF(\mathbf{P}) + (1 - \omega)\lambda E(\mathbf{P}) \tag{4.21}$$

where λ is the scaling factor and ω is the weighting factor. The scaling factor λ is used to balance the two objectives. The increase of the scaling factor favors the predominance of the total emission objective function over the total operating cost objective function. Value of $\lambda = 3000$ was found to be the best compromise between the two objectives. In this study the weighting factor ω is selected to be varying randomly $\omega = rand[0, 1]$ and λ is chosen to be 3000. With the proposed MOMADS method, the total operating cost and emissions are reduced to 48.3012 \$/day and 41.8015 kg/day, respectively.

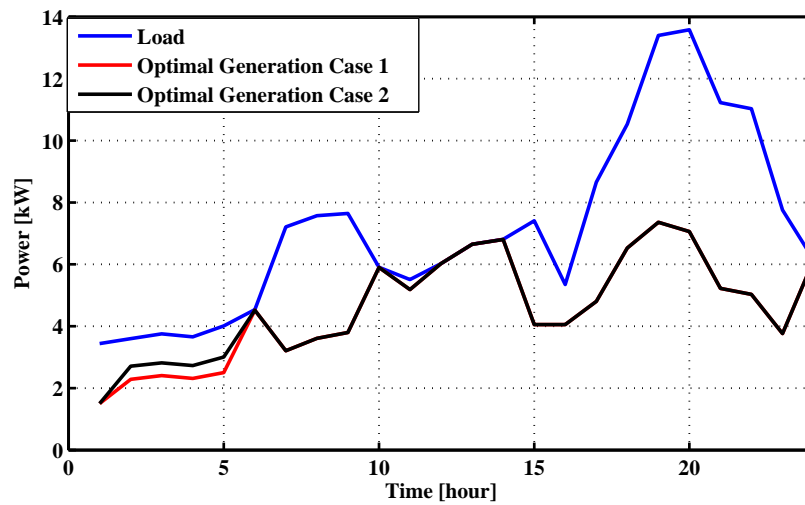


Figure 4.27: Effect of purchased power tariffs on the MG optimal operation using MOMADS Scenario 3.

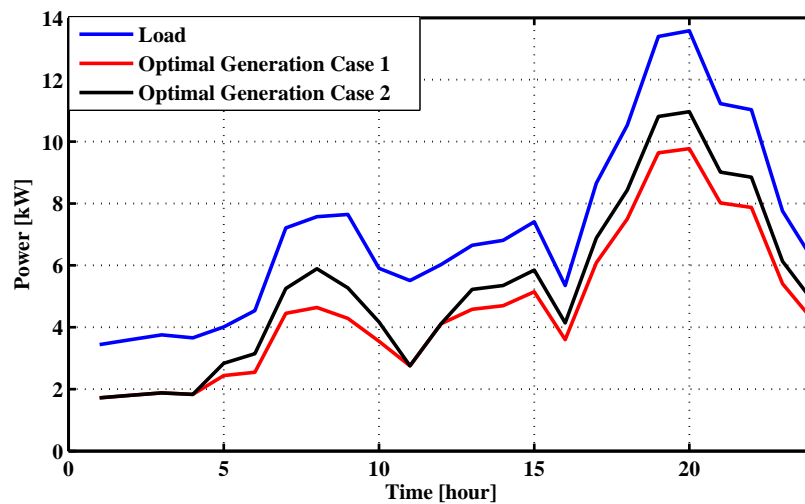


Figure 4.28: Effect of purchased power tariffs on the MG optimal operation using MOSQP Scenario 3.

MOMADS is more capable of handling the multiobjective optimization problem of the MG when the problem becomes more complex, e.g, when more constraints and purchased and sold power are considered. It is also noticeable from Figures 4.29 and 4.30 that MOMADS has a good distribution of the powers given to the microsources.

Table 4.7: Cost savings and emissions reductions of the MG using multiobjective optimization: Scenario 3

	Average Cost & Emissions		Average difference with respect to the optimal case			
	Cost \$/Day	Emissions kg/Day	cost \$/Day	Emissions kg/Day	Cost%	Emissions%
Case A	95.3091	229.4895	47.0079	187.6880	97.32%	449.00%
Case B	68.6616	61.3615	20.3604	19.5600	42.15 %	46.79 %
Case C	113.7293	13.0826	65.4281	-28.7189	135.46%	-68.70 %
Case D	53.5643	58.9397	53.5643	11.7628	10.90 %	28.14%
MOSQP	49.3980	44.0851	1.0968	2.2836	2.27%	5.46%
MOMADS	48.3012	41.8015	00.0000	00.0000	0%	0%

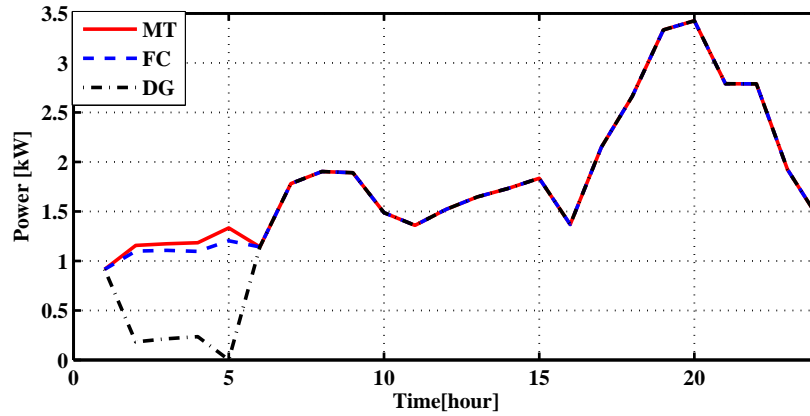


Figure 4.29: Power Generation distribution using MOSQP Scenario 3.

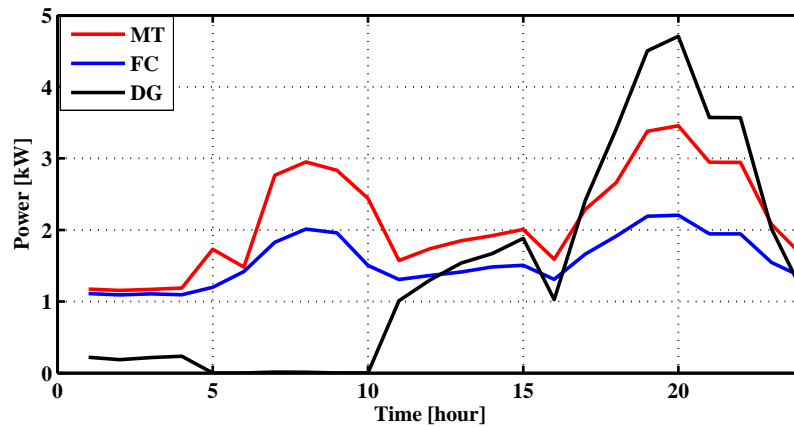


Figure 4.30: Power Generation distribution using MOMADS Scenario 3.

4.6 Conclusions.

Objective functions to determine the optimum operation of a MG with respect to the load demand and environmental requirements are constructed and presented in a new form. The optimization problem includes a variety of energy sources that are likely to be found in a microgrid: fuel cells, diesel engines, microturbines, PV arrays, wind generators, and battery storages. Constraint functions are added to the optimization problem to reflect some of the additional considerations often found in a small-scale generation system. The results of the optimal power operating costs and emissions curves for the MG ensure that the optimization works very well and can give the optimal power to the generators after taking the operating costs and emissions into account. The effectiveness of the suggested approach is confirmed through the agreement between the optimized settings and the output from the algorithm. The responses are effected by several variables such as weather conditions, sold and purchased tariffs, and of course, the actual power demand. The results show the capability of the proposed system model and the proposed algorithm to achieve both reduction in the operating costs and meeting the load demand. The proposed procedure can be implemented with different loads and for periods more than one day.

Chapter 5

MicroGrid Online Management Using Multiobjective Genetic algorithms

5.1 Introduction

This chapter develops a novel intelligent technique to manage the operation of MG units for residential or industrial utilization. Genetic algorithms (GAs) are used to find optimal settings of the MG units depending on detailed economic and environmental models. This approach is applied to the three scenarios described in Chapter 4. The objective is to develop an intelligent management tool, which can be used for environmentally constrained economic problems of the MG. The problem can be classified as a multiobjective optimization and nonlinear programming problem. The purpose of the tool is to find the optimal amount of the generated power by minimizing the operating cost and the emission level simultaneously while satisfying the load demand and operational constraints. The trade-off curve is obtained by forming an objective function which combines the operating costs and emission level objectives. The next step is to use GA to determine the global optimum solutions.

5.2 Genetic algorithms

Genetic algorithms (GAs) and the closely related evolutionary algorithms are a class of global non-gradient methods which have grown in popularity. Reference [98] presents a comprehensive study of genetic algorithms. Genetic algorithms are modeled after mechanisms of natural selection. Each optimization parameter (x_n) is encoded by a gene using an appropriate representation, such as a real number or a string of bits. The corresponding genes for all parameters x_1, \dots, x_n form a chromosome capable of describing an individual design solution. A set of chromosomes representing several individual design solutions comprises a population where the fittest are selected to reproduce. Mating is performed using crossover to combine genes from different parents to produce children. The children are inserted into the population and the procedure starts over again. The

general form of genetic algorithms is presented in Figure 5.1. Content of each block in this flow chart is explained in greater details in the following.

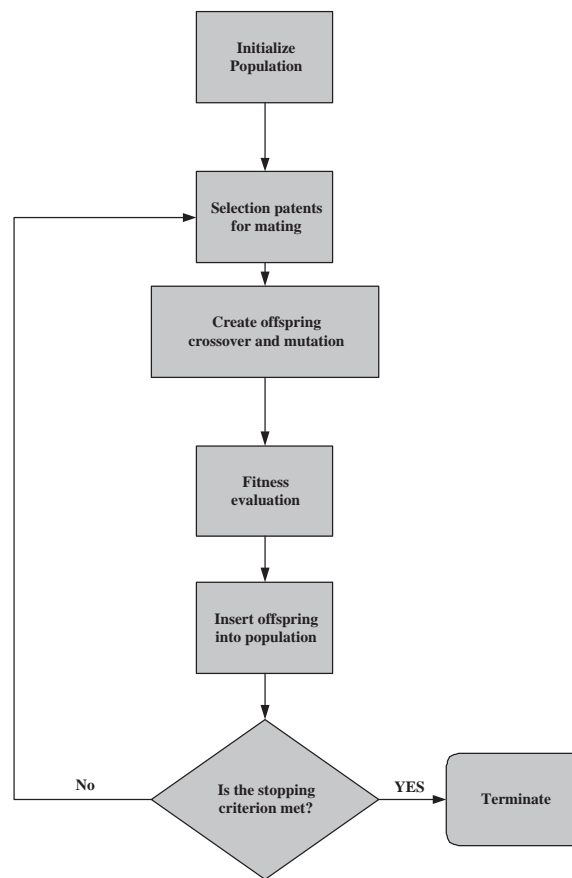


Figure 5.1: Flow chart of a general form of the genetic algorithm

Initialization

In the initialization, one generates, often randomly, a population from which new generations are formed. At this point one also needs to define the terminating condition so that the algorithm stops running once an acceptable solution is found.

Crossover

Crossover is one of the genetic operators used in producing new candidates using the features of the existing ones. The crossover procedure is illustrated in Figure 5.2 below.

The crossover procedure consists of three parts. First one selects two parents from the population. Then the crossover points are selected. The selection of crossover points is done at random, usually so that the distribution from which the points are drawn from is uniform. In Figure 5.2, two crossover points are marked with dotted lines. Once the points are defined, two offsprings are generated by interchanging the values between the two parents as illustrated in Figure 5.2. In the genetic algorithm, crossover is the operator that spreads the favorable characteristics of the members around the population. A number of different crossover techniques have been presented in the literature.

Mutation

Mutation is the operator that causes totally new characteristics to appear in the members of the population. In many cases the mutations, result in offsprings that are worse than

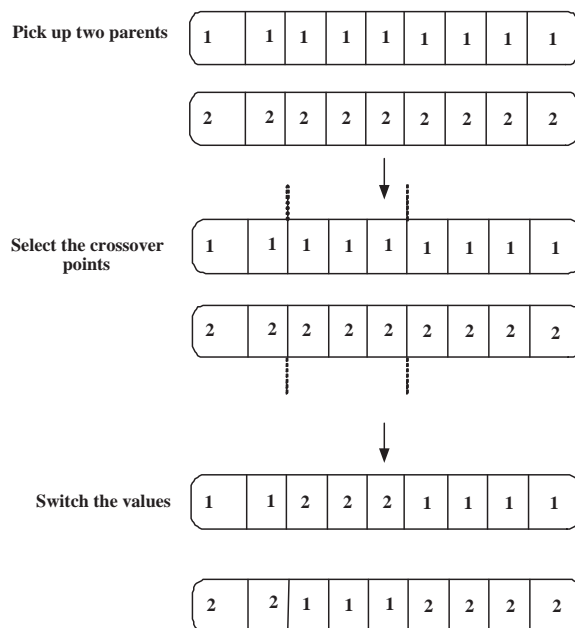


Figure 5.2: Crossover procedure

the other members, but sometimes the result has characteristics that make it better. Figure 5.3 demonstrates the mutation operation. First, one selects a member from the population to be mutated and a point of mutation. Then the value at the point of mutation is replaced by another value that is picked randomly from the set of all possible values.

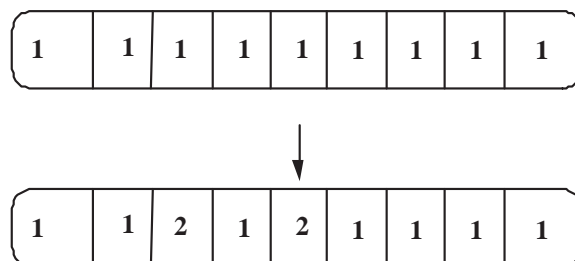


Figure 5.3: Mutation

Evaluation

After the population is manipulated using the genetic operators, the fitness of each new offspring is evaluated. To do this one needs to have a numerical function and a fitness function.

Selection

In the selection, the weakest individuals in the population are eliminated. Most fit offsprings survive to the next generation.

Population size specifies how many individuals there are in each generation. With a large population size, the genetic algorithm searches the solution space more thoroughly, thereby reducing the chance that the algorithm will return a local minimum that is not a global minimum. However, a large population size also causes the algorithm to run more slowly. Population size of 100 is used in this study.

Mutation options specify how the genetic algorithm makes small random changes in the individuals in the population to create mutation children. Mutation provides genetic diversity and enable the genetic algorithm to search a broader space. The mutation function, adds a random number taken from a Gaussian distribution with mean 0 to each entry of the parent vector. Gaussian mutation function is applied in this study.

Crossover options specify how the genetic algorithm combines two individuals, or parents, to form a crossover child for the next generation. Crossover function specifies the fraction of the next generation, other than elite children, that are produced by crossover. Set Crossover fraction to be a fraction between 0 and 1, either by entering the fraction in the text box or moving the slider. The value 0.8 is used.

Selection options specify how the genetic algorithm chooses parents for the next generation. The Tournament selection is employed in the thesis. This chooses each parent by choosing Tournament players at random and then pikes the best individual out of that set to be a parent. Tournament size must be at least 2. The value of Tournament size 4 is used.

5.3 Multiobjective genetic algorithms (MOGA)

The simplest and most obvious approach to multiobjective optimization is to combine the objectives into one aggregating function, and to treat the problem like a single objective optimization problem. Therefore, it is commonly used because of its simplicity and computational efficiency as in Chapter 4.

The weighted sum approach combines k objectives f_i using weights, $w_i, i = 1, \dots, k$:

$$fitness = w_1 f_1(\mathbf{P}) + w_2 f_2(\mathbf{P}) + \dots + w_k f_k(\mathbf{P}) \quad (5.1)$$

The weights are real numbers, $w_i \geq 0$ and \mathbf{P} as in (4.1)

5.4 Results and Discussion

Following the same procedure as proposed in Chapter 4, the optimization model is applied to the load shown in Figure 4.3 and MOGA is used to solve the problem in the three scenarios.

5.4.1 Scenario 1

Table 5.1 shows the operating costs and emissions objective functions which are optimized individually. The first case occurs when the operation cost is optimized and the second case when the emission objective is optimized. Then the problem is solved as a

Table 5.1: The objective functions when optimized individually Scenario 1

	P_L (kW/Day)	Total Emission (kg/Day)	Total Cost (\$/Day)	Optimal Generation (kW/Day)
Case 1	171.2924	85.1738	32.5497	171.5044
Case 2	171.2924	68.6615	51.1472	171.2954

MO optimization problem where both operation costs and emissions are optimized simultaneously. In order to see the diversity of the Pareto optimal set over the trade-off surface, the trade-off relation can be obtained by minimizing (4.20).

Figure 5.4 shows the relationship trade-off curve between the two objectives, where the Pareto optimal set has a number of non-dominated solutions. Two of them represent the best cost and best emission. The best selection of the power generators of the MG using MOGA is given in Table 5.2 and in Figure 5.5. It can be concluded that the proposed approach is capable of reducing the operation cost from 51.1472 \$/Day to 32.5497 \$/Day and the emission level from 85.1738 kg/Day to 68.6615 kg/Day while the load is satisfied all the time.

Figure 5.6 shows the hourly costs and emissions. The costs and emissions are high only when the DG is fully in the peak time, which means that the proposed approach has reached an optimal setting. Furthermore, because the DG has the highest cost and emission, it is the least preferable generation unit.

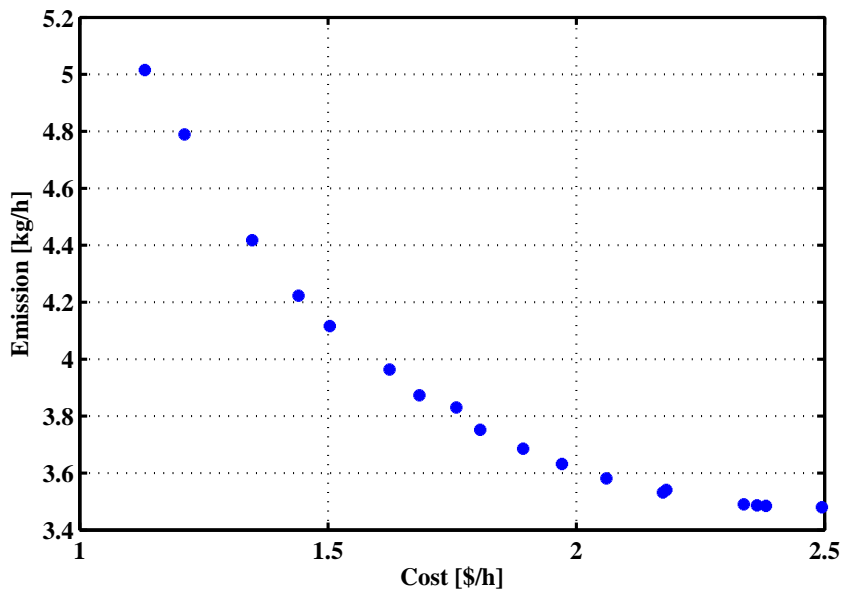


Figure 5.4: Trade- off in operating cost and emission using GA Scenario 1.

Table 5.2: The best selection per day of the power generators of the MG using MOGA Scenario 1

P_L (kW/Day)	Optimal Generation (kW/Day)	Total Cost (\$/Day)	Total Emission (kg/Day)
171.2924	171.3003	39.0442	73.0406

5.4.2 Scenario 2

As mentioned in Chapter 4, more constraints in Scenario 2 are added to the operation costs. The results when the two objectives of the total operating costs and total emissions level are optimized individually are summarized in Table 5.3. The results explore the extreme points for the costs and emissions. Furthermore, the added constraints could de-

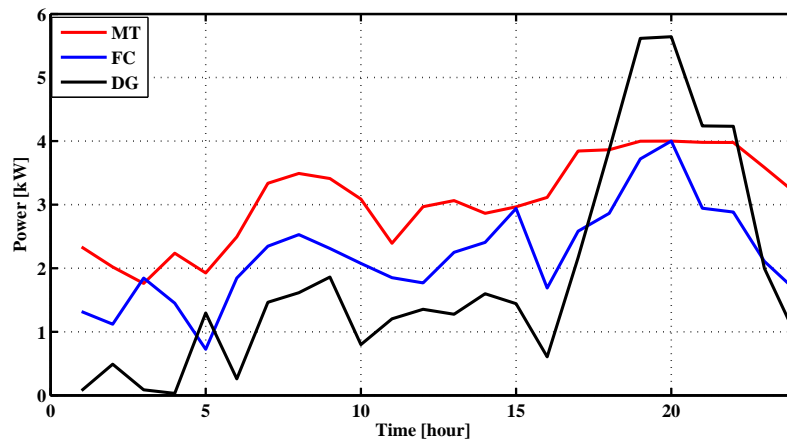


Figure 5.5: The hourly power curves using GA Scenario 1.

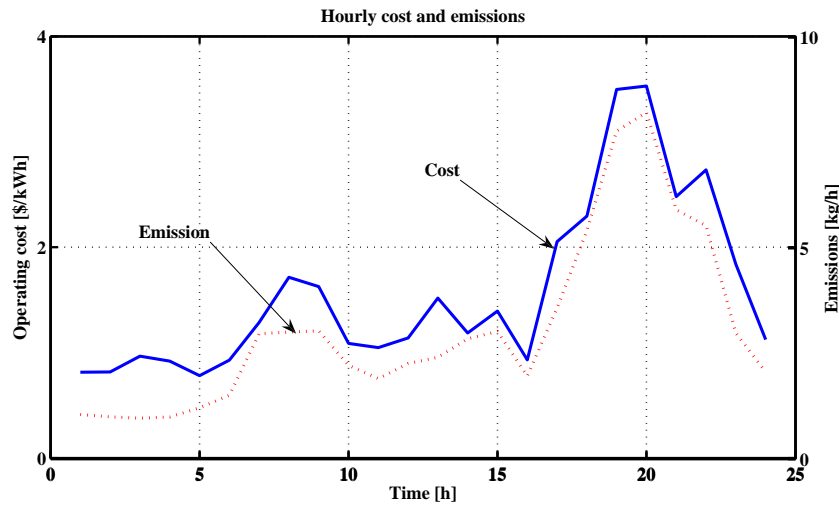


Figure 5.6: Hourly operating cost and emission using MOGA Scenario 1.

crease the operation costs and emissions level compared to the results obtained from Scenario 1. Figure 5.7 depicts the trade-off curve of the Pareto-optimal set obtained by minimizing (4.20) subjected to the constraints considered in Scenario 2. The figure demonstrates how an operational policy may be chosen as a compromise between the operation cost and the emission.

Table 5.3: The The objective functions when optimized individually Scenario 2

	P_L (kW/Day)	Total Emission (kg/Day)	Total Cost (\$/Day)	Optimal Generation (kW/Day)
Case 1	171.4009	76.7318	45.7703	171.9298
Case 2	171.4009	68.2841	51.6224	171.4024

Table 5.4 shows the results when the problem is solved as a multiobjective optimization problem. It can be seen also that the operating costs and emission level are reduced compared to Scenario 2 in Chapter 4.

Figures 5.8 and 5.9 illustrate the power curves and hourly cost and emission using MOGA. In both figures, the cost and emission are high during the peak time. Also the DG is fully on and the load is handled well.

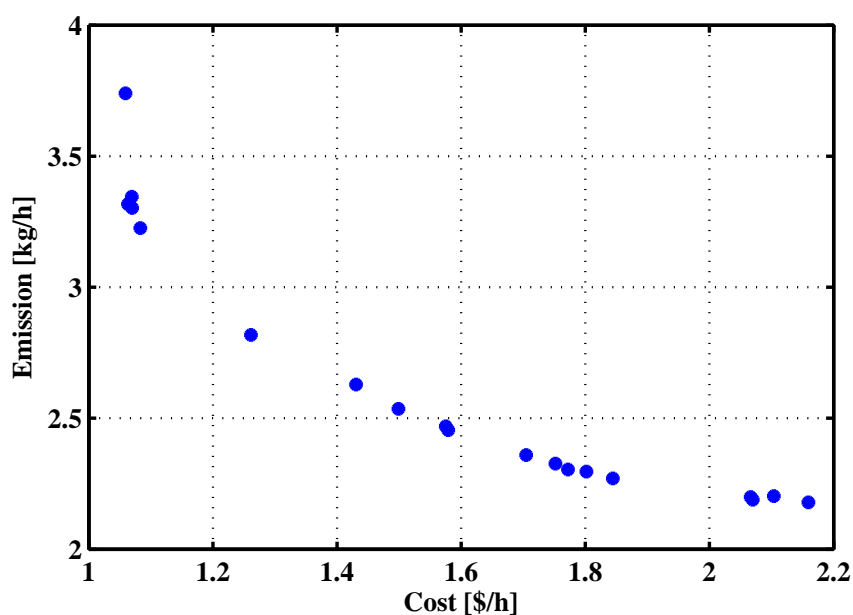


Figure 5.7: Trade- off in operating cost and emission using GA Scenario 2.

Table 5.4: The best selection of the power generators of the MG using MOGA Scenario 2

P_L (kW/Day)	Optimal Generation (kW/Day)	Total Cost (\$/Day)	Total Emission (kg/Day)
171.4009	171.4029	50.6136	68.6519

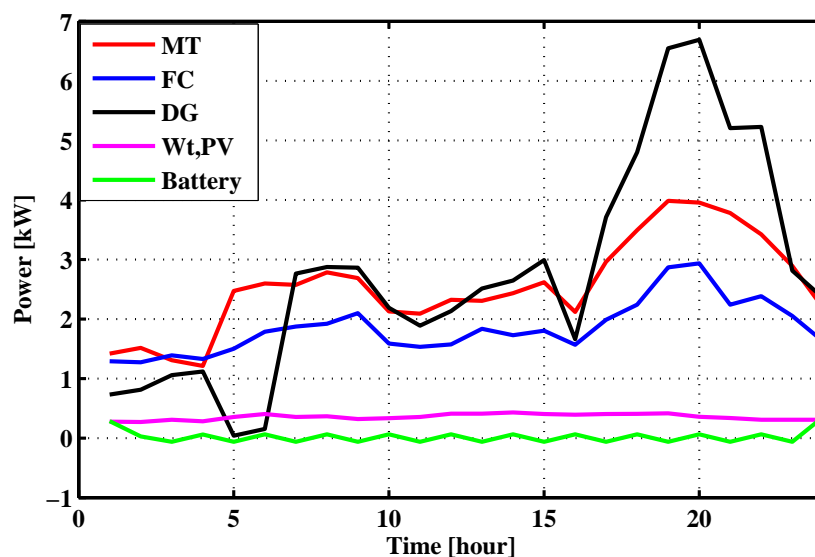


Figure 5.8: The hourly power curves using GA Scenario 2.

5.4.3 Scenario 3

Here the purchased tariff is 0.12 \$/kWh, the sold tariff 0.07 \$/kWh and the cost and emission functions are optimized individually. The result obtained is shown in Table 5.5. The emission is reduced to 14.5988 (kg/Day) when optimized individually, whereas the cost is increased to 85.2773 (\$/Day) in the second case. It can be noticed that the different tariff prices have an effect on the operation cost objective functions. With the same tariffs,

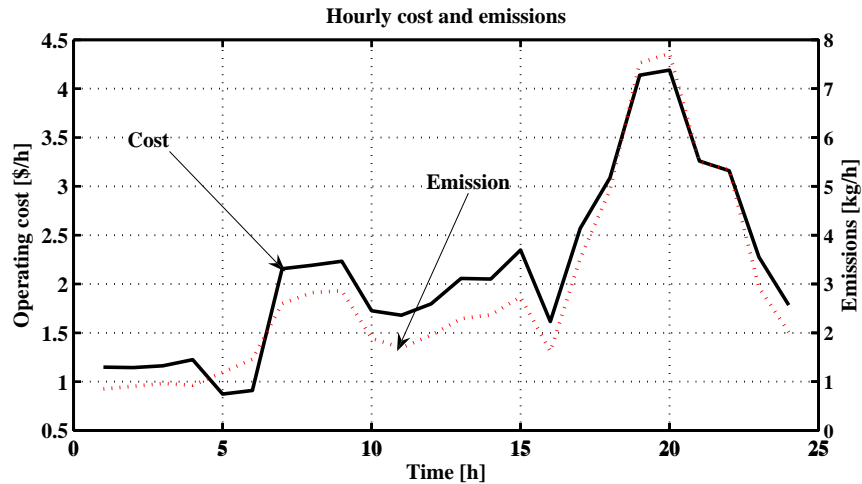


Figure 5.9: Hourly operating cost and emission using MOGA Scenario 2.

Table 5.5: The objective functions when optimized individually using MOGA Scenario 3

	P_L (kW/Day)	T E(kg/Day)	T C(\$/Day)	O G (kW/Day)	S.P (kW/Day)	P.P (kW/Day)
Case 1	171.4009	219.8892	85.2773	345.6814	174.2805	00.0000
Case 2	171.4009	14.5988	114.9525	19.0519	00.0000	152.3490

the hourly cost and emission are illustrated in Figure 5.10, which shows that the cost and emissions are high when the DG is fully operated and the load is high.

Figures 5.11 and 5.12 show the operation point of the minimum operating cost and they indicate the minimum emission level for the different tariffs. These figures reveal that when θ in equation (4.20) varies from 0 to 1, the operating cost continuously increases, but the emission level decreases. Therefore, the test results clearly explain the trade-off between economy and environmental protection requirements for different tariffs.

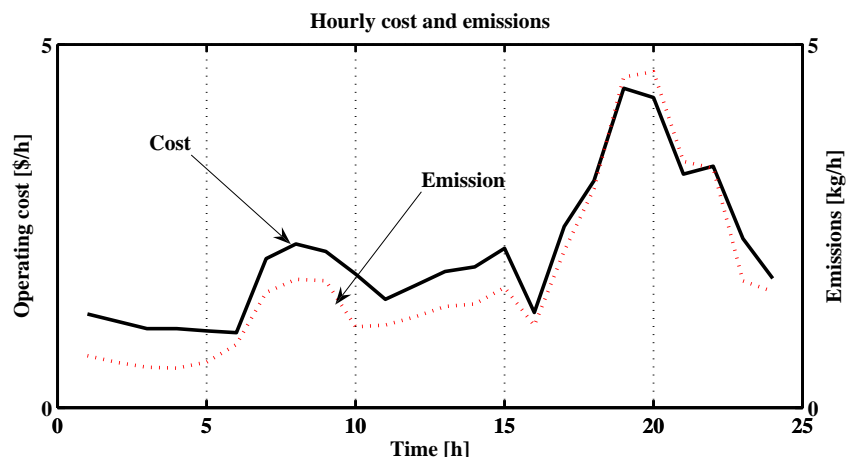


Figure 5.10: Hourly operating cost and emission using MOGA Scenario 3.

As in Chapter 4, the effect of changing the sold and purchased tariffs is studied here in four different cases as shown in Table 5.6 and Figures 5.13 and 5.14. For Cases 1 and 2 the effect of changing the purchased tariffs is studied. In Case 1, the sold power is 0.04 \$/kWh and the purchased tariff is 0.1 \$/kWh, while in Case 2 the value of the purchase tariff has increased to 0.16 \$/kWh and the sold one is the same as in Case 1. As expected,

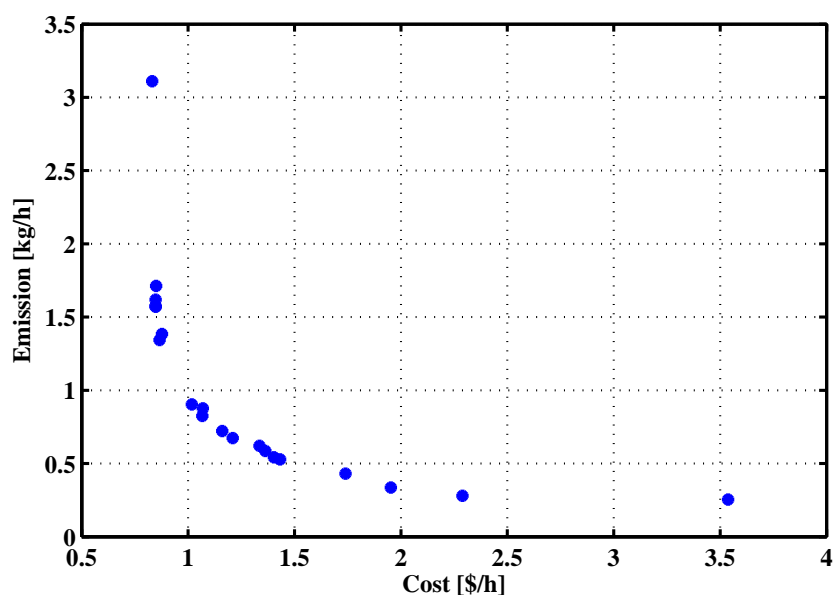


Figure 5.11: Trade- off in operating cost and emission using MOGA Scenario 3 and for $P = 0.12$ and $S = 0$.

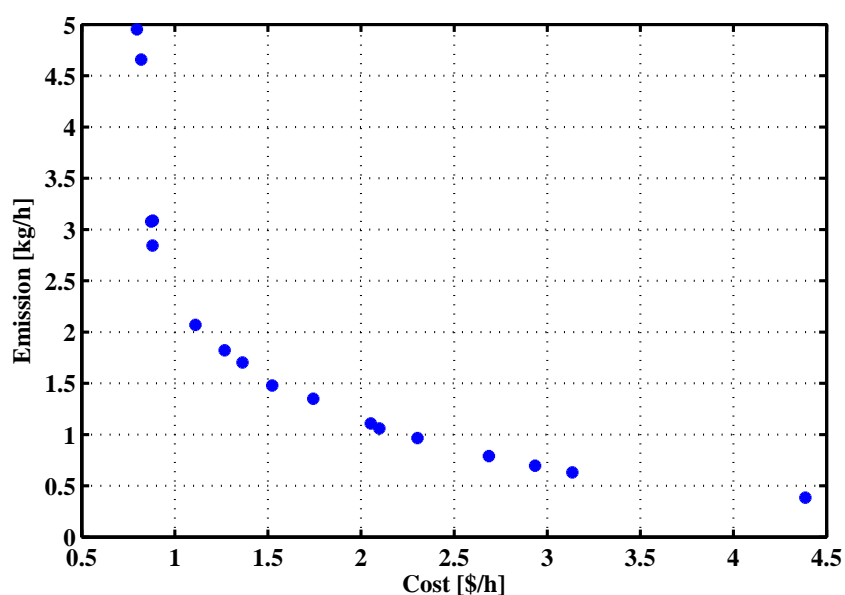


Figure 5.12: Trade- off in operating cost and emission using MOGA at Scenario 3 and for $P = 0.16$ and $S = 0.1$.

the MG increases the optimal generation when the purchased tariffs increase. It is more economical to buy power from the main grid if the purchased tariff is 0.1 \$/kWh.

Changes in the sold tariffs are considered in Cases 3 and 4. In these cases, the purchased tariff is kept constant at 0.12 \$/kWh, while the sold tariff is 0.0 \$/kWh in Case 3 and 0.04 \$/kWh in Case 4. It is noticeable that the MG generates more power when the sold tariffs are increased. However, there is an increase in the cost and emission per day. Higher values of the sold power tariffs give the possibility to produce more power to meet the load demand.

A direct comparison of the outcomes achieved by different cases is presented in Table 5.7. The results obtained using the proposed technique to minimize the total cost and

Table 5.6: The effect of the Purchased and Sold tariffs on the optimal Generation using MOGA and Scenario 3

	Load (kW/Day)	Optimal Generation (kW/Day)	Total Cost(\$/Day)	Total Emission(kg/Day)
Case 1	171.4009	120.4416	49.3850	39.1980
Case 2	171.4009	135.0016	52.0921	46.9082
Case 3	171.4009	124.5539	50.6185	41.3060
Case 4	171.4009	125.4585	50.9941	41.7836

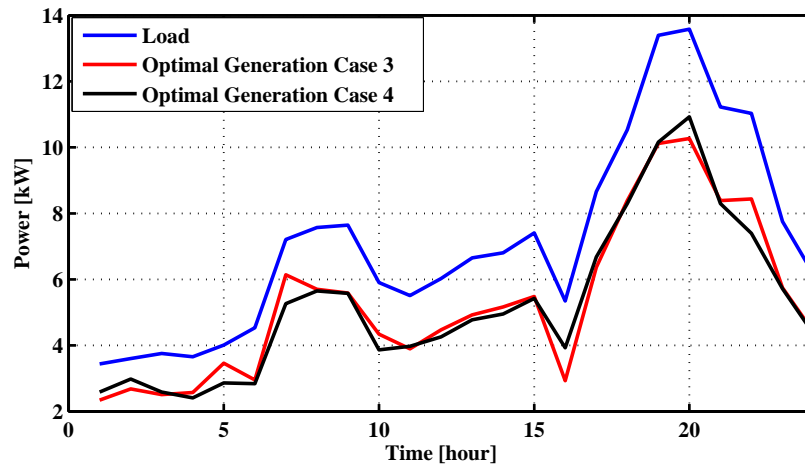


Figure 5.13: Effect of sold power tariff on the MG optimal operation using MOGA Scenario 3.

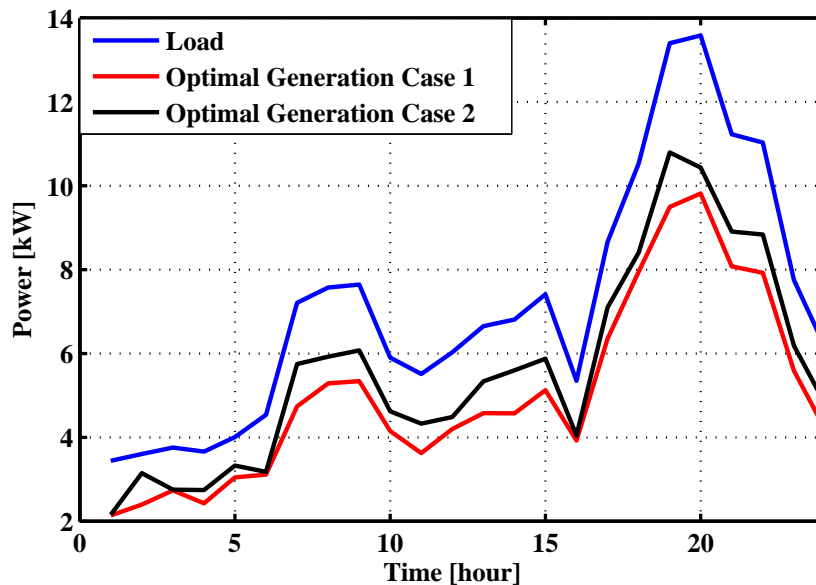


Figure 5.14: Effect of purchased power tariff on the MG optimal operation using MOGA Scenario 3.

total emissions is compared with the same strategies of settings as in Chapter 4. The first method is to operate the DG, FC, and MT at their rated power for the whole day (Case A). The second method is to optimize the operating costs individually (Case B). The scenario in the third is to optimize the emissions objective functions individually (Case C). The same result obtained from Case A in Chapter 4 is attained here and leads to the same conclusion. In the second scenario, the cost is reduced somewhat, but the emissions are

increased. In the third case, the cost increases while the emissions decrease and the optimal choice is to purchase more power from the main grid.

Finally, the problem is treated as a single objective optimization problem (Case D). Equation (4.21) is minimized to check the effectiveness of the proposed technique. The objective function is a linear combination of the cost and emission objectives.

With the proposed MOGA method, the total operating cost and emission are 48.7863 \$/day and 43.1379 kg/day respectively. Furthermore, the MOGA is slower than the other techniques in Chapter 4.

Table 5.7: Cost savings and emissions reductions of the MG using multiobjective optimization Scenario 3

	Average Cost & Emissions		Average difference with respect to the optimal case			
	Cost \$/Day	Emissions kg/Day	cost \$/Day	Emissions kg/Day	Cost%	Emissions%
Case A	95.3299	229.4895	46.5228	186.3516	95.3600 %	431.99 %
Case B	85.2773	219.8892	36.4910	176.7513	74.80 %	409.74 %
Case C	114.9525	14.5988	66.1662	-28.5391	135.62 %	-66.16 %
Case D	50.1359	74.0180	1.3496	30.8801	2.77 %	71.58 %
MOGA	48.7863	43.1379	00.0000	00.0000	00.0000	00.0000

5.5 Conclusions.

This chapter has presented the GA approach to solve the multiobjective problem. From the results obtained, optimization of the above-formulated objective functions using MOGA, yields not only a single optimal solution, but a set of Pareto optimal solutions, in which one objective cannot be improved without sacrificing other objectives. For practical applications, however, one solution is needed to be selected, which will satisfy the different goals to some extent. Such a solution is called the best compromise solution. One of the challenging factors of the trade-off decision is the imprecise nature of the decision maker's judgment.

Initially in all the three scenarios, minimum and maximum values of each original objective function are computed in order to obtain the last compromise solution. Minimum values of the objectives are obtained by giving full consideration to one of the objectives and neglecting the others. In this study, two objective functions are considered. Operating costs and emission level are optimized individually to obtain minimum values of the objectives. Owing to the conflicting nature of the objectives, emission level has to have maximum values when operating cost is minimum.

The GA transforms the original multiobjective optimization problem into a single-objective problem and, thus, the set of noninferior solutions can be easily obtained. Compared with the other conventional strategies of settings, the proposed approach significantly reduces the operating cost and emission level, while satisfying the load demand required by the multiobjective MG problem.

Chapter 6

MicroGrid Online Management Using Game Theory

6.1 Introduction

One of the main contributions in this thesis is a novel procedure to solve the MG management problem based on Game Theory and multiobjective optimization. The contribution is discussed in this chapter.

Game Theory is a collection of mathematical models formulated to study the situations of conflicts and cooperation. More precisely, it is a general theory of rational behavior for situations in which rational decision makers (players) have available with them a finite number of courses of action, each leading to a well-defined outcome or end with gains and losses expressed in terms of numerical payoffs associated with each combination of courses of action for each decision maker [99]. Game theory studies the phenomenon of negotiation between rational agents in conflict situations and in a very general setting. Game theory does not cover the games of changes where the decision makers do not have any influence on the results [100].

6.2 Game Theory

The cooperative game theory approach of solving a multi objective optimization problem of MG management can be stated as follows [25]. Two players are assumed to correspond to two objectives; one for operating cost and one for the emission level. While playing the game, each player will try to improve his own conditions that is, to decrease the value of his own objective function. The players will start to bargain from their respective reference (starting) values and put a joint effort in maximizing a subjective criterion (supercriterion) formed by themselves. It is assumed that each player has analyzed his own criterion before starting the game to find the maximum possible benefit he can obtain. This will also help him in guaranteeing against the worst value. This analysis is necessary since each player should know the extreme conditions of his own and others so that none of them is bargaining from a reference value which is unrealistic (i.e., unacceptable to the other player).

In reference [101], this method is applied to a three degree-of-freedom spring-and-damper system. The relative displacement and transmitted force are minimized subject to limits on the design variables, which are the mass, spring constant, and damping coefficient for each degree-of-freedom. In [26], controlled two-bar and twelve-bar trusses are actively optimized. There are four objective functions: weight, "control effort", effective damping response time, and performance index, which provides a measure of the total system energy. The crosssectional areas of the structural members are the design variables. Limits are placed on the damping ratios and cross-sectional areas. In [25], this approach is applied to the probabilistic design of an eighteen-speed gear train. Reliability in bending and in wear is maximized while the weight is minimized. The width of each gear is used as a design variable. In [102], a comparative study of several methods of multiobjective optimization has been carried out using two structural design optimization problems. The method is theoretically designed to reach a near Pareto optimal design and it is introduced so that the game theory can be practically applied without much deviation from its original form. Although the final design is aimed to be near Pareto optimum, the use of this method requires some additional work from the designer.

To increase the computational efficiency of the game theory method [103] it is proposed in [25] that the Pareto optimal solution generation and the maximization of the supercriterion are performed simultaneously. This may be done by combining the Pareto optimal solution generation and the supercriterion into one objective by subtracting the supercriterion from the Pareto optimal objective. This new objective may be minimized by a standard, single objective optimization program. This formulation, however, does change the characteristic of the optimization problem so that it is neither truly minimizing the Pareto objective nor it is truly maximizing the supercriterion. The constrained MO problem is formulated using the modified game theory as follows:

1. Form a constant initial design vector, minimize each of the n objectives separately and record the values of the other objectives at each optimal design vector. According to the game theory, the Pareto optimal solution is determined by solving the following problem [103]:

$$\mathbf{F}(\mathbf{P}) = \{CF(\mathbf{P}), E(\mathbf{P})\} \quad (6.1)$$

subject to

$$h_i(\mathbf{P}) = 0 \quad i = 1, \dots, q \quad (6.2)$$

$$g_j(\mathbf{P}) \leq 0 \quad j = 1, \dots, p \quad (6.3)$$

$$P_i^{\min} \leq P_i \leq P_i^{\max}, \quad \forall_i = 1, \dots, N \quad (6.4)$$

where the number of the objective functions = 2, and $\mathbf{F}(\mathbf{P}) : \mathbb{R}^n \rightarrow \mathbb{R}^2$. The vector of objective functions is denoted by $\mathbf{F}(\mathbf{P}) = (F(\mathbf{P}_1), F(\mathbf{P}_2))$. The decision variable vector $\mathbf{P} = (P_1, P_2, \dots, P_N)^T$ consists of all design variables in the problem and may be bounded. The collection of equality constraints, $\mathbf{H}(\mathbf{P}) = (h_1(\mathbf{P}_1), h_2(\mathbf{P}_2), \dots, h_q(\mathbf{P}_i))^T$, is an equality constraint vector, and similarly the inequality constraint vector, $\mathbf{G}(\mathbf{P}) = (g_1(\mathbf{P}_1), g_2(\mathbf{P}_2), \dots, g_p(\mathbf{P}_i))^T$ is less or equal to zero.

2. Due to the computational complexities when using the game theory approach, a modification to the method was proposed [25]. The solution is expected to be near optimal solution obtained by the original game theory. Normalize the objectives so that no objective due to its magnitude will be favored. The following normalization procedure gives zero as the optimum value and one as the worst value of the operating cost objective function:

$$CF_n(\mathbf{P}) = \frac{CF(\mathbf{P}) - CF(\mathbf{P}^*)}{CF_w - CF(\mathbf{P}^*)} \quad (6.5)$$

where CF_w is the worst of $CF(\mathbf{P})$ and it is defined as the maximum value of $CF(\mathbf{P})$. It is determined from $CF_w = \max_{j=1,2,\dots,N} CF(\mathbf{P}_j^*)$.

The minimum value of $CF(\mathbf{P})$ is called the best value of $CF(\mathbf{P})$, which is shown as $CF(\mathbf{P}^*)$, where \mathbf{P}^* is the optimal design vector obtained when only $CF(\mathbf{P})$ is minimized.

3. Formulate the supercriterion S : The supercriterion gives an indication as to how far the objective function is from its worst value at any design. Therefore, the higher the value of S , the lower cost and emission in terms of compromise solution.

This normalization procedure gives zero as the minimum value and one as maximum of the operating cost objective function.

$$S = 1 - CF_n(\mathbf{P}) \quad (6.6)$$

S always has value between zero and one due to the normalization with the same magnitude as the normalized objective.

4. Formulate a Pareto optimal objective FC using the normalized objective

$$FC(\mathbf{P}) = \sum_{i=1}^N c_i CF_i(\mathbf{P}) + c_2 E(\mathbf{P}) \quad (6.7)$$

subject to $c_1 + c_2 = 1$

5. Since FC has to be minimized and S has to be maximized, a new objective is created (for minimization)

$$OBJ(\mathbf{P}) = FC(\mathbf{P}) - S(\mathbf{P}) \quad (6.8)$$

subject to the three scenario constraints.

6.3 Results and Discussion

Multiobjective game theory is tested with the three different scenarios presented in Chapter 3. The method attempts to produce a good balance between the two objective functions in (6.1) by trying to keep them close to their optimum values and hence aims at reaching a Pareto optimal design. The first player, who corresponds to the operation cost objective, cannot claim a value lower than the minimum of his objective function. Furthermore, it is also guaranteed that the cost will never exceed the worst value which is its maximum. The same procedure is also true for the emission level objective function.

6.3.1 Scenario 1

Scenario 1 is studied, when the MG is working in the islanding mode. Figure 6.1 shows the trade-off between the operating cost and emission objective functions. Each point on the trade-off curve is a noninferior solution and corresponds to a unique set of generator schedules. The optimal generated powers of the sources are shown in Figure 6.2, in which the MT is the cheapest and is the lowest emission power source while the power is nearly full all the time. The second choice is the FC, and the poorest choice is the DG as it has the highest cost and emission. Figure 6.3 illustrates the hourly cost and emission of the MG, where the cost and emission level are high when the load is high. Table 6.1 presents the compromise output from the optimal configuration of the algorithm, in which 35.2130 \$/Day is obtained for the operating cost function and 76.4520 kg/Day for the emission level.

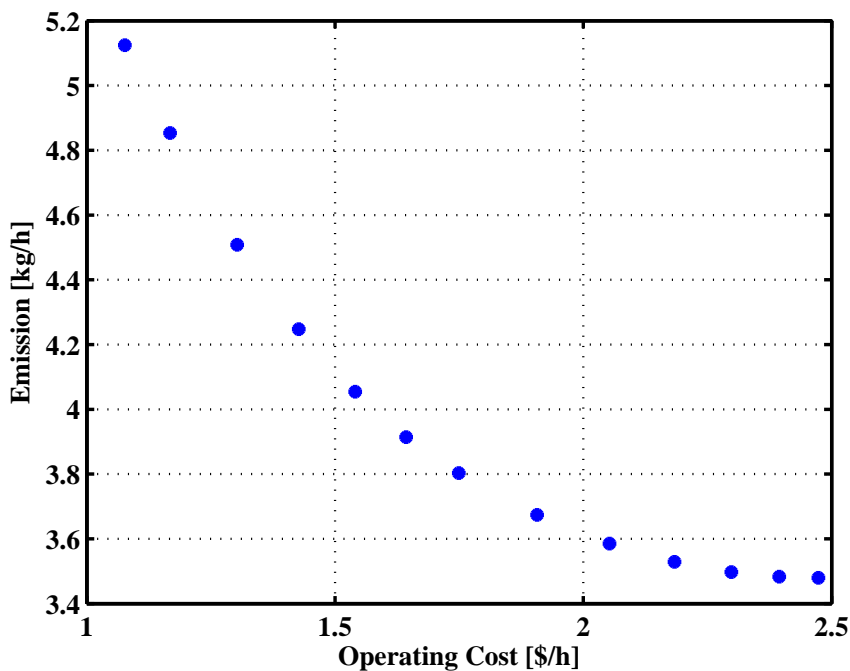


Figure 6.1: Trade- off in operating cost and emission using MOGT Scenario 1.

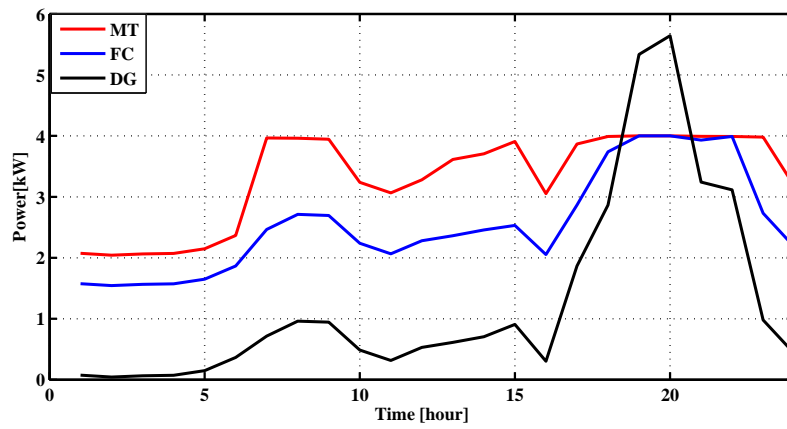


Figure 6.2: The hourly power curves using MOGT Scenario 1.

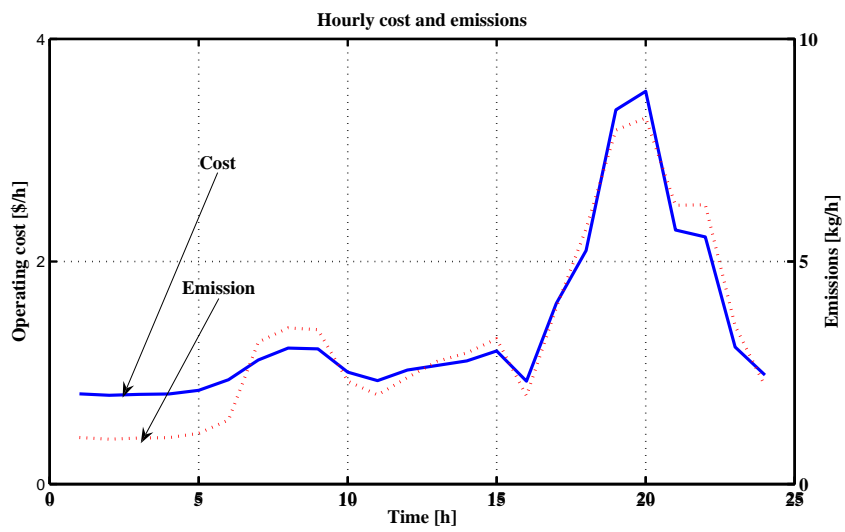


Figure 6.3: Hourly operating cost and emission using MOGT Scenario 1.

Table 6.1: The best selection of the power generators of the MG using MOGT: Scenario 1

P_L (kW/Day)	Optimal Generation (kW/Day)	Total Cost (\$/Day)	Total Emission (kg/Day)
171.2924	171.2928	35.2130	76.4520

6.3.2 Scenario 2

The proposed algorithm is then applied to Scenario 2, when the MG is working in the islanding mode. Table 6.2 presents the response of the algorithm to the load demand. The results shown in Figure 6.4 display the output power from the generators. The curves have almost the same shape as in Scenario 1. The figure also shows that the constraints (4.16) and (4.17) are inactive. The hourly cost and emission of the sources, when working optimally, are shown in Figure 6.5. They are high when all the sources are working nearly full efficiency. The distribution of the nondominated solutions obtained with the proposed approach is given in Figure 6.6. The results show that the proposed approach is superior and preserves the diversity of the nondominated solutions over the trade-off front.

Table 6.2: The best selection of the power generators of the MG using MOGT: Scenario 2

P_L (kW/Day)	Optimal Generation (kW/Day)	Total Cost (\$/Day)	Total Emission (kg/Day)
171.4009	171.4009	36.0704	77.1775

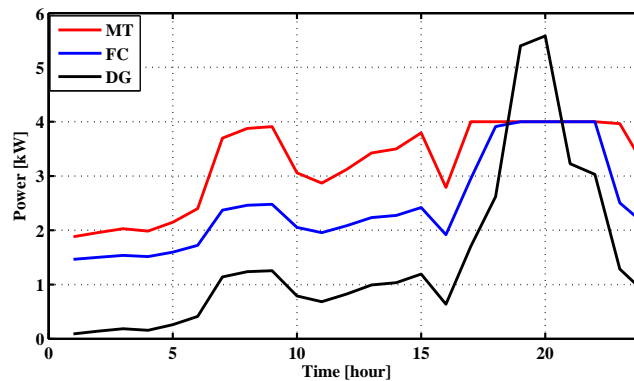


Figure 6.4: The hourly power curves using MOGT Scenario 2.

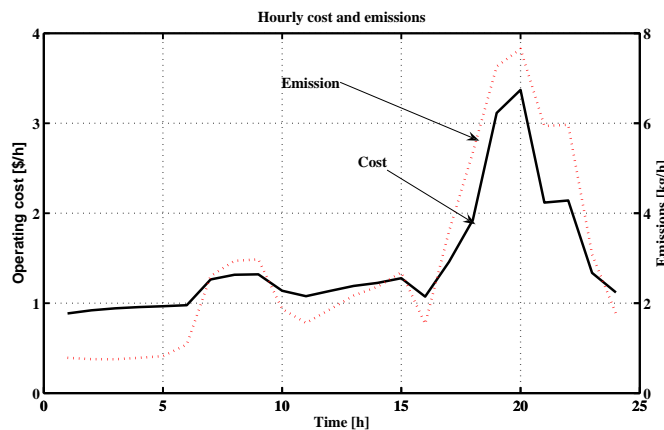


Figure 6.5: Hourly operating cost and emission using MOGT Scenario 2.

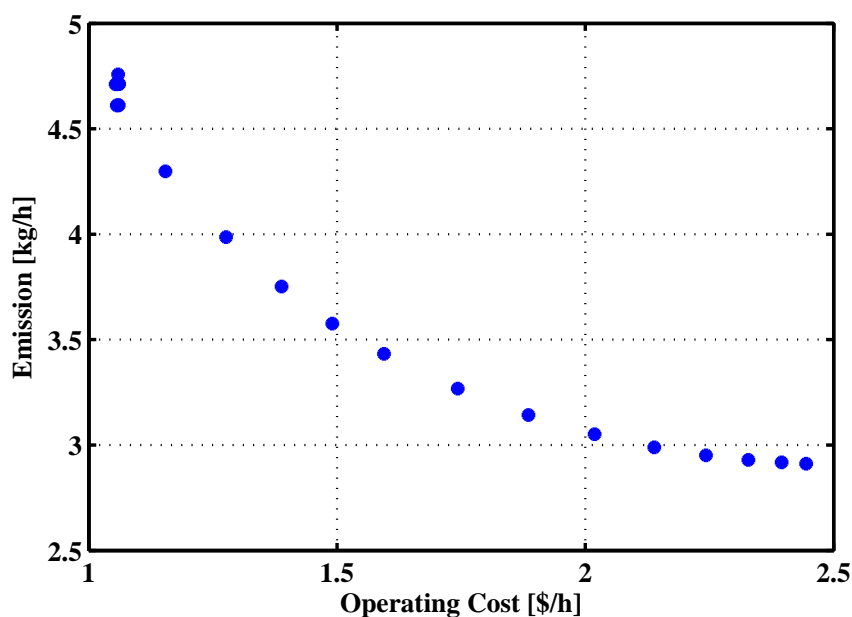


Figure 6.6: Trade- off in operating cost and emission using MOGT Scenario 2.

6.3.3 Scenario 3

In this Scenario, the MG is connected to the main grid. At first, to explore the extreme values of the operating cost and emission level objective functions, they are optimized individually for purchased tariff equal to 0.12 \$/kWh and the sold tariff 0.07 \$/kWh. The result obtained is shown in Table 6.3. The emission is reduced to 31.3689 (kg/Day) when optimized individually (Case 2), whereas the cost increased to 58.5249 (\$/Day). In Case 1 the operating cost is optimized individually. The total operating cost is found to be 40.7757(\$/Day) and the total emission 53.1386(kg/Day). It can be noticed that the presence of the tariff prices has an effect on the operation cost objective functions.

Table 6.3: The objective functions when optimized individually using MOGT: Scenario 3

	P_L (kW/Day)	T E(kg/Day)	T C(\$/Day)	O G (kW/Day)	S.P (kW/Day)	P.P (kW/Day)
Case 1	171.1044	53.1386	40.7757	138.3802	00.0000	32.7242
Case 2	171.1044	31.3689	58.5249	89.8034	00.0000	81.3009

With the same tariffs the problem is solved as a multiobjective optimization problem. The hourly cost and emission are illustrated in Figure 6.7, which shows that the cost and emissions are high when the DG is fully operated, and the load is high. Figure 6.8 shows the optimal generated power. It is noticeable that the DG is turned off most of the time and switched on only when the power from other sources is not enough to meet the load demand.

The Pareto optimal front for different tariffs are shown in Figures 6.9 and 6.10. These figures ensure that the Pareto optimal front have a good diversity characteristic of non-dominated solutions. Furthermore, the problem is efficiently solved by Game Theory. The results also represent the operation point of the minimum operating cost, and indicate the minimum emission level for different tariffs.

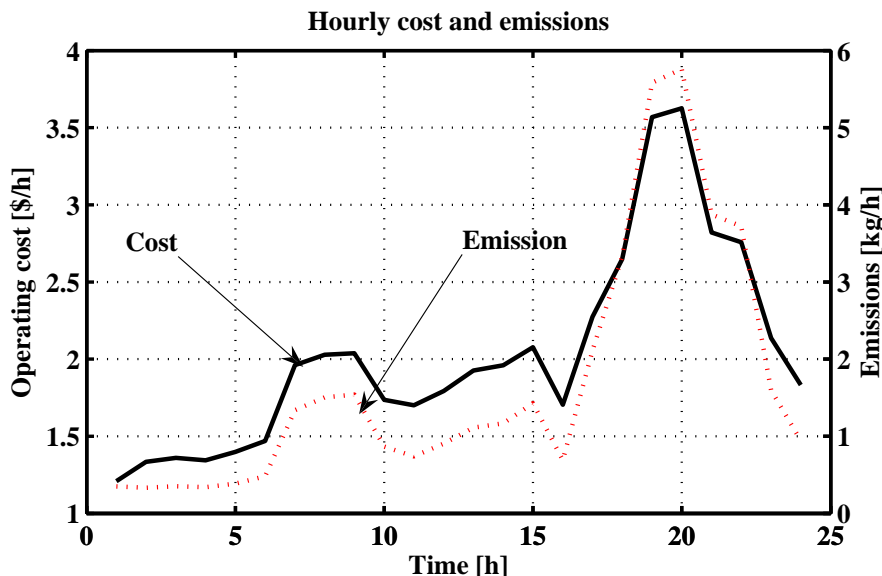


Figure 6.7: Hourly operating cost and emission using MOGA Scenario 3.

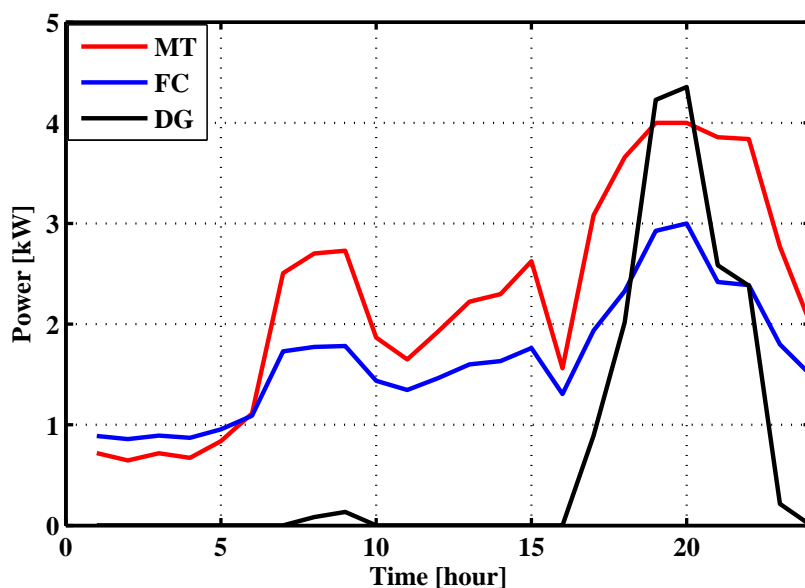


Figure 6.8: The hourly power curves using MOGT Scenario 3.

As in Chapters 4 and 5, the effect of changing the purchased and sold tariffs is studied here in four different cases as given in Table 6.4 and Figure 6.11. In Cases 1 and 2 changing the purchased tariffs is studied. In Case 1, the sold power is 0.04 \$/kWh and the purchased tariff is 0.1 \$/kWh. In Case 2, the value of the purchased tariff has increased to 0.16 \$/kWh and the sold tariff is the same as in Case 1. As expected the MG increases the optimal generation when the purchased tariff value increases. It is more economical to buy power from the main grid. Changes in the sold tariff is considered in Cases 3 and 4. The purchased tariff is kept constant at 0.12 \$/kWh, while the sold tariff is 0.0 \$/kWh in Case 3 and 0.04 \$/kWh in Case 4. From Table 6.4 it is noticeable that the MG generates the same power when increasing the sold tariffs. However, there is no increase in the cost and emission per day. The optimal generated power is always less than the load, which means that changing the sold tariff has no effect on the optimal generation.

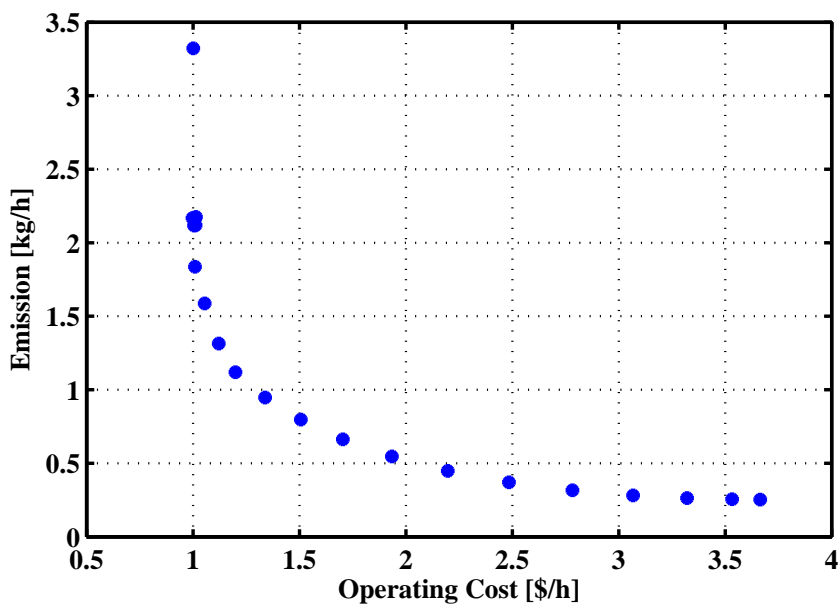


Figure 6.9: Trade- off in operating cost and emission using MOGT Scenario 3 and for P = 0.12 and S= 0.

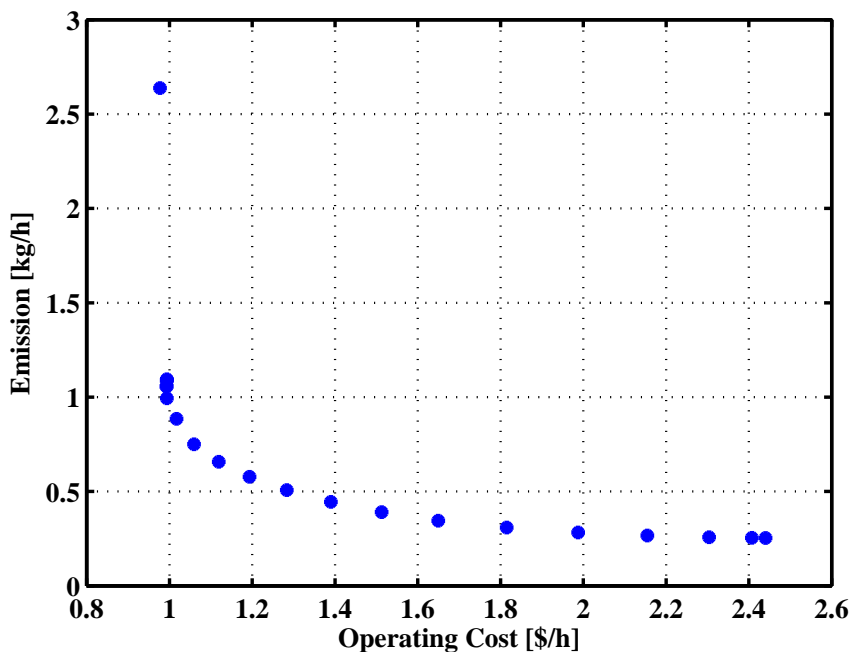


Figure 6.10: Trade- off in operating cost and emission using MOGT at Scenario 3 and for P = 0.16 and S= 0.1.

Table 6.4: The effect of the Purchased and Sold tariffs on the optimal Generation using MOGT: Scenario 3

	Load (kW/Day)	Optimal Generation (kW/Day)	Total Cost(\$/Day)	Total Emission(kg/Day)
Case 1	171.4009	108.1694	45.4938	39.8396
Case 2	171.4009	113.7652	54.1840	41.2879
Case 3	171.4009	110.5522	48.7014	40.4481
Case 4	171.4009	110.5522	48.7014	40.4481

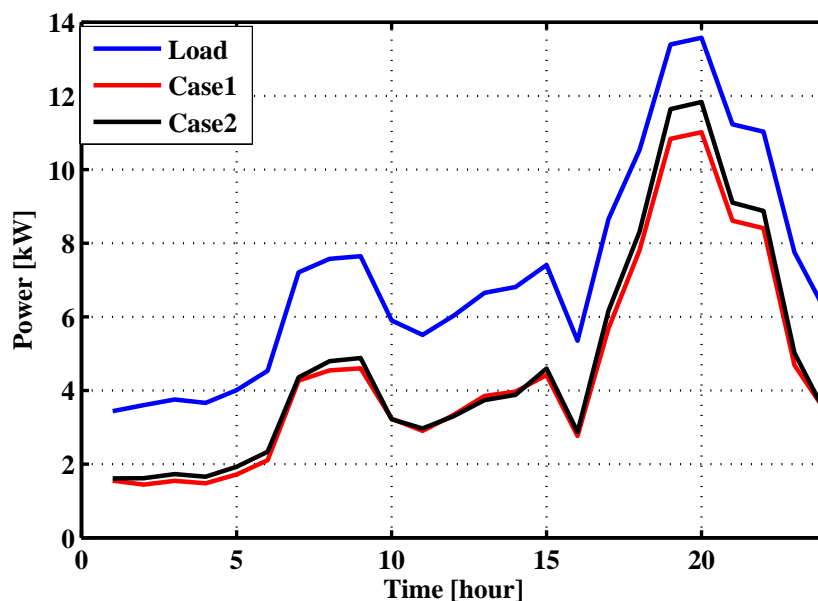


Figure 6.11: Effect of purchased power tariffs on the MG optimal operation using MOGT Scenario 3.

A direct comparison of the outcomes achieved by the different cases is presented in Table 6.5. The results obtained using our proposed technique to minimize the total cost and total emissions are compared with the same strategies of settings as in Chapters 4 and 5. The first case is when the DG, FC, and MT operate at their rated power for the whole day (case A). In the second case the costs are optimized individually (case B). The third case is to optimize the emission objective function individually (case C).

The same result obtained for Case A in Chapters 4 and 5 is reached here and leads to the same conclusion. In the second case, the cost is reduced somewhat, but the emissions are increasing. In Case C, the cost increase while the emissions decreased compared to Case B and the optimal choice is to purchase more power from the main grid.

With the proposed MOGT method, the total operating cost and emissions are 47.4326 \$/day and 41.4918 kg/day respectively. It can be noticed that the MOGT is more capable of handling the multiobjective optimization problem of the MG when the problem becomes more complex. Furthermore, the MOGT is slower than the other techniques discussed in Chapter 4 although the results are better here.

Table 6.5: Cost savings and emissions reductions of the MG using multiobjective optimization: Scenario 3

	Average Cost & Emissions		Average difference with respect to the optimal case			
	Cost \$/Day	Emissions kg/Day	cost \$/Day	Emissions kg/Day	Cost%	Emissions%
Case A	95.3091	229.4895	47.8765	187.9977	100.94 %	453.10%
Case B	59.8804	39.0681	12.4478	-2.4237	26.24 %	-5.84%
Case C	28.2629	62.9865	-19.1697	21.4947	-40.41 %	51.80 %
MOSQP	49.3980	44.0851	1.9654	2.5933	4.14 %	6.25 %
MOMADS	48.3012	41.8015	0.8686	0.3097	1.83 %	0.75 %
MOGA	48.7863	43.1379	1.3537	1.6461	2.85 %	3.97 %
MOGT	47.4326	41.4918	00.0000	00.0000	00.0000	00.0000

6.4 Conclusions

A new approach for solving multiobjective management problem of the MG has been presented. Game Theory helps the proposed method to efficiently search and to actively explore solutions. The introduced technique is able to handle the changes in the purchased tariff effectively by increasing the generated power, while changing the sold tariff has no effect on the generated power as it is smaller than the load. The significant merits of the proposed approach are that it can automatically adjust the generated power to meet the changes in the load demand. However, the proposed method requires more time in comparison with the techniques investigated in Chapters 4 and 5. The results confirm that the proposed MOGT outperforms the setting, in both reducing the operating cost and emission level, according to the power demand and constraints for the MG.

Chapter 7

Conclusions and Future Work

7.1 Conclusions

In this final chapter, the importance, aims and outcomes of this research are highlighted and summarized. The research is discussed in terms of what it aims for and how it could contribute to the power industry's needs. It also explores, how the research of MGs could be extended and improved and how this might be done.

By making optimal use of the small and varied energy sources which comprise MGs, MGs may be able to make a significant contribution to the distributed power generation. For instance, if the sun is shining, the PV array may provide power; if it is windy the wind turbine will generate the power; if it is neither or if more power is needed, the fuel cell, diesel engine, and micro-turbine or main supply can be used. The key is how to orchestrate the power sources in the optimal manner. The inclusion of batteries in a MG system allows excess power produced to be stored, or alternatively, the excess power could be put into the main grid. In this way it is expected that MGs could reduce pollution and deliver reliable energy in a variety of situations as discussed in Chapter 1.

To understand the behaviour of a Microgrid, the thesis develops models suitable for overall analysis and design. The aim of the work is to model both for optimization and for understanding the steady-state behaviour of the MG's individual power sources. The final goal is to lay a groundwork which would allow efficient management of the MGs by minimizing the operating costs and reducing emission level while meeting the load demand. More specifically, steady-state and optimization models for diesel engines, fuel cells, photovoltaic cells, micro-turbines, wind turbines, and battery storage have been developed. All models developed will allow studies of different scenarios that provided an understanding of MGs for online management application.

The online management of MGs for three different scenarios is addressed to understand the behaviour of the MG in islanding and utility connected situations. Single and multi-objective functions are presented of the optimization producer. Two techniques to solve the single objective problem of the MG are applied. They are SQP and MADS in Chapter 3. For the multiobjective case MOMADS and MOSQP are used as presented in Chapter 4. MOGA is applied in Chapter 5. Finally, the MOGT approach is explained and applied for the same problem in Chapter 6..

7.2 Modelling of the MG components

7.2.1 Modelling of the Diesel Engine

The general structure of the fuel actuator system is usually represented as a first order phase-lag network, which is characterized by a gain, and time constant. The output of the actuator is the fuel-flow. Fuel flow is then converted into mechanical torque after a time delay and engine torque constant, diesel engine can be represented by such a model.

An economic model for the Diesel Generator is constructed from real manufactural data. The diesel fuel consumption data of a 6-kW diesel generator set (Cummins Power DNAC 50 Hz) is used to model the fuel cost function.

7.2.2 Modelling of the Fuel Cell

Dynamic responses of the output power, voltage, and current are obtained by modelling Solid Oxide Fuel Cell (SOFC). The responses of pressure difference between hydrogen and oxygen could also be studied. The response time of a SOFC is limited by the time constants of the fuel processor, which are normally large and cannot be made smaller for a given fuel cell due to physical limitations imposed by the parameters of the corresponding chemical reactions. Therefore, the response time of the plant cannot be enhanced by manipulating its input. Technological changes in the fuel cell plant are required if the fuel cell power plant is to operate in a stand alone mode, which requires load-following capabilities. Alternatively, other technical solutions should be sought; for example, the combined use of fuel cell modules and a gas turbine, or the use of an external energy storage, such as batteries, a flywheel, or a superconducting magnetic energy storage device. The developed SOFC system model appears suitable for the time scale to be used in our dynamic simulation.

An economic model of the FC is obtained from the the efficiency curve of the PEMFC. The efficiency curve is used to develop the cell efficiency as a function of the electrical power.

7.2.3 Modelling of the MicroTurbine

The microturbine model has been developed to investigate the responses of the output power, shaft speed and DC link voltage for different levels of power demand. The simulated model and the results obtained for various operating conditions permit to predict the performance of the microturbine. The simulation results demonstrate that the established model provides a useful tool suitable to study and to perform accurate analysis of most electrical phenomena that occur when a microturbine is connected to the grid. The simulation results obtained for different levels of power demand show the usefulness of the model and its accuracy.

As in the case of a FC, the same procedure is applied to the MT to obtain an economic model of the MT. However, the parameters and curves are modified to properly describe the performance of the MT unit.

7.2.4 Modelling of the Wind Turbine

Modelling of the wind turbine with a doubly fed induction generator and also the development of models of the most important current wind turbine types for power system dynamics simulations are completely covered. First, the basic working principle of the wind turbine is discussed. Then, an overview over the most important types of wind turbines is given: they are the constant speed wind turbine with a squirrel cage induction generator, and the variable speed wind turbine with a doubly fed induction generator and the one with a direct drive synchronous generator. The structure of the model of each turbine type is depicted, after which equations for each of the subsystems are given. Finally, the models are used in simulations in order to investigate the impact of changing the wind speed on the active power, pitch angle, rotor speed, and also to study the power curve of the wind turbine. Measured wind sequence data is used to simulate the responses of active power, rotor speed, pitch angle. Wind turbine responses with a designed signal which has different values of wind speed are also simulated. From these, it can be seen that the responses of the simulated input and measured input wind speed have almost the same range of fluctuations of the output power. The range of the response of the rotor speed fluctuations are similar, the behavior of the response of the pitch angle is different as there was no pitch controller in the design model.

The WT in the optimization model is modeled using industrial data. The actual AIR403 power curve of the wind turbine is obtained from the owner's manual, in order to find the mathematical equations representing the power curve.

7.2.5 Modelling of the Photovoltaic Cell

Having a simple but equivalent model of a photovoltaic cell allows the extraction of the device's electrical characteristics. The model is presented and analyzed. The current voltage relationship of the PV is determined by the shunt and series resistances and the magnitude of the current source. From the model equations, it can be seen that the open circuit voltage is logarithmically proportional to the magnitude of the current source. The short circuit current is directly proportional to illumination intensity. The solar cell current ranges from zero to short circuit current. The solar cell voltage ranges from zero to open circuit voltage, U_{oc} . As the current increases, the voltage decreases due to the series resistance. As the voltage increases, the current decreases due to the shunt resistance. Since power is the product of voltage and current, the current that will produce the maximum power current will be found to be somewhere between zero and the short circuit current, and the maximum power voltage somewhere between zero and open circuit voltage.

The PV characteristics are presented in operating conditions that differ from the Standard Test Condition (STC). The effect of solar irradiation and ambient temperature on PV characteristics are modeled. The effect of solar intensity is modeled by considering that power output of the PV module is directly proportional to the irradiance. On the other hand, the temperature effect is represented by a temperature coefficient of power.

7.3 The Online Management of the MG

7.3.1 Online Management using MADS

A new approach for optimizing the performance of the MG for residential or industrial applications is presented. The single objective operating cost function is optimized using SQP and MADS methods for three different scenarios proposed in Chapter 3. The MADS has a proven good capability to handle the operation management problem of the selected MG units when supplying the load. Analyzing the obtained results demonstrates a significant reduction in the daily operating costs using the MADS, which contributes to improving the economic feasibility of the MG units. Supplying the load using MADS shows a lower daily operating cost compared to SQP.

7.3.2 Multiobjective using MOMADS

When the emission level is added as an objective function, the problem is solved with multiobjective optimization techniques. MOSQP and MOMADS are applied to the problem in Chapter 4. Constraint functions and three scenarios are added to the optimization problem to reflect some of the additional considerations often found in a small-scale generation system. The results of the optimal power operating costs and emissions curves for the MG ensure that the optimization works very well and can give the optimal power to the generators after taking the operating costs and emissions into account.

7.3.3 Multiobjective using MOGA

A novel approach to solve the Multiobjective problem of Chapter 4 is to use genetic algorithms, the MOGA approach. Initially in all three scenarios, minimum and maximum values of each original objective function are computed in order to obtain the best compromise solution. Minimum values of the objectives are obtained by giving full consideration to one of the objectives and neglecting the others. Comparison with MOSQP and MOMADS, the proposed approach significantly reduces the operating costs and the emission level, while satisfying the load demand required for the multiobjective MG problem. The main disadvantage is that it will take quite a long time to obtain the optimal setting.

7.3.4 Multiobjective using MOGT

A new approach for solving the multiobjective management problem using game theory, MOGT, is proposed. Game Theory helps the optimization algorithm to search efficiently and explore actively solutions. The introduced technique is able to handle the changes in the purchased tariff effectively by increasing the generated power, while the sold tariff changes have no effect on the generated power as it is smaller than the load. The significant merits of the proposed approach are that the proposed method can automatically adjust the generated power to meet the changing load demand. However, the proposed method requires more time in comparison with the techniques discussed in Chapters 4, 5.

7.4 Microgrid Modelling and the Future

The next step in this research is to learn more about how the sources interact with each other. More specifically their relationship to each other needs to be defined. If all goes as anticipated and the MG system is developed, the control of the system will likely be imbedded within the electronics. It is possible to use specialized controllers to get a more stable response and to use each power source more efficiently. This should certainly be researched and considered once the power sources interaction and relationship with each other and the mains have been defined. Other aspects that could be developed further are the individual sources within the MG. This could be done at two levels. The first is the consideration of other variables for each source. For example, the wind speed is not considered for the PV array and in some conditions it would prove quite significant. Also, working in pu is more desirable than actual values: the full conversion of the microsources to pu would be useful. Another issue is to keep the model up-to-date with the technology. In the area of PV arrays and micro turbines technology is rapidly changing and improving.

The final important aspect is to obtain some actual MG data (rather than data from individual power sources). During this research work we were unable to find any actual data about implemented MGs. This is likely due to MGs being such a new idea and therefore no data is currently available.

7.5 Final Remarks and Future Work

In this presented work, modelling and online management of components of a MG system has been successfully done. Models, which allow for investigation of the individual power sources behaviour, have been developed. The work was carried out by doing extensive research and by using a design process to implement each system individually. Testing and development through understanding was also a significant part of this work. The goals of this work have been met and it is anticipated that further research and development will be carried out on the system, with the goal that MGs will be able to make a valid, greener, contribution to the world's growing energy needs. The future steps will be introducing more constraints to the optimization problem, study also the communication infrastructure used to communicate between the microsources and central controller.

References

- [1] N. Jenkins, R. Allan, P. Crossley, D. Kirschen, and G. Strbac. *Embedded Generation*. The Institution of Electrical Engineers, UK, 2000.
- [2] T. E. Hoff, H. J. Wenger, and B. K. Farmer. Distributed generation: An alternative to electric utility investments in system capacity. *Energy Policy*, 24(2):137 – 147, 1996.
- [3] B. Lasseter. Microgrids [distributed power generation]. In *IEEE Power Engineering Society Winter Meeting, 2001.*, volume 1, 146–149, Columbus, Ohio, Feb 2001.
- [4] R. Lasseter. Microgrids. In *IEEE Power Engineering Society Winter Meeting, 2002*, volume 1, 305 – 308, New York, NY, 2002.
- [5] Y. Zoka, H. Sasaki, N. Yorino, K. Kawahara, and C.C. Liu. An interaction problem of distributed generators installed in a microgrid. In *Proc. of IEEE on Electric Utility Deregulation, Restructuring and Power Technologies Conference*, volume 2, 795 – 799, Hong Kong, April 2004.
- [6] The future of village power supply in remote areas. [Online]. Available: <http://www.iset.uni-kassel.de/>.
- [7] A. F. Farret and M. G. Simoes. *Integration of Alternative Sources of Energy*. John Wiley & Sons, Ltd, New Jersey, 2006.
- [8] S. Meliopoulos. Challenges in simulation and design of μ grids. In *Proc. of the 2002 IEEE/PES Winter Meeting, New York, NY, 2002*.
- [9] G. Venkataramanan and M. Illindala. Microgrids and sensitive loads. In *Proc. IEEE Power Eng. Soc. Winter Meeting, 2002*, volume 1, 316 – 322, 2002.
- [10] J. M. Correa, S. Chakraborty, M. G. Simoes, and F. A. Farret. A single phase high frequency ac microgrid with an unified power quality conditioner. In *Proc. IEEE-Industry Applications Conference*, volume 2, 956 – 962, Oct. 2003. Conference Record of the 38th IAS Annual Meeting, SaltLake City, UT.
- [11] Microgrids: reliable power in a small package. [Online]. Available: <http://www.lbl.gov/Science-Articles/Archive/EETD-microgrids.html>.
- [12] R. Lasseter, A. Akhil, C. Marnay, J. Stephens, J. Dagle, R. Guttromson, A. Meliopoulos, R. Yinger, and J. Eto. White paper on integration of distributed energy resources. the certs microgrid concept. Tech. rep, 2002.
- [13] C. A. Hernandez-Aramburo, T. C. Green, and N. Mugniot. Fuel consumption minimization of a microgrid. *IEEE Transactions on Industry Applications.*, 41(3):673 – 681, May/June 2005.

-
- [14] S. B. Patra, J. Mitra, and S. J. Ranade. Microgrid architecture: A reliability constrained approach. In *Power Engineering Society General Meeting, 2005. IEEE*, volume 3, 2372 – 2377, June 2005.
- [15] J. H. Talaq, F. El-Hawary, and M. E. El-Hawary. A summary of environmental/economic dispatch algorithms. *IEEE Transactions on Power Syst*, 9(4):1508 – 1516, Aug. 1994.
- [16] J. Nanda, D. P. Kothari, and K. S. Lingamurthy. Economic emission load dispatch through goal programming technique. *IEEE Transactions on Energy Conversion*, 3:26 – 32, March.1988.
- [17] J. Nanda, H. Lakshman, and M. L. Kothari. Economic emission load dispatch with line flow constraints using a classical technique. In *Proc. Inst. Elect. Eng., Gen., Transm. Distrib*, volume 141, 1 – 10, Jan. 1994.
- [18] C. M. Huang, H. T. Yang, and C. L. Huang. Bi-objective power dispatch using fuzzy satisfaction-maximizing decision approach. *IEEE Transactions on Power Systems*, 12:1715 – 1721, Nov. 1997.
- [19] L. C. Chao, Ji. H. L., and T. S. Ching. New approach with a genetic algorithm framework to multi-objective generation dispatch problems. *European Transactions on Electrical Power*, 15:381 – 395, 2005.
- [20] M. A. Abido. Multiobjective evolutionary algorithms for power dispatch problem. *IEEE Transactions on Evolutionary Computation*, 10(3):315 – 329, June 2006.
- [21] A. M. Azmy and I. Erlich. Online optimal management of pem fuel cells using neural networks. *IEEE Transactions on Power Delivery*, 20(2):1051 – 1058, April 2005.
- [22] M. A. Abido. Environmental/economic power dispatch using multiobjective evolutionary algorithms. *IEEE Transactions on Power Syst*, 18(4):1529 – 1537, November 2003.
- [23] R.T. Marler and J.S. Arora. Survey of multiobjective optimization methods in engineering. *Structural Multidisciplinary Optimization*, 26:369 – 395, 2004.
- [24] C. Audet, J. E. Dennis, and Jr. Mesh adaptive direct search algorithms for constrained optimization. *SIAM Journal on Optimization.*, 17(1):188 – 217, 2006.
- [25] S. S. Rao and T. I Freiheit. A modified game theory approach to multiobjective optimization. *Journal of Mechanical Design*, 113:286 – 291, 1991.
- [26] S. S. Rao, V. B. Venkayya, and N. S. Khot. Game theory approach for the integrated design of structures and controls. *AIAA Journal*, 26:463 – 469, 1988.
- [27] W. Morgantown. Emission rates for new dg technologies. The Regulatory Assistance Project, May 2001. [Online]. Available: <http://www.raponline.org/ProjDocs/DREmsRul/Collfile/DGEmissionsMay2001.pdf>.
- [28] S. Häggmark, V. Neimane, U. Axelsson, P. Holmberg, G. Karlsson, K. Kauhaniemi, M. Olsson, and C. Liljergren. Aspects of different distributed generation technologies, CODGUENT WP. March 2003. [Online]. Available: <http://www.energia.fi/attachment.asp?Section=1353&Item=10792>.

-
- [29] G. S. Stavrakakis and G. N. Kariniotakis. A general simulation algorithm for the accurate assessment of isolated diesel-wind turbines systems interaction. I. A general multimachine power system model. *IEEE Transactions on Energy Conversion*, 10(3):577 – 583, Sept 1995.
- [30] B. Kuang, Y. Wang, and Y. L. Tan. An H_∞ controller design for diesel engine systems. In *Power System Technology, International Conference Proceedings*, volume 1, 61 – 66, Dec. 2000.
- [31] S. Roy, O. P. Malik, and G. S. Hope. A least squares based model fitting identification technique for diesel prime movers with unknown dead time. *IEEE Transactions on Energy Conversion*, 6(2):251 – 256, June 1991.
- [32] S. Roy, O. P. Malik, and G. S. Hope. An adaptive control scheme for speed control of diesel driven power-plants. *IEEE Transactions on Energy Conversion*, 6(4):605 – 611, Dec. 1991.
- [33] Y. Hu, M. Cirstea, M. McCormick, and L. Haydock. Modelling and simulation of a variable speed stand-alone generator system. In *Proc. of Power Electronics and Variable Speed Drives, 2000. Eighth International Conference*, pages 372 – 377, Sept. 2000.
- [34] S. Roy, O. P. Malik, and G. S. Hope. A k- step predictive scheme for speed control of diesel driven power plant. *IEEE Transactions on Industry Application*, 29(2):389 – 396, March/April 1993.
- [35] W. Y. Yang, W. Cao, T-S. Chung, and J. Morris. *Applied Numerical Methods Using Matlab*. John Wiley & Sons Inc, Canada, 2005.
- [36] A. J. Wood and B. F. Wollenberg. *Power Generation, Operation and Control*. John Wiley & Sons, Ltd, New York, 1996.
- [37] C. D. Walters and B. G. Sheble. Genetic algorithm solution of economic dispatch with valve point loading. *IEEE Transactions on Power Systems*, 8(3):1325 – 1332, August 1993.
- [38] [online]. available: www.cumminspower.com/commercial1/diesel/s-1215.pdf. Technical report.
- [39] W. Morgantown. Fuel Cell Handbook. 6th Edition, EG&G Technical Services, Virginia, November 2002. [Online]. Available: <http://www.rwth-aachen.de/lbz/linksframe.html>.
- [40] J. A. Smith, M. H. Nehrir, V. Gerez, and S. R Shaw. A broad look at the workings, types, and applications of fuel cells. In *Power Engineering Society Summer Meeting*, volume 1, 70 – 75, Chicago, USA, July 2002.
- [41] M. W. Ellis, M. R. Von Spakovsky, and D. J Nelson. Fuel cell systems: efficient, flexible energy conversion for the 21st century. In *Proc. of the IEEE*, volume 89, pages 1808 – 1818, Dec. 2001.
- [42] A. R Sakhare, A. Davari, and A. Feliachi. Control of stand alone solid oxide fuel cell using fuzzy logic. In *Proc. of the 35th Southeastern Symposium on System Theory, 2003*, volume 35, pages 473 – 476, 16-18 March 2003.

-
- [43] J. Padulles, G. W. Ault, C. A. Smith, and J. R. McDonald. Fuel cell plant dynamic modelling for power systems simulation. In *Proc. of 3rd Universities Power Engineering Conference*, volume 34, 21 – 25, 1999.
- [44] K. Sedghisigarchi and A. Feliachi. Dynamic and transient analysis of power distribution systems with fuel cells-part i: fuel-cell dynamic model. *IEEE Transactions on Energy Conversion*, 19(2):423 – 428, 2004.
- [45] Y. Zhu and K. Tomsovic. Development of models for analyzing the load- following performance of microturbine and fuel cells. *Electric Power System Research Journal*, Dec. 2001.
- [46] F. Barbir and T. Gomez. Efficiency and economics of proton exchange membrane PEM fuel cell. *Int. Journal of Hydrogen Energy*, 21(10):891 – 901, October 1996.
- [47] T. Kreutz and J. Ogden. Assessment of hydrogen-fueled proton exchange membrane fuel cells for distributed generation and cogeneration. In *Proc. of the 2000 US DOE Hydrogen Program Review*, United States Department of Energy, 2000.
- [48] C. Sharma. Modeling of an island grid. *IEEE Transaction on Power System*, 13(3):971 – 978, August 1998.
- [49] W. G. Scott. Micro- turbine generators for distribution systems. *IEEE Industry Applications Magazine*, 4(4):57 – 62, May/June 1998.
- [50] H. Nikkhajoei and M. R. Iravani. Modeling and analysis of a micro-turbine generation system. In *IEEE Power Engineering Society Summer Meeting*, volume 1, 167 – 169, Chicago, USA, July 2002.
- [51] S. Haugwitz. Modelling of microturbine systems. Master’s thesis, Department of Automatic Control, Lund Institute of Technology, Lund, Sweden, May 2002.
- [52] R. Lasseter. Dynamic models for micro-turbines and fuel cells. In *IEEE Power Engineering Society Summer Meeting*, volume 2, 761 – 766, British Columbia, Canada, July 2001. NREL Report No. SR-560-32527.
- [53] S. Campanari and E. Macchi. Technical and tariff scenarios effect on microturbine trigenerative applications. *Journal of Engineering for Gas turbines and Power*, 126:581 – 589, July 2004.
- [54] S. Campanari, L. Boncompagni, and E. Macchi. Microturbines and trigeneration: Optimization strategies and multiple engine configuration effects. *Journal of Engineering for Gas turbines and Power*, 126:92 – 101, January 2004.
- [55] T. Ackermann. *Wind Power in Power Systems*. John Wiley & Sons, Ltd, Royal Institute of Technology, Stockholm Sweden, 2005.
- [56] J. G. Slootweg, S. W. H. de Haan, H. Polinder, and W. L. Kling. Modeling wind turbines in power system dynamics simulations. In *Power Engineering Society Summer Meeting, 2001. IEEE*, volume 1, 22 – 26, Vancouver, Canada, 15-19, July 2001.
- [57] E. S. Abdin and W. Xu. Control design and dynamic performance analysis of a wind turbine-induction generator unit. *IEEE Transactions on Energy Conversion*, 15(1):91 – 96, March 2000.

-
- [58] S. A. Papathanassiou and M. P. Papadopoulos. Mechanical stresses in fixed-speed wind turbines due to network disturbances. *IEEE Transactions on Energy Conversion*, 16(4):362 – 367, Dec. 2001.
- [59] J. Tamura, M. Ueno, Y. Matsumura, and S. Kimoto. Transient stability simulation of power system including wind generator by pscad/emtdc. In *Proc. of 2001 IEEE Porto Power Tech Conference*, volume 4, Sept. 2001.
- [60] S. A. Papathanassiou and M. P. Papadopoulos. Dynamic behavior of variable speed wind turbines under stochastic wind. *IEEE Transactions on Energy Conversion*, 14(4):1617 – 1623, Dec. 1999.
- [61] F. D. Kanellos, S. A. Papathanassiou, and N. D. Hatziargyriou. Dynamic analysis of a variable speed wind turbine equipped with a voltage source ac/dc/ac converter interface and a reactive current control loop. In *Proc. of Electrotechnical Conference*, volume 3, 986 – 989, May 2000.
- [62] S. Heier. *Grid Integration of Wind Energy Conversion Systems*. John Wiley & Sons, Ltd, Chicester, UK, 1998.
- [63] J. G. Slootweg, S. W. H. de Haan, H. Polinder, and W. L. Kling. General model for representing variable speed wind turbines in power system dynamics simulations. *IEEE Transactions on Power Systems*, 18(1):144 – 151, Feb. 2003.
- [64] Database of wind characteristics. [Online]. Available: <http://www.winddata.com>.
- [65] R. Chedid, H. Akiki, and S. Rahman. A decision support technique for the design of hybrid solar- wind power systems. *IEEE Transaction on Energy Conversion*, 13(1):76 – 83, March 1998.
- [66] M. K. C. Marwali, H. Ma, S. M Shahidehpour, and K. H. Abdul-Rahman. Short term generation scheduling in photovoltaic-utility grid with battery storage. *IEEE Transaction on Power System*, 13(3):1057 – 1062, August 1998.
- [67] [online]. available: www.nooutage.com/pdf/swwp_air403_landman.pdf. Technical report.
- [68] M. Pipattanasomporn. *A Study of Remote Area Internet Access with Embedded Power Generation*. PhD thesis, Faculty of the Virginia Polytechnic Institute and State University, Alexandria, Virginia, December 2004.
- [69] R. Mukund. *Wind and solar power systems*. CRC Press, CRC Press LLC, 2000 N.W., Corporate Blvd., Boca Raton, Florida 33431, 1999.
- [70] B. Lindgren. *A Power Converter for Photovoltaic Applications*. PhD thesis, Department of Electric Power Engineering, Chalmers University of Technology, Göteborg, Sweden, 2000.
- [71] K. H. Hussein, I. Muta, T. Hoshino, and M. Osakada. Maximum photovoltaic power tracking: an algorithm for rapidly changing atmospheric conditions. In *Generation, Transmission and Distribution, IEE Proceedings*, volume 142, 59 – 64, Jan 1995.
- [72] C. T. Chiang, T. S. Chiang, and H. S. Huang. Modeling a photovoltaic power system by cmac-gbf. In *Proc. of 3rd World Conference on Photovoltaic Energy Conversion*, 2431 – 2434, Osaka, Japan, 11-18 May 2003.

-
- [73] M. F. Ishengoma and E. E. Norum. Design and implementation of a digitally controlled stand-alone photovoltaic power supply. In *Nordic Workshop on Power and Industrial Electronics (Norpie 2002)*, Stockholm, Sweden, 12-14 Aug. 2002.
- [74] E. S. Gavanidou and A. G. Bakirtzis. Design of a stand alone system with renewable energy sources using trade off methods. *IEEE Transaction on Energy Conversion*, 7(1):42 – 48, 1992.
- [75] F. Lasnier and T. G. Ang. *Photovoltaic Engineering Handbook*. IOP Publishing Ltd, Adam Hilger, New York., 1990.
- [76] R. Chedid and S. Rahman. Unit sizing and control of hybrid wind-solar power systems. *IEEE Transactions on Energy Conversion*, 12(1):79 – 85, March 1997.
- [77] M. A. Abramson. Second order behavior of pattern search. *SIAM Journal on Optimization*, 16(2):515 – 530, 2005.
- [78] C. Audet, J. E. Dennis, and Jr. A pattern search filter approach for nonlinear programming without derivatives. *SIAM Journal on Optimization*, 14(4):980 – 1010, 2004.
- [79] A. J. Booker, J. E. Dennis, Jr., P. D. Frank, D. B. Serafini, and V. Torczon. Optimization using surrogate objectives on a helicopter test example. *Optimal Design and Control, Progress in Systems and Control Theory*, 49 – 58, 1998.
- [80] M. Kokkolaras, C. Audet, J. E. Dennis, and Jr. Mixed variable optimization of the number and composition of heat intercepts in a thermal insulation system. *Optimization and Engineering*, 2(1):5 – 29, 2001.
- [81] M. A. Abramson and C. Audet. Convergence of mesh adaptive direct search to second order stationary points. *SIAM Journal on Optimization.*, 17(2):606 – 619, 2006.
- [82] F. A. Mohamed and H. N. Koivo. System modelling and online optimal management of microgrid. In *Proc. of Sixth International Workshop on Large-Scale Integration of Wind Power and Transmission Networks for Offshore Wind Farms*, pages 470 – 478, TU Delft, Delft, The Netherlands, Oct. 2006.
- [83] F. A. Mohamed and H. N. Koivo. System modelling and online optimal management of microgrid with battery storage. In *Proc. of International Conference on Renewable Energies and Power Quality (ICREPQ'07)*, Universidad de Sevilla, Sevilla, Spain, March 2007.
- [84] S. O. Orero and M. R. Irving. Large scale unit commitment using a hybrid genetic algorithm. *International Journal of Electrical Power & Energy systems.*, 19(1):45 – 55, 1997.
- [85] S. Häggmark, V. Neimane, U. Axelsson, P. Holmberg, G. Karlsson, K. Kauhaniemi, M. Olsson, and C. Liljegren. Aspects of different distributed generation technologies, CODGUNet WP 3. In *Vattenfall Utveckling Ab 2003-03-14*, May 2003.
- [86] S. Bernow and D. Marron. Valuation of environmental externalities for energy planning and operations. In *Tellus Institute Report 90-SB01 Boston, MA*, May 1990.
- [87] M. Pipattanasomporn, M. Willingham, and S. Rahman. Implications of on-site distributed generation for commercial/industrial facilities. *IEEE Transactions on Power Systems.*, 20(1):206 – 212, February 2005.

-
- [88] V. Michel, B. Sascha, B. Britta, Herve C., K. Nipon, K. Franz, M. Didier, M. Jens, R. Jurgen, S. Philipp, S. Tawachai, and X. Vallve. Expandable hybrid systems for multi-user mini-grids. In *Proc. of 17th European Photovoltaic Solar Energy Conference*, 2330 – 2335, Munich, Germany, Oct. 2001.
- [89] A. Zahedi and A. Kalam. Balancing cost and performance in a pv /wind/battery hybrid power system. In *Proc. of Australasian Universities Power Engineering Conference (AUPEC'00)*, 280 – 283, Brisbane, Australia, 2000.
- [90] G. Liu, J. Yang, and Whidborne J. *Multiobjective optimisation and control*. Research Studies Press LTD, Baldock, 2003.
- [91] V. Bhaskar, S. K. Gupta, and A. K. Ray. Applications of multiobjective optimization in chemical engineering. *Reviews Chem. Eng*, 16:1 – 54, 2000.
- [92] J. Andersson. A survey of multiobjective optimization in engineering design. Technical Report LiTH-IKP-R-1097, Department of Mechanical Engineering, 2000.
- [93] M. Elmusrati, J. Riku, and H. Koivo. Multiobjective distributed power control algorithm for cdma wireless communication systems. *IEEE Transaction on Vehicular Technology*, 56(2):779 – 788, March 2007.
- [94] F. A. Mohamed and H. N. Koivo. Online management of microgrid with battery storage using multiobjective optimization. In *Proc. of IEEE International Conference on Power Engineering, Energy and Electrical Drives (POWERENG 2007)*, Setúbal, Portugal, Apr. 2007.
- [95] F. A. Mohamed and H. N. Koivo. System modelling and online optimal management of microgrid using multiobjective optimization. In *Proc. of IEEE International Conference on Clean electrical power - ICCEP 2007*, pages 148 – 153, Capri, Italy, May 2007.
- [96] F. A. Mohamed and H. N. Koivo. Microgrid online management and balancing using multiobjective optimization. In *Proc. of IEEE Power Tech 2007*, Lausanne, Switzerland, July 2007.
- [97] K. Miettinen. *Nonlinear multiobjective optimization*. Kluwer Academic Publishers, Boston, 1998.
- [98] D. E. Goldberg. *Genetic Algorithms in Search, optimization, and Machine Learning*. Addison Wesley, Reading, 1989.
- [99] D. Dutta, A. Goel, and J. Heidermann. Oblivious aqm and nash equilibria. *SIGCOMM Computer Communications Review*, 32(3):398 – 406, July 2002.
- [100] A. T. Rextin, Z. Irfan, and Z. A. Uzmi. Games networks play a game theoretic approach to networks. In *Proc. of 7th International Symposium on Parallel Architectures Algorithms and Networks*, 451 – 456, Hong Kong, SAR, China, May 2004.
- [101] S. S. Rao and S. K. Hati. Optimum design of shock and vibration isolation systems using game theory. *Journal of Eng. Optim*, 4:215 – 226, 1980.
- [102] M. Sunar and R. Kahraman. A comparative study of multiobjective optimization methods in structural design. *Turkish Journal of Engineering and Environmental Sciences*, 25:69 – 78, 2001.

- [103] S. S Rao and S. K. Hati. Game theory approach in multicriteria optimization of function generating mechanisms. *Journal of Mechanical Design*, 101:398 – 406, 1979.
- [104] S. S Rao and T. I Freiheit. Modified game theory approach to multiobjective optimization. *Journal of Mechanisms, Transmissions, and Automation in Design*, 113:286 – 291, 1991.
- [105] M. A. Abramson. *Pattern Search Algorithms for Mixed Variable General Constrained Optimization Problems*. PhD thesis, Rice Univeristy, Houston, Texas, August 2002.

Appendix A

Appendix

A.1 The General Pattern Search Algorithm

For simplicity, our discussion will focus primarily on the case of unconstrained minimization: minimize $CF(\mathbf{P})$.

We assume that CF is continuously differentiable, but that information about the gradient of CF is either unavailable or unreliable. Since the inception of pattern search methods, various techniques have also been used to apply them to solve the general nonlinear programming problem (3.1)

A.1.1 Generalized pattern search

We will consider the NLP problem,

$$\min_{x \in X} CF(\mathbf{P}) \tag{A.1}$$

where $CF : X \rightarrow \mathcal{R} \cup \{\infty\}$, $X = \{\mathbf{P} \in \mathcal{R}^n : l \leq \mathbf{A}\mathbf{P} \leq u\}$, $A \in \mathcal{R}^{m \times n}$ is a real matrix, $l, u \in (\mathcal{R} \cup \{\pm\infty\})^n$, and $l \leq u$.

A key point is that if an iterate falls outside of the domain X , it is simply ignored [105].

This differs in construction from that of some proposed methods, where the algorithm is applied to $CF_{\mathbf{P}} = CF + \varphi_{CF}$ rather than CF , where φ_{CF} is the indicator function for CF ; that is, it is zero for any point in X and 1 outside of X .

While $l = u$ is allowed in the formulation, equality constraints are problematic in practice because points outside of X are not evaluated by the algorithm, and any roundoff error would eliminate feasible points from being considered. Thus, to use these methods in practice, variables ought to be eliminated until all the constraints can be expressed as $l < u$.

The GPS algorithm is a direction-based method, whose convergence theory is based on searching in directions that form a positive spanning set. A finite set of positive spanning directions D is used to construct (theoretically) a mesh on which GPS iterates lie. This is based on the positive basis theory, and is done with the idea that, if CF is sufficiently smooth in a neighborhood of \mathbf{P}_k and $\nabla CF(\mathbf{P}_k) \neq 0$, then at least one direction $d \in D$ must be a descent direction. Thus, for some sufficiently small value of $\Delta_k > 0$, there

exists a point $y = \mathbf{P}_k + \Delta_k d$ satisfying $CF(y) < CF(\mathbf{P})$. Specifically, at iteration k , the mesh M_k is defined as:

$$M_k = \left\{ \mathbf{P}_k + \Delta_k D z \in X : z \in Z_+^{|D|} \right\} \quad (\text{A.2})$$

where \mathbf{P}_k is the current iterate, $\Delta_k > 0$ is a parameter that controls the fineness of the mesh, and Z_+ is the set of nonnegative integers. For convenience, the positive spanning set D is represented here as a real $n \times |D|$ matrix whose columns are the vectors in the set.

The positive spanning directions must also satisfy the mild restriction,

$$D = GZ \quad (\text{A.3})$$

where $G \in \mathfrak{R}^{n \times n}$ is a nonsingular generating matrix, and $Z \in Z^{n \times |D|}$. A common choice for G is the identity matrix.

A.1.2 The Basic GPS Algorithm

In the GPS algorithm, each iteration is characterized by an optional global search step and a local poll step. In the search step, the objective function CF is evaluated at a finite number of points lying on the current mesh M_k in an attempt to try to find a new point with a better function value than the incumbent. Any strategy may be used (including none), as long as the number of mesh points it evaluates is finite.

In the poll step, a positive spanning set $D_k \subseteq D$ is chosen from which the poll set is constructed. Again, we represent D_k also as a matrix whose columns are the members of the set. It is a function of k and \mathbf{P}_k ; *i.e.*, $D_k = D(k, P_{i_k}) \subseteq D$. The poll set P_k is constructed as the neighboring mesh points in each of the directions in D_k ; *i.e.*,

$$O_k = \{ \mathbf{P}_k + \Delta_k d \in X : d \in D_k \} \quad (\text{A.4})$$

The function CF is evaluated at points in O_k until the points have all been evaluated, or until one with a lower objective function value is found. The set of trial points is defined as $T_k = S_k \cup O_k$, where S_k is the finite set of mesh points evaluated during the search step. The following definitions define the two possible outcomes of the search and poll steps [105].

Definition 1: If $CF(y) < CF(\mathbf{P}_k)$ for some $y \in T_k$, then y is said to be an improved mesh point.

Definition 2 If $CF(\mathbf{P}_k) \leq f(y)$ for all $y \in O_k$, then \mathbf{P}_k is said to be a mesh local optimizer.

If either the search or poll step is successful to find an improved mesh point, then it becomes the new incumbent \mathbf{P}_{k+1} , and the mesh is coarsened according to the rule,

$$\Delta_{k+1} = \tau^{m_k^+} \Delta_k, \quad (\text{A.5})$$

where $\tau > 1$ is rational and fixed over all iterations, and the integer m_k^+ satisfies $0 \leq m_k^+ \leq m_{max}$ for some fixed integer $m_{max} \geq 0$.

If the poll and search steps both fail to find an improved mesh point, then the mesh

local optimizer should remain unchanged, while the mesh is refined according to the rule,

$$\Delta_{k+1} = \tau^{m_k^-} \Delta_k \quad (\text{A.6})$$

where

$\tau > 1$ is defined as above, $\tau^{m_k^-} \in (0, 1)$, and the integer $\tau^{m_k^-}$ satisfies $m_{\min} \leq \tau^{m_k^-} \leq -1$ for some fixed integer m_{\min} .

Furthermore, for any integer $k \geq 0$, there exists the integer r_k such that

$$\Delta_k = \tau^{r_k} \Delta_0 \quad (\text{A.7})$$

The generalized Pattern search algorithm is in the form [105]:

Initialization:

Let \mathbf{P}_0 be such that $CF(\mathbf{P}_0)$ is finite, and let $M_0 \subset X$ be the mesh defined by $\Delta_0 > 0$ and x_0 .

For $k = 0, 1, 2, \dots$, perform the following:

1. Search step: Employ some finite strategy seeking an improved mesh point; *i.e.*, $\mathbf{P}_{k+1} \in M_k$ such that $CF(\mathbf{P}_{k+1}) < CF(\mathbf{P}_k)$.

2. Poll step: If the search step was unsuccessful, evaluate CF at points in the poll set P_k until an improved mesh point \mathbf{P}_{k+1} is found (or until done).

3. Update: If search or poll finds an improved mesh point, Update \mathbf{P}_{k+1} , and set $\Delta_{k+1} \geq \Delta_k$;

Otherwise, set $\mathbf{P}_{k+1} = \mathbf{P}_k$, and set $\Delta_{k+1} < \Delta_k$.

A.2 Mesh Adaptive Direct Search (MADS) Methods

The MADS class of algorithms, introduced in [24], is designed for nonsmooth optimization problems. The convergence analysis of MADS ensured necessary optimality conditions of the first [24] and second [81] orders under certain assumptions.

A.2.1 Features of the MADS algorithm

Each iteration k of a MADS algorithm is characterized by two steps. First, an optional search step over the space of variables, as long as it is a finite process and all trial points lie on a mesh. If no better point is found or no global search is used, the algorithm goes to a mandatory local exploration step (mandatory because it ensures convergence). Second is the poll step, at most $2n$ trial mesh points near the incumbent solution are selected (the poll set) and evaluated. If no better neighbor is found, the mesh is refined [24].

If an improved mesh point $\mathbf{P}_{k+1} \in X$ is found, the mesh is kept the same or coarsened, and then \mathbf{P}_{k+1} is the next incumbent. The exploration directions vary at each iteration, and become dense with probability 1. This is the main difference between the pattern

search and MADS algorithms.

$$CF_X = \begin{cases} CF(\mathbf{P}) & \text{if } \mathbf{P} \in X \\ +\infty & \text{otherwise} \end{cases} \quad (\text{A.8})$$

Then, MADS is applied to the unconstrained barrier problem

$$\min_{\mathbf{P}} CF_X(\mathbf{P}) \quad (\text{A.9})$$

The feasible region X can be nonlinear, non-convex, non-differentiable, or disjoint. There are no hypotheses made on the domain, except that the initial point must be feasible. The convergence results depend on the local smoothness of CF (and not CF_X , which is obviously discontinuous on the boundary of) and on the tangent cone at the limit point produced by the algorithm.

A.2.2 The MADS algorithm Description

A general form for MADS is proposed in [24]. This general framework is then specialized to a specific algorithmic implementation. The algorithm is very similar to GPS, with differences in the POLL step, and the new size parameter. The main algorithm is summarized in the following steps:

A.2.3 Initialization

MADS is an iterative algorithm, and the iteration number is denoted by the index k . Then the iteration counter k is set to 0. The user must specify the starting point \mathbf{P}_0 such that $CF_X(\mathbf{P}_0) < \infty$, and an initial mesh size parameter $\Delta_0^m \in \mathbb{R}_+$.

Then, the algorithm defines:

the poll size parameter $\Delta_k^p = \sqrt{\Delta_k^m}$;

the fixed positive basis needed to generate polling directions $D = \{\pm e_i, i = 1, 2, \dots, n\}$: where e_i is the i^{th} coordinate direction;

$M_k = \bigcup_{\mathbf{P} \in S_k} \{\mathbf{P}_k + \Delta_k^m D z \mid z \in N^{2n}\}$: the mesh, where S_k

is the set of points where the objective function CF had been evaluated by the start of iteration k .

MADS then proceeds to the quest for an improved mesh point.

A.2.4 Search Step

The goal of this step is to provide flexibility to the algorithm. with the optional search allows the evaluation of CF_X at any finite set of mesh points. The search and possibly the Poll step is performed until an improved mesh point \mathbf{P}_{k+1} is found on the mesh M_k .

A.2.5 Poll Step

This step ensures the convergence of the algorithm. It begins by defining the poll set $P_k = \{\mathbf{P}_k + \Delta_k^m d \mid d \in D_k\} \subset M_k$. Where D_k is a positive spanning set such that for each $d \in D_k$,

- Non-negative combinations of the elements of the set D_k span the entire space \mathbb{R}^n ;
- While k goes to infinity, the elements of D_k do not collapse to a lower dimensional subspace;
- Each d in D_k may be written as $d = Du$ with $u \in N^2n$ (it is a positive integer combination of the columns in D);
- The distance from the frame center \mathbf{P}_k to a poll point $\mathbf{P}_k + \Delta_k^m d, \forall d \in D_k$ is bounded above by the poll size parameter:

$$\|\Delta_k^m d\|_\infty \leq \Delta_k^p.$$

The number of possible directions for building P_k is of the order of $(\Delta_k^m)^{-n}$. As Δ_k^m becomes small, the number of possible poll points increases. It is shown in [24] that the set of normalized directions formed by (A.10) is dense in the unit circle with a probability of 1.

$$\bigcup_{k=1}^{\infty} \left\{ \frac{d}{\|d\|} \mid d \in D_k \right\} \quad (\text{A.10})$$

There are two strategies for the evaluation of set P_k . The opportunist one is to terminate iteration k whenever there is a decrease in f . The exhaustive one consists of evaluating the entire poll set P_k and then choosing the feasible point leading to the largest decrease of the objective function value CF . If no improvement of f is made with the poll step, i.e., when it is shown $CF_X(\mathbf{P}_k) \leq CF_X(\mathbf{P}) \forall x \in P_k$, then \mathbf{P}_k is declared a "mesh local optimizer".

A.2.6 Parameters update

This step uses a resizing factor of 4 to update mesh and poll parameters. We define \mathbf{P}_{k+1} as being the better point obtained by either the search or the poll step, or being a mesh local optimizer. According to the result of step 2, the algorithm applies:

- if $CF_X(\mathbf{P}_{k+1}) = CF_X(\mathbf{P}_k)$ then $\Delta_{k+1}^m = \frac{1}{4} \Delta_k^m$;
- if $CF_X(\mathbf{P}_{k+1}) < CF_X(\mathbf{P}_k)$ then $\Delta_{k+1}^m = \min \{1, 4\Delta_k^m\}$.

This redefinition of the mesh parameter (the poll size parameter is defined as in initialization step) ensures that $\liminf_{k \rightarrow \infty} \Delta_k^p = \liminf_{k \rightarrow \infty} \Delta_k^m = 0$. The algorithm updates $k \rightarrow k+1$ and then goes to the termination step.

A.2.7 Termination

The user must specify some termination criterion, such as a minimal value on the mesh size parameter Δ_k^m , a maximal number of objective function evaluations, or a maximal number of consecutive unsuccessful function evaluations. As soon as one termination criterion is reached, the algorithm terminates. Otherwise, it returns to step 2.

A.2.8 Convergence Analysis

The main results of the convergence analysis of [24] will be summarized. Under the assumptions $P_0 \in X$, that $CF(P_0)$ is finite, and that all iterates \mathbf{P}_k produced by the MADS algorithm lie in a compact set. The convergence analysis relies on the two following hypotheses:

- Function $CF_X : \mathbb{R}^n \rightarrow \mathbb{R} \cup \{\infty\}$ and an initial point \mathbf{P}_0 ($CF_X(\mathbf{P}_0) < \infty$) are available;
- The set $\{\mathbf{P}_k\}$ of iterates produced by MADS lies in a compact set.

Next the type of optimality results guaranteed by MADS is presented. The idea is to prove that there are no feasible descent directions at \hat{P} ; this is the concept of a KKT (Karush- Kuhn-Tucker) point. The set of feasible descent directions is a type of "tangent cone" and is defined according to the domain's constraints.

Let \hat{P} be a point in \mathbb{R}^n and v be some direction in \mathbb{R}^n . If CF is a differentiable function, then the directional derivative at \hat{P} in the direction v is defined by:

$$CF'(\hat{P}; v) = \lim_{t \rightarrow 0} \frac{CF(\hat{P} + tv) - CF(\hat{P})}{t} \quad (\text{A.11})$$

where $t \in \mathbb{R}_+$. If all constraint functions are differentiable, the tangent cone can be defined as

$$T_X(\hat{P}) = \left\{ v \in \mathbb{R}^n \mid v^T \nabla g_i(\hat{P}) \leq 0, \forall i \text{ such that } g_i(\hat{P}) = 0 \right\} \quad (\text{A.12})$$

The necessary first-order optimality condition for the smooth case may be stated as: Suppose that $CF(\mathbf{P})$ is continuously differentiable near $\hat{P} \in X$.

A necessary condition for \hat{P} to be a local minimizer is that:

$$CF'(\hat{P}; v) \geq 0 \forall v \in T_X(\hat{P}).$$

The point \hat{P} is called a KKT stationary point.

In the context of the present work, however, we are concerned with non-smooth functions, and so the directional derivative $CF'(\hat{P}; v)$ and/or the tangent cone $T_X(\hat{P})$ may not necessarily exist. Under the assumption that the function f is Lipschitz near \hat{P} , i.e., that there exists a scalar $K \in \mathbb{R}_+$ such that:

$$\left| \frac{f(\hat{P}) - CF(y)}{\hat{P} - y} \right| \leq K \quad (\text{A.13})$$

for any y in some open neighborhood of \hat{P} , the generalized Clarke derivative of CF at \hat{P} in the direction v is defined as:

$$CF^o(\hat{P}; v) = \lim_{y \rightarrow \hat{P}} \sup_{t \downarrow 0} \frac{CF(y + tv) - CF(y)}{t} \quad (\text{A.14})$$

Note that CF^o is a generalization of CF' , in the sense that if CF is differentiable, then $CF^o = CF'$ [14]. Similarly as (7), a vector $v \in \mathbb{R}^n$ is said to be Clarke-tangent to $X \subset \mathbb{R}^n$ at a point $\hat{P} \in X$ if for any sequence $\{y_k\} \in X$ that converges to \hat{P} , and for any sequence $\{t_k\} > 0 \in \mathbb{R}$ converging to 0, there exists a sequence of vectors $\{w_k\}$ converging to v such

that $y_k + t_k w_k \in X$. The set $T_X^{Cl}(\hat{P})$ of Clarke-tangent vectors is called Clarke tangent cone at \hat{P} .

Some references also provides conditions ensuring that $T_X^{Cl}(\hat{P}) = T_X(\hat{P})$ [24]. In the context of non-smooth optimization, the necessary optimality condition may be stated as:

Suppose that $CF(\mathbf{P})$ is Lipschitz near $\hat{P} \in X$. A necessary condition for \hat{P} to be a local minimizer is that:

$$CF^o(\hat{P}; v) \geq 0 \forall v \in T_X^{Cl}(\hat{P})$$

The point \hat{P} is called a Clarke-KKT stationary point.

[24] consider the limit \hat{P} of a convergent subsequence of mesh local minimizers on meshes that get infinitely fine. They show the existence of such points and provide a hierarchy of convergence results based on the local smoothness of the functions.

Their main convergence result is that if $CF(\mathbf{P})$ is Lipschitz near $\hat{P} \in X$, and if either X is closed or $\text{int}(T_X^{Cl}(\hat{P})) \neq \emptyset$, then \hat{P} is a Clarke-KKT stationary point.

In the case where there are no constraints ($X = \mathbb{R}^n$) or when the optimum does not lie on the boundary ($\hat{P} \in \text{int}(X)$), then the tangent and Clarke tangent cones include all directions in \mathbb{R}^n . The optimality conditions reduce to $\nabla CF_X(\hat{P}) = 0$ for the continuously differentiable case, and to $0 \in \partial CF(\hat{P})$ for the non-smooth case, where $\partial CF(\hat{P})$ is the generalized gradient.

Appendix B

Appendix

B.1 The numerical values used to simulate Fuel Cell model

P_{ref}	Real power reference	100 kW
T	Absolute temperature	1273 K
F	Faraday's constant	96 487 C/mol
R	Universal gas constant	8314 J/(kmol K)
E_0	Ideal standard potential	1.18 V
N_0	Number of cells in series in the stack	384
K_r	Constant, $K_r = N_0/4F$	0.996×10^{-6} kmol/(s A)
U_{max}	Maximum fuel utilization	0.9
U_{min}	Minimum fuel utilization	0.8
U_{opt}	Optimal fuel utilization	0.85
K_{H_2}	Valve molar constant for hydrogen	8.43×10^{-4} kmol/(s atm)
K_{H_2O}	Valve molar constant for water	2.81×10^{-4} kmol/(s atm)
K_{O_2}	Valve molar constant for oxygen	2.52×10^{-3} kmol/(s atm)
τ_{H_2}	Response time for hydrogen flow	26.1 s
τ_{H_2O}	Response time for water flow	78.3 s
τ_{O_2}	Response time for oxygen flow	2.91 s
r	Ohmic loss	0.126 V
T_e	Electrical response time	0.8 s
T_f	Fuel processor response time	5 s
r_{H-O}	Ratio of hydrogen to oxygen	1.145
PF	Power factor	1

HELSINKI UNIVERSITY OF TECHNOLOGY CONTROL ENGINEERING

Editor: H. Koivo

- Report 141 Pöyhönen, S.
Support Vector Machine Based Classification in Condition Monitoring of Induction Motors. June 2004.
- Report 142 Elmusrati, M. S.
Radio Resource Scheduling and Smart Antennas in Cellular CDMA Communication Systems. August 2004.
- Report 143 Tenno, A.
Modelling and Evaluation of Valve-Regulated Lead-Acid Batteries. September 2004.
- Report 144 Hyötyniemi, H.
Hebbian Neuron Grids: System Theoretic Approach. September 2004.
- Report 145 Hyötyniemi, H. (ed.)
Complex Systems: Science at the Edge of Chaos - Collected papers of the Spring 2003 postgraduate seminar. October 2004.
- Report 146 Paanasalo, J.
Modelling and Control of Printing Paper Surface Winding. June 2005.
- Report 147 Mohamed, F.
Microgrid Modelling and Simulation. March 2006.
- Report 148 Mäenpää, T.
Robust Model Predictive Control for Cross-Directional Processes. May 2006.
- Report 149 Kantola, K.
Modelling, Estimation and Control of Electroless Nickel Plating Process of Printed Circuit Board Manufacturing. March 2006.
- Report 150 Virtanen, T.
Fault Diagnostics and Vibration Control of Paper Winders. June 2006.
- Report 151 Hyötyniemi, H.
Neocybernetics in Biological Systems. August 2006.
- Report 152 Hasu, V.
Radio Resource Management in Wireless Communication: Beamforming, Transmission Power Control, and Rate Allocation. June 2007.
- Report 153 Hrbek, J.
Active Control of Rotor Vibration by Model Predictive Control - A simulation study. May 2007.
- Report 154 Mohamed, F. A.
Microgrid Modelling and Online Management. January 2008.

ISBN 978-951-22-9234-9

ISSN 0356-0872

Yliopistopaino, Helsinki 2008